UNIVERSITÄT DUISBURG ESSEN

Offen im Denken

Universität Duisburg-Essen

Fakultät für Chemie

Theoretical calculations of the molecular interactions of polypyrrole oligomers doped with heptafluorotantalate ions

Dissertation

to obtain the doctoral degree in natural sciences

Dr. rer. nat.

Presented by
Felipe Giraldo Nohra
born in Bogotá, Colombia

Essen, 31th May 2021

Die vorliegende Arbeit wurde in der Zeit von Oktober 2014 bis Mai 2021 an der Fakultät für Chemie der Universität Duisburg-Essen im Arbeitskreis von Prof. Dr. Georg Jansen angefertigt.

Disputationstermin: 04.10.2021

Gutachter : Prof. Dr. Georg Jansen.

Prof. Dr. Eckhard Spohr

Vorsitzender: Jun-Prof. Dr. Corina Andronescu

DOI: 10.17185/duepublico/74905
URN: urn:nbn:de:hbz:464-20211020-104519-9

Acknowledgements

In the first place, I want to thank very deeply my advisor, Prof. Dr. Georg Jansen for his support during these 7 years of altogether work, for believing in me since the first contact and accepting me in his group, and for the guidance and help through the development of this work.

Thanks to Prof Dr. Eckard Spohr for being the Reviewer of my work, providing appropriate corrections and comments to present an excellent Dissertation.

Thanks to my group companions: Robert, Briac, Felix, Dennis, Rebekka, Iris and Lukasz for their help in my thesis, and making more enjoyable my hours of work.

Most importantly, I want to thank my family, my Mother Flor, for her unconditional love, support, lessons, education and patience, that endly gave result in this stage of my life, I hope to continue making you proud for many years more, to my sister Carolina, for guiding me in the real world, giving me impulse in this stage, growing together with you is until now one of the biggest honours a sibling can have, despite our quarrels, or disputes, my gratitude for your role until now is unmatchable.

Special thanks to Prof. Dr. Wolfram Baumann whose guidance, made me take all my way to Germany, and finally obtain my doctor title.

My gratitude as well to one of my closest friends that could have appreciated this achievement, Dr. Sc. José Luis Villaveces (RIP), for introducing me to what doing chemistry from computers is like, for 10 years of friendship and learning I will never forget.

A special mention to Dr. Jorge Daniel Gamarra, for giving me the start material to begin this work.

And finally, thanks to my father (RIP), who I know that he would be proud of this work, the man I loved the most.

Kurzzusammenfassung

Seit ihrer Entdeckung im Jahre 1977 sind leitende Polymere als eine potentiell technisch relevante Art von Materialen bekannt. Die Forschung dazu ist inzwischen weit fortgeschritten und es wurden viele Varietäten mit verschiedenen Eigenschaften und Nutzungsmöglichkeiten entwickelt. Dotierung durch Ionen ist eine der Methoden, den Leitungsprozess der Materialien zu verbessern. Eines der am häufigsten verwendeten Materialien ist Polypyrrol, unter anderem wegen seiner mechanischen Eigenschaften. Experimente haben gezeigt daß die Einlagerung von Metallionen in seiner Matrix die Leitfähigkeit verbessert. Dabei haben Tantalationensalze gute Ergebnisse gezeigt. Wechselwirkungen und Struktur dieser Materialen sind dennoch nicht ganz verstanden.

Ausgangspunkt der vorliegenden Arbeit waren experimentelle Ergebnisse zur Synthese von mit Heptafluorotantalationen dotiertem Polypyrrol, wo Cyclovoltammetrie Daten zufolge eine sehr starke Wechselwirkung mit der Matrix vorliegt. Durch die Nutzung quantenchemischer Methoden, insbesondere dispersionskorrigierter Dichtefunktionaltheorie, sollten Informationen zu Struktur und Ionisierung von Aggregaten aus Oligopyrrolen und Heptafluorotantalationen gewonnen werden, in der Erwartung, daß sich diese auf das amorphe dotierte Polypyrrol-Material übertragen lassen.

Es wurden also zunächst Geometrieoptimierungen für Aggregate verschiedenster Größe durchgeführt, die aus mehreren Oligopyrrolketten mit einer Kettenlänge bis zu sieben und einem bis drei Heptafluorotantalationen bestehen. Durch die Betrachtung verschiedenster Konformationen dieser Aggregate wurden Einblicke in die strukturbestimmende Rolle von Wasserstoffbrückenbindungen, Coulomb-Abstoßung zwischen den Anionen und Stapelung der Polypyrrolketten gewonnen. Dabei wurde unter anderem festgestellt, dass sich die Anionen in "Taschen" der in der Pyrrolmonomer alternierenden Oligopyrrolketten einlagern, die Anionen von bis zu fünf Ketten umgeben sein können und daß mehrere Anionen trotz ihrer Coulomb-Abstoßung auch in unmittelbar benachbarten Taschen eingelagert werden können. Anschließend wurden analoge Rechnungen von ein- und mehrfach oxidierten Aggregaten durchgeführt, um vertikale und adiabatische Ionisierungsenergien zu bestimmen sowie Strukturveränderungen der Aggregate nach

Ionisierung zu beleuchten. So wurde unter anderem gezeigt, daß Oxidation in der Tat zu delokalisierten positiven Ladungen auf den Oligopyrrolketten führt.

Da experimentelle Ergebnisse zumeist in Gegenwart von Lösungsmitteln erzielt werden wurde schließlich der Einfluss von Mikrosolvatation der Aggregate untersucht. Hier wurden zwei verschieden Lösungsmittel betrachtet: einerseits Wasser als das gebräuchlichste Lösungsmittel und andererseits Acetonitril, welches für die Experimente im vorliegenden Fall benutzt wurde. Diese Lösungsmittel unterscheiden sich hinsichtlich ihrer Molekülgröße, ihres Dipolmoments und ihrer Fähigkeit, Wasserstoffbrückenbindungen einzugehen. In Strukturoptimierungen nicht-oxidierter und oxidierter Oligopyrrol-Heptfluorotantalataggregate mit bis zu zwei Dutzend Lösungsmitttelmolekülen zeigten sich Phänomene wie Einschiebung von Wassermolekülen in Wasserstoffbrückenbindungen zwischen Anionen und Pyrrol und die Verbrückung zweier Anionen durch Wassermoleküle, die im Falle von Acetonitril natürlich nicht auftreten können. Beiden Lösungsmitteln war aber gemeinsam, dass sie die Autoxidation der Pyrrolketten in den Aggregaten etwas reduzieren: während die Aggregate ohne Lösungsmittel energetisch dann am stabilsten waren, wenn ein Elektron pro eingelagertem Anion abgegeben wurde,verminderte sich die optimaler Anzahl abgegebener Elektronen bei einigen Konformationen der mikrosolvatisierter Aggregate.

Index

Chapter 1: Introduction

1.1 Theoretical background

The history of the conducting polymers goes back to the year of 1977[1], when (because of a mistake), doped polyacetylene was synthesized[2]. This material showed a conductivity close to that of copper, making it the first known intrinsically conducting polymer (ICP). However, doped polyacetylene is quite sensitive to air and moisture[3]. As a consequence, research in this field turned to find monomers with better stability and with similar properties (π-electron delocalisation, low energy optical transitions, low ionisation potentials and high electron affinities). Among these we can list polyaniline, polypyrrole, polythiophene, polyphenylene, polyphenylvinylene, and many others. In the year 2000 a Nobel Prize was awarded to Heeger, MacDiarmid, and Shrikawa for “the discovery and development of conductive polymers".[4]

Among the most important features of these materials, at first place their mixed-type conductivity (ionic and electronic) should be highlighted. The first conductivity type is ionic because it involves ions due to the dopants. The second type is electronic and involves the conjugated π- electron system in the polymer. Another important feature is that these materials can interchange continually between oxidised and reduced states upon applying electric impulses to them. This phenomenon can be seen by cyclic voltammetry studies, implying that they can act as capacitors.[1,3]

A wide variety of examples in this respect can be found, where polypyrrole and other conducting polymers are used for charge storage, especially when used with inorganic materials such as graphene, as can be seen in an experiment by Oliveira *et al.*[5] (Fig.**1**) where polypyrrole and functionalized graphene sheets were fused using different polymerization techniques in order to obtain nanocomposites which could act as supercapacitors.

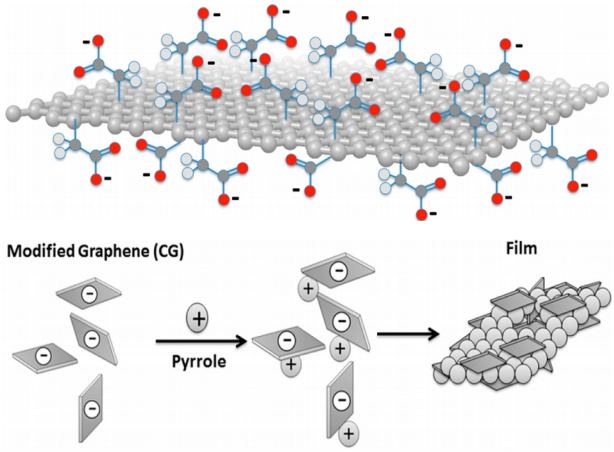

Figure **1**. A functionalized graphene sheet.[5]

On the other hand, polypyrrole could be useful as well in the medical area, as shown by a study of Runge *et al.*[6], where polypyrrole issued in the synthesis of a hydrogel in order to achieve nerve regeneration; this material is obtained through inserting polypyrrole inside an oligopolyethyleneglycol fumarate hydrogel, helping to stimulate nerve cells regeneration.

Another field in which polypyrrole shows growing potential is photocatalysis. For example, Dimitrijevic *et al.*[7], use nanocomposites of TiO_2 and polypyrrole, where the polymer acts as an electron provider through photosensitivity and transferring charge to TiO_2 and to the composite interface(Fig. **2**).

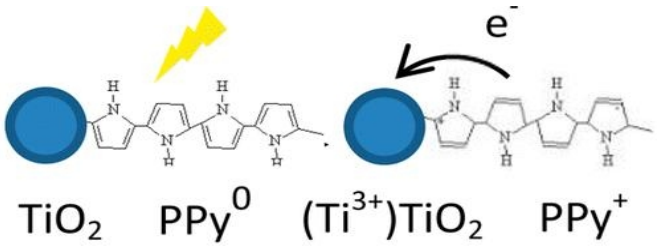

Figure **2**. Polypyrrole functionalized TiO_2 nanoparticles.[7]

Polypyrrole has even found use as a potential sorbent in the research made by Parakhonskiy *et al.*[8], where this polymer has shown capabilities to encapsulate hydrogen bubbles and other potential chemical hazards as well (Fig. **3**).

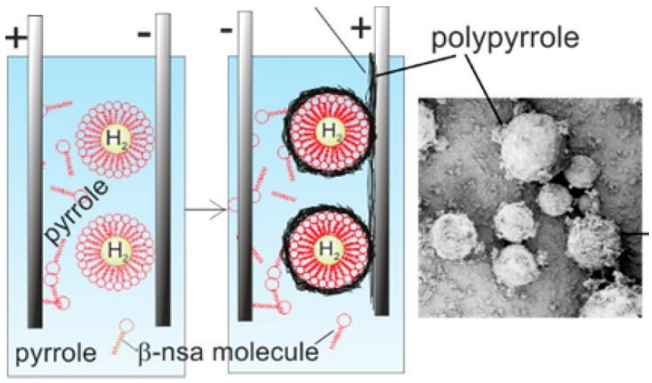

Figure **3**. Encapsulation of hydrogen by polypyrrole.[8]

In the environmental field for example, polypyrrole is able to form aggregates with mercaptoacetic acid (MAA) which can remove toxic metal ions, as shown by Ragunath *et al.*[9] They also demonstrated other uses such as a reducing and antimicrobial agent, and for gas sensing as well.

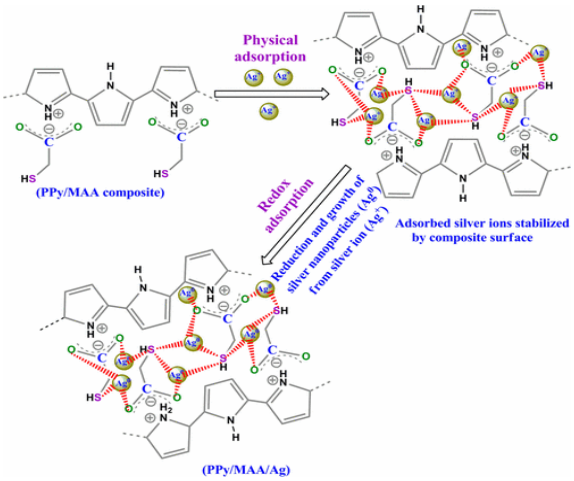

Figure **4**. Composite formation between polypyrrole and MAA.[9]

Recently, interest in the synthesis of hybrid materials that involve compounds of transition metal ions (oxides, or salts) has increased. However, the charge transfer mechanism and application range of these materials is not known or defined yet[10,11].

1.2 Polypyrrole, synthesis and doping

Polypyrrole is synthesized from pyrrole in two ways: chemical and electrochemical. The chemical synthesis consists in oxidising the monomers with chemical oxidants like copper

or iron salts. The reaction yield here is determined by many factors like the solvent, the reaction time, initial pyrrole/oxidant ratio, and temperature. This way of synthesis in general has the advantage of yielding a more crystalline product than obtained electrochemically[12].

The electrochemical method, however, has numerous other advantages over the chemical synthesis. It is thus possible to obtain a membrane over an electrode surface, because of anodic deposition, depending on parameters like temperature, electrolyte concentration, electrode material, applied potential or current, temperature and species concentration. The main advantages found in this type of synthesis are that it is fast, clean, of high reproducibility and yield, and also allows to have more control in the final properties of the obtained films. The mechanism of this type of synthesis is not completely understood however. A proposed general polymerization mechanism[13] is summarized in Figures **5** and **6**.

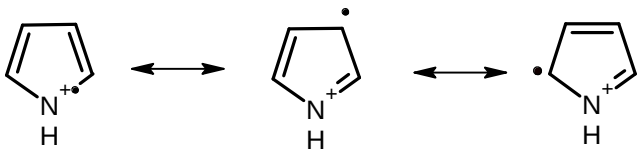

Figure **5**. Resonance forms of the pyrrole after oxidation

Beginning with the oxidised resonance forms of pyrrole (cf. Fig. **5**), the third one of which has the largest contribution, it dimerises with another radical cation, expelling two protons to gain aromaticity. The new dimer, which has a more extended conjugated π- electron system, is even more readily oxidised under the same conditions, thus successively adding more monomers to the growing chain (Fig. **6**).

Formation of a more conjugated system implies that it will easily be possible to change its oxidation state, and then to obtain electrical conductivity. As already mentioned above, it is also important to note that to have charge transport, ions must be introduced in order to create what is known as electrochemical doping. This can be achieved if the material is immersed in an electrolyte solution and in contact with an electrode. During this process the generated charges in the polymer are balanced by counter ions which are referred as dopants[14]. Depending on the ion acting as dopant[11], there will be anionic or cationic exchange between the polymer and the medium, and the structure of the polymer will

change as well. Doping involves as well oxidation and reduction of the polymer backbone; oxidation removes electrons, producing a positively charged polymer (p-doping). In a similar way reduction adds electrons to the back bone generating a negative polymer (n-doping).

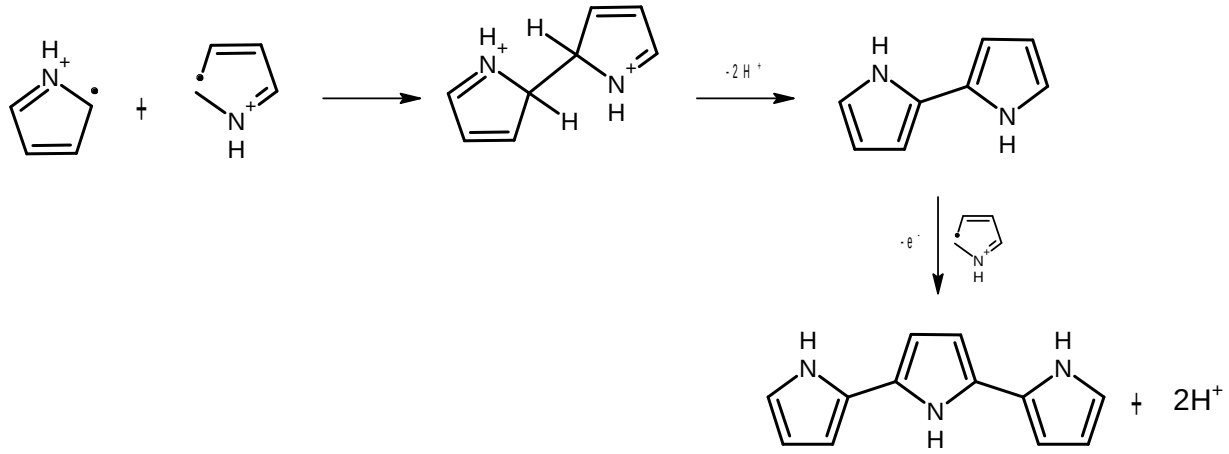

Figure **6**. Chain growth, adding a new monomer.

1.3 Context of the project, objectives and methods

Gamarra *et al.*[15] synthesized polypyrrole membranes by electrochemical methods which were doped with potassium heptafluorotantalate. The experimental methods that were applied to the polymer like cyclic voltammetry to determine the redox values and SEM photographies of the membranes, showed that tantalum stands into the membranes. The redox values show a cationic interchange, indicating a strong interaction between the tantalate and the polymer. This leads to the following question: How strong is the interaction between the polymer with the metallic ion and how does this affect the material conductivity?

The main goal in this PhD project thus is to study aggregates composed of one to three heptafluorotantalate ions and surrounding oligopyrrole chains, through quantum chemical calculations in order to get insight into structural motifs of the amorphous material. Here different oxidation states of the aggregates will be considered to gain information on structural and energetic changes upon electron removal. From this set of data, the role of specific interactions such as hydrogen bridges between heptafluorotantalate and pyrrole subunits, and stacking between oligopyrrole chains will be highlighted. Furthermore,

microsolvation of the aggregates varying numbers of water and acetonitrile molecules will be computationally investigated to shed some light on the influence of a solvent on their structural properties.

The methodology consists in first modeling the proposed system with one of the existent programs of molecular modeling (MOLDEN, TMoleX, Avogadro). In this way a preliminary model of heptafluorotantalate ion with one pyrrole molecule will be created, followed by rising up the monomer number and the number of anions. Then, these model structures will be refined with quantum chemical methods such as dispersion-corrected density functional theory (BP+D) and second-order Møller-Plesset theory (MP2), using standard packages such as Turbomole, and Molpro[16-22]. Furthermore, calculations will be carried out for the systems in a certain range of oxidation numbers, taking into account that interaction changes can occur with changes in the oxidation state. Finally, the influence of solvent molecules such as water and acetonitrile on the aggregates will also be considered in a microsolvation approach.

1.4 Computational methods

1.4.1 Density functional theory (DFT)

Density functional theory[23] is a computational method used in theoretical chemistry and solid state physics to determine the properties of a many body system, more specifically for the purpose of this project, the properties of molecules. In DFT the energy of the systems is considered to be a functional of the electron density. The theory is based on the Hohenberg-Kohn theorem, which states that the ground state electronic density is unique for every system. A basic advantage of DFT over other quantum chemical methods which use electronic wavefunctions is that the density depends on 3 spatial coordinates only, whereas wavefunctions depend on three spatial and a spin coordinate for each of the electrons. To improve the accuracy of the energy calculations, usually the Kohn-Sham variant of DFT is used. In Kohn-Sham DFT the calculation of the total energy is divided in 3 parts: (i) the kinetic energy funcional of “non-interacting electrons” (meaning that each electron, or, more precisely, each pseudo-electron does not interact with the others), (ii) the easily calculated Coulomb interaction of the electrons with the nuclei creating the “external potential” and the Coulomb interaction among themselves, and (iii) finally the

functional of correlation and exchange of the electrons which also includes the deviation of the kinetic energy of the electrons from that of the pseudo electrons (a.k.a. non-interacting electrons). The first part is easy to calculate for the pseudo-electron system which is described by a Slater determinant containing the Kohn-Sham orbitals. The density of the pseudo electron system, i.e., the sum of the KS orbital densities, is required to have the same density as the real system while the third part is only known in special cases (as the homogeneous electron gas) and in general must be approximated [23].

DFT calculations have been applied to optimize metal complexes of polymer structures[24-29] as for example in a work by Guo *et al.* where a complex of polypyrrole with cobalt modeling a material for lithium batteries was optimized with DFT to find the best structure (Fig. **7**)[30].

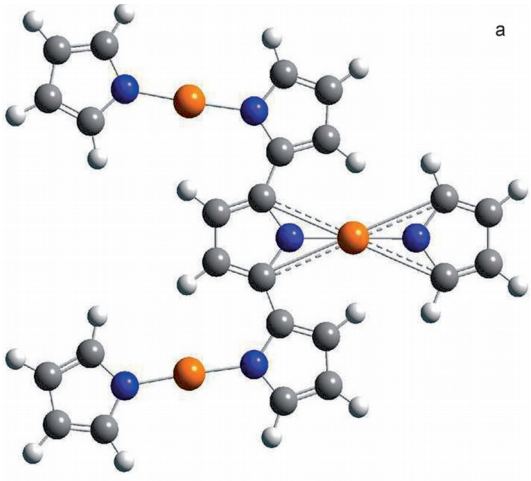

Figure **7**. Monolayer of the polypyrrole-cobalt complex.[30]

Standard DFT functionals suffer from problems with the description of dispersion interactions and thus are not readily applicable to the treatment of interactions between molecules. Yet, this difficulty was overcome by the addition of empirical dispersion corrections to the energy expression[30,31]. In this dispersion-corrected form named DFT+D the methodology should be a useful and efficient tool for the purpose of the proposed project.

1.4.2 Electron correlation methods

The Hartree-Fock method[32,33] generates simple one-determinant (or few-determinant, in some open-shell cases) approximations to the solution of the Schrödinger equation, replacing the electron-electron interaction with an average interaction term. With a sufficiently large basis set, the HF method accounts for ~99% of the energy. Yet, the remaining ~1% contribution is really necessary in order to describe chemical phenomena involving relatively small energy changes correctly. This energetic difference between HF and the true energy in a given basis set is called the electron correlation energy, it corresponds to the motion of electrons being correlated.

The electron correlation effect can be taken into account with the help of additional Slater determinants in which one, two, three.. of the occupied Hartree-Fock orbitals are replaced with one, two, three... so-called “virtual” orbitals, i.e., orbitals, which are also solutions of the Hartreee-Fock equations, yet with higher orbital energy. Thus in electron correlation methods the electronic wavefunction becomes:

$$\Psi = a_o \Phi_{HF} + \sum_{i=1} a_i \Phi_i$$

Electron correlation approaches differ from one another in how they calculate the coefficients (a_i) for the additional determinants (the coefficient for the HF function (a_0) being determined by the normalization condition).

1.4.3 Second order Møller-Plesset perturbation method (MP2)

The Møller-Plesset method is one of the most often used methods for electron correlation in computational chemistry. Here first an unperturbed Hamiltonian operator is chosen to be the sum of the Fock operators for all electrons. The perturbation then becomes the exact potential operator of electron-electron interaction minus the average interaction already contained in the Fock operator. With this “fluctuation potential”, corrections to the Hartree-Fock energy are calculated. In second-order Møller-Plesset theory (MP2) corrections up to the square of the fluctuation potential are taken into account.[34]

The MP2 energy is conviniently evaluated from two-electron integrals over molecular orbitals (MOs) and the corresponding orbital energies, needing only those that involve the combination of two occupied and two virtual MOs. This means that in practical calculations for a system with a few hundred basis functions the MP2 energy can be calculated with a similar cost as the HF energy when additional tricks such as density-fitting and/or smart integral-presercening and orbital localisation techniques are applied. Since MP2 accounts for about 80-90% of the correlation energy it is the most economical method to include electron correlation (apart from the indirect treatment of electron correlation in the framework of DFT as discussed above)[35-42].

Chapter 2: Methodology

2.1 Procedure for the calculations

In order to know the geometrical parameters of the polymer and to get the first insights about the energy values, we will begin with calculating the pieces that compose this material: the pyrrole and the heptafluorotantalate(V). As a reasonable start, we looked up first for crystallographic data for each one of the components; and from there, we carried out DFT+D optimizations for these structures in gas phase using pyrrole-oligomers consisting of 1, 2 and 3 monomers . The next step consisted in modelling different configurations using the Avogadro[43] software and subsequent quantum chemical geometry optimization of them. Considering the form of the tripyrrole, further systems will be built. These systems will consist in the first place, in different configurations of two tripyrroles and one TaF_7^{2-} ion.

Then we will explore bigger structures, adding two more tripyrroles, leaving geometrical configurations with 4 trimers. Furthermore, we will try to establish structural motifs which could be found in the amorphous doped polypyrrole material. For example, it was tested how close two TaF_7^{2-} ions could be as well as how long must be an oligomer chain to hold them. Further calculations with 2, 4 and 6 chains will be carried out in order to study not only the ion-pyrrole interaction but also the interaction between chains. Starting from the converged structures, we will reoptimize each one of the aggregates with different charges, adding add up to one positive charge per chain, in order to calculate vertical and adiabatic ionisation potentials along with geometrical changes due to non covalent interactions, and from here, to establish how easy or hard it is for a system to oxidise one or more of its chains.

We will then add solvent molecules to the converged structures to see how the interactions with the solvent could change the geometry of each one of the systems; these calculations will be carried out submitting the structures to increasing numbers of randomly distributed solvent molecules, using water and acetonitrile for this purpose and doing further calculations on micro-solvated oxidised pyrrol-oligomer systems as well.

2.2 Technical details

In this section, we will specify the computational tools that were used to carry out the optimizations for the structures above described:

All quantum chemical calculations were undertaken with the TURBOMOLE program package[17,44-47] making use of dispersion-corrected density functional theory (DFT+D). We chose the Becke-Perdew (BP) exchange-correlation functional[48,49] in combination with a third-generation dispersion correction[50] and the triple-zeta valence quality basis set def2-TZVP[51] for all computations. For reasons of computational efficiency the resolution-of-the-identity (RI) approximation[52] will be employed in the determination of energies and energy gradients as required for geometry-optimization.

While all of the investigated systems were computed at the dispersion-corrected BP level of theory for some systems additionally DFT+D geometry optimizations employing the B97[53,54] functional were made. Furthermore, for the sake of checking accuracy second order Møller-Plesset (MP2) in the RI approximation[55] were undertaken for some of the aggregates. Here we used def2-TZVPP and def2-QZVPP orbital basis sets[56] along with the corresponding auxiliary basis[52,56] sets for the RI approximation. Whenever dimeric systems were treated with MP2, the counterpoise correction (CPC) procedure of Boys and Bernardi[57,58] was used during the geometry optimization, i.e., for both, energies and gradients (these calculations will be labelled as CPC MP2).

In order to calculate the total binding energy for aggregates with neutral oligopyrroles, the following formulae will be used:

$$E_{bind} = X * E(Py_n) + Y * E(TaF_7^{-2}) - E((TaF_7)_Y (Py_n)_X)^{-2Y}$$

Here $E(Py_n)$ is the energy of one oligopyrrole, “n” is the number of units of the oligopyrrole (n= 3 or 5), $E(TaF_7^{2-})$ is the energy of the heptafluorotantalate (V) ion, the last term corresponds to the energy of the aggregate, and finally, X and Y are the number of oligomers and TaF_7^{2-} ions respectively.

For the systems with solvent molecules the formula reads:

$$E_{bind} = X * E(Py_5) + Y * E(TaF_7^{-2}) + Z * E(S) - E((TaF_7)_Y (Py_5)_X)^{-2Y} S_Z$$

Where $E(Py_5)$ is the energy of one pentapyrrole conformer, $E(TaF_7^{2-})$ is the energy of the heptafluorotantalate (V) ion, S is a solvent molecule, the coefficients X,Y and Z correspond to the number of units which compose the aggregate, and the last term corresponds to the energy of the aggregate which has X pentapyrroles, Y heptafluorotantalates and Z solvent molecules. For the aggregates involving oxidised oligopyrroles Py_n^+ the above formulae were modified in the following way: the total charge now is $-2Y+Q$, where Q is the number of oxidised olygopyrroles, and $X*E(Py_n)$ becomes $(X-Q)*E(Py_n) + Q*E(Py_n^+)$.

It should be noted that in each case $E(Py_n)$ and $E(Py_n^+)$ refer to the energy of the most stable conformer, i.e., the alternating conformer (see below).

Chapter 3: Fundamental components

3.1 Heptafluorotantalate ion

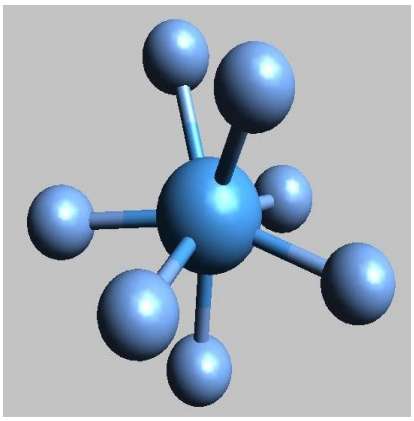

Figure **9**. BP+D structure of the heptafluorotantalate(V) ion (TaF_7^{2-}).

	Exp.[59]	BP86 + D3	B97 + D3	MP2-TZVPP	MP2-QZVPP
Ta-F1	1.976	2.016	2.016	1.984	1.986
Ta-F2	1.952	2.004	1.995	1.982	1.985
Ta-F3	1.965	1.996	2.003	1.969	1.986
Ta-F4	1.954	1.996	2.002	1.971	1.950
Ta-F5	1.937	2.002	1.996	1.984	1.985
Ta-F6	1.919	1.997	2.001	1.972	1.950
Ta-F7	1.953	1.996	1.999	1.969	1.986
Energy (Ha)		-756.832868	-756.488601	-755.352681	-755.603294

Table **1**. Ta-F distances in Å of the heptafluorotantalate(V) ion (TaF_7^{2-}) with different methods.

According to reference [59], the dopant TaF_7^{2-} has essentially a monocapped trigonal prism structure. However, the interaction of the fluorine ions distorts the whole structure from true C_{2v} symmetry, rather leading to an unsymmetrical strucure (C_1 point group). Crystallographic data[59] for K_2TaF_7 give an average Ta-F bond length of 1.951 Å , with two F atoms being significantly further away from Ta (1.965 and 1.976 Å, respectively), and two F atoms being significantly closer (1.937 and 1.919 Å, respectively). The neighbourhood to K^+ ions in the crystal is certainly an important contributing factor to the sizable differences of the bond lengths. This, of course, is not the case for *in vacuo* calculations of the TaF_7^{2-} ion, and indeed here we observe smaller intervals for the Ta-F

bond lengths: with DFT+D (with both functionals) they range from 1.995 to 2.016 Å, with an average value of 2.001 Å (Fig. **9** and Table **1**).

Though on average shorter, *i.e.*, 1.977 Å, MP2/def2-TZVPP geometry optimization yields a similar spread of the Ta-F distances, which vary from 1.969 to 1.984 Å. The MP2/def2-QZVPP geometry optimization, on the other hand, illustrates the sensitivity of the TaF_7^{2-} structure towards details of the theoretical treatment: though the average Ta-F distance with 1.975 Å is hardly changed by the change of the orbital basis set, respectively, the distance spread with 1.950 to 1.986 Å becomes significantly larger, and the geometry now resembles more closely that of a pentagonal bipyramid.
All in all, the heptafluorotantalate ion should perhaps best be considered as weakly structured concerning the positions of the fluorine atoms. Taking the MP2 results as benchmark for a free TaF_7^{2-} ion we note that BP+D at the BP+D3/def2-TZVP level overestimates the average Ta-F distance by nearly 0.03 Å.

3.2. Structures of Py_n with n=1,2,3

Comparing our calculated geometries for the pyrrole monomer (**10a**, cf. Fig. **10** and Table **2**) to the results of microwave spectroscopy[60] we observe the strongest disagreement for the NH bond, which is about 0.016 Å too long with BP+D, while it is better reproduced with MP2 . All other bonds deviate by less than 0.008 Å with BP+D and by even less than 0.004 Å with MP2, and also the computed bond angles agree very well with experiment, *i.e.*, within 0.2° for both, BP+D and MP2, proving the suitability of the used method.

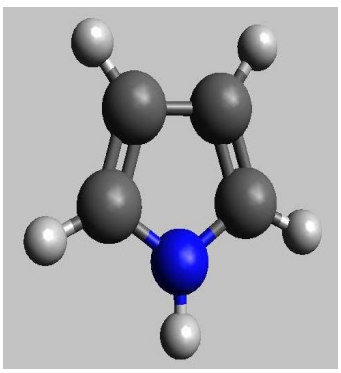

10a)

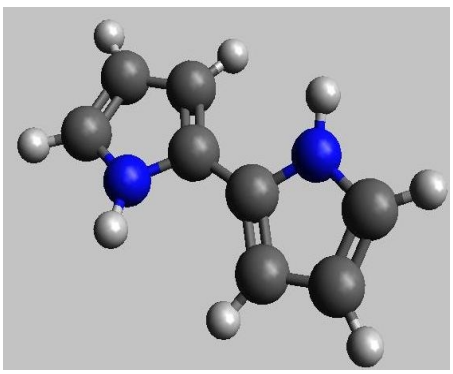

10b)

Figure **10.1**. BP+D structures of pyrrole and different oligopyrrole conformations.

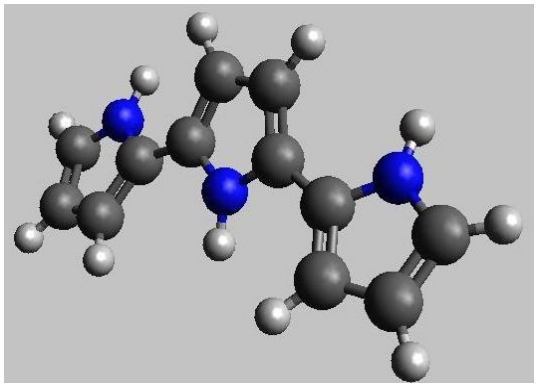
10c)

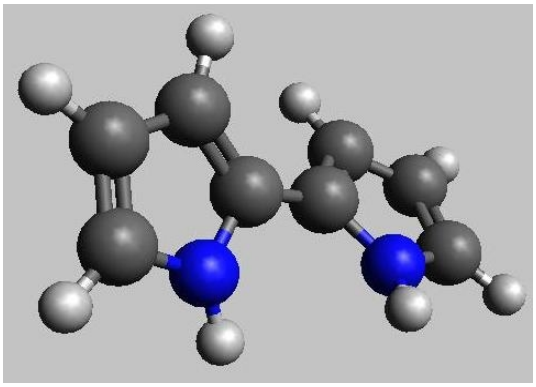
10d)

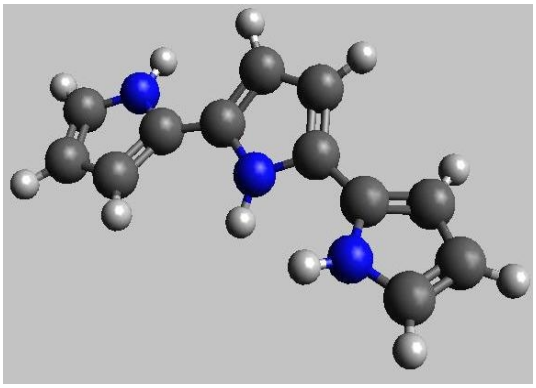
10e)

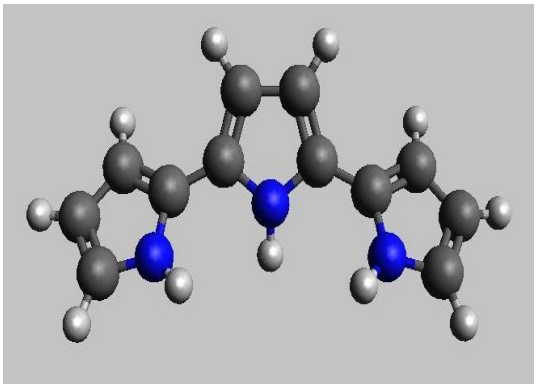
10f)

Figure **10.2**. BP+D structures of pyrrole and different oligopyrrole conformations.

	Exp.[60]	BP86 + D3	B97 + D3	MP2-TZVPP	MP2-QZVPP
N-H	0.996	1.012	1.007	1.004	1.003
C-N	1.370	1.377	1.377	1.368	1.366
C=C	1.382	1.383	1.382	1.382	1.380
C-C	1.417	1.425	1.425	1.416	1.414
C-H (1)	1.076	1.084	1.081	1.075	1.075
C-H (2)	1.077	1.085	1.082	1.076	1.075
Energy (Ha)		-210.266703	-210.095923	-209.737118	-209.801484

Table **2**. Bond distances in Å for the pyrrole monomer (**10a**) with different methods.

The most stable structure of dipyrrole can be called “alternating”, *i.e.*, an arrangement with the two NH bonds of the two monomeric units pointing in opposing directions (**10b**). As it is known for a long time[60] this conformation (also denoted as anti-gauche) is not fully planar: with BP+D we find a C=C-C=C torsion angle of 156.9° (taking a double bond of carbons from one pyrrole and the opposing pair in the immediately neighbouring monomer) with BP and of 161° with B97+D for the bond linking the two pyrrole subunits, while the double-zeta Hartree-Fock calculations of Kofranek *et al.*[61] gave 150.8°. With MP2 we find 146.0° and 147.5° with the triple- and quadruple-zeta basis sets, respectively. C=C-C=C torsion angles different from 180° are also found the for tripyrrole

(**10c**) and the larger oligo- and polypyrroles. Yet, “parallel” conformations of dipyrrole and tripyrrole with the NH bonds of all monomeric units pointing in the same direction are also possible: in the case of dipyrrol the parallel conformation (**10d**) lies only 8.1 kJ/mol for BP, 8.3 kJ/mol for B97 and 7.0 kJ/mol with MP2/def2-TZVPP and with MP2/def2-QZVPP above the alternating one. This conformation (also denoted as syn-gauche) was also predicted in the Hartree-Fock calculations of Kofranek *et al.*[61], with an an energy difference to the alternating conformation of 10.1 kJ/mol and a C=C-C=C torsion angle of about 45°. The torsion angles of 46.0° and 45.3° as obtained with MP2 and triple- and quadruple-zeta basis sets, respectively, agree very well with this, while with BP+D a smaller torsion angle of 33.0° was obtained.

	BP86 + D3	B97 + D3	MP2-TZVPP	MP2-QZVPP
Torsion angle 10b	156.9	161.0	146.0	147.5
Torsion angle 10c	159.0	163.0	148.7	150.1
Torsion angle 10d	33.0	31.3	46.0	45.3
Torsion angle 10e	29.7	27.5	40.4	39.9
Torsion angle 10f anti	158.6	161.2	148.9	148.9
Torsion angle 10f gauche	30.4	28.0	40.8	40.8
Isomerization energy 10b-d	8.1	8.3	7.0	7.0
Isomerization energy 10c-e	15.2	15.6	14	14
Isomerization energy 10c-f	6.8	7.1	6.0	6.1
Energy 10a	-210.266703	-210.095923	-209.737118	-209.801484
Energy 10b	-419.351331	-419.002892	-418.306227	-418.432571
Energy 10c	-628.436751	-627.910671	-626.876141	-627.064426
Energy 10d	-419.348257	-418.999740	-418.303574	-418.429921
Energy 10e	-628.434158	-627.907982	-626.870809	-627.059096
Energy 10f	-628.430968	-627.904744	-626.873850	-627.062106

Table **3**. Torsion angles for the studied pyrrole oligomers in degrees, and isomerization energies in kJ/mol. Total energies in Hartrees (Ha).

Summarizing the differences between the benchmark MP2 results and the BP+D3/def2-TZVP level results we note that the latter reproduce relative conformer stabilities within about 1 kJ/mol, while the strongest disagreement in geometrical parameters are found for the N-H distance, too long by about 0.02 Å, and the C=C-C=C torsion angles between pyrrole subunits, which tend to be too close to planarity by about 10°.

In the case of tripyrrole a partially parallel conformation with one of the terminal pyrrole units pointing into the opposing direction of the other two (**10e**) lies 6.8 kJ/mol (6.0 kJ/mol

with MP2/def2-TZVPP and 6.1 kJ/mol with MP2/def2-QZVPP) above the alternating conformation according to BP+D. Note that this changes the arrangement of the pyrrole dipoles from ↓↑↓ to ↑↑↓ , *i.e.* a repulsive arrangement of the terminal dipoles is replaced with an attractive arrangement, explaining why it costs less energy to switch a terminal pyrrole in Py_3 than in Py_2. Switching the alignment of the central pyrrole unit from ↓↑↓ to ↓↓↓ (**10f**) costs 15.2 kJ/mol (14.0 kJ/mol with MP2/def2-TZVPP and MP2/def2-QZVPP).

In a particular "parallel" arrangement (↑↑) of two or more neighbouring pyrrole units may lead to significant deviations from planarity of the pyrrole subunits themselves: presumably for steric reasons and electrostatic repulsion between the positively charged hydrogen atoms the NH bonds are no longer located within the ring plane. For example, the C=C-N-H torsion angle of the central pyrrole unit in the fully parallel arrangement **10f** of Py_3 is 156.4°, and the corresponding torsion angles on both terminal pyrrole subunits are 168.5° (162.8° and 171.8°, respectively, with MP2/def2-TZVPP and MP2/def2-QZVPP). Note that also fully "alternating" (↑↓) conformers of Py_n are non-planar – however, here rather due to the slight torsion around the C-C bonds linking neighbouring Pyrrole monomers, while each monomer itself is nearly planar. As already observed for Py_2, BP+D also in case of the alternating configuration of Py_3 yields the C=C-C=C torsion angle between neighbouring pyrrole subunits about 10° closer to planarity than MP2 (159.1° with BP+D, 148.7° and 150.1° with MP2 using triple- and quadruple-zeta basis sets, respectively).

The case of pentapyrrole (exclusively calculated with BP+D) makes it very obvious that the notion of "parallel" pyrrole units is somewhat oversimplified: switching of the central pyrrole unit (from ↓↑↓↑↓ to ↓↑↑↑↓) leads to a structure which clearly can no longer be considered a linear chain of pyrrole units but rather becomes a bent chain (an effect, which is also noticeable in Py_3). This is accompanied by a destabilisation of 11.2 kJ/mol, *i.e.*, 4 kJ/mol less destabilisation than switching of the central pyrrole in Py_3 since unfavourable dipole-dipole interactions between second next neighbours are replaced with favourable interactions. A fully "parallel" arrangement (↓↓↓↓↓) of all pyrrole units in Py_5 lies 28.7 kJ/mol above the alternating conformation, and, in fact, it has a hemicircular chain shape. Though one could argue that any non-alternating arrangement of pyrrole

units within a polypyrrole material is structurally and energetically unfavourable, an interaction with TaF_7^{2-} ions might change the situation, as we will see in the following.

3.3.Structures and binding energies for $[TaF_7(Py_n)_x]^{2-}$ with n=1,2,3 and x=1,2,4

To acquire an initial understanding of the incorporation of TaF_7^{2-} ions into polypyrrole we started with the smallest possible building blocks, *i.e.*, one TaF_7^{2-} ion and one mono-, di-, or tripyrrole. Not unexpectedly, the most important contact between TaF_7^{2-} and mono- or oligopyrrole is due to a hydrogen bridge between a NH group of a pyrrole unit and a fluorine atom from TaF_7^{-2}. In case of the monomer Py_1 this is assisted by an „auxiliary“ contact between a CH-group in α-position and another fluorine atom of TaF_7^{2-} (**11a**), leading to a total binding energy E_{bind} of 143.4 kJ/mol at the BP86+D3 level (please note that we define E_{bind} using its conventional sign convention, *i.e.*, as the energy *required* to dissociate the interacting system into the most stable conformations of its components, the latter for the oligopyrroles always corresponding to fully *alternating* conformations).

This is a fairly strong binding, nearly seven times stronger than that of the hydrogen bridge between two water molecules[62] and only about three times weaker than a covalent C-C single bond[63]. This strong binding is satisfactorily confirmed by counterpoise-corrected geometry optimizations at the second-order Moller-Plesset (MP2) level of theory: with the def2-TZVPP basis set the counterpoise-corrected binding energy amounts to 127.1 kJ/mol, while with the def2-QZVPP basis set 129.3 kJ/mol were obtained, *i.e*. corresponding to about 10% deviation from BP+D (*cf.* Table **4**). Note that no counterpoise correction was used during the geometry optimizations at the BP+D/def2-TZVP level since for DFT methods the basis set superposition error is expected to be much smaller than for conventional electron correlation treatments such as MP2.

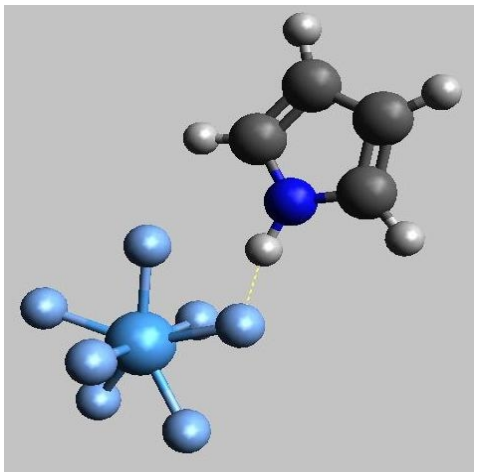

11a)

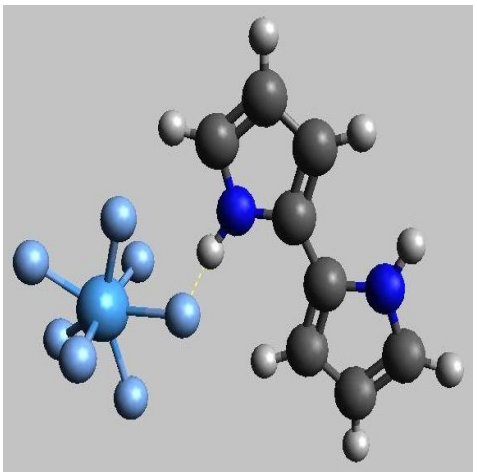

11b)

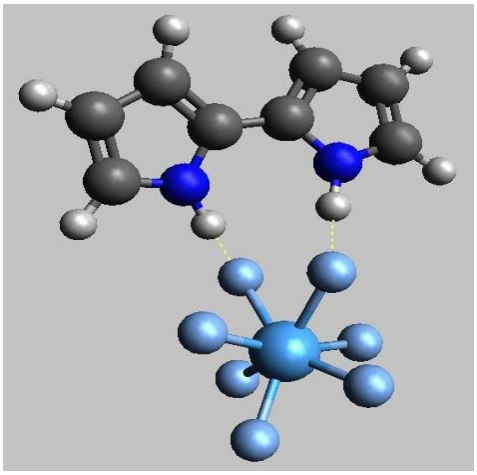

11c)

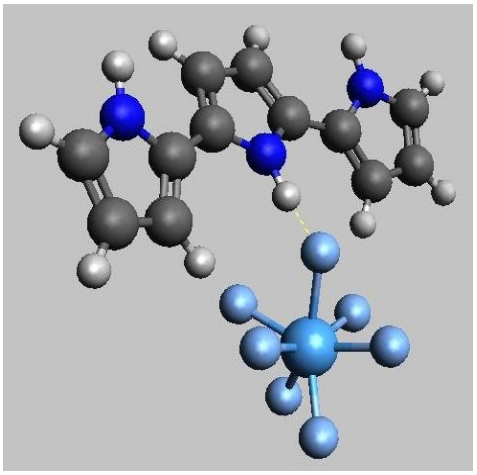

11d)

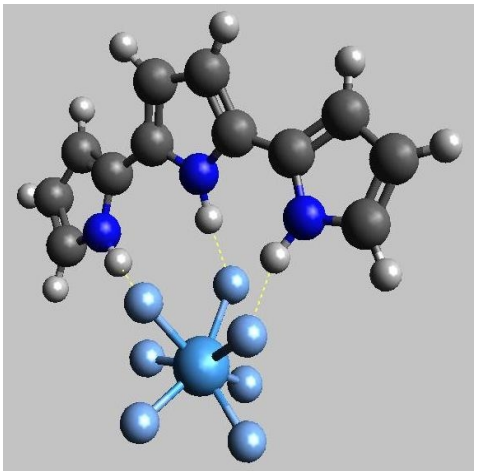

11e)

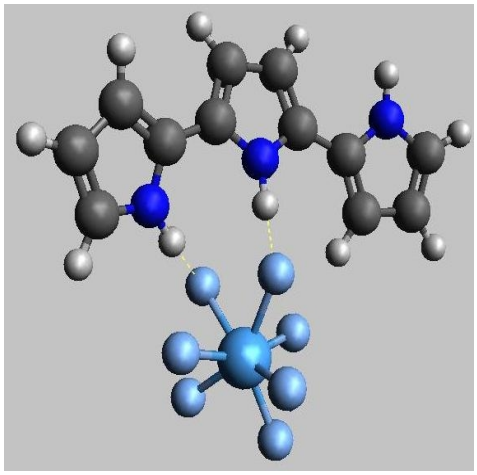

11f)

Figure **11.1**. BP+D structures of pyrrole (a) and different oligopyrrole dimer (b,c) and trimer (d,e,f) conformers interacting with one TaF_7^{2-} ion.

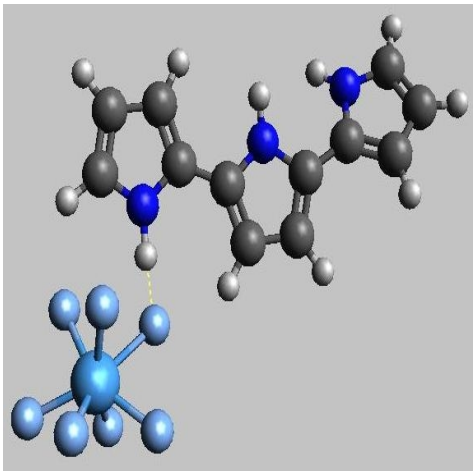

11g)

Figure **11.2**. BP+D structure of a pyrrole trimer interacting with one TaF_7^{2-} ion.

In case of the complex of alternating Py_2 with TaF_7^{2-} (**11b**), an auxiliary contact between the first fluorine atom and a CH group in β position of the second pyrrole unit is observed in addition to the contacts already present in $[TaF_7(Py_1)_1]^{2-}$. Switching of the second pyrrole around the C-C-bond linking the two monomers enables a second NH...F hydrogen bridge (10c), which is accompanied by a dramatic change of the total BP+D/def2-TZVP binding energy E_{bind} from 163.5 kJ/mol in the alternating to 235.3 kJ/mol in the parallel conformation. The corresponding values at the CPC MP2/def2-QZVPP level are about 10-12% lower (*cf.* Table **4**).

In case of the alternating conformation ↓↑↓ of Py_3 interacting with T^{2-} one observes a NH...F contact between the central pyrrole unit and two CH...F contacts of the adjacent pyrrole units with two different F atoms of TaF_7^{2-} in a „pocket“ type arrangement (**11d**), with a binding energy of 174.8 kJ/mol at the BP+D level. Here another confomer with a fully parallel Py_3 (↓↓↓) leading to a total of three NH..F contacts (**11e**) could be obtained as well, characterized by what may be regarded as a switching of the two outer pyrrole units of Py_3 around the pyrrole-linking C-C bonds. As shown above, in free Py_3 this switching (here more appropriately regarded as switching of the central pyrrole unit) costs about 15.2 kJ/mol. Yet, upon interaction with the TaF_7^{2-} ion two new NH...F hydrogen bridges are established in place of the two weaker CH...F contacts, resulting in a dramatic increase of the magnitude of the binding energy to 299.4 kJ/mol at the BP+D level.

Not surprisingly, the binding energy of the remaining arrangement ↑↑↓ of $[TaF_7(Py_3)_1]^{2-}$ (**11f**) with 245.0 kJ/mol is in between those of the other conformations of $[TaF_7(Py_3)_1]^{2-}$

when the TaF_7^{2-} ion faces the two parallel Pyrrole units, resulting in two NH...F hydrogen bridges. On the other hand, when the TaF_7^{2-} ion faces the two alternating Pyrrole units essentially the same binding mode as in the interaction of TaF_7^{2-} with alternating Py_2 is observed (one NH...F hydrogen bridge, one CH...F contact to the same F atom, **10g**), leading to a similar binding energy of 177.9 kJ/mol. The corresponding binding energies at the CPC MP2/def2-TZVPP and CPC MP2/def2-QZVPP levels of theory as collected in Table 1 are about 10 % smaller with exception of **10d** where the deviation becomes somewhat larger (16%).

Binding energies (kJ/mol)	B86+D3/ def2-TZVP	MP2/ def2-TZVPP	MP2/ def2-QZVPP
11a	143.4	127.1	129.3
11b	163.5	138.2	143.2
11c	227.2	202.4	205.4
11d	174.8	142.0	146.9
11e	299.4	269.5	273.3
11f	245.0	212.5	217.2
11g	177.9	148.8	153.2
Energies (Ha)			
11a	-967.1541910472	-965.143531	-965.143530
11b	-1176.246480209	-1173.718767	-1173.718766
11c	-1176.270748111	-1173.744426	-1173.744421
11d	-1385.336184315	-1382.292515	-1382.292515
11e	-1385.383646771	-1382.342618	-1382.342615
11f	-1385.362936056	-1382.320165	-1382.320165
11g	-1385.337378459	-1382.292964	-1382.292964

Table **4**. Calculated binding and total energies for the structures shown in Figure **11**. All binding energies were determined with respect to the alternating conformers of Py_2 and Py_3, respectively.

Basically the same contact modes are also observed when TaF_7^{2-} interacts with *two* mono-, di- and tripyrroles. For mono- , $[TaF_7(Py_1)_2]^{2-}$, and dipyrrole, $[TaF_7(Py_2)_2]^{2-}$, only “coplanar” conformations with the Py_1 and Py_2 at opposing sides of TaF_7^{2-}, and, in consequence, unfavourable dipole-dipole interactions between the pyrroles, were investigated: not unsurprisingly, here the binding energies (now referring to the dissociation of, e.g., $[TaF_7(Py_2)_2]^{2-}$ into TaF_7^{2-} + 2 Py_2) were somewhat smaller than twice the E_{bind} of $[TaF_7(Py_1)_1]^{2-}$ and $[TaF_7(Py_2)_1]^{2-}$, *i.e.*, 265.2 and 295.1 kJ/mol, respectively. Note that here and in the following all binding energies were obtained with BP+D/def2-TZVP.

In the more relevant case of $[TaF_7(Py_3)_2]^{2-}$ several conformers were studied (*cf.* Fig. **12**). Once again, when two alternating Py_3 are arranged at opposing sides of the TaF_7^{2-} ion as in structure **12a** a binding energy of somewhat less than twice the E_{bind} for a TaF_7^{2-} ion interacting with a single alternating Py_3 is obtained, *i.e.*, 305.4 kJ/mol. Rotating one of the Py_3 by 90° as in **12b** has hardly any influence, yielding an E_{bind} of 303.1 kJ/mol. Ignoring interactions between the fairly distant Py_3 chains one thus may infer an average BP+D "embedding energy" of roughly 150 kJ/mol per pocket when two chains surround TaF_7^{2-}, *i.e.*, about 15% less than when only one chain is present. The binding energy increases to 311.6 kJ/mol when the two Py_3 are more or less on the same side of the TaF_7^{2-} ion (**12c**), where the "angled" arrangement of the two Py_3 allows the establishment of a CH...π contact between them. Interestingly, an even higher binding energy of 329.7 kJ/mol is obtained when the TaF_7^{2-} ion links to alternating Py_3 chains in a "non-pocket-like" manner (**12d**), presumably due to a less unfavourable arrangement of the Py unit dipoles in the two Py_3 chains and, on average, larger distances between them. A dramatic increase in the binding energy to 518.1 kJ/mol is observed when each of the two Py_3 chains assumes a parallel (↓↓↓)conformation, allowing for a total of six NH...F hydrogen bridges (**12e**).

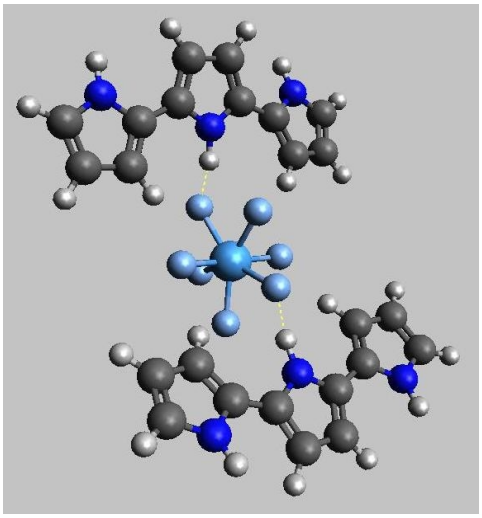

12a)

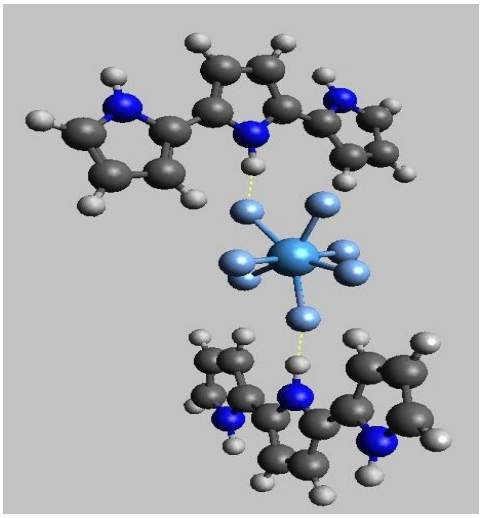

12b)

Figure **12.1**. BP+D structures of two tripyrroles interacting with one TaF_7^{2-} ion.

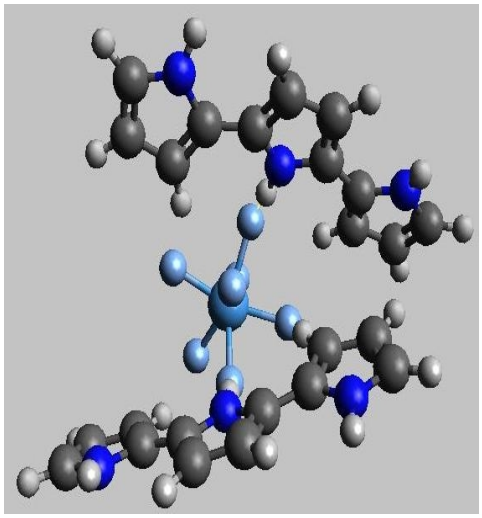

12c)

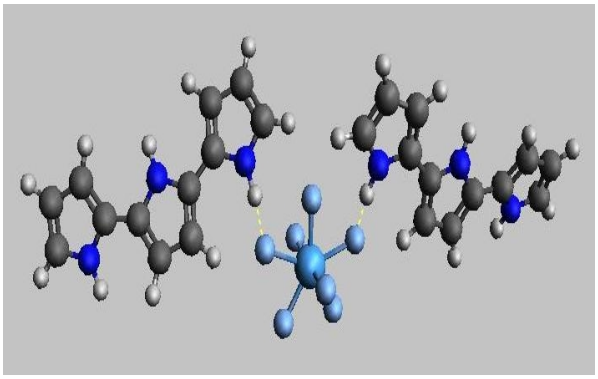

12d)

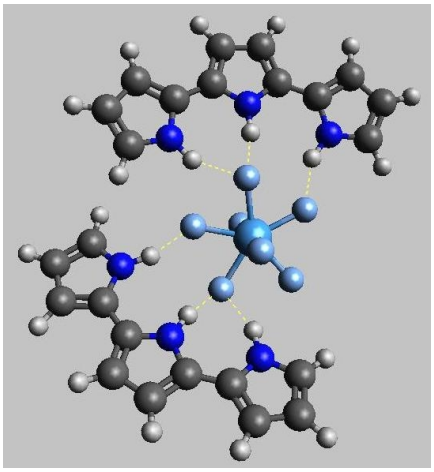

12e)

Figure **12.2.** BP+D structures of two tripyrroles interacting with one TaF_7^{2-} ion.

In view of the geometrical parameters to be discussed for larger systems presented in the following we define the structure observed for the alternating conformation ↓↑↓ of Py_3 interacting with TaF_7^{2-} as an "ideal pocket" conformation. It is characterized by a NH...F distance of 1.49 Å and two CH..F distances of 2.11 Å, respectively, on the BP+D/def2-TZVP level of theory. Adding a second tripyrrole in an antiparallel conformation to obtain structure **12a** of $TaF_7^{2-}(Py_3)_2$ changes the NH..F distance to 1.59 Å, while the CH..F distances become 2.33 Å and 2.26 Å, respectively. Thus all distances increase by about 0.1 Å for NH...F and in average by 0.2 Å for CH...F with respect to the "ideal pocket" conformation of $TaF_7^{2-}(Py_3)_1$, as to be expected for reasons of the dipole-dipole repulsion between the two Py_3 chains.

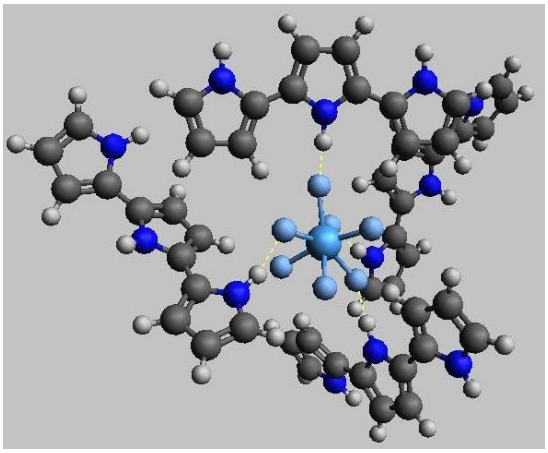

13a)

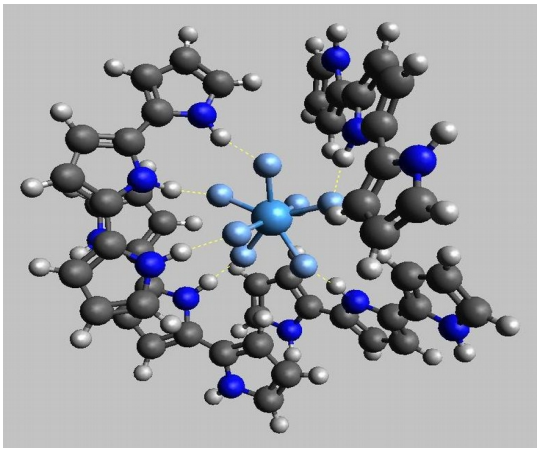

13c)

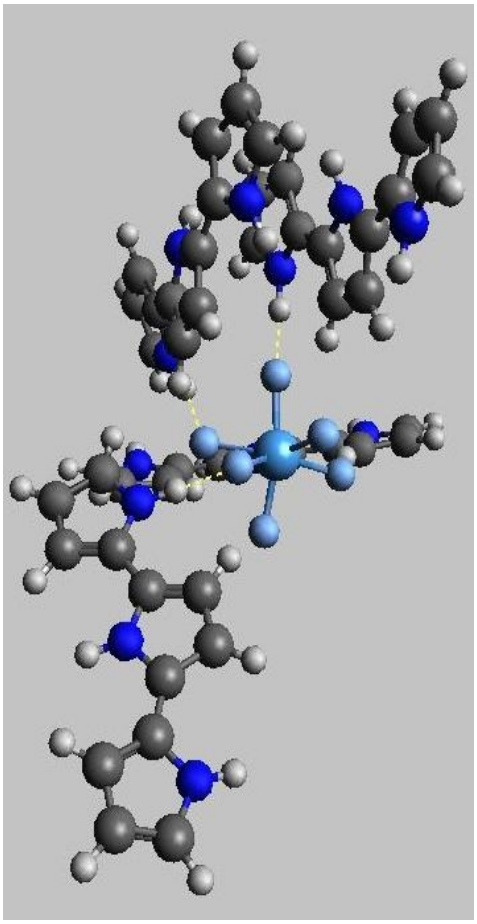

13b)

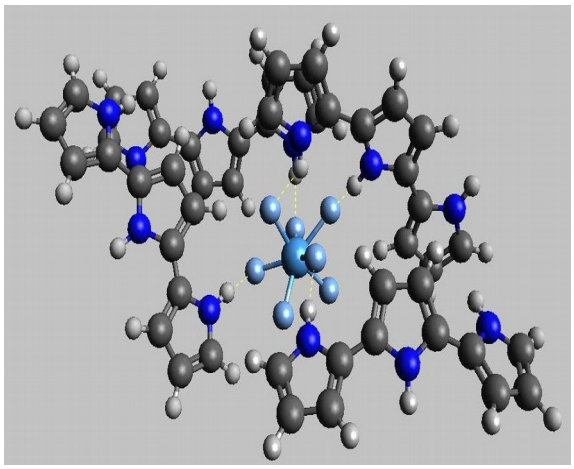

13d)

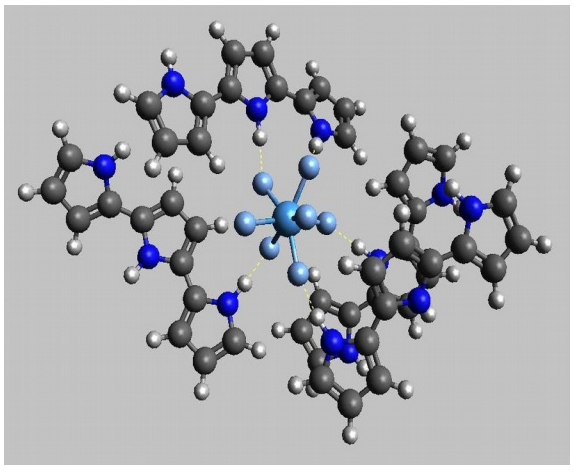

13e)

Figure **13.1**. BP+D structures of four tripyrroles interacting with one TaF_7^{2-}.

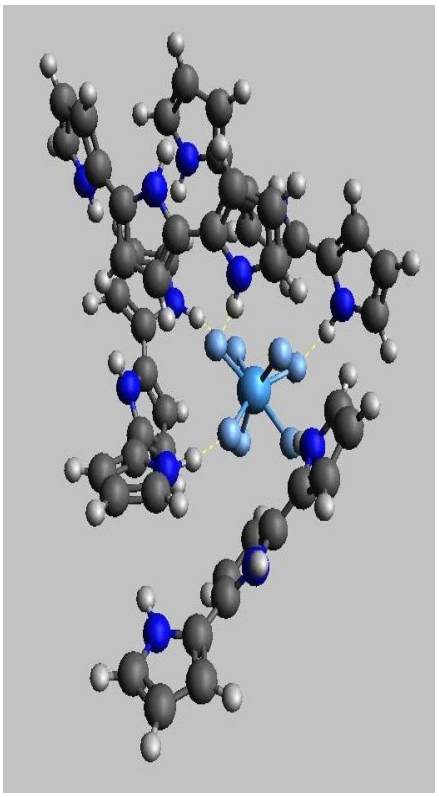

13f)

Figure **13.2**. BP+D structures of four tripyrroles interacting with one TaF_7^{2-}.

System	Energy (Ha)	Binding Energy (kJ/mol)
13a	-3270.796109	567.73
13b	-3270.809843	603.79
13c	-3270.830347	657.63
13d	-3270.830938	659.18
13e	-3270.837864	677.36
13f	-3270.837880	677.40

Table **5**. Energetic data of the presented trimer structures of four tripyrrole onteractions with one TaF_7^{2-}.

Next we carried out another set of calculations, considering the fact that the negative ion is located inside the polypyrrole matrix; this time embedding the heptafluorotantalate ion into 4 alternating tripyrroles (↓↑↓) in full pockets (NH...F binding with the central pyrrole) in the starting structures contructed with Avogadro. But after many attempts, none of the conformers shown in Fig. 13 obtained after the DFT+D structure optimization fitted to this objective. Beginning with structure **13a**, all 4 tripyrroles retained their alternating conformation (↓↑↓). Yet, only two of them remained in full pocket configuration while the others formed only half-filled pockets, probably due to the relatively high number of oligomers concentrated in the same space. The resulting binding energy of 567.7 kJ/mol

is the lowest among all $[TaF_7(Py_3)_4]^{2-}$ conformers. For structure **13b**, with 4 alternating (↓↑↓) tripyrroles as well, the anion sits in three half pockets and a full pocket (in the back). On the other hand, here we have probably an additional NH-π interaction between two of the oligomers, resulting in a binding energy of 603.8 kJ/mol. In **13c** there are one fully paralell (↓↓↓) and three alternating (↓↑↓) oligomers. The former displays 3 NH...F hydrogen bonds to the central ion, while the rest of them adopt a normal full pocket (only the central pyrrole binding to the ion with an NH...F bridge) configuration, resulting in a total number of 6 NH...F hydrogen bridges. Correspondingly, the binding energy with 657.6 kJ/mol is higher than in **13a** and **13b**, where only 4 NH...F bonds exist. Interestingly, **13d** has a very similar binding energy (659.2 kJ/mol). Here, one Py_3 adopts a semi paralell (↑↓↓) conformation allowing for 2 NH...F bonds. The remaining 3 alternating (↓↑↓) Py_3 adopt a half pocket configuration, resulting in a overall 5 hydrogen bonds.

As in the case of **13d** also **13e** shows one semi parallel (↑↓↓) and 3 alternating (↓↑↓) Py_3 conformations, with the semi parallel establishing two NH...F bonds. But now only two alternating oligomers form half pockets, while the third one forms a full pocket. Correspondingly, the binding energy of **13e** is 18 kJ/mol larger than that of **13d**. Finally, in **13f** one observes 4 alternating (↓↑↓) Py_3. While 3 of them bind to TaF_7^{2-} in half pocket arrangements, the remaining oligomer is strongly twisted, binding to TaF_7^{2-} with the two outermost pyrrole units through NH...F bonds while switching the central pyrrole out of plane. This results in a total number of 5 NH...F bonds and a binding energy which is virtually identical to that of **13e**, despite the large structural differences.

Chapter 4: Complex Aggregates

4.1 Structures and binding energies for $[(TaF_7)_2(Py_5)_y]^{2x-}$ with x=2,3 and y = 1,2

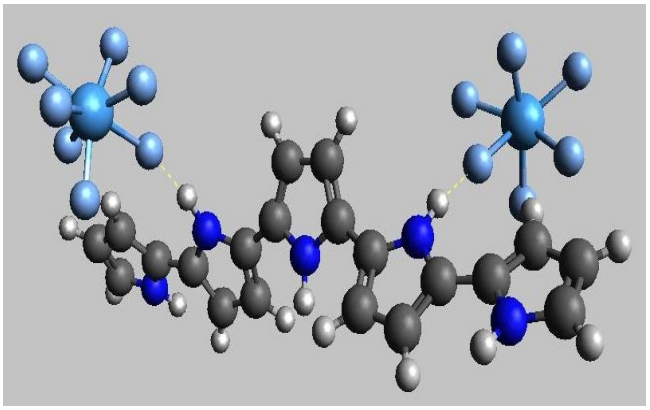

14a)

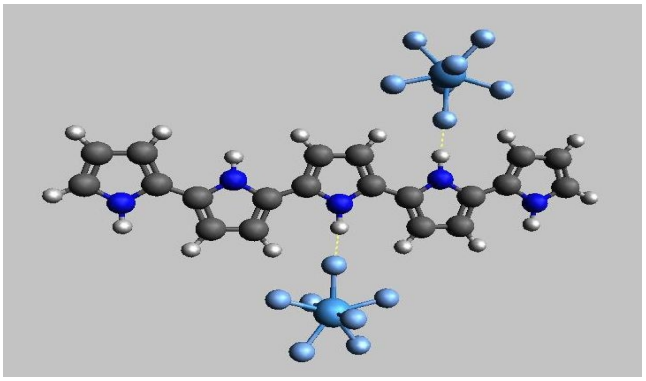

14b)

Figure **14**. BP+D structures of one pentapyrrole interacting with two TaF_7^{2-} ions.

Evidently, there is a strong Coulomb repulsion between two twofold negatively charged heptafluorotantalate ions. Thus, the question under which conditions the binding of heptafluorotantalate to polypyrrole can overcome this repulsion is most interesting for the capacity of polypyrrole to store the anions. The smallest oligopyrrole, which could accommodate two neighbouring heptafluorotantalate ions in two neighbouring binding pockets is pentapyrrole. Based on the N...N and H...H distances of 7.14 and 7.07 Å respectively, as found between the second and fourth pyrrole subunits in the fully alternating conformation of Py_5 we infer an “ideal pocket-pocket distance” of 7.1 Å. Two twofold negatively charged ions (spherical, or nearly so) in this distance have a huge Coulomb repulsion of 783 kJ/mol, whereas the energy of binding of each TaF_7^{2-} in its pocket is expected to amount to only about 150-170 kJ/mol (*vide supra*). Nevertheless, we investigated the capacity of pentapyrrole to bind two TaF_7^{2-} ions (*cf.* Fig. **14**).

Accordingly, we first put one ion in each of the two neighbouring pockets on the same side of a planar pentapyrrole: after geometry optimization, the TaF_7^{2-} surprisingly ions remained in these pockets. Yet the pentapyrrole chain became strongly twisted in an attempt to lower Coulomb repulsion between the TaF_7^{2-} anions through increasing their distance, which in the final geometry was found to be 13.0 Å between the Ta atoms (**14a**), yielding a strongly reduced Coulomb repulsion of 428.2 kJ/mol between the TaF_7^{2-} ions. We nevertheless get a *negative* binding energy of -197.7 kJ/mol for the resulting structure **14a**, showing that it is only a metastable system. Placing the TaF_7^{2-} ions in two pockets on opposing sides of the chain, leads to another metastable structure (**14b**) in which the pentapyrrole chain remains approximately planar, with a somewhat smaller Ta...Ta distance of 11.4 Å corresponding to an approximate TaF_7^{2-}...TaF_7^{2-} repulsion of 486.2 kJ/mol. Despite the slightly smaller inter-ion distance, **14b** with a binding energy of -182.8 kJ/mol is a little more stable than **14a**, This is probably due to better screening of the inter-ion repulsion, thanks to the Py_5 chain lying between the ions in **14b** combined with the energetic cost of twisting the chain in **14a,** which we calculated to amount to 49.8 kJ/mol, through comparison of the energy (Ha) of Py_5 in the geometry of **14a** with that of the optimized alternating structure of Py_5. From the difference of the inter-ion repulsion in **14b** and the total aggregate binding energy, one obtains an average energy of about 152 kJ/mol for “embedding” of each of the TaF_7^{2-} ions into one oligopyrrole pocket. Repeating the same calculation for **14a**, and taking the energetic cost of the chain twisting in this case into account, we arrive at an average energy of 140 kJ/mol for embedding each TaF_7^{2-} in a pocket . One should note that here these pockets are fairly strongly bent and thus far from “ideal”. Combining the binding motifs of **14a** and **14b**, *i.e.*, placing two TaF_7^{2-} ions in neighbouring pockets on the same side of the chain and a further TaF_7^{2-} ion on the opposing side, did not yield a stable structure: one of the TaF_7^{2-} ions unhitched from the chain during geometry optimization.

We then placed two TaF_7^{2-} ions in between two pentapyrrole chains, arranged in such a way that the TaF_7^{2-} ions sit in neighbouring pockets of each chain: this structure after geometry optimization turned out to be stable and to retain approximate planarity of both pentapyrrole chains. However, the two chains do not remain in the same plane (cf. **15a** in Fig. 15). The Ta...Ta distance in this structure is only 9.20 Å, meaning that the approximate Coulomb repulsion between the anions amounts to 604.1 kJ/mol. The total

binding energy with respect to dissociation into two TaF_7^{2-} ions and two alternating Py_5 chains amounts to 47.0 kJ/mol, *i.e.*, **15a** is a weakly stable aggregate. Making the simplifying assumption that its stabilisation is entirely due to the energy of embedding of the two TaF_7^{2-} ions into four pockets of the pentapyrrole chains, we get an average embedding energy of about 160 kJ/mol. To highlight the effect of ion distance, we optimized another structure (**15b**), changing the location of the TaF_7^{2-} ions from two full pockets in both chains to one pocket and a half pocket in both chains. Geometry optimization yielded that the TaF_7^{2-} ions roughly retained their position in one of the chains but occupy two half pockets in the other. The increase of more than 3 Å of the inter-ion distance (12.4 Å) clearly helped to stabilise the aggregate, increasing the binding energy to 137.5 kJ/mol. In the configuration **15c**, the two TaF_7^{2-} ions occupy "half-pockets" only (full pockets would be possible in heptapyrrole chains). The pentapyrrole chains are nearly coplanar in this structure (the N...Ta...N angle around the central TaF_7^{2-} ion being 85°). The structure is characterized by a positive binding energy of 282.8 kJ/mol and a Ta...Ta distance of 17.9 Å.

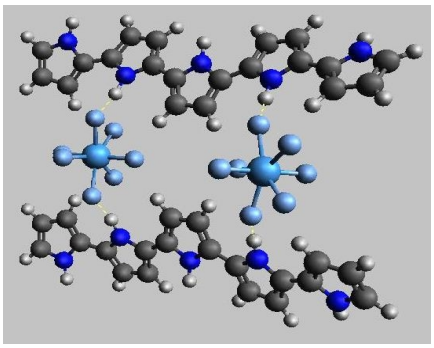

15a)

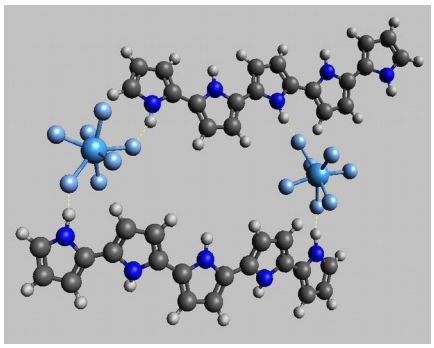

15b)

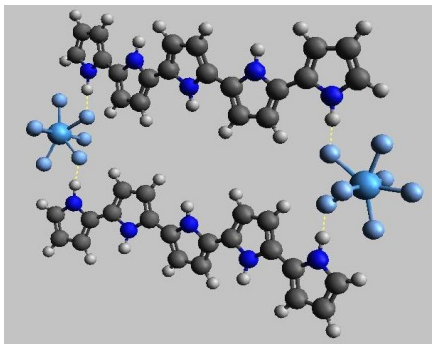

15c)

Figure **15**. Three BP+D configurations of two chains of pentapyrrole holding two TaF_7^{2-} ions.

Surprisingly, we have found that two pentapyrrole chains are even able to accommodate three TaF_7^{2-} ions: a corresponding geometry optimized structure with a strongly negative binding energy of -546.1 kJ/mol is shown in Fig. **16**. In this metastable aggregate the central TaF_7^{2-} ion displays distances from the other two TaF_7^{2-} ions of 11.1 and 11.2 Å, respectively.

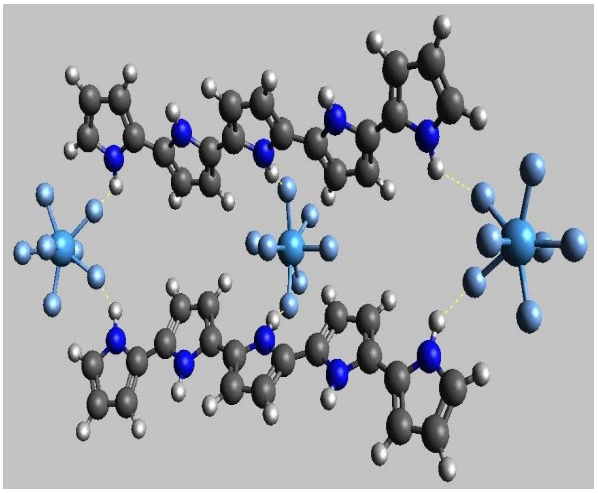

16a)

Figure **16**. BP+D structure of two chains of pentapyrrole holding three TaF_7^{2-} ions.

4.2 Structures and binding energies for $[(TaF_7)_2(Py_5)_x]^{4-}$ with x=4,5,6

While in the previous section we investigated the question of how many TaF_7^{2-} ions can be stabilised by one or two pentapyrrole chains, here we turn the question around and ask how many pentapyrrole chains can surround two TaF_7^{2-} ions, i.e., the minimum number of ions where each pentapyrrole chain has a chance to stay approximately planar. We started with 4 different conformers with four pentapyrrole chains (Fig. **17**), placing the TaF_7^{2-} ions in some of the different pocket and half-pocket arrangements as observed above. From the resulting optimized structures one notes a π-stacking tendency of the pentapyrrole chains, a phenomenon observed in many structures containing aromatic systems[67-69] , which can be ascribed to attractive dispersion forces between the π systems of the aromatic rings (*cf.* Fig. **17**).

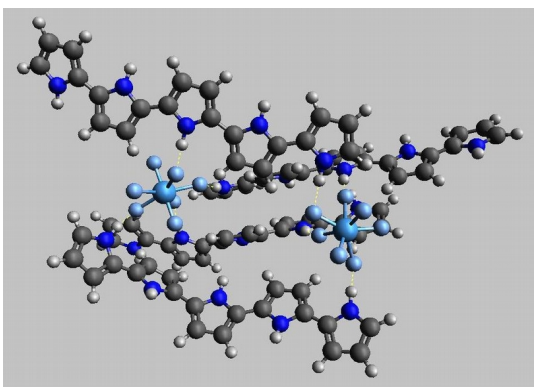

17a)

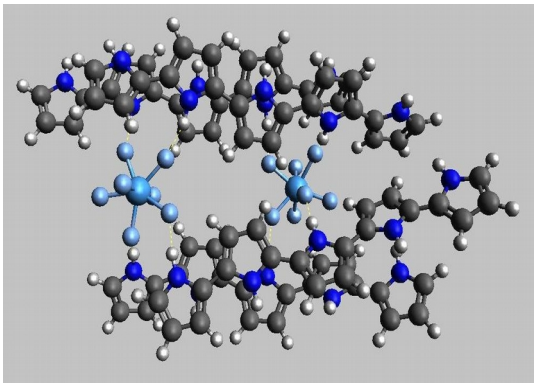

17b)

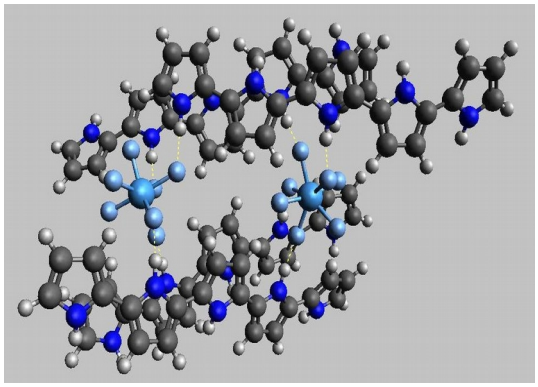

17c)

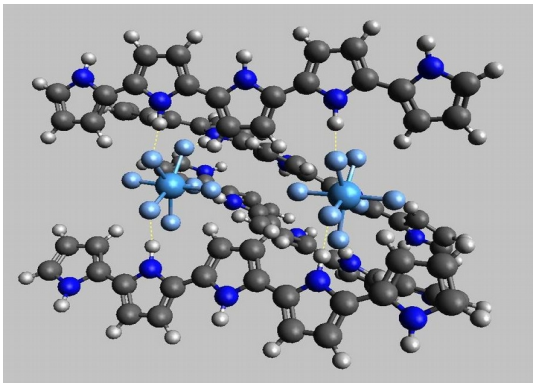

17d)

Figure **17**. Different BP+D configurations of four chains of pentapyrrole holding two TaF_7^{2-} ions.

The structure **17a** shows a non organized distribution of the oligomers, with the two at the front of the figure in a slightly twisted configuration, while the two at the back are almost parallel due to π-stacking. The structures **17b** and **17c** resemble each other, organizing themselves in parallel pairs through π-π interactions. The last one (**17d**) resembles structure **17a** whith only two stacked chains. Their binding energies amount 630.6 (**17a**) , 689.3 (**17b**) , 654.3 (**17c**) and 597.7 (**17d**) kJ/mol respectively. Considering also the distances between the two tantalate ions which are 10.0 (**17a**), 8.9 (**17b**), 8.6 (**17c**) and 7.7 (**17d**) Å respectively, after sustraction of the Coulomb interaction between the anions we obtained the average energy data for pocket embedding as follows: 148 (**17a**), 164 (**17b**), 163 (**17c**), and 165 (**17d**) kJ/mol where it was asumed that eight pockets are occupied, irrespective of “full” or “half occupation. This is in remarkable agreement with the average embedding energies found so far: clearly, our estimates of average “embedding” energies are grossly simplifying in implicitly including all attractive and repulsive interaction contributions between the oligopyrrole chains such as π-stacking and dipole-dipole interactions, and also all energetic costs of chain deformations. Apparently, these contributions cancel to some extent.

We then added two further pentapyrrole chains. However, geometry optimizations of the starting structures led to aggregates where only five pentapyrrole chains were hosting the TaF_7^{2-} ions in their pockets while the sixth chain unhitched. It thus appears that two TaF_7^{2-} ions can stabilise at most five pentapyrrole chains around them. We found three different conformers with this composition: a first one, in which a group consisting of two stacked pentapyrroles and another group consisting of three pentapyrrole chains leave the TaF_7^{2-} ions partially exposed in a large and a small groove (**18a**), a second arrangement where four Py_5 chains are π-stacked and the fifth chain is an unstacked solitary chain (**18b**), and a third structure where two different stacks, each composed of two chains, and an unstacked solitary chain surround the TaF_7^{2-} ions (**18c**). All of these conformers show a tendency of the pentapyrrole stacks to somewhat helically wind around the TaF_7^{2-} ions, and they all are stable against dissociation into their components (5 Py_5 + 2 TaF_7^{2-}), with binding energies of 904.8 (**18a**), 875.4 (**18b**), and 855.5 kJ/mol (**18c**), respectively. The Ta...Ta distances amount to 8.8 (**18a**), 7.6 (**18b**), and 7.7 Å (**18c**), respectively, yielding inter-ion Coulomb repulsion energies of 631.5 , 731.2 , and 721.7 kJ/mol. Taking these into account and considering each TaF_7^{2-} as embedded in five oligopyrrole pockets we obtain average embedding energies of 154 (**18a**), 161 (**18b**), and 158 kJ/mol (**18c**), respectively.

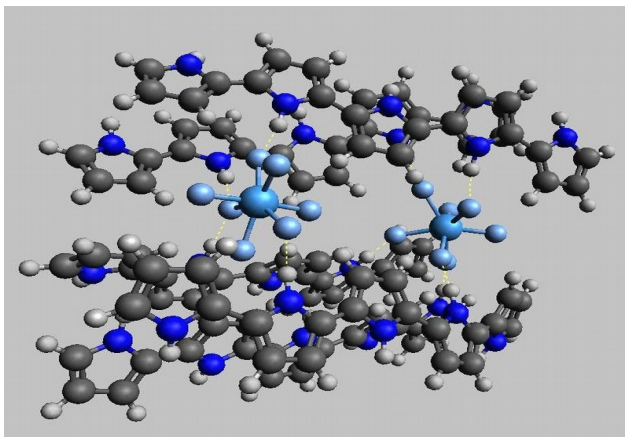

18a)

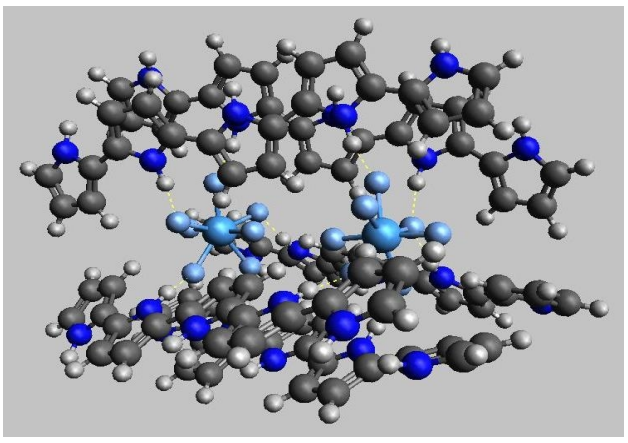

18b)

Figure **18.1**. BP+D structures of five chains of pentapyrrole holding two TaF_7^{2-} ions.

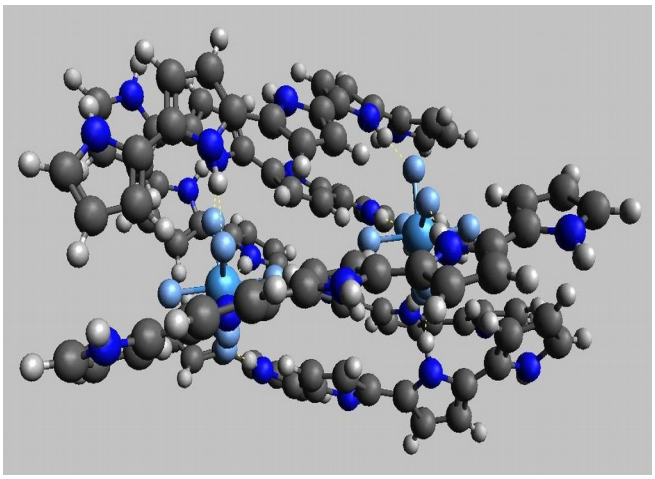

18c)

Figure **18.2**. BP+D structures of five chains of pentapyrrole holding two TaF_7^{2-} ions.

4.3 Structures and binding energies for $[(TaF_7)_3(Py_7)_x]^{6-}$ with x=2,5

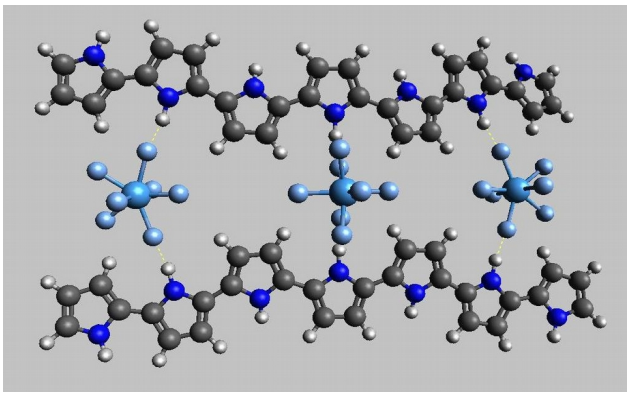

(a)

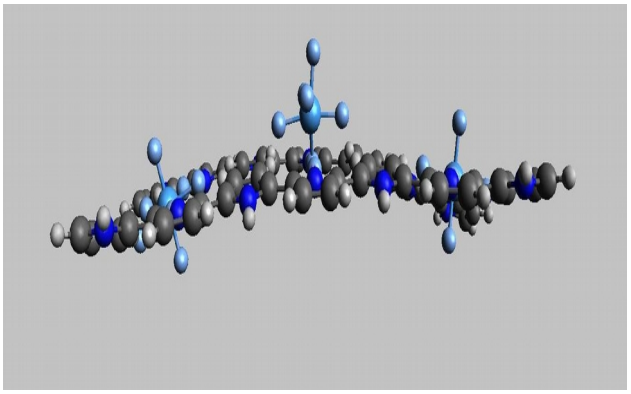

(b)

Figure **19**. BP+D structure of two chains of heptapyrrole holding tree T^{2-} ions. View from the top (a) and from the side (b).

Further calculations with heptamers (Py_7) were made studying first a system composed of two chains and three TaF_7^{2-} ions. The obtained structure shows a slight curvature for both chains, and a central ion which is no longer fully embedded in pockets of the chains, because of the large Coulomb repulsion between the anions. The obtained binding energy is -543.7 kJ/mol, suggesting a metastable aggregate. Increasing the number of oligomers surrounding the TaF_7^{2-} ions to five a stable aggregate is obtained with a positive binding energy of 667.2 kJ/mol, perhaps thanks to the increased possibility for hydrogen bonding between anions and oligopyrroles, but also due to π-π interactions between the chains. The latter lead to two different slightly helical π stacks consisting of two and three heptapyrroles, respectively (Fig. **19**), while the anions nearly perfectly sit on a straight

line. The distances between the central and the two terminal TaF_7^{2-} ions are 7.3 and 7.5 Å, respectively, *i.e.*, very close to the "ideal pocket" distance of 7.1 Å inferred from the alternating conformation of Py_5 (*vide supra*). The total Coulomb repulsion between the three anions amounts to 1875.9 kJ/mol. From this and the binding energy of the aggregate an average embedding energy of about 170 kJ/mol is estimated for each of the fifteen different TaF_7^{2-}-pocket contacts.

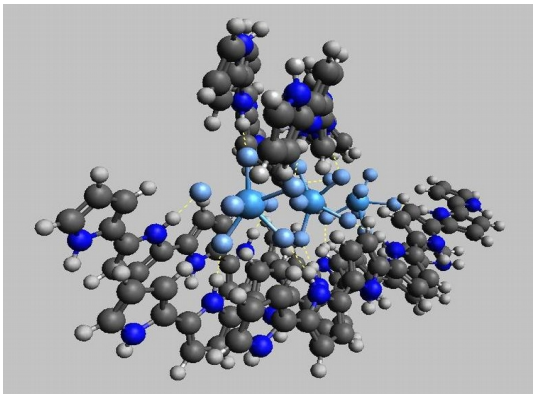

(a)

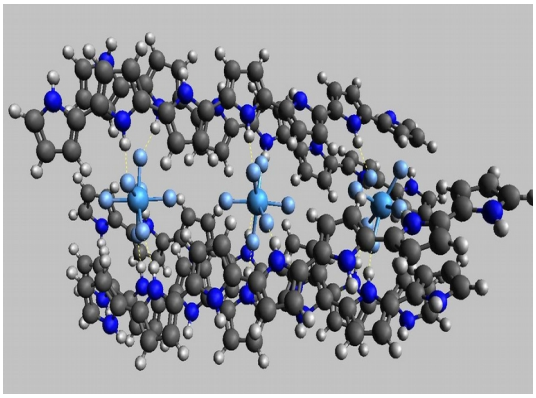

(b)

Figure **20**. BP+D structure of five chains of heptapyrrole holding tree T^{2-} ions. View from the side (a) and front (b).

4.4 Average noncovalent distances

In the ideal pocket configuration as defined by $[TaF_7(Py_3)_1]^{2-}$ (*vide supra*) the noncovalent NH...F distance was found to be 1.49 Å and the CH...F distance to be 2.11 Å. Table 2 shows average noncovalent bond distances for nearest neighbour NH...F and CH...F contacts and their standard deviations for the larger aggregates studied here (taking all optimized configurations of a particular aggregate into account, and considering only NH...F distances smaller than 2.0 Å and CH...F distances smaller than 3.0 Å). First of all, it is evident that the average distances in all of the larger aggregates significantly increase as compared to those observed for the ideal pocket in $[TaF_7(Py_3)_1]^{2-}$. For all of the systems with two oligopyrrole chains the NH...F distances increase by about 0.1 Å and the CH...F distances by roughly 0.2 Å – a direct consequence of the repulsion between the dipoles on the two oligopyrrole chains, which in most of the studied configurations lie on opposing sides of the TaF_7^{2-} ion(s). A further increase of the NH...F distances by one or two tenths of an Å and of the CH...F distances by roughly 0.1 Å is observed upon addition of further oligopyrrole chains in each case, due to an increased number of possibilities for

dipole-dipole repulsion between oligopyrrole chains in combination with geometrical constraints imposed by their π stacking.

Besides ideal pocket-like configurations the statistical data shown in Table 2 take also into account (i) aggregate structures, where only half-pockets are occupied by TaF_7^{2-}, and (ii) non-alternating pyrrole chains. Nevertheless, from these BP+D level data it seems safe to conclude that in the TaF_7^{2-} doped polymeric material the average NH...F distances will amount to 1.7 – 1.8 Å and the CH...F distances to 2.3 – 2.5 Å, at least as long as the polypyrrole remains uncharged.

NH..F Bond. Dist (Å)	$[T(Py_3)_2]^{2-}$	$[T(Py_3)_4]^{2-}$	$[T_2(Py_5)_2]^{4-}$	$[T_2(Py_5)_4]^{4-}$
Average	1.58	1.74	1.59	1.69
Std. Dev.	0.11	0.08	0.05	0.08
% Std. Dev.	6.6	4.8	2.9	4.6
CH..F Bond. Dist (Å)				
Average	2.27	2.32	2.28	2.42
Std. Dev.	0.19	0.17	0.11	0.21
% Std. Dev.	8.3	7.2	4.7	8.6

Table **6.1**. Average NH...F and CH...F distances and their standard deviations for the series of aggregates calculated with BP+D. (Here T= TaF_7^{2-}).

NH..F Bond. Dist (Å)	$[T_2(Py_5)_5]^{2-}$	$[T_3(Py_7)_2]^{6-}$	$[T_3(Py_7)_5]^{6-}$
Average	1.71	1.59	1.59
Std. Dev.	0.05	0.06	0.05
% Std. Dev.	2.7	4	2.9
CH..F Bond. Dist (Å)			
Average	2.43	2.35	2.46
Std. Dev.	0.16	0.3	0.12
% Std. Dev.	6.6	12.6	4.7

Table **6.2**. Average NH...F and CH...F distances and their standard deviations for the series of aggregates calculated with BP+D. (Here T= TaF_7^{2-}).

Chapter 5: Aggregates with charged oligopyrrole chains

In this chapter we will elucidate how the oxidation of the structures described above affects their geometry, energies and internal interactions, keeping in mind that we are dealing with a conducting material. The topics that we will discuss here are: (i) the Mulliken partial charges for the different groups of the calculated structures and (ii) the energies and geometrical changes observed when the same structures were calculated in different oxidation states.

5.1 ionisation potentials of TaF_7^{2-} and Py_n (n=1,2,3,5)

The first factor to take into account when studying charged structures is the energetic cost of giving/accepting electrons. This means to calculate the energy for each step of the proposed ionisation. In Table **7**, we list the first vertical and adiabatic ionisation potentials of the components of the studied aggregates. These were determined from the energy differences between the non oxidised and singly oxidised structures without ("vertical") and with ("adiabatic") geometry re-optimization of the latter using BP+D3. The pyrrole monomer alone needs 809 kJ/mol to instantaneously loose an electron and still 786 kJ/mol after geometry relaxation of the cation. For the oligomers we can see that ionisation potential diminishes as the number of units in a pyrrole chain grows, due to the better delocalisation of the charge through the carbon backbone. On the other hand, instantaneously extracting an electron from the double anion TaF_7^{2-} costs several times less energy, as it was to be expected, and even an order of magnitude less energy accounting for geometry relaxation.

	Vertical IP	Adiabatic IP	Total energy
TaF_7^{2-}	120.50	54.48	-756.812117
Py	801.26	786.24	-209.967242
Py_2	664.55	646.23	-419.105194
Py_3	599.16	583.39	-628.214549
Py_5	532.96	521.64	-1046.408848

Table **7.** Vertical and aediabatic ionisation potentials (IP) in kJ/mol of the fundamental components and total energies in Hartrees of the geometry-optimized oxidised components.

5.2 Mulliken populations for selected structures

Considering the fact that we are modelling a conducting material, it must be taken into account that prescence of charged species is inherent to the nature of this type of systems. Here, we will carry out BP+D geometry optimizations in order to see how positive charges will distribute in the oligomers, assuming that the heptafluorotantalate ion concentrates the negative charge in itself. However, we first want to confirm this hypothesis through calculating the Mulliken partial charges in some of the optimized structures, already described in the previous chapter, for different total charges of some aggregates. Corresponding results are found in Fig. **21** and Tables **7.1**-**7.3**.

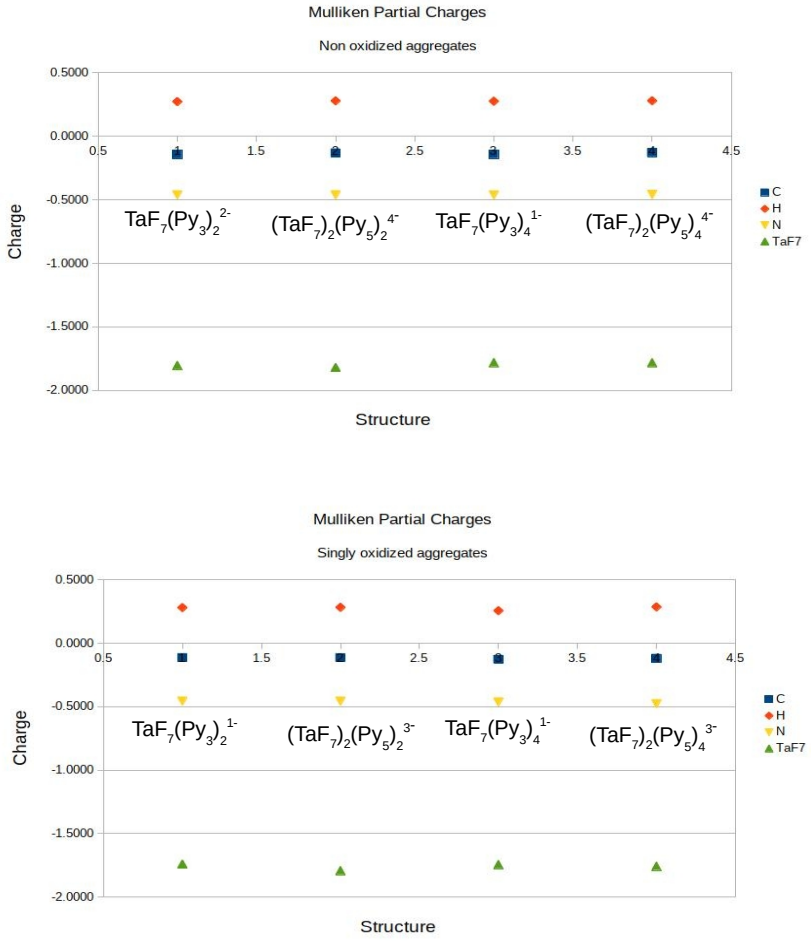

Figure **21.1**. Average Mulliken charges for each oligopyrrole atom and the heptafluorotantalate ion in various aggregates (up), with corresponding charges after single (down) oxidation.

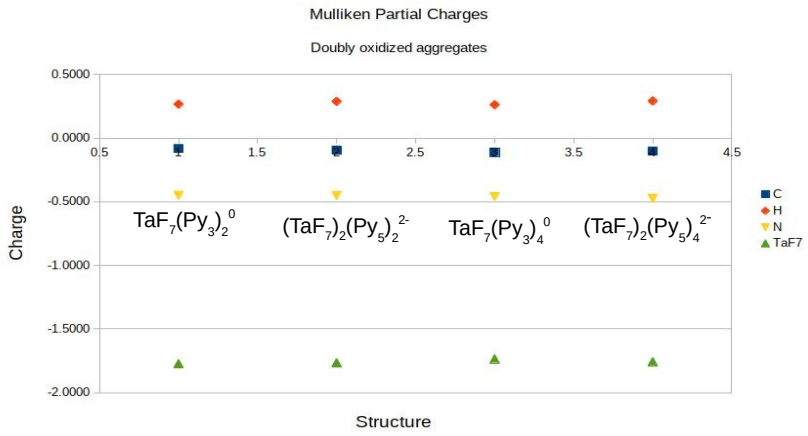

Figure **21.2.** Average Mulliken charges for each oligopyrrole atom and the heptafluorotantalate ion in various aggregates after double oxidation.

	$TaF_7(Py_3)_2^{-2}$	$(TaF_7)_2(Py_5)_2^{4-}$	$TaF_7(Py_3)_4^{2-}$	$(TaF_7)_2(Py_5)_4^{4-}$
C	-0.1433	-0.1312	-0.1422	-0.1288
H	0.2728	0.2790	0.2764	0.2800
N	-0.4599	-0.4599	-0.4607	-0.4585
TaF_7	-1.8038	-1.8205	-1.7816	-1.7827

Table **8.1.** Average Mulliken charges for each oligopyrrole atom and the heptafluototantalate ion in non oxidised aggregates.

	$TaF_7(Py_3)_2^{1-}$	$(TaF_7)_2(Py_5)_2^{3-}$	$TaF_7(Py_3)_4^{1-}$	$(TaF_7)_2(Py_3)_4^{3-}$
C	-0.1130	-0.1131	-0.1266	-0.1184
H	0.2823	0.2840	0.2574	0.2876
N	-0.4541	-0.4547	-0.4609	-0.4751
TaF_7	-1.7404	-1.7927	-1.7446	-1.7577

Table **8.2.** Average Mulliken charges for each oligopyrrole atom and the heptafluototantalate ion in singly oxidised aggregates.

	$TaF_7(Py_3)_2^{0}$	$(TaF_7)_2(Py_5)_2^{2-}$	$TaF_7(Py_3)_4^{0}$	$(TaF_7)_2(Py_5)_4^{2-}$
C	-0.0818	-0.0945	-0.1113	-0.1020
H	0.2666	0.2887	0.2622	0.2913
N	-0.4491	-0.4502	-0.4586	-0.4751
TaF_7	-1.7736	-1.7658	-1.7357	-1.7577

Table **8.3.** Average Mulliken charges for each oligopyrrole atom and the heptafluototantalate ion in doubly oxidised aggregates.

The most important observation from the preceeding figure and the tables is that the charge on the heptafluorotantalate ion is not strongly affected by oxidation of the

aggregate: in the non-oxidised aggregates with roughly -1.8*e* it is close to the expected formal charge of -2*e*, and even upon oxidation it varies by less than 0.1*e*. Thus, in the following we will continue to use TaF_7^{2-} to designate heptafluorotantalate, irrespective of the aggregates oxidation state.

This, in turn means that indeed the oligopyrrole chains are oxidised, i.e. become positively charged in the aggregates. At first sight, this is amazing, considering that in the non-aggregated fundamental compounds it is much easier to oxidise the heptafluorotantalate ion. Yet, evidently the increase in the magnitude of the binding energy between TaF_7^{2-} and positively charged (rather than neutral) oligopyrroles overcompensates for the higher ionisation potential of the latter. Futhermore, the preceeding figures and tables demonstrate that the positive charge of an oxidised oligopyrrole is fairly evenly distributed over all of its backbone atoms and can not be ascribed to a single type of atom. It also should be noted that here and in the following a notion such as “single oxidation” does not imply that only one of the chains looses an electron when the aggregate contains several oligopyrrole chains: In the case of two chains, for example, each chain rather looses half of an electron, i.e., the oxidation state is also delocalised over the several chains.

5.3 Structures and binding energies for $[TaF_7(Py_3)_y]^{x-}$ with x=0,1 and y = 2,4

The converged structures described in Chapter 4 (Fig. 11,12,14 and 15) were submitted to further geometry optimizations after oxidation, considering at first two groups of systems: one with two pyrrole trimers and the other with four pyrrole trimers. In each group two charged states were calculated: total aggregate charge -1 (only one oxidised oligomer) and 0 (two oxidised oligomers); always taking the converged structures described in Chapter 4 as start geometries. It must be stated clearly that in the latter case (total charge = 0) the calculations had to be carried out in triplet configuration, for the sake of reaching convergence. The aggregates with a total charge of -1 have a doublet spin configuration. All calculations used unrestricted open shell Kohn-Sham theory.

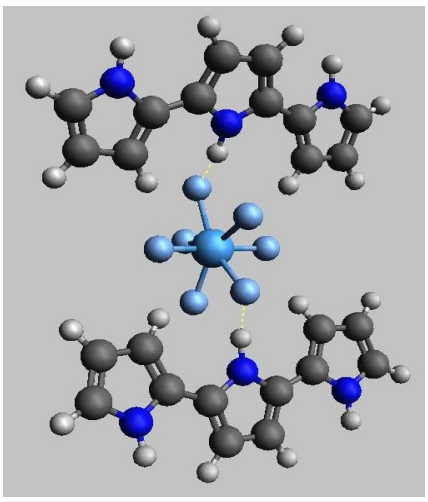

22a)

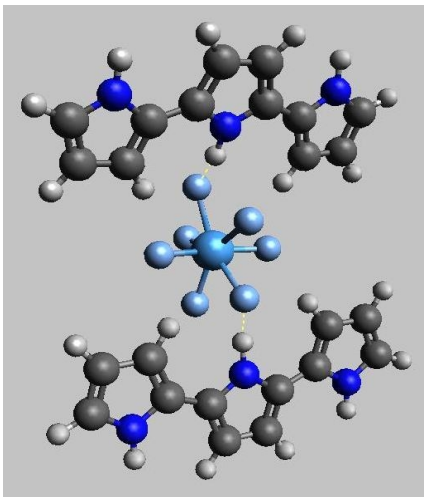

22b)

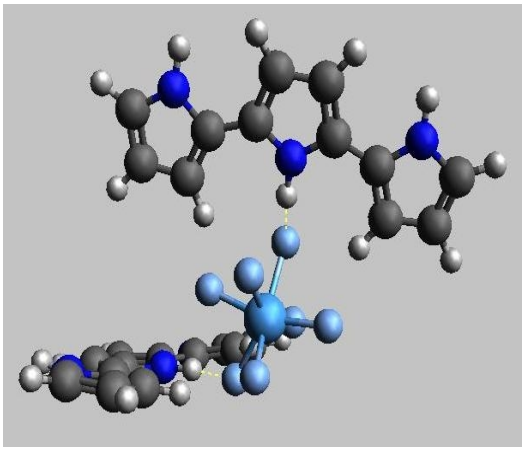

22c)

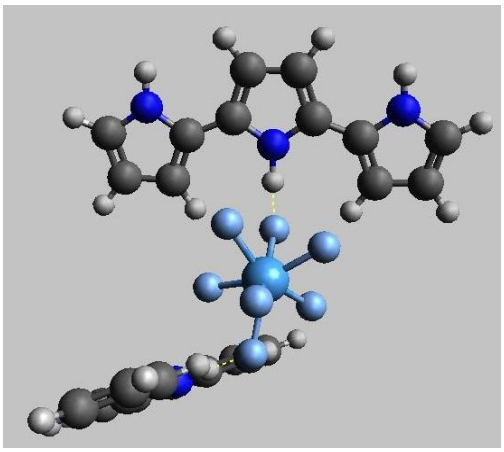

22d)

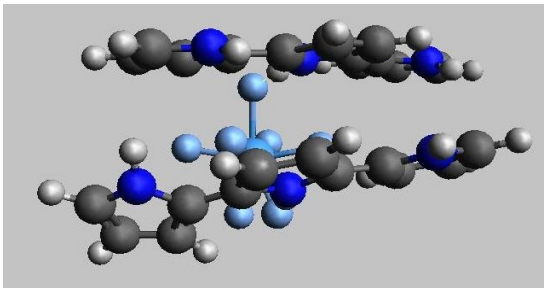

22e)

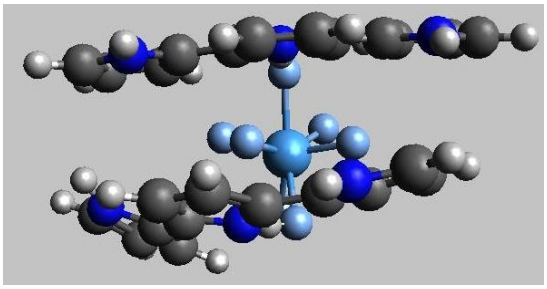

22f)

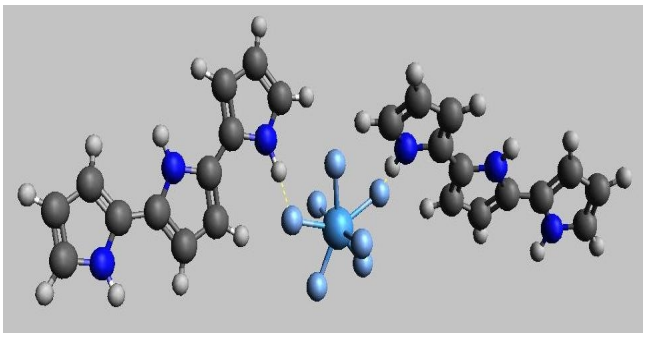

22g)

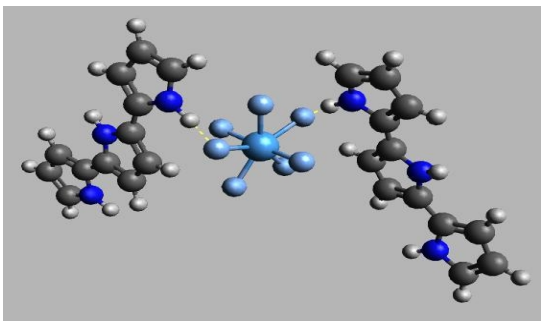

22h)

Figure **22.1.** BP+D structures of the some configurations of two tripyrrole oligomers holding a TaF_7^{2-} ion using two overall charges: -1 (a,c,e,g) and 0 (b,d,f,h).

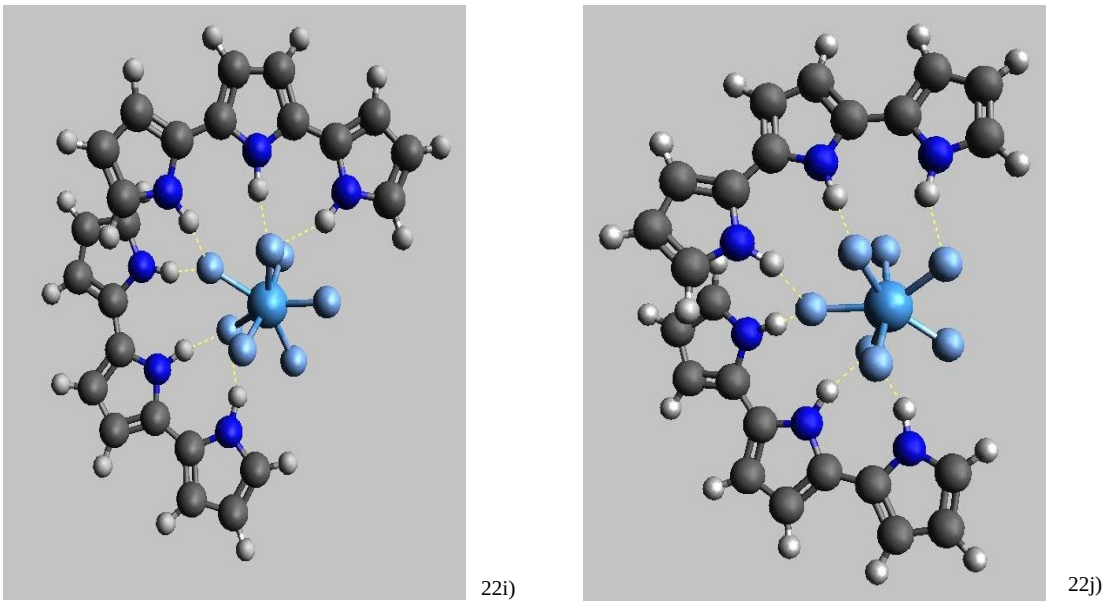

22i) 22j)

Figure **22.2.** BP+D structures of the some configurations of two tripyrrole oligomers holding a TaF_7^{2-} ion using two overall charges: -1 (i) and 0 (j).

Table **9** collects the total energies of the non oxidised aggregates along with those of the singly and doubly oxidised aggregates before ("vertical") and after ("adiabatic") geometry reoptimization. From these the vertical and adiabatic ionisation potentials were determined, which are also given in Table 8. All vertical ionisation potentials (IP) happen to be positive, meaning that it costs energy to ionise the aggregate. As expected, it costs much more energy to doubly oxidise an aggregate than a single oxidation: the first vertical IPs vary from 41 to 90 kJ/mol, while removing a second electron costs further 311-349 kJ/mol. Structure relaxation after removal of the first electron stabilises most aggregates by 10-20 kJ/mol, with exception of aggregate **12c**, where the structural stabilisation amounts to about 44 kJ/mol, meaning that the structurally relaxed oxidised aggregate **22e** is about 3 kJ/mol lower in energy than ist non-oxidised parent structure. This, actually, is the first occurrence of a negative adiabatic IP (indicating the possibility of autoionisation) observed in this work. Comparing Figs. **12c** and **22e** we note that indeed the large relaxation energy is accompanied by large geometrical changes: while in **12c** both tripyrroles are approximately parallel, but quite distant from each other, in **22e** they are considerably closer, increasing their attractive π-stacking interactions. In addition, one of the terminal pyrrole units twists out of the plane of its neighbours allowing for a NH...π interaction with the other tripyrrole. A major geometrical change is also observed upon relaxing the structure of the singly oxidised aggregate **12b**, leading to **22c**, in which the two tripyrroles are no longer on opposing sides of TaF_7^{2-}.

Total Energy (Ha)

Vertical Energy (Ha)

System	Energy CS^{-2}		System	Energy CS^{-1}		System	Energy CS^{0}
12a	-2013.822681		22a	-2013.803918		22b	-2013.684949
12b	-2013.821823		22c	-2013.801683		22d	-2013.683315
12c	-2013.825049		22e	-2013.809464		22f	-2013.685913
12d	-2013.831957		22g	-2013.797824		22h	-2013.665043
12e	-2013.903719		22i	-2013.882013		22j	-2013.757804

Adiabatic Energy (Ha)

	System	Energy CS^{-1}		System	Energy CS^{0}
	22a	-2013.807564		22b	-2013.698966
	22c	-2013.808614		22d	-2013.701817
	22e	-2013.826299		22f	-2013.707345
	22g	-2013.802062		22h	-2013.690338
	22i	-2013.888497		22j	-2013.772525

Ionization potential (kJ/mol) (Vertical)

System	En. Diff. (En CS^{-1} - En CS^{-2})		System	En. Diff. (En CS^{0} – CS^{-1})		System	En. Diff. (CS^{0} – CS^{-2})
12a	49.26		22a	312.35		22b	361.62
12b	52.88		22c	310.77		22d	363.65
12c	40.92		22e	324.38		22f	365.30
12d	89.62		22g	348.62		22h	438.23
12e	56.99		22i	326.11		22j	383.10

Ionization potential (kJ/mol) (Adiabatic)

System	En. Diff. (En CS^{-1} - En CS^{-2})		System	En. Diff. (En CS^{0} – CS^{-1})		System	En. Diff. (CS^{0} – CS^{-2})
12a	39.69		22a	285.12		22b	324.82
12b	34.68		22c	280.40		22d	315.08
12c	-3.28		22e	312.31		22f	309.03
12d	78.49		22g	293.33		22h	371.82
12e	39.97		22i	304.49		22j	344.45

Table **9.** Total energy and ionisation energy values in kJ/mol, for the transition between different charged states of $[TaF_7(Py_3)_2]$.

Clearly, one would expect that structure relaxation is more important after removal of two electrons, and this is confirmed by comparing the corresponding vertical and adiabatic IPs (cf. Table **9**): the relaxation energies now amount to 35-67 kJ/mol. Nevertheless, the converged doubly oxidised aggregates strongly resemble the singly oxidised and optimized structures, as seen in Figs. **22a**-**22j**. Overall, the doubly oxidised aggregates are 309-372 kJ/mol less stable than their non-oxidised parent structures.

The vertical first IPs of the aggregates composed of one TaF_7^{2-} and four tripyrroles are all positive and larger than those of the aggregates with only two tripyrroles: according to Table **9** they amount to 65-95 kJ/mol. Geometry relaxation (cf. Fig. **23**) stabilises the singly oxidised aggregates in most cases by less than 10 kJ/mol, yielding adiabatic IP in

between 51-86 kJ/mol. An explanation for the higher vertical IP $[TaF_7(Py_3)_4]^{2-}$ as compared to $[TaF_7(Py_3)_2]^{2-}$ is found in the higher average NH...F and CH...F distances of the former (cf. Table 5.1) meaning that the Coulomb interaction between the TaF_7^{2-} anion and Py_3^+ is less stabilising in (vertical) $[TaF_7(Py_3)_4]^{2-}$ than in $[TaF_7(Py_3)_2]^{2-}$.

While relaxation of the structure of the oxidised aggregate in principle could change the situation, it is less efficient in the aggregates with four Py_3 chains than in those with two chains -as indicated by the smaller relaxation energies- which may probably be attributed to the increased “stiffness” of the larger aggregates. While vertical and adiabatic IPs are in the narrow intervals of 85-95 kJ/mol and 76-86 kJ/mol for nearly all the $[TaF_7(Py_3)_4]^{2-}$ aggregates, the exception is structure **13c** with its vertical IP of 65 kJ/mol and an adiabatic IP of 51 kJ/mol. This difference can be explained through the structure (**23c**, left): it is not only the aggregate with more NH...F bonds than the others, but also more NH-π and π-π interactions. This facilitates the formation of attractive interactions like ion-π or dipole-ion.

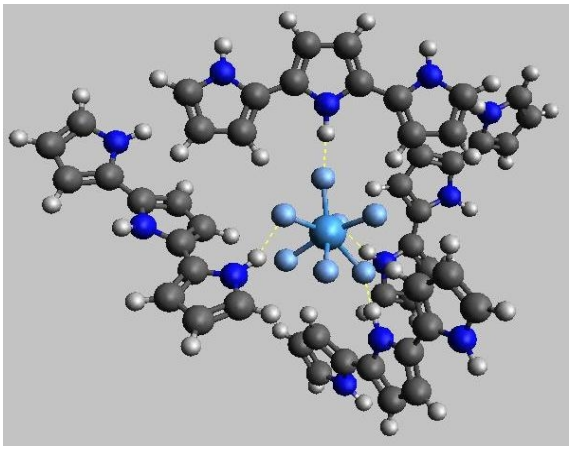

23a)

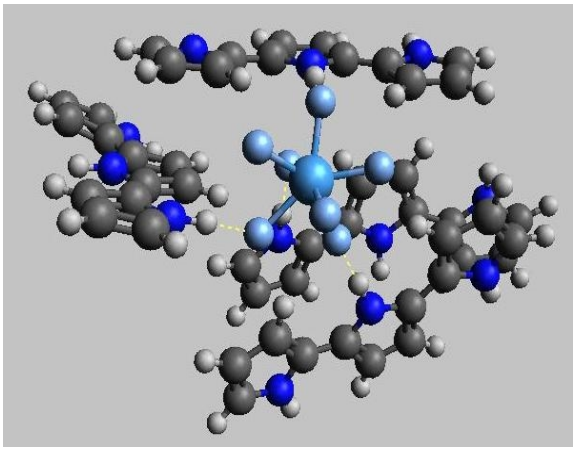

23b)

Figure **23.1**. BP+D structures of six different configurations of four tripyrrole oligomers holding a TaF_7^{2-} ion using two overall charges: -1 (a) and 0 (b).

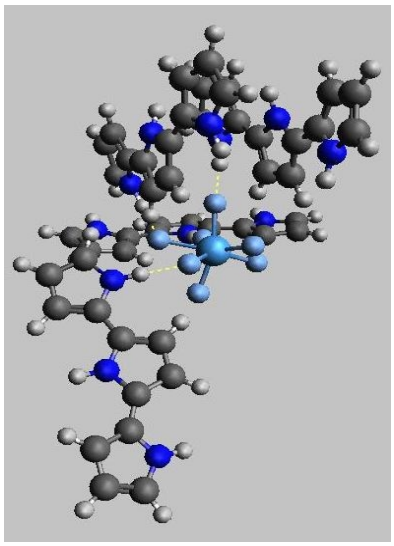

23c)

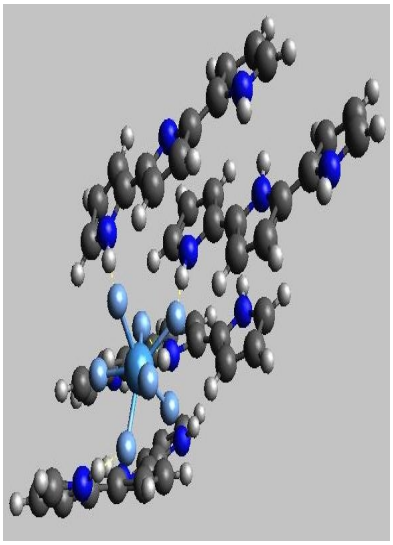

23d)

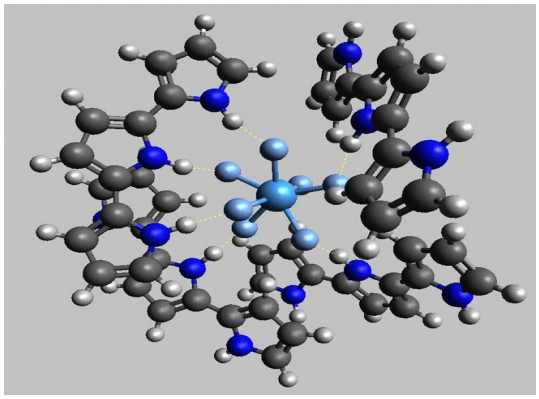

23e)

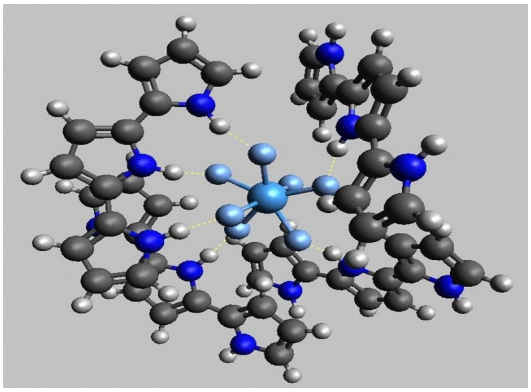

23f)

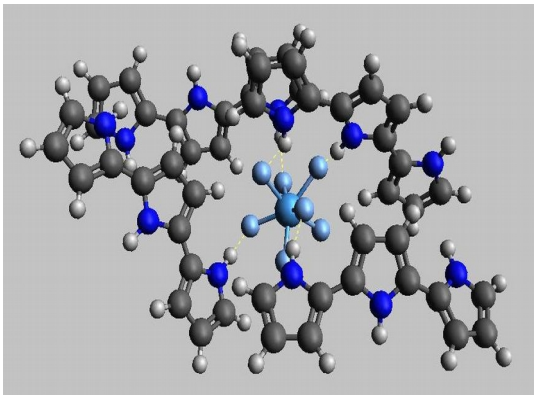

23g)

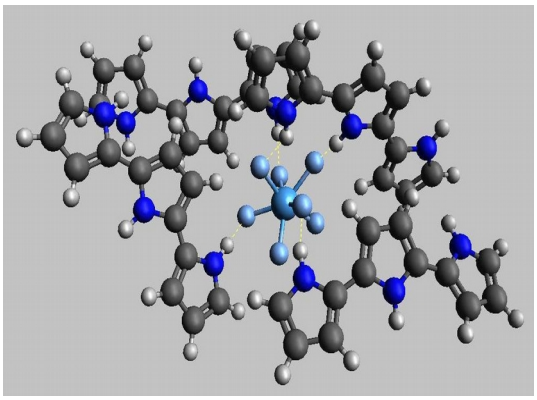

23h)

Figure **23.2**. BP+D structures of six different configurations of four tripyrrole oligomers holding a TaF_7^{2-} ion using two overall charges: -1 (c,e,g) and 0 (b,d,f).

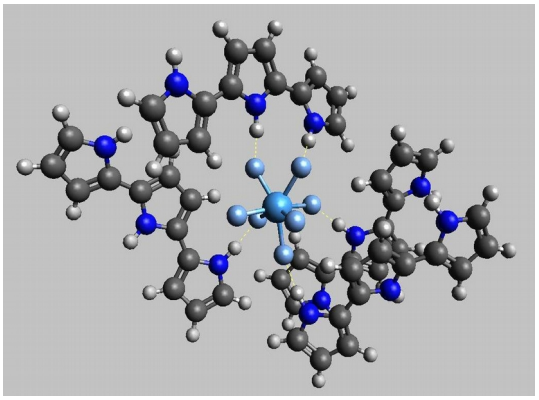
23i)

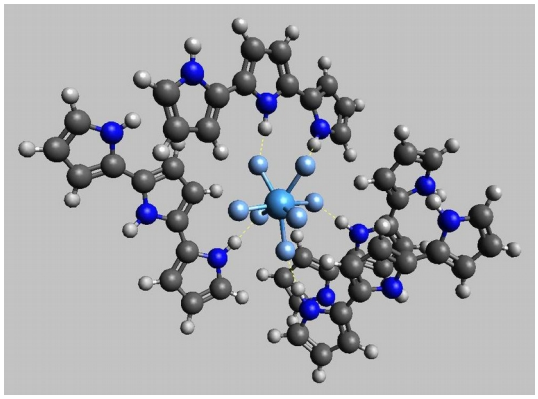
23j)

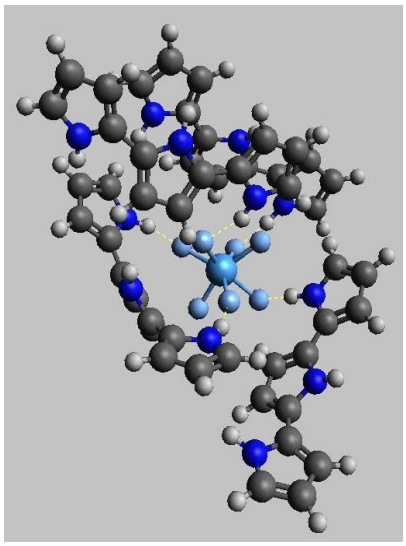
23k)

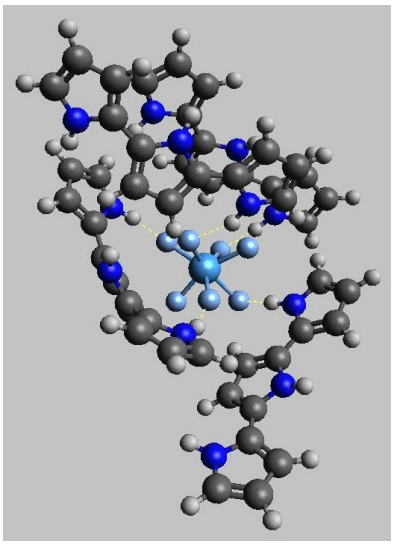
23l)

Figure **23.3**. BP+D structures of six different configurations of four tripyrrole oligomers holding a TaF_7^{2-} ion using two overall charges: -1 (a) and 0 (b).

When we go further in the oxidation process, in the step from total aggregate charge -1 to 0, ionisation energies of 294-329 kJ/mol need to be invested, leading to total vertical IPs of 360-424 kJ/mol (cf. Table 10). Allowing the doubly oxidised aggregates to relax in most cases releases 20-30 kJ/mol, with exception of conformers **23a** and **23c** which display large relaxation energies of nearly 120 kJ/mol. Here it is possible to observe clear structural changes in the doubly oxidised aggregates (cf. Figs. 23b and 23d), and in both cases, their oligomers fold themselves in order to form and enhance NH-π, π-π and ion-π interactions.

Total Energy (Ha) (Vertical)

System	Energy CS^{-2}		System	Energy CS^{-1}		System	Energy CS^{0}
13a	-3270.796109		23a	-3270.761795		23b	-3270.646548
13b	-3270.809843		23c	-3270.777606		23d	-3270.662339
13c	-3270.830347		23e	-3270.805457		23f	-3270.693471
13d	-3270.830938		23g	-3270.797601		23h	-3270.678096
13e	-3270.837864		23i	-3270.804534		23j	-3270.687153
13f	-3270.837880		23k	-3270.801657		23l	-3270.676397

Total Energy (Ha) (Adiabatic)

System	Energy CS^{-1}		System	Energy CS^{0}
23a	-3270.763999		23b	-3270.691627
23c	-3270.780814		23d	-3270.703460
23e	-3270.810761		23f	-3270.705158
23g	-3270.801594		23h	-3270.686794
23i	-3270.806975		23j	-3270.696098
23k	-3270.805125		23l	-3270.687185

Ionization Energy (kJ/mol) (Vertical)

System	En. Diff. (En CS^{1-} - En CS^{2-})		System	En. Diff. (En CS^{0} - CS^{1-})		System	En. Diff. (En CS^{0} - CS^{2-})
13a	90.09		23a	302.58		23b	392.67
13b	84.64		23c	302.63		23d	387.27
13c	65.35		23e	294.02		23f	359.37
13d	87.53		23g	313.76		23h	401.29
13e	87.51		23i	308.18		23j	395.69
13f	95.10		23k	328.87		23l	423.97

Ionization Energy (kJ/mol) (Adiabatic)

System	En. Diff. (En CS^{1-} - En CS^{2-})		System	En. Diff. (En CS^{0} - CS^{1-})		System	En. Diff. (En CS^{0} - CS^{2-})
13a	84.30		23a	190.01		23b	274.32
13b	76.22		23c	203.09		23d	279.31
13c	51.42		23e	277.26		23f	328.68
13d	77.04		23g	301.41		23h	378.45
13e	81.10		23i	291.11		23j	372.21
13f	86.00		23k	309.65		23l	395.65

Table **10**. Total energy and ionisation energy values in kJ/mol, for the transition between different charged states of $[TaF_7(Py_3)_4]$.

Comparing the binding energies of the non oxidised aggregates containing two Py_3 (cf. Table **11**) with those containing four Py_3 (Table 11) we note that the latter are roughly two times higher (in the order of 568-677 kJ/mol) than the former (in the order of 303-330 kJ/mol -with exception of **12e** with its two Py_3 with parallel ↑↑↑ conformation). This was already observed in the preceeding chapter and simply reflects the increased number of pocket and half pocket embedding possibilities in the two types of aggregates. The binding energies of the singly oxidised aggregates are 500-590 kJ/mol higher than those of the non-oxidised aggregates in case of the aggregates containing two Py_3, and 500-530 kJ/mol higher in case of the aggregates containing four Py_3 chains. From this we may infer

that the Coulomb attraction between TaF_7^{2-} and Py_3^+ amounts to roughly 500-600 kJ/mol. The binding energies of the doubly oxidised aggregates $[TaF_7(Py_3)]^0$ are only about 270-300 kJ/mol higher than those of their singly oxidised counterparts $[TaF_7(Py_3)]^{1-}$ since now there is an additional repulsive contribution between two Py_3^+. Comparing this to the increase of the binding energy observed above from the comparison between $[TaF_7(Py_3)]^{2-}$ and $[TaF_7(Py_3)]^{1-}$ we may estimate this interchain Coulomb repulsion to roughly be 200-300 kJ/mol. Similar considerations hold for the aggregates containing four Py_3 chains, where the binding energies of the doubly oxidised $[TaF_7(Py_3)_4]^0$ are 280-390 kJ/mol higher than those of their singly oxidised counterparts $[TaF_7(Py_3)_4]^{1-}$.

System	Energy CS^{-2}		System	Energy CS^{-1}		System	Energy CS^{0}
12a	305.38		22a	849.08		22b	1147.34
12b	303.12		22c	851.83		22d	1154.83
12c	311.59		22e	898.27		22f	1169.34
12d	329.73		22g	834.63		22h	1124.69
12e	518.14		22i	1061.57		22j	1340.47

Table **11**. Binding energies for different charged states in kJ/mol of $[TaF_7(Py_3)_2]$.

System	Energy CS^{-2}		System	Energy CS^{-1}		System	Energy CS^{0}
13a	567.73		23a	1066.82		23b	1460.20
13b	603.79		23c	1110.97		23d	1491.26
13c	657.63		23e	1189.59		23f	1495.72
13d	659.18		23g	1165.52		23h	1447.51
13e	677.36		23i	1179.65		23j	1471.93
13f	677.40		23k	1174.80		23k	1448.54

Table **12.** Binding energies for different charged states of $[TaF_7(Py_3)_4]$.

5.4 Structures and binding energies for $[(TaF_7)_2(Py_5)_y]^{x-}$ with x= 0,1,2,3,4 and y = 2,4

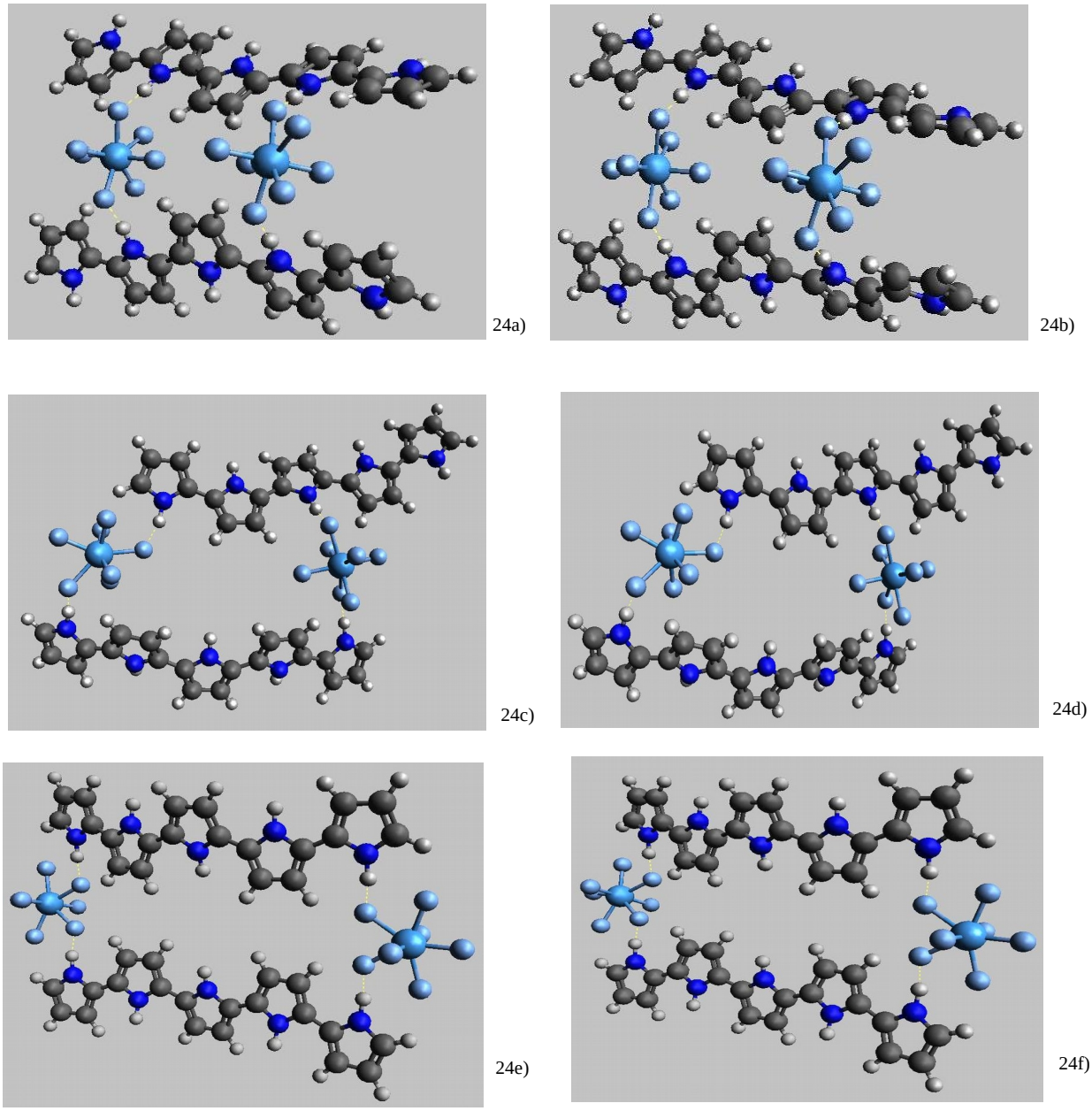

Figure **24**. BP+D structures of six different configurations of two pyrrole pentamers holding two TaF_7^{2-} ion using two overall charges: -3 (a,c,e) and -2 (b,d,f).

As discussed in Chapter 4.1, aggregates between two TaF_7^{2-} and two neutral pentapyrrole chains are slightly to significantly stable against dissociation into two free ions and two separated Py_5 chains, depending on the interionic distance in the aggregate. They are, however, not stable against oxidation, and again, the distance between the TaF_7^{2-} ions plays an important role here. The first vertical IPs are all negative for the three considered aggregates, i.e., energy is released upon emitting an electron, and the closer the two

negative ions in the aggregate, the more energy is released: from 183 over 228 to 285 kJ/mol when the interion distance decreases from 17.9 over 12.4 to 9.2 Å (cf. Table **12**). Subsequent geometry relaxation of the singly oxidised aggregates releases another 10-22 kJ/mol, leading to adiabatic first IPs of -192 to -299 kJ/mol.

Total Energy (Ha) (Vertical)

System	Energy CS^{-4}		System	Energy CS^{-3}		System	Energy CS^{-2}
15a	-3606.898710		24a	-3607.007281		24b	-3607.033366
15b	-3606.933162		24c	-3607.020016		24d	-3607.026177
15c	-3606.988499		24e	-3607.058002		24f	-3607.047966

Total Energy (Ha) (Adiabatic)

System	Energy CS^{-3}		System	Energy CS^{-2}
24a	-3607.012671		24b	-3607.052710
24c	-3607.028565		24d	-3607.049517
24e	-3607.061719		24f	-3607.062346

Ionization Potential (kJ/mol) (Vertical)

System	En. Diff. (En CS^{3-} - En CS^{4-})		System	En. Diff. (En CS^{2-} - CS^{3-})		System	En. Diff. (CS^{2-} - CS^{4-})
15a	-285.05		24a	-68.48		24b	-353.54
15b	-228.03		24c	-16.17		24d	-244.21
15c	-182.48		24e	26.35		24f	-156.13

Ionization Potential (kJ/mol) (Adiabatic)

System	En. Diff. (En CS^{3-} - En CS^{4-})		System	En. Diff. (En CS^{2-} - CS^{3-})		System	En. Diff. (CS^{2-} - CS^{4-})
15a	-299.20		24a	-105.12		24b	-404.33
15b	-250.48		24c	-55.01		24d	-305.49
15c	-192.24		24e	-1.65		24f	-193.89

Table **12.** Total energy in Ha, ionisation potential values in kJ/mol, for the transition between different charged states of of $[TaF_7(Py_5)_2]$.

Binding Energy (kJ/mol)

System	Energy CS^{-4}		System	Energy CS^{-3}		System	Energy CS^{-2}
15a	47.03		24a	867.87		24b	1494.64
15b	137.48		24c	909.60		24d	1486.25
15c	282.76		24e	996.65		24f	1519.94

Ta-Ta distance (Å)

System	Energy CS^{-4}			Energy CS^{-3}			Energy CS^{-2}
15a	9.195		24a	8.814		24b	8.552
15b	12.44		24c	11.499		24d	11.083
15c	17.935		24e	17.766		24f	17.583

Table **13.** Binding energies in kJ/mol and interion distance in Å for the different charged states $[TaF_7(Py_5)_2]$.

Remarkably, two of the $[(TaF_7)_2(Py_5)_2]^{4-}$ aggregates also voluntarily emit a second electron: the aggregates **15a** and **15b** with their smal Ta-Ta distance below 13 Å have negative second IPs of -68.5 and -16.2 kJ/mol, respectively, and only in case of the aggregate **15c** energy (26.4 kJ/mol) is required to perform a second oxidation step at the fixed geometry of the non-oxidised aggregate. Geometry relaxation, however, also in the latter case allows the twofold oxidised aggregate to become more stable than its singly oxidised counterpart. So, all of the considered $[(TaF_7)_2(Py_5)_2]^{2-}$ aggregates finally are more stable than the $[(TaF_7)_2(Py_5)_2]^{3-}$ aggregates which, in turn, were already significantly more stable than the non-oxidised $[(TaF_7)_2(Py_5)_2]^{4-}$ aggregates.

It is also noteworthy that geometry relaxation in the singly oxidised aggregates leads to a shortening of the Ta-Ta distances by 0.2-0.9 Å while the Ta-Ta distances in the optimized doubly oxidised aggregates are even by 0.4-1.3 Å shorter than in the non-oxidised aggregates (cf. Table **13**), an effect which may be attributed to the attractive TaF_7^{2-}…. Py_5^+ interactions in combination with a more efficient screening of the repulsive TaF_7^{2-}….TaF_7^{2-} Coulomb interactions through Py_5^+ (in comparison to Py_5). Furthermore it should be noted that the doubly oxidised aggregate with the shortest Ta-Ta distance, where both TaF_7^{2-} ions sit in “ideal” pockets, now is nearly as stable (by 1495 kJ/mol) against full dissociation into its components as that with the largest Ta-Ta distance where both TaF_7^{2-} occupy half pockets only, which requires 1520 kJ/mol for dissociation (cf Table **13**).

From here, the number of pentamers was raised up to four, carrying out calculations for four different aggregate conformations (Fig.**25**-**28**). In each case up to fourfold oxidation was considered, i.e., aggregates with total charges -3,-2,-1, and 0. As before high spin unrestricted Kohn-Sham theory was employed, i.e., considering doublet, triplett, quartett and quintett spin states, respectively.

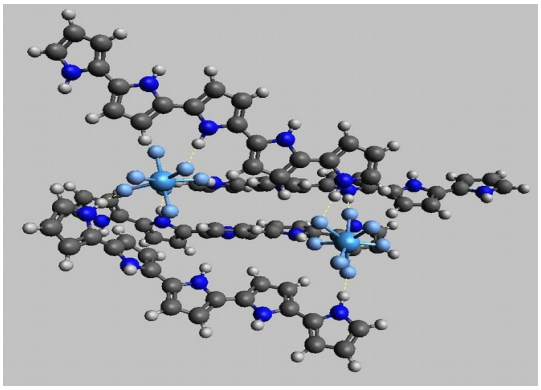
25a)

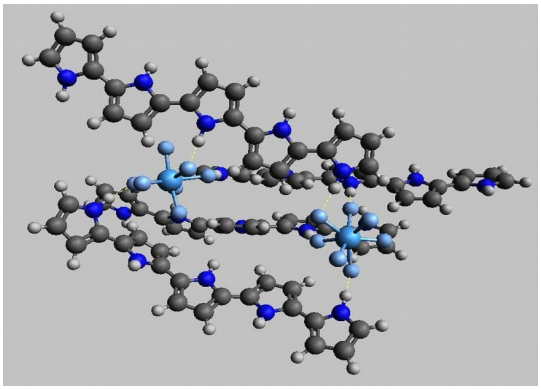
25b)

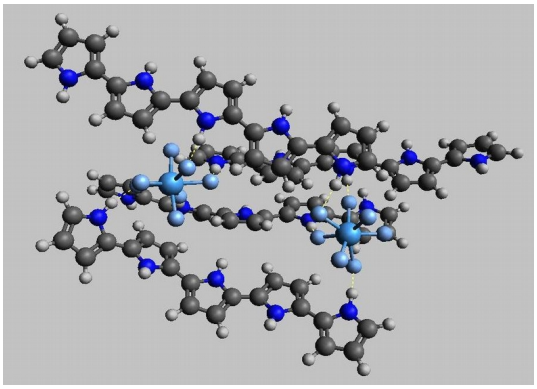
25c)

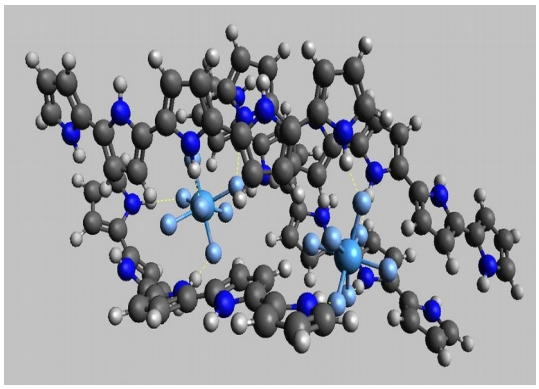
25d)

Figure **25**. First configuration of 4 pentamers and two TaF_7^{2-} ions in its four optimized oxidation states -3 (a), -2 (b), -1 (c), 0 (d).

For the first oxidation step of $[(TaF_7)_2(Py_5)_2]^{4-}$ essentially the same trend is observed as was already described above: the vertical first IP is negative and its magnitude increases with decreasing Ta-Ta distance (cf. Table **14**), releasing between 222 kJ/mol and 274 kJ/mol for the four aggregate structures considered. Geometry relaxation leads to additional stabilisation by a bit less than 10 kJ/mol in each case (cf. Table **15**, the corresponding optimized structures are denoted as **25a**-**28a**, respectively), resulting in adiabatic first IPs of -231 to -284 kJ/mol. The second oxidation step is also exothermic, releasing 38 to 83 kJ/mol (cf. Table 13), which again is inversely correlated with the Ta-Ta distance. As expected, geometry relaxation is a bit more stabilising in the twofold oxidised structures, amounting to one to two dozend kJ/mol and resulting in adiabatic IP of -292 to -383 kJ/mol for twofold oxidation.

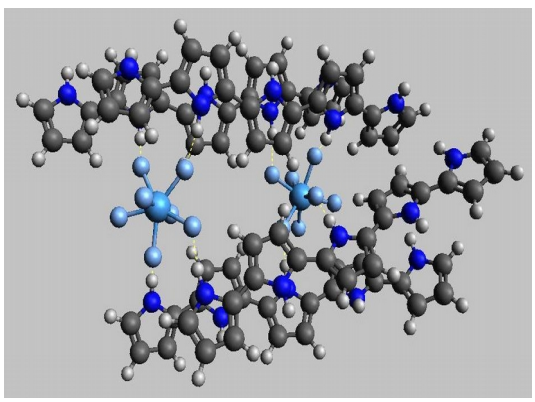

26a)

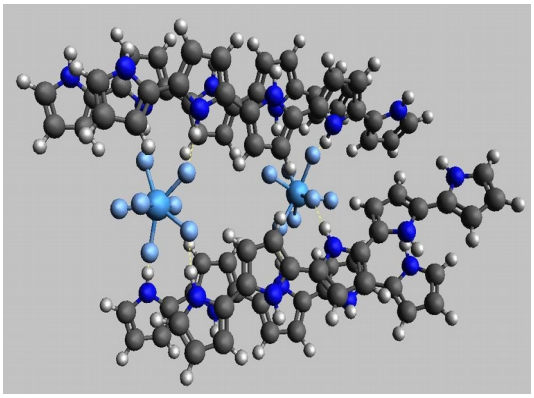

26b)

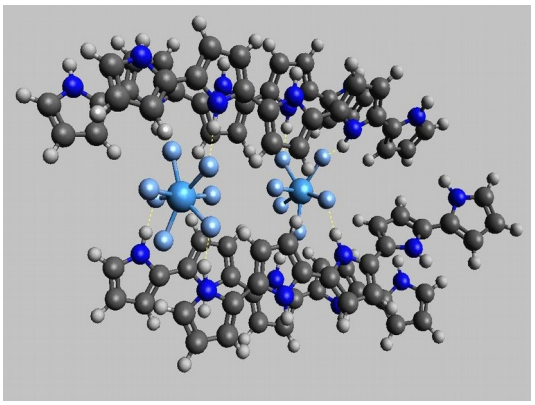

26c)

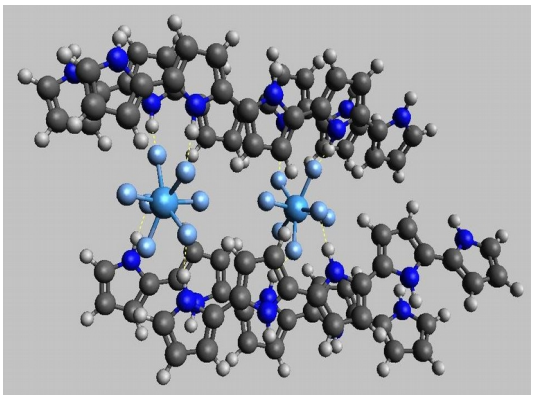

26d)

Figure **26**. Second configuration of 4 pentamers and two TaF_7^{2-} ions in its four optimized oxidation states -3 (a), -2 (b), -1 (c), 0 (d).

Further oxidation, however, requires energy: going from $[(TaF_7)_2(Py_5)_4]^{2-}$ to $[(TaF_7)_2(Py_5)_4]^{1-}$ needs more than 130 kJ/mol for the aggregates **24 – 27** in the geometries of **24a**-**27a**, respectively, and still about 60 kJ/mol for aggregate **28** when its geometry is fixed to that of **28a**. The reason for the significantly smaller amount of energy needed for the third ionisation step of **28** as compared to the other aggregates is probably the significantly smaller Ta-Ta distance in **28**: oxidation of Py_5 chains here is particularly helpful in stabilising the electronic structure of the aggregate through anion-cation attraction and shielding of the anion-anion repulsion -a tendency, which is already noticeable in the first two oxidation steps. While this trend reverses for the fourth vertical ionisation step of **28**, which with 351 kJ/mol costs 16-35 kJ/mol more than for the other aggregates, “instantaneous” oxidation of the four pyrrole chains in **28** without geometry relaxation overall necessitates only 52 kJ/mol, while in case of aggregate **25** with its significantly larger Ta-Ta distance 217 kJ/mol are required.

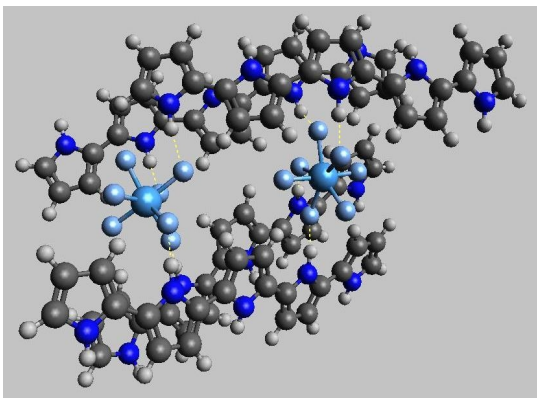
27a)

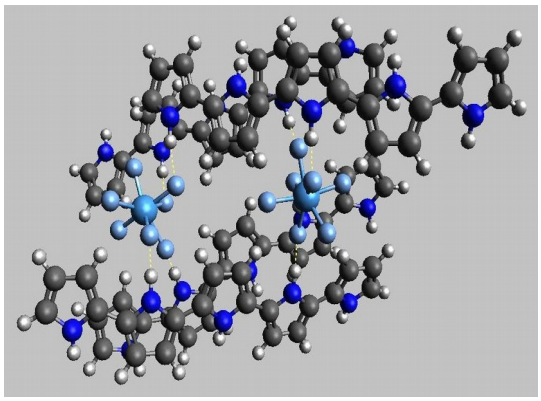
27b)

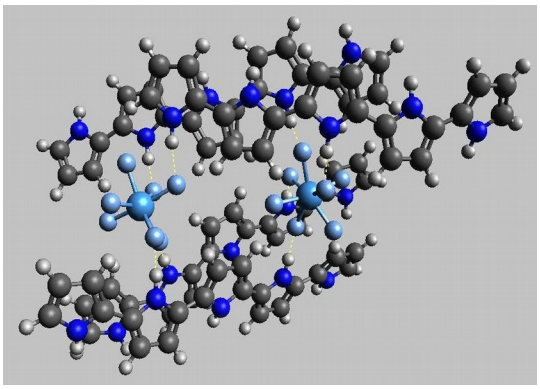
27c)

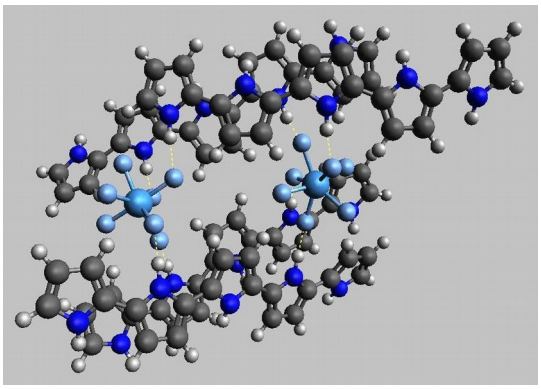
27d)

Figure **27**. Third configuration of 4 pentamers and two TaF_7^{2-} ions in its four optimized oxidation states -3 (a), -2 (b), -1 (c), 0 (d).

The possibility of geometry relaxation in the oxidised aggregates, however, decreases the energy differences in the adiabatic IP of the four considered aggregate structures: now they range from 61 kJ/mol for aggregate **26** to -33 kJ/mol for aggregate **28** (Table 14). Yet, the more relevant finding is perhaps the consistent decrease in the anion-anion distances observed with each oxidation step for each one of the aggregates when geometry relaxation is taken into account (cf. Table 14). This is particularly relevant in aggregate **28**, where the TaF_7^{2-} anions occupy full pockets in each of the four Py_5 chains. While in the non-oxidised aggregate a Ta-Ta distance of 7.67 Å is obtained, in the twofold oxidised aggregate the Ta-Ta distance of 7.23 Å is already fairly close to the “ideal pocket-pocket distance” of 7.1 Å as inferred in Chapter 4.1.

The Ta-Ta distance even further decreases with threefold and fourfold oxidation. It should not be forgotten, however, that twofold oxidation represents the energetic minimum for each of the considered aggregates, as clearly visible from Fig. 29 which plots the total energy of the aggregates as a function of the charged state. This graph furthermore demonstrates that the conformer **28b** of $[(TaF_7)_2(Py_5)_4]^{2-}$ is the second-most stable

conformer (only conformer **26b**, with several “half pocket” occupations, is more stable). As concerning the total binding energies of the aggregates, the trends are as to be expected: oxidation of a first Py_5 chain increases the energy required to dissociate the aggregate into its components by roughly 800 kJ/mol, oxidation of a second Py_5 increases it by further 600 kJ/mol, while oxidation of the third and fourth Py_5 increase E_{bind} by roughly 400 and less than 300 kJ/mol, respectively, due to increased cation-cation repulsion.

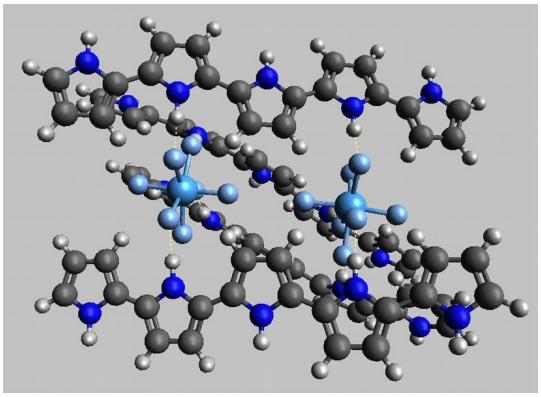

28a)

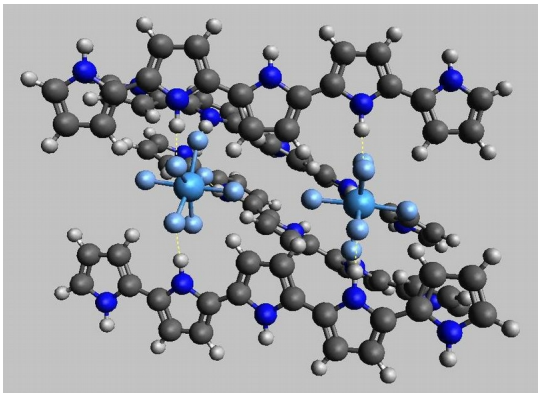

28b)

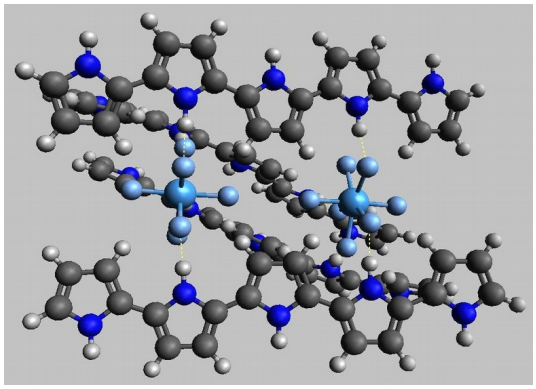

28c)

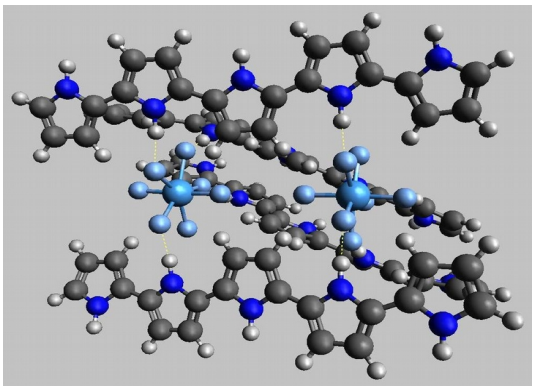

28d)

Figure **28**. Third configuration of 4 pentamers and two Ta^{-2} ions in its four optimized oxidation states -3 (a), -2 (b), -1 (c), 0 (d).

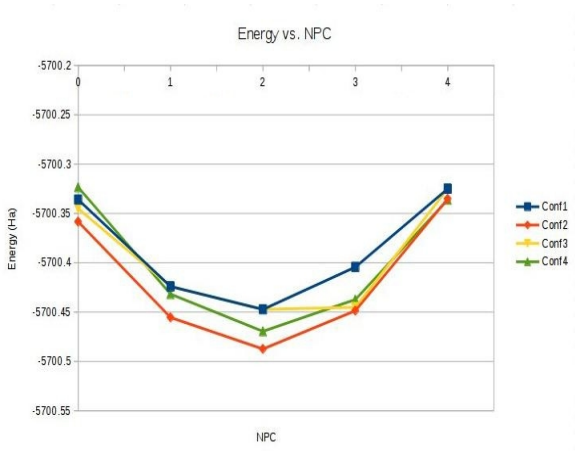

Figure **29**. Graph of total energy in hartrees (Ha) vs. the number of positive charges (NPC) added for the four considered conformers of $[(TaF_7)_2(Py_5)_4]$.

Total Energy (Ha)

System	Energy CS^{-4}	Energy CS^{-3}	Energy CS^{-2}	Energy CS^{-1}	Energie CS^{0}
Conf1	-5700.336053	-5700.420758	-5700.435140	-5700.380590	-5700.253482
Conf2	-5700.358389	-5700.452012	-5700.473163	-5700.418286	-5700.290736
Conf3	-5700.345086	-5700.446222	-5700.475384	-5700.424748	-5700.304302
Conf4	-5700.323519	-5700.428033	-5700.459701	-5700.437299	-5700.303782

Ionization Potential (kJ/mol) (Vertical)

System	En. Diff.(CS^{3-}-CS^{4-})	En. Diff.(CS^{2-}-CS^{3-})	En. Diff. (CS^{1-}-CS^{2-})	En. Diff. (CS^{0}-CS^{1-})	En. Diff. (CS^{0}-CS^{4-})
Conf1	-222.39	-37.76	143.22	333.72	216.79
Conf2	-245.81	-55.53	144.08	334.89	177.62
Conf3	-265.53	-76.56	132.94	316.23	107.08
Conf4	-274.40	-83.14	58.82	350.55	51.82

Table **14**. Total energy in Ha and vertical ionisation energy in kJ/mol for the transition between different charged states $[(TaF_7)_2(Py_5)_4]$.

Total Energy (Ha)

System	Energy CS^{-4}	Energy CS^{-3}	Energy CS^{-2}	Energy CS^{-1}	Energie CS^{0}
Conf1	-5700.336053	-5700.424034	-5700.447283	-5700.404379	-5700.325008
Conf2	-5700.358389	-5700.455448	-5700.487386	-5700.448579	-5700.335233
Conf3	-5700.345086	-5700.449576	-5700.484621	-5700.445097	-5700.336778
Conf4	-5700.323519	-5700.431736	-5700.469489	-5700.437299	-5700.336136

Ionization Potential (kJ/mol) (Adiabatic)

System	En. Diff.(CS^{3-}-CS^{4-})	En. Diff.(CS^{2-}-CS^{3-})	En. Diff. (CS^{1-}-CS^{2-})	En. Diff. (CS^{0}-CS^{1-})	En. Diff. (CS^{0}-CS^{4-})
Conf1	-230.99	-61.04	112.64	208.39	29.00
Conf2	-254.83	-83.85	101.89	297.59	60.80
Conf3	-274.34	-92.01	103.77	284.39	21.81
Conf4	-284.12	-99.12	84.51	265.60	-33.12

Ta-Ta distance (Å)

System	Energy CS^{-4}	Energy CS^{-3}	Energy CS^{-2}	Energy CS^{-1}	Energie CS^{0}
Conf1	9.974	9.788	9.571	9.378	8.075
Conf2	8.876	8.624	8.353	7.578	7.409
Conf3	8.55	8.308	8.072	7.891	7.787
Conf4	7.672	7.422	7.233	7.066	6.937

Table **15**.Total energy in Ha and adiabatic ionisation energy in kJ/mol, and inter Ta distances for the transition between different charged states $[(TaF_7)_2(Py_5)_4]$.

Total Energy (Ha)

System	Energy CS^{-4}	Energy CS^{-3}	Energy CS^{-2}	Energy CS^{-1}	Energie CS^{0}
Conf1	-5700.336053	-5700.424034	-5700.447283	-5700.404379	-5700.325008
Conf2	-5700.358389	-5700.455448	-5700.487386	-5700.448579	-5700.335233
Conf3	-5700.345086	-5700.449576	-5700.484621	-5700.445097	-5700.336778
Conf4	-5700.323519	-5700.431736	-5700.469489	-5700.437299	-5700.336136

Binding Energy (kJ/mol)

System	Energy CS^{-4}	Energy CS^{-3}	Energy CS^{-2}	Energy CS^{-1}	Energie CS^{0}
Conf1	630.62	1383.26	1965.94	2374.94	2688.19
Conf2	689.26	1465.73	2071.23	2490.99	2715.04
Conf3	654.34	1450.32	2063.97	2481.84	2719.10
Conf4	597.71	1403.48	2024.24	2461.37	2717.41

Table **16**.Total energies in Ha and binding energies in kJ/mol for the different charged states $[(TaF_7)_2(Py_5)_4]$.

Chapter 6: Aggregates with solvent molecules

A further aspect of this work is the solution medium's influence on the storage of the heptafluorotantalate ions inside the polypyrrole. In this context, systems with water molecules as the most usual protic solvent were calculated: for these different configurations with two or four pentamers were considered, to which in the first case (2 chains) between 4 and 12 water molecules were added in random positions and in the second case (four chains) between 8 and 24 water molecules. Similarly, up to 14 acetonitrile molecules in random positions were added to get some insight on the influence of this aprotic solvent on the heptafluorotantalate/pentapyrrole aggregates. All systems were calculated using DFT using the exchange funtional BP86 with a third generation dispersion correction (BP+D3) in combination with a triple-zeta basis-set (def2-TZVP).

6.1 Structures and binding energies for $[(TaF_7)_2(Py_5)_2(H_2O)_x]^{4-}$ with x= 4,6,8,10,12

For each one of the three different conformations obtained for a system composed of two TaF_7^{2-} ions and two pentapyrrole chains (Py_5), groups of 4, 6, 8, 10, and 12 water molecules (WM) at randomly distributed positions were added. Here we show the results of the calculations done for each one of these conformations and how water affects them when the WM number is raised.

The first aggregate considered is that with two heptafluorotantalate anions in two immediately neighbouring pockets of two pentapyrrole chains (Figs **30**). Adding four WM leads to an interesting phenomenon: one of the WM inserts into a NH..F bridge, replacing it with one NH..O and two H..F contacts (cf. **30b**), and leading to an increase of the distance between the two Ta atoms from 9.2 to 10.8 Å. While such a WM insertion is not observed upon adding 6 WM, the resulting structure **30c** shows another interesting phenomenon: here a WM bridges the two anions, establishing a H..F contact with each of them. Similarly, ion-bridging WM are also observed in the structures with 8 (**30d**) and 10 WM (**30e**), where in the latter case additionally insertion of a WM into a former NH..F contact is found. Bridging WM obviously decrease the Ta..Ta distance to values between 8.6 and 8.1 Å (cf. Table 13.2). They thus help to make the distance between the Ta centers matching the "ideal pocket-pocket distance" of 7.1 Å as inferred in Chapter 4.1. In

structure **30d** the two pentapyrrole chains can more or less be considered as lying in the same plane, whereas this does not hold for the other aggregates. In particular, the aggregate with 12 WM (**30f**) is strongly distorted from the "unsolvated" aggregate **30a**: here the pentapyrrole chains themselves no longer retain a roughly planar geometry, and also the Ta..Ta distance elongates to 10.7 Å, which may be ascribed to the lack of bridging WM in this aggregate and the formation of individual solvation shells around each heptafluorotantalate ion. Yet, even in this case there is no complete detachment of the anions from their pockets, as indicated by the presence of "surviving" NH..F contacts.

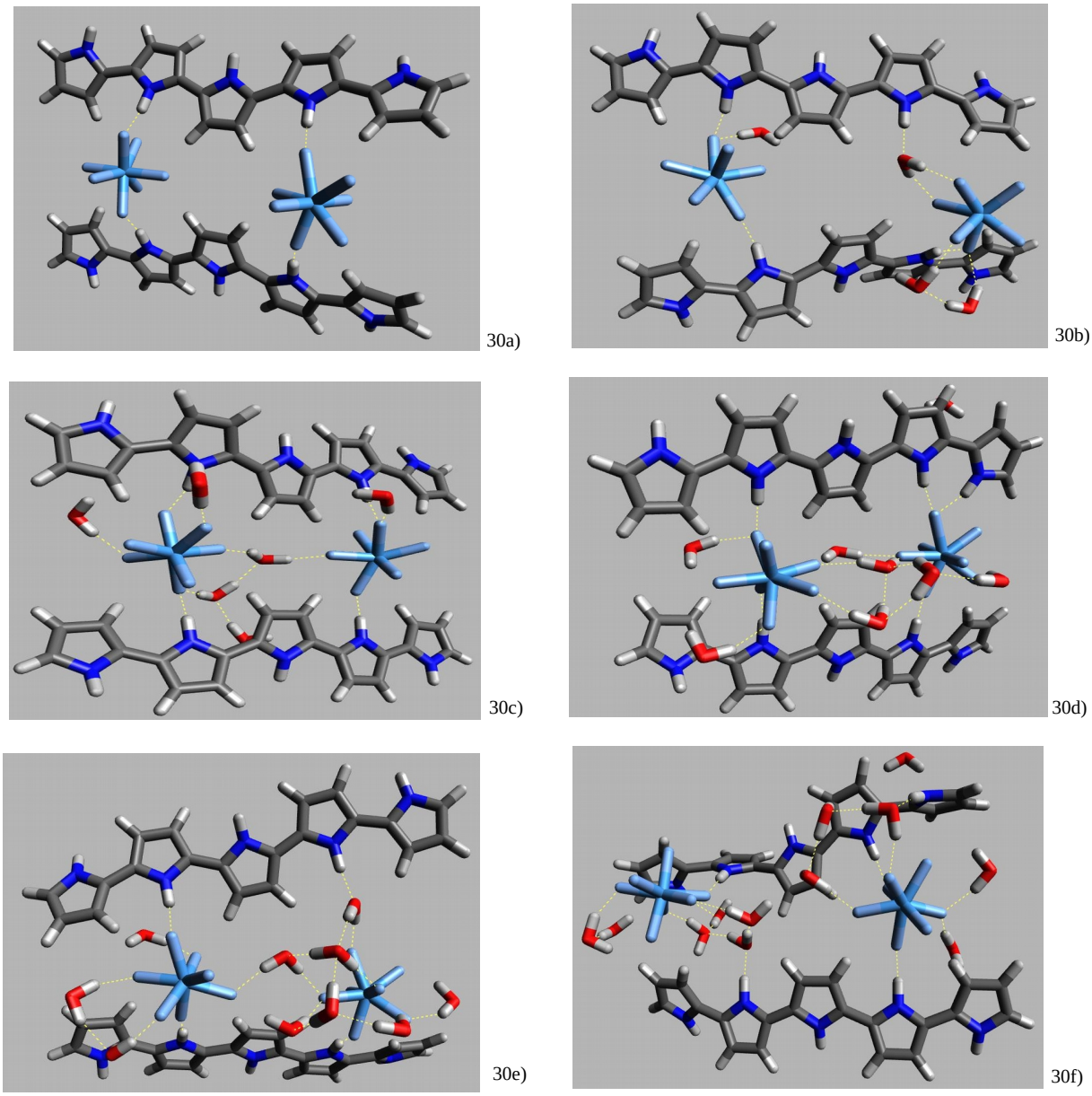

Figure **30**. Optimized structures for the first configuration with 2 Py_5-chains und 2 TaF_7^{2-} ions in this order: a) pure structure with b) 4 WM. 6 c), 8 d), 10 e) and 12 f) WM.

In the second aggregate to which WM were added the anions occupy two half-pockets on one chain and a half-pocket along with a full pocket on the other. Before addition of WM this leads to a Ta..Ta distance of 12.4 Å, which in nearly all of the solvated aggregates (cf. Fig. **31**) increases: from slightly (12.9 Å in **31f**) to drastically (17.2 Å in **31e**). It should be noted that in the aggregates with the largest Ta..Ta distances, i.e., **31d** and **31e**, a WM has inserted in the NH..F contact of the former "full" pocket, allowing the second anion to partially move out of the full pocket towards the end of the corresponding pentapyrrole chain. In the only aggregate with a decreased Ta..Ta distance upon solvation, i.e., structure **31c**, a WM occupying a full pocket in the middle position of one of the chains establishes a hydrogen bridge to one of the heptafluorotantalate ions, thus pulling the latter a little bit towards ths other anion.

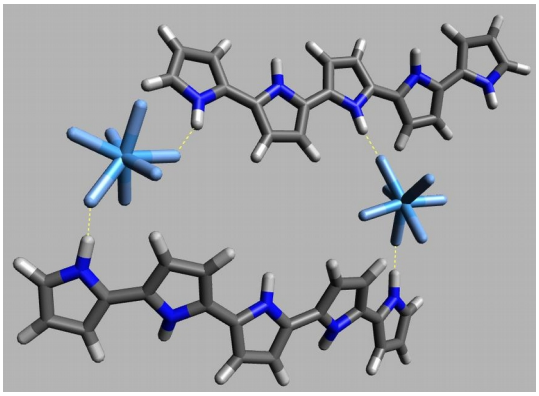

31a)

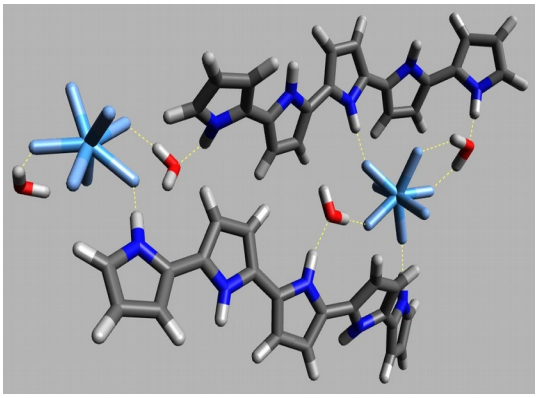

31b)

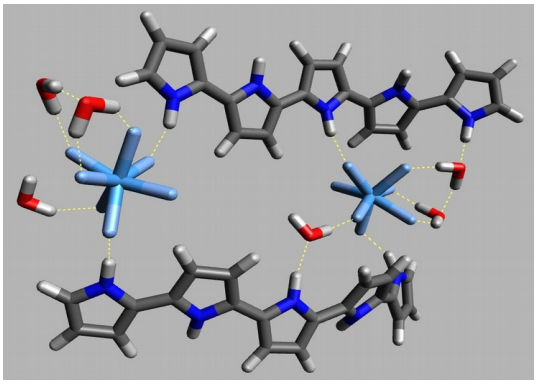

31c)

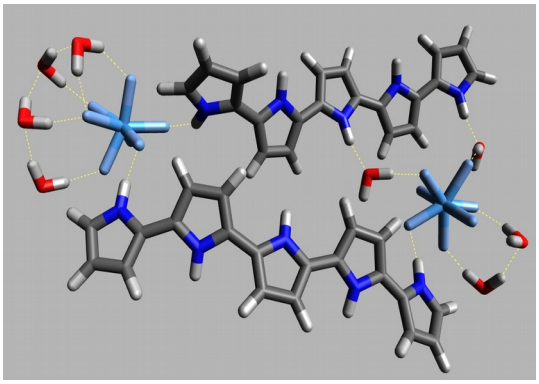

31d)

Figure **31**. Optimized structures for the second configuration with 2 Py_5-chains und 2 TaF_7^{2-} ions in this order: pure structure a) , with b) 4 6 c) and 8 d).

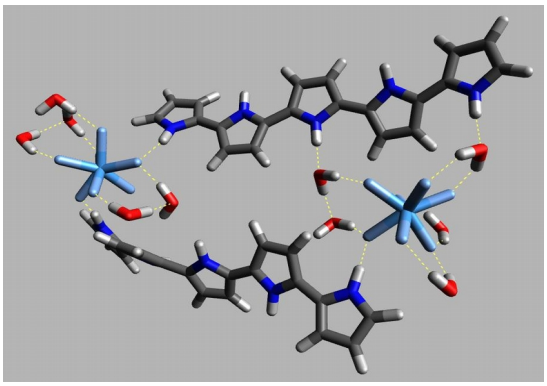
31e)

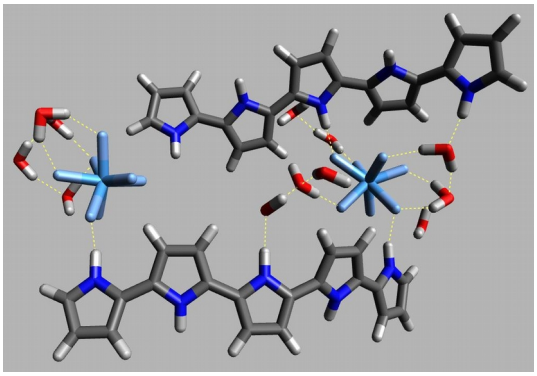
31f)

Figure **31.2**. Optimized structures for the second configuration with 2 Py_5-chains und 2 TaF_7^{2-} ions in this order: 10 e) and 12 WM f).

In the third of the considered aggregates between two pentapyrrole chains and two anions the latter occupy half-pockets only, meaning that in the unsolvated structure they display a fairly large Ta..Ta distance of 17.9 Å (cf. **32a**). Adding four WM increases this distance by more than 1 Å, due to a combination of an insertion of a WM molecule into a NH..F bridge and an out-of-plane bending of one of the chains (cf. **32b**). This bending allows for the establishment of an OH..π bridge between a pyrrole unit in one chain and a WM occupying a full pocket in the other chain. Such a bending does not occur upon addition of 8 and 10 WM, respectively (cf. **32c** and **32d**).

These structures rather display the possibility of inserting several water molecules between the anions, completed to a chain of 5 WM with an uninterrupted hydrogen bridge network between them and the anions in case of structure **32d**. In both cases the Ta..Ta distance reduces by about 0.8 Å as compared to the unsolvated aggregate. Neither the aggregates with 10 (**32e**) nor with 12 WM (**32f**) display such a perfect hydrogen-bridged WM chain between the anions, but they demonstrate that the accumulation of a number of WM between the anions is possible without strongly affecting the Ta..Ta distance.

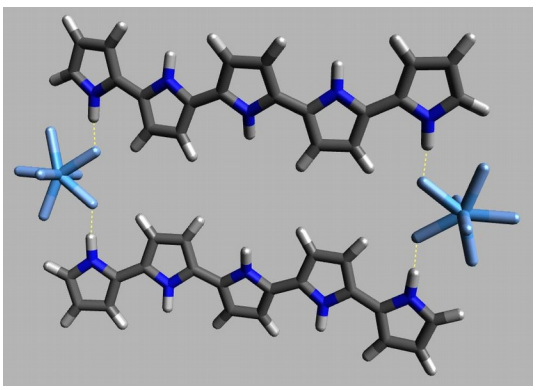
32a)

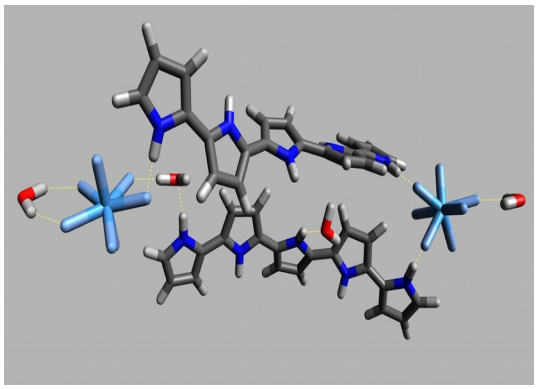
32b)

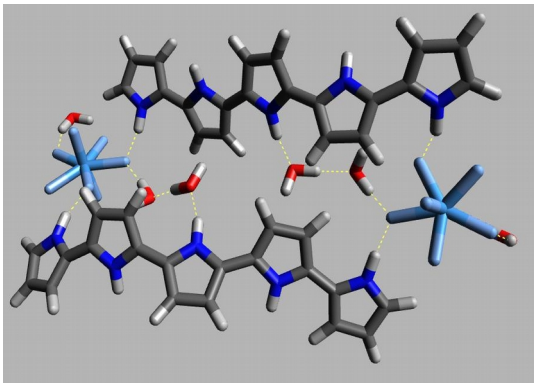
32c)

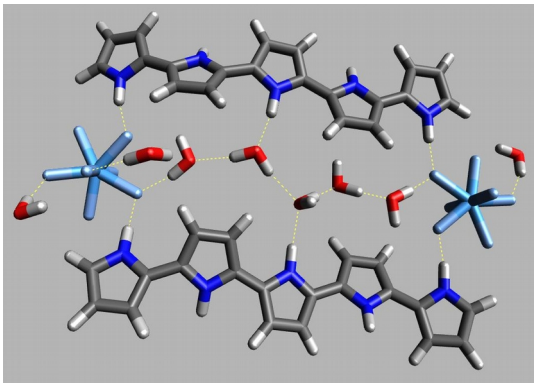
32d)

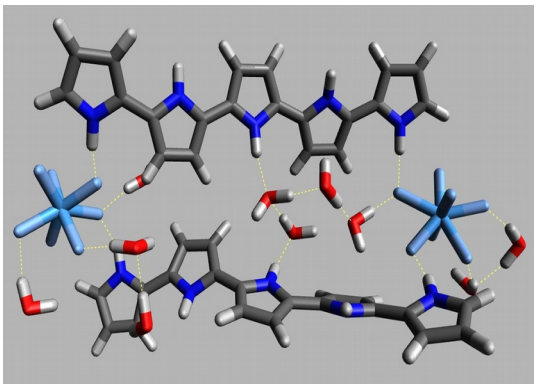
32e)

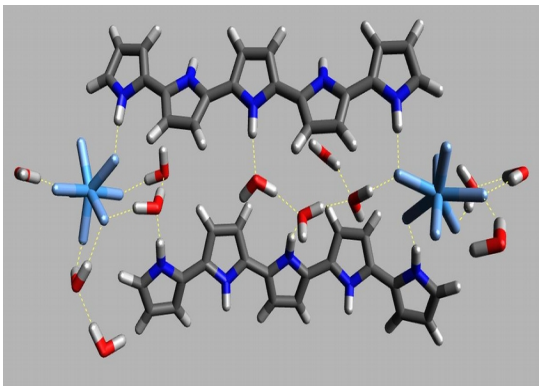
32f)

Figure **32**. Optimized structures for the third configuration with 2 Py_5-chains und 2 TaF_7^{2-} in this order: pure structure a), with b) 4 WM. 6 c), 8 d), 10 e) and 12 WM f).

Total Energy (Ha)

System	Fig. 30	Fig. 31	Fig. 32
a	-3606.898710	-3606.933162	-3606.988499
b	-3912.890460	-3912.960577	-3912.976770
c	-4065.874336	-4065.945442	-4065.972792
d	-4218.882182	-4218.965719	-4218.963421
e	-4371.872974	-4371.945230	-4371.955380
f	-4524.877282	-4524.903341	-4524.933982

Binding Energy (kJ/mol)

System	Fig. 30	Fig. 31	Fig. 32
a	47.03	137.48	282.76
b	367.87	551.96	594.47
c	496.78	683.47	755.28
d	688.63	907.96	901.93
e	835.71	1025.42	1052.07
f	1018.27	1086.69	1167.14

Ta-Ta distance (Å)

System	Fig. 30	Fig. 31	Fig. 32
a	9.20	12.44	17.94
b	10.80	14.53	19.18
c	8.62	11.80	17.16
d	8.33	16.17	17.14
e	8.11	17.16	17.72
f	10.67	12.88	18.17

Table **17**. Total energy, binding energy values and Inter Ta distances for different configurations.

The binding energy of an aggregate here is defined as the energy required to dissociate an aggregate into its individual constituents, i.e., isolated anions, oligopyrrole chains and solvent molecules. While it is clear that total energies of aggregates must increase with the number of added WM, one would also expect an increase in the corresponding binding energies, due to the interactions of the WM with anions, oligopyrrole chains, and other WM. Table **17** demonstrates that this is indeed the case. Averaging over all of the aggregates each individual WM is seen to add about 83 kJ/mol to the total binding energy. The most significant excpetions to this are found for aggregate 31b with 104 kJ/mol per WM and aggregate 32f with 74 kJ/mol per WM.

6.2 Structures and binding energies for $[(TaF_7)_2(Py_5)_4(H_2O)_x]^{4-}$ with x= 8,12,16,20,24

Following a similar protocol as in the previous section next the influence of solvent molecules on aggregates consisting of two heptafluorotantalate anions and four pentapyrrole chains was investigated. Due to the increased size of the aggregates, now more WM were added, i.e., between 8 and 24, this time in steps of four WM.

There is one stack of π-π interacting pentapyrrole chains in the first of the considered structures (Fig. **33**) while the two other pentapyrrole chains of the aggregate do not interact directly with each other. This basically does not change upon the addition of an increasing number of WM, yet the details of the geometric arrangement of the chains are significantly influenced. For example, in the aggregate with 8 WM a terminal dipyrrole unit of one of the π-stacked chains rotates to enable a bridging WM between an NH group and one of the anions (cf. **33b**). This WM in **33c** (12 WM) is replaced by a small "network" of two WM terminating in the π system of a pyrrole unit belonging to another chain, while in **33d** (16 WM) the terminus of the "2 WM network" is the anion, each time provoking a change in the relative orientation of the terminal two pyrrole units with respect to the remaining three pyrrole units. Perhaps the most significant changes, however, are observed for the aggregates with 20 (**33e**) and 24 (**33f**) WM: in **33e** the π-stacked pentapyrrole chains partially assume a curved conformation in order to maximize their participation in hydrogen bond networks while maintaining their stacking, and in **33f** the π-stacked arrangement (which usually involves three pyrrole units from each chain) is even partially dissolved (now involving only two pyrrole units from each chain) in favour of H bond network participation. All in all, the distances between the anions are not too strongly influenced by the number of WM, falling into the range of about 9.8 to 10.6 Å, with exception of aggregate **33e** where it drops to 8.5 Å, (cf. Table **18.2**), presumably due to the curvature of the π-stacked chains observed here.

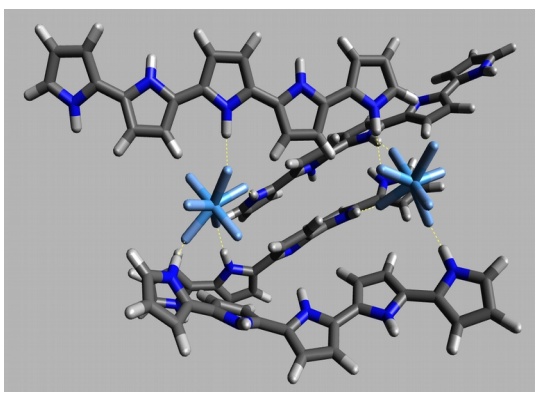

33a)

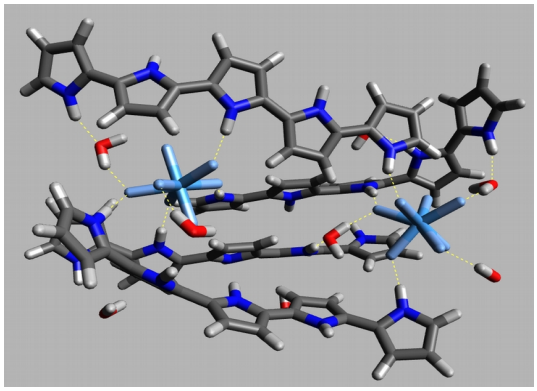

33b)

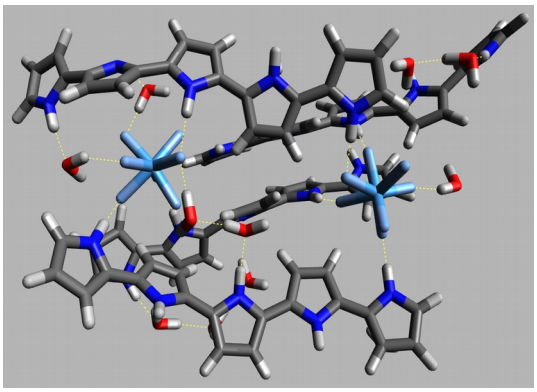

33c)

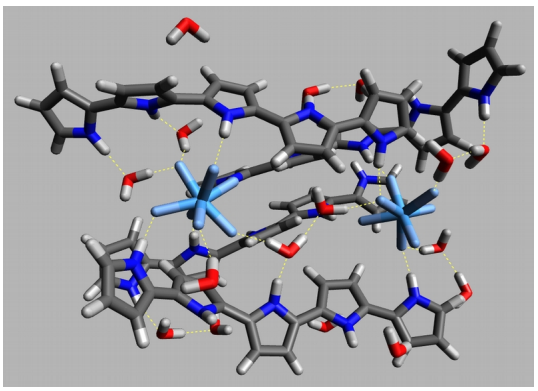

33d)

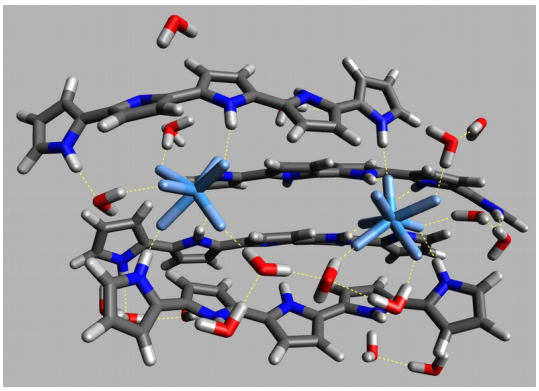

33e)

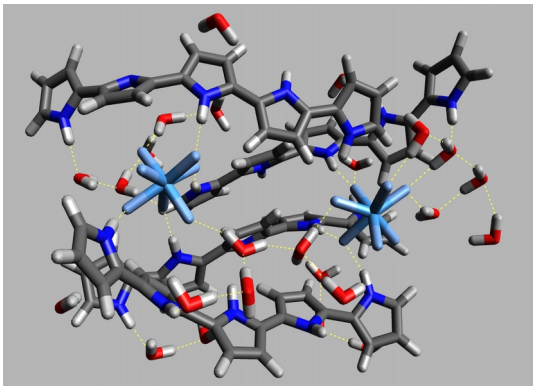

33f)

Figure **33**. Optimized structures for the first configuration with 4 Py_5-chains und 2 TaF_7^{2-} in this order: pure structure a) 8 b), 12 c), 16 d), 20 e) and with 24 f) WM.

In the second aggregate considered here one observes two stacks of parallel pentapyrrole chains. This arrangement seems to be relatively stiff when it comes to changes of the geometry provoked by WM (cf. Fig. **34**): the aggregates from 8 to 24 added WM show only minor modifications of the chain geometry, suggesting an overall greater importance of π-stacking in comparison to the hydrogen bridges. In this type of aggregate, a significant portion of the WM attaches to the pentapyrrole chains, rather than to the anions, and the dependence of the Ta..Ta-distance on the number of attached WM is

somewhat stronger as that observed for the previous aggregate: it varies between 8.1 and 10.0 Å (cf.Table **18.2**).

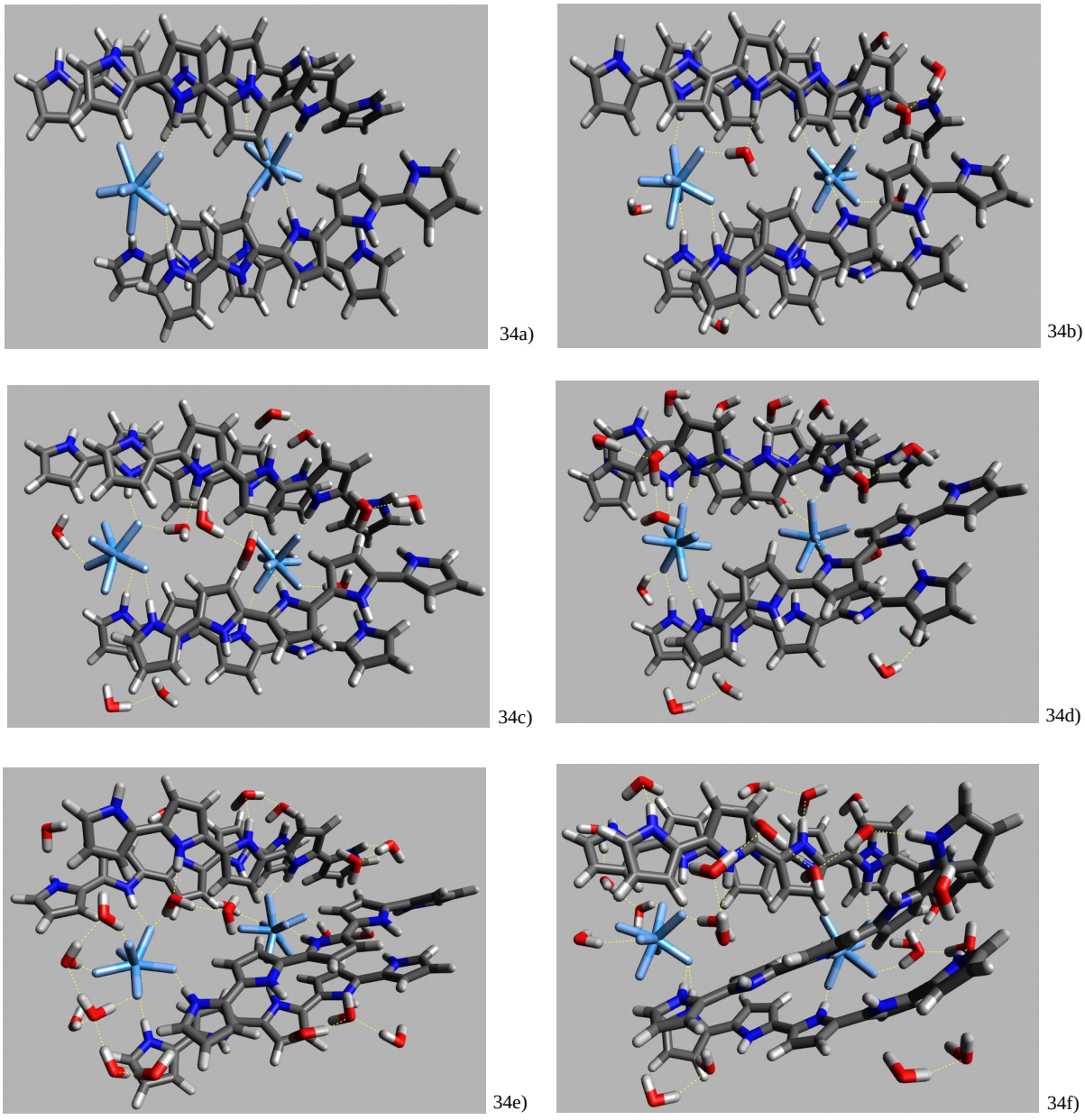

Figure **34**. Optimized structures for the first configuration with 4 Py_5-chains und 2 TaF_7^{2-} in this order: pure structure a) 8 b), 12 c) and 16 d) 20 e) and with 24 f) WM.

The third of the aggregates considered here can also be described as containing two stacks of Py5 chains, linking the two anions. Again, no qualitative changes of this situation are found upon adding more and more WM (cf. Fig. **35**). Here, however, the WM tend to form solvation shells around the anions and in some cases even "bridging" networks

involving both anions (cf. **35b** and **35d**). Still, the Ta..Ta distances with 8.0 - 9.8 Å are very similar to those found for the second aggregate.

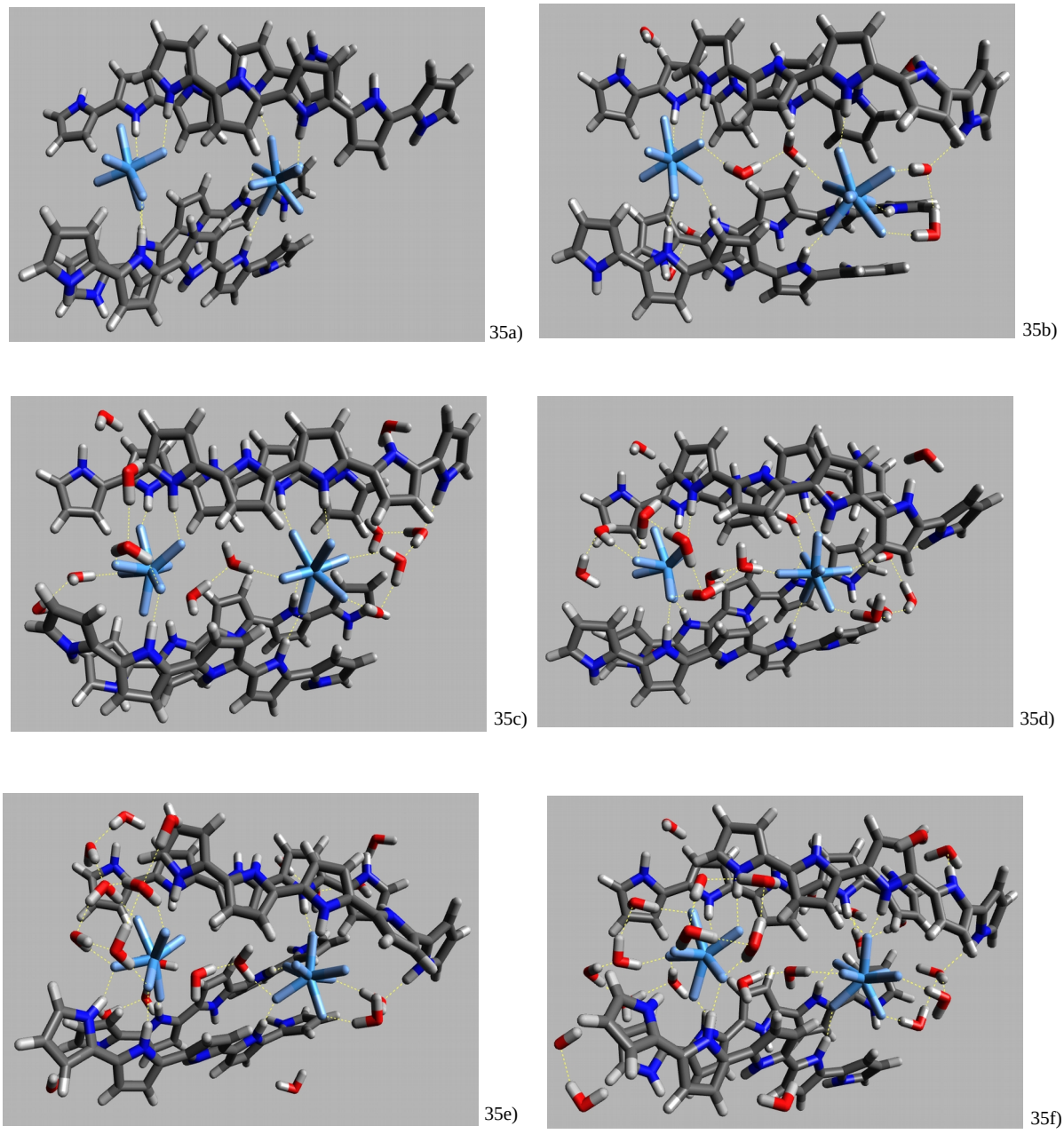

Figure **35**. Optimized structures for the first configuration with 4 Py_5-chains und 2 TaF_7^{2-} in this order: pure structure a) 8 b), 12 c), and 16 d) 20 e) and with 24 f) WM.

The final aggregate resembles the first aggregate in that there is a single stack consisting of Py5 chains and two further chains with no direct contact. However it differs strongly in the Ta..Ta distance when no WM are added: with 7.7 Å in **36a** it is 2.2 Å shorter than in **33a** (cf. Table **18.2**). The increased flexibility of the chain arrangement as compared to the

aggregates shown in Figs. **34** and **35** is clearly visible in rotations of pyrrole units. The relatively short distance between the anions is kept in most of the aggregates where WM were added, ranging from 7.4 Å in **36d** to 7.9 Å in **36c** (cf. Table **18.2**). The only exception is structure **36f**, where the Ta..Ta distance becomes 8.4 Å, presumable due to the rotation of a terminal pyrrole unit in one of the π-stacked chains which to some extent destroys the corresponding pocket conformation.

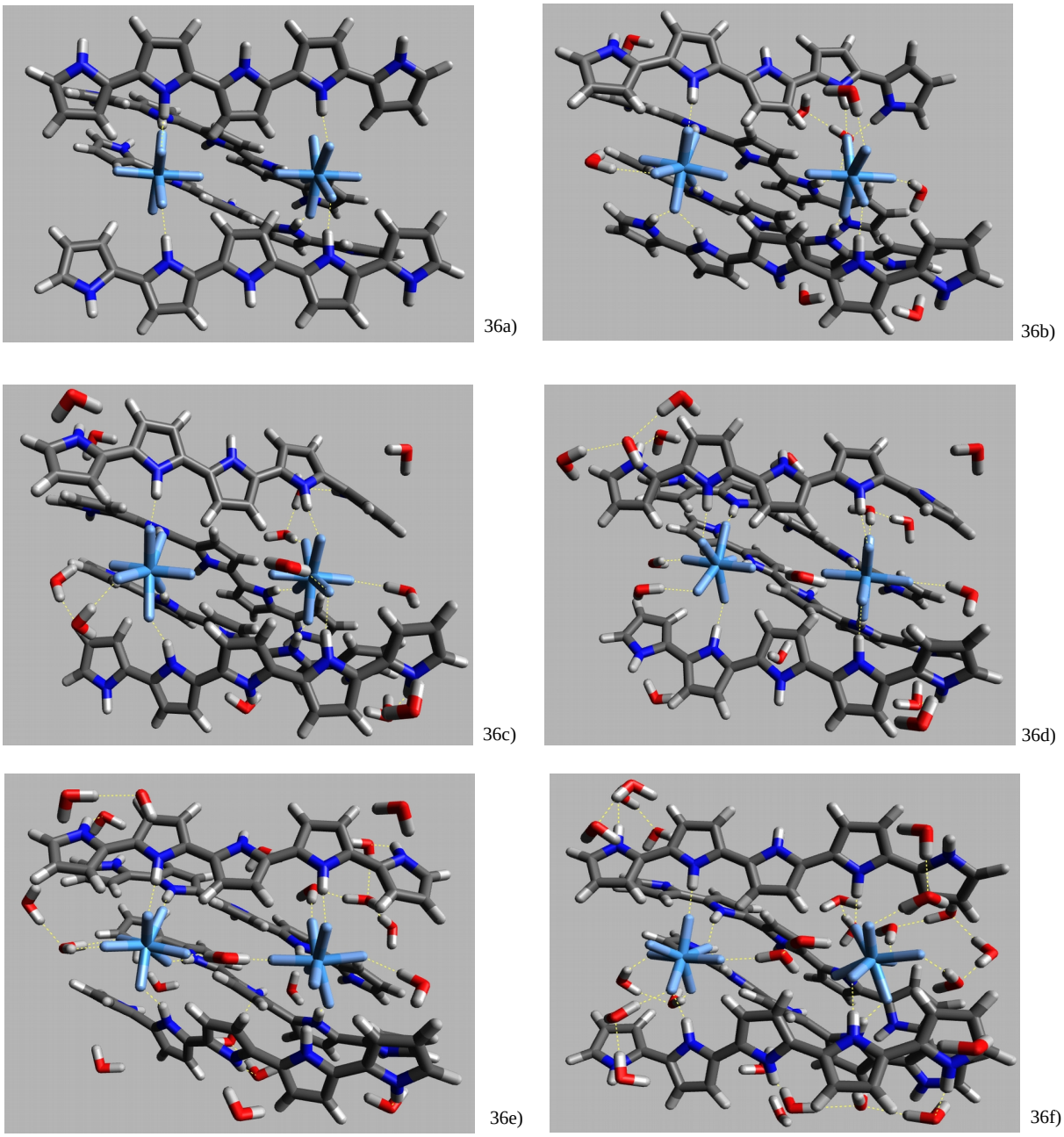

Figure **36**. Optimized structures for the first configuration with 4 Py_5-chains und 2 TaF_7^{2-} in this order: pure structure a) 8 b), 12 c), 16 d), 20 e) and with 24 f) WM.

From the binding energies shown in Table **18.1** one may calculate average binding energies for each water molecule by substracting the corresponding aggregates binding energy as determined without water molecules from that for a number n of WM and dividing the result by n, as it has already been done in the previous discussion of Table **17** in Chapter **6.1**. The binding energy per WM as obtained by averaging over all aggregates now is found to amount to 73 kJ/mol, i.e., it is reduced by about 10 kJ/mol as compared to the corresponding number for the smaller aggregates. This reduction is likely due to the fact that in the larger aggregates considered here a larger number of the WM are found at larger distances from the heptafluorotantalate ions. These WM usually are rather attached to the pyrrole chains and the interaction with the pyrrole chains must be weaker since it is not of ion-dipole character. Note that also the spread of the average WM binding energies for the individual aggregates is reduced in comparison to the smaller aggregates: the lowest value of 65 kJ/mol now is found for aggregate **36d**, and the highest value of 87 kJ/mol for aggregate **36b**.

Total Energy (Ha)

System	Fig. 33	Fig. 34	Fig. 35	Fig. 36
a	-5700.336053	-5700.358389	-5700.345086	-5700.323519
b	-6312.324758	-6312.328374	-6312.315063	-6312.326470
c	-6618.272800	-6618.296222	-6618.274931	-6618.263286
d	-6924.260068	-6924.260997	-6924.251227	-6924.197900
e	-7230.273031	-7230.252339	-7230.256695	-7230.215450
f	-7536.215535	-7536.229227	-7536.201803	-7536.189272

Binding Energy (kJ/mol)

System	Fig. 33	Fig. 34	Fig. 35	Fig. 36
a	630.62	689.26	654.34	597.71
b	1285.97	1295.46	1260.51	1290.46
c	1492.06	1553.55	1497.65	1467.08
d	1801.13	1803.57	1777.92	1637.91
e	2177.67	2123.34	2134.78	2026.49
f	2369.21	2405.16	2333.16	2300.26

Table **18.1**. Total energy in Ha for different oxidation states and binding energy values in kJ/mol, for different configurations.

Ta-Ta distance (Å)

System	Fig. 33	Fig. 34	Fig. 35	Fig. 36
a	9.974	8.876	8.550	7.672
b	10.585	9.802	9.791	7.728
c	10.637	9.888	8.176	7.875
d	9.834	8.083	7.960	7.360
e	8.477	9.011	8.260	7.728
f	9.865	10.007	8.313	8.395

Table **18.2**. Inter Ta distances for different configurations.

6.3 Structures and binding energies for $[(TaF_7)_2(Py_5)_x(CH_3CN)_y]^{4-}$ with x=2,4 y=4,6,8,10,12,14

Given the fact that the experimental studies were carried out using acetonitrile (ACN) as a solvent, geometry optimizations of representative heptafluorotantalate-oligopyrrole aggregates with added ACN molecules were undertaken. In contrast to water, ACN is a nonprotic solvent. Thus it cannot act as a hydrogen bridge donor. However, it may accept hydrogen bridges from the NH groups of pyrrole units. More importantly, the dipole moment of ACN is 3.92 D[64] and thus more than double than the 1.85 for a WM.[65] As a consequence, ion-dipole interactions are expected to play a more important role than in the water-solvated aggregates considered hitherto. As before, first the influence of solvent molecules on three aggregates of two pentapyrrole chains and two anions was studied, adding 4-12 ACN molecules in steps of two.

The structures of the first series of aggregates displayed in Fig.37 clearly indicate the importance of the ion-dipole interactions: in all of them most of the ACN molecules orient their positive ends, i.e. their methyl groups, towards one of the anions. Since the anions in this series of aggregates are relatively close together (Ta..Ta distances between 8.0 and 9.5 Å according to Table 19), the ACN molecules sometimes also seem to orient their positive end towards a point in between the two anions (cf., for example, ACN molecules in the foreground of **37e** and **37f**). The attachement of ACN molecules has a strong effect on the pyrrole chains: already with four ACN molecules significant deviations from planarity are observed for one of the chains, and with increasing numbers of ACN molecules these deviations become stronger and affect both chains. The structural influence of WM in the same kind of aggregate was less dramatic (cf. Fig. 30), which can certainly be attributed to the smaller size of the WM: when a much more voluminous ACN

molecule is pulled towards an anion, it may have to push a pyrrole unit out of its way, as a consequence of steric repulsion (a.k.a. exchange-overlap interactions).

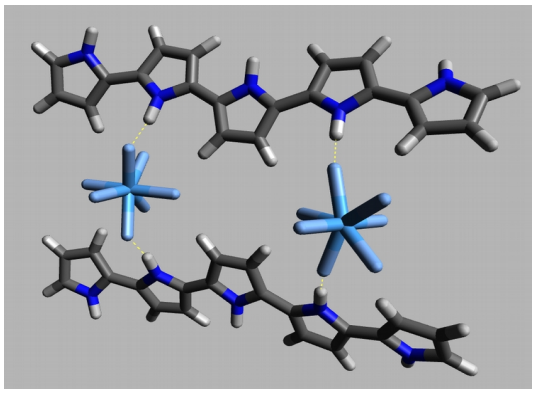

37a)

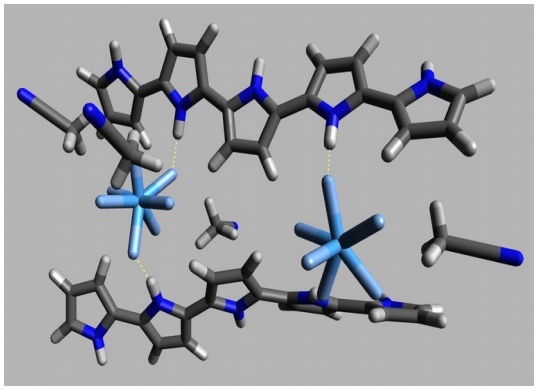

37b)

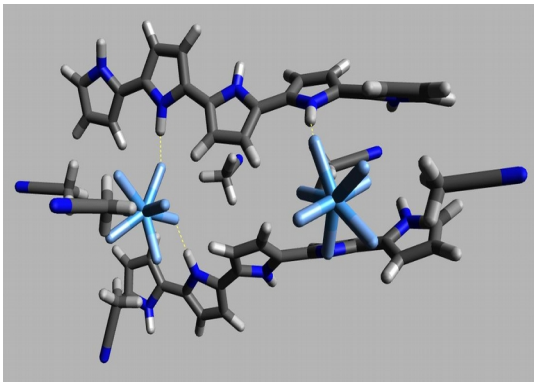

37c)

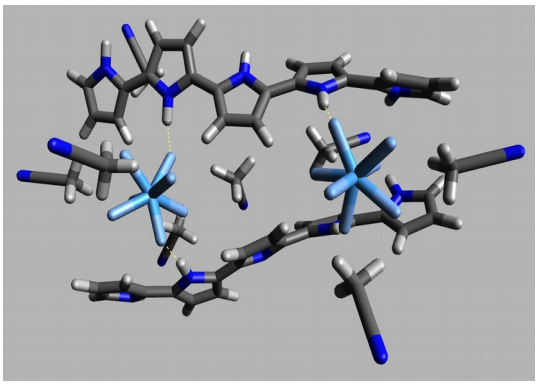

37d)

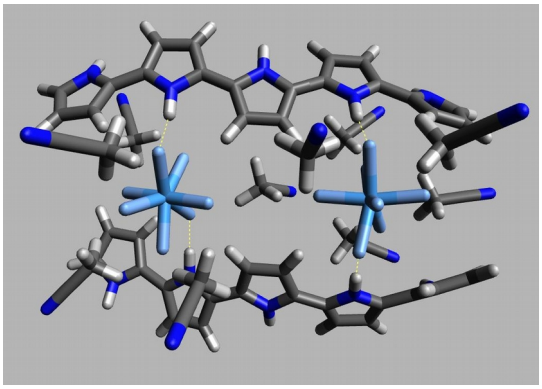

37e)

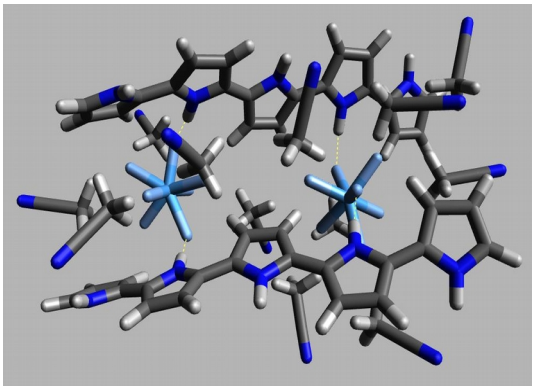

37f)

Figure **37**. Optimized structures for the first configuration with 4 Py_5-chains und 2 TaF_7^{2-} in this order: pure structure a), b) 4, 6 c), 8 d), 10 e) and with 12 f) ACN molecules.

The overall structure of the second of the considered aggregates (cf. Fig. 38) in most cases is conserved upon adding ACN molecules, in the sense that both chains stay at opposite sides of the anions, with more or less strong deviations from chain planarity. This may be explained by the fact that the two tantalate ions are fairly exposed in this type of aggregates so that the ACN can easily access them with their positive ends, i.e., the

methyl groups. Occasionally hydrogen bridges between a pyrrole NH group and the N atom of ACN are observed, as in aggregates **38b** and **38f**. A noteworthy exception to the series is aggregate **38d**, where 8 ACN molecules were added: here one of the chains completely detaches from one of the anions which, however, is still linked to the other chain, and accomodates three ACN molecules at its exposed side. As a consequence the interion distance grows to 17.9 Å, whereas in the remainig structures of the series it varies in the small interval between 11.7 and 12.6 Å (cf. Table **14**).

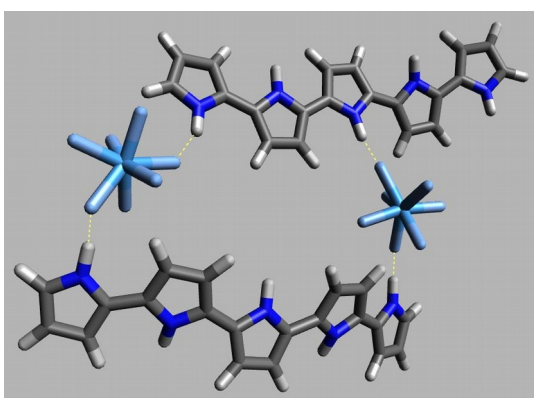

38a)

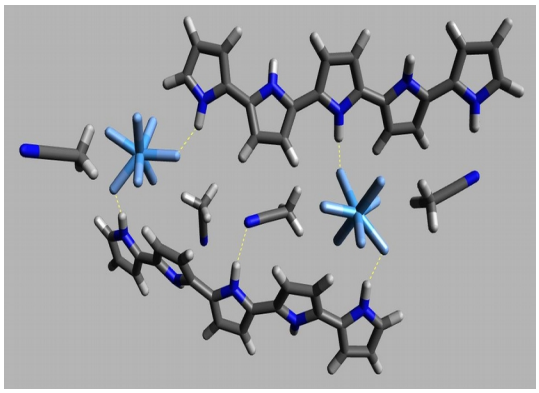

38b)

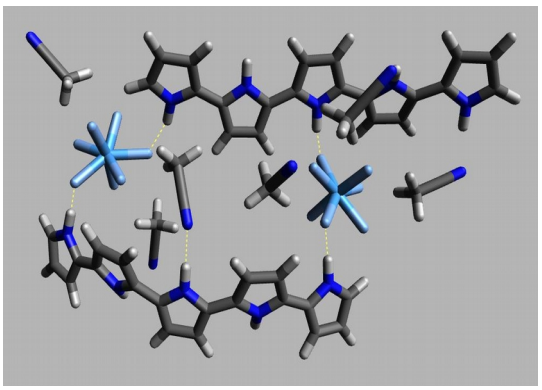

38c)

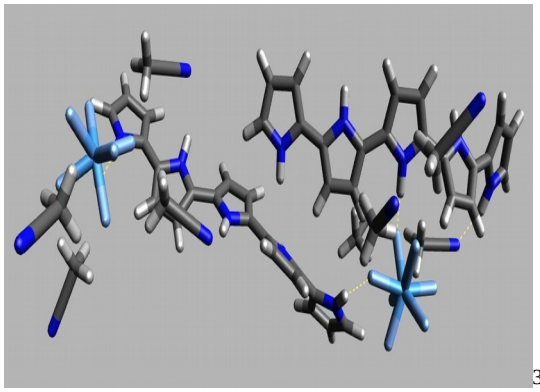

38d)

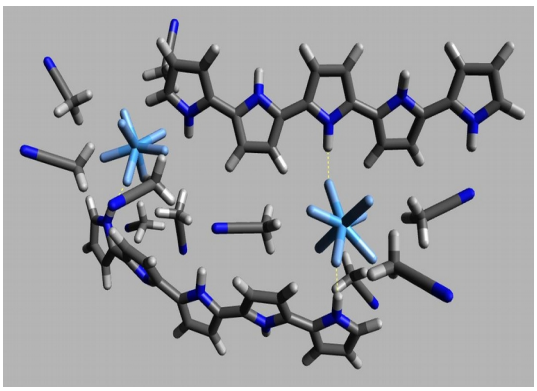

38e)

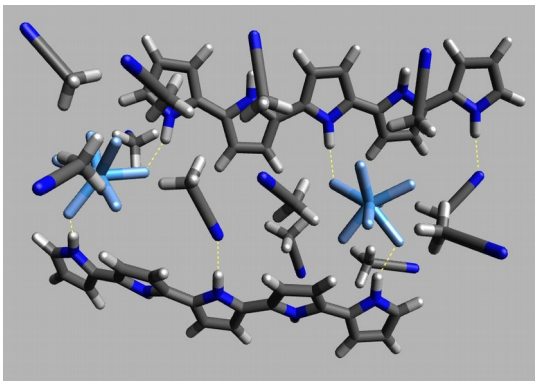

38f)

Figure **38**. Optimized structures for the first configuration with 4 Py_5-chains und 2 TaF_7^{2-} in this order: pure structure a), b) 4, 6 c), 8 d), 10 e) and with 12 f) ACN molecules.

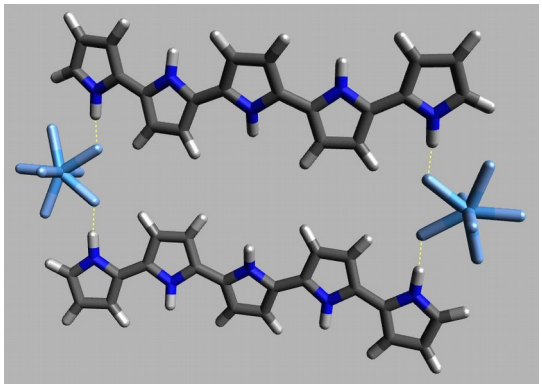
39a)

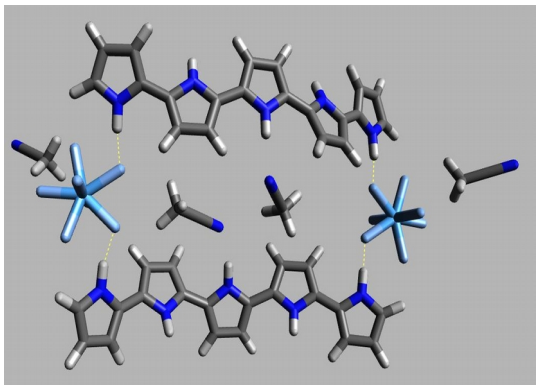
39b)

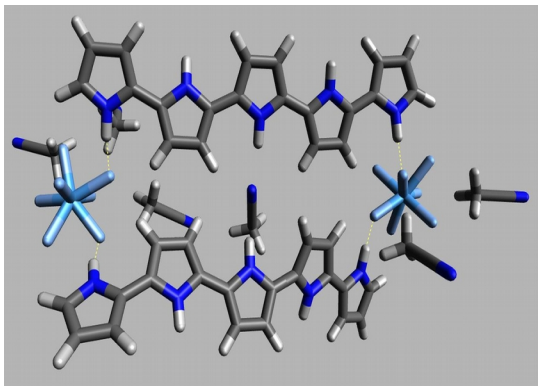
39c)

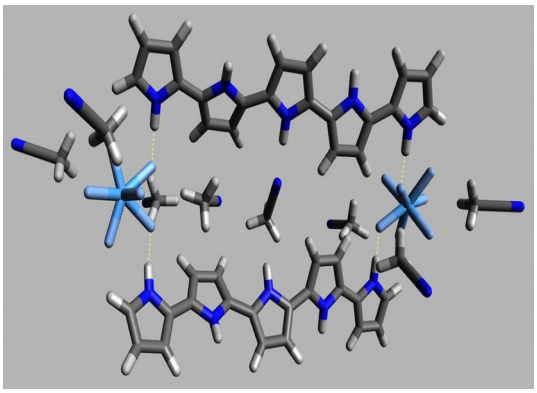
39d)

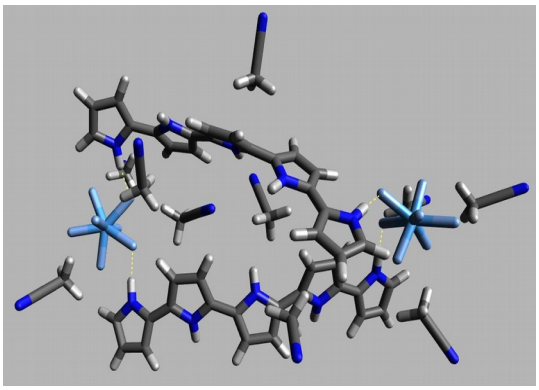
39e)

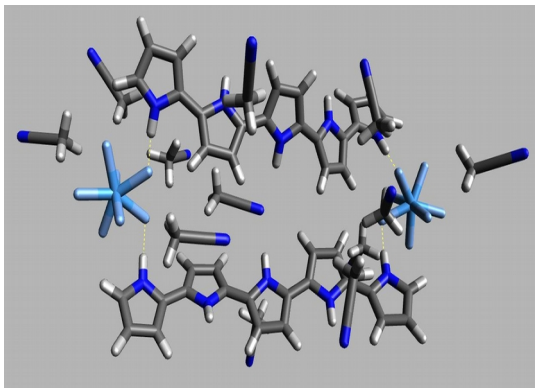
39f)

Figure **39**. Optimized structures for the first configuration with 4 Py_5-chains und 2 TaF_7^{2-} in this order: pure structure a), b) 4, 6 c), 8 d), 10 e) and with 12 f) ACN molecules.

Total Energy (Ha)

System	Fig. 37	Fig. 38	Fig. 39
a	-3606.898710	-3606.933162	-3606.988499
b	-4138.303957	-4138.334727	-4138.358172
c	-4404.013439	-4404.033802	-4404.051406
d	-4669.703942	-4669.735977	-4669.727422
e	-4935.384829	-4935.405545	-4935.399540
f	-5201.079811	-5201.077349	-5201.073330

Binding Energy (kJ/mol)

System	Fig. 37	Fig. 38	Fig. 39
a	47.03	137.48	1090.31
b	450.71	531.50	1636.34
c	670.57	724.03	1813.54
d	840.59	924.70	1945.52
e	985.37	1039.75	2067.27
f	1167.15	1160.68	2193.42

Ta-Ta distance (Å)

System	Fig. 37	Fig. 38	Fig. 39
a	9.195	12.44	17.935
b	9.342	12.064	16.893
c	9.524	11.686	17.476
d	9.333	17.866	17.418
e	8.024	12.646	17.052
f	8.16	12.073	17.935

Table **19**. Total energy, binding energy and inter ionic distances for different structures of $[(TaF_7)(Py_5)_2ACN_n]^{2-}$

In the third aggregate series the heptafluorotantalate ions are 17.9 Å apart when no ACN molecules are present, and this distance in general it reduces by addition of ACN molecules: while the Ta..Ta distance is kept at 17.9 Å when 12 ACN molecules are present, it is only 16.9 Å with four ACN molecules, with the other cases lying in between (Table 14). The large distance between the anions certainly helps in keeping the overall aggregate structure intact, i.e. all of the structures have both pentapyrrole chains linked to the anions with their chain ends through NH..F hydrogen bridges, and the chains are roughly opposing each other. A larger structural distortion is observed for aagregate **39e**, with one of the chains severely twisting to produce a kind of hemi-helical arrangement. As before, most of the ACN molecules orient their methyl groups towards one of the anions, while the strong chain twist of structure **39e** may be attributed to an ACN molecule with an NH..N bridge to one of the chains and CH_3..π interaction to the other.

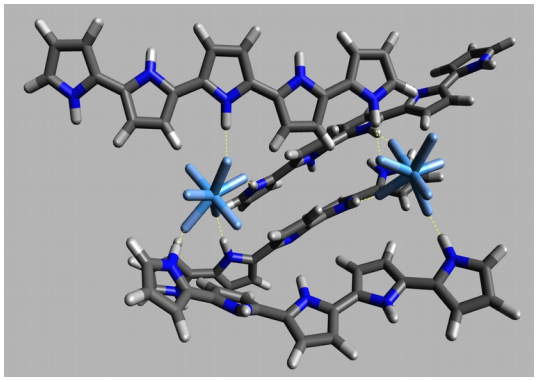

40a)

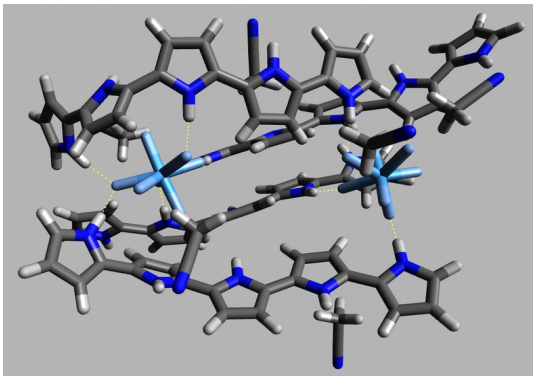

40b)

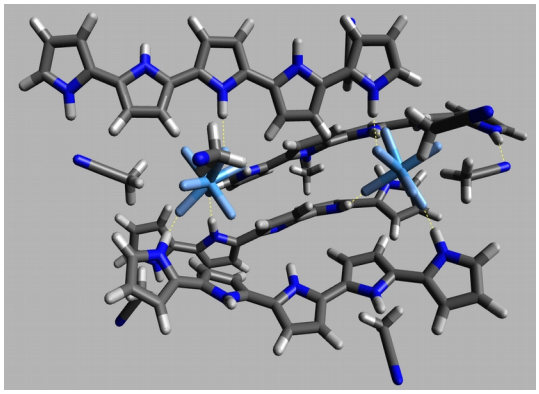

40c)

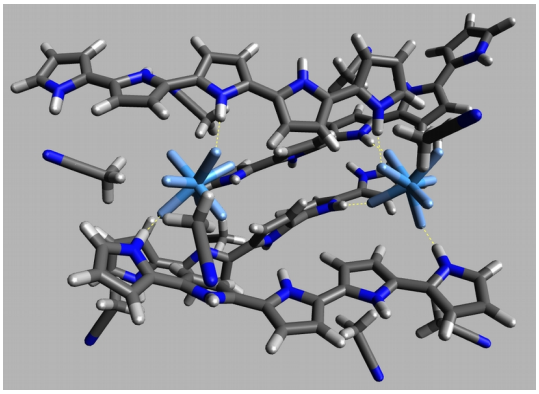

40d)

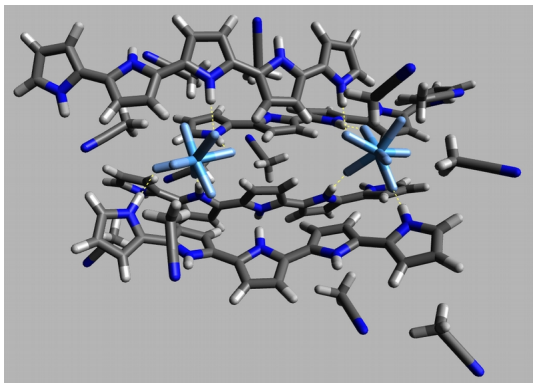

40e)

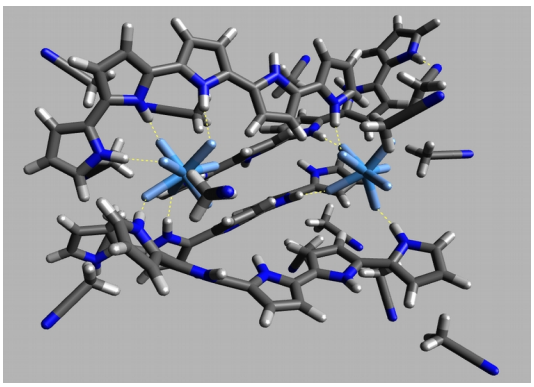

40f)

Figure **40**. Optimized structures for the first configuration with 4 Py_5-chains und 2 T-ions in this order: pure structure a), 6 b), 8 c), 10 d), 12 e) and with 14 f) ACN.

It is interesting to compare the average binding energies of ACN molecules as a function of their number with the corresponding values for water molecules. These average binding energies were calculated in complete analogy to those for water, by substracting the total aggregate binding energy including ACN molecules (cf. Table 14) from that of the corresponding aggregate without ACN and dividing by the number of ACN molecules. Again, this number obviously includes energy contributions from restructuring of the anion-oligopyrrole aggregate, besides accounting for energetic consequences of interactions of the ACN dipoles with the anions or the pyrrole chains and dipole-dipole

interactions between the ACN molecules, etc. While the average WM binding energy was found to vary between 74 and 104 kJ/mol for the analogous aggregates of two anions and two pentapyrrole chains (cf. Chapter 6.1) and did not display any clear trends with increasing numbers of WM, this is completely different for the ACN microsolvated aggregates. Here each added ACN molecule lowers the average ACN binding energy: from 99 - 137 kJ/mol for 6 ACN molecules down to 33 - 46 kJ/mol for 14 ACN molecules, where in each case the highest binding energies are found for the structures shown in Fig. 39 and the lowest for those of Fig. 38, while those for the aggregates shown in Fig. 37 agree within 1 - 2 kJ/mol with the latter. While in the case of water solvation additional WM may attach to to a hydrogen bridge network without strong disturbances this is not the case for ACN molecules: for the small numbers of ACN molecules considered here each additional ACN molecule is likely to orient its positive end towards one of the anions, meaning that unfavourable dipole-dipole interactions with other ACN molecules orienting themselves to the same anion must come into play.

System	Total Energy	Binding Energy	Ta-Ta Distance
40a	-5700.336053	630.618489	9.974
40b	-6497.409675	1146.234575	9.776
40c	-6763.080210	1263.830591	9.519
40d	-7028.760459	1406.931354	9.980
40e	-7294.449266	1572.502942	9.385
40f	-7560.128613	1713.234405	9.469

Table **20**. Total energy in Ha, binding energy in kJ/mol and inter ionic distances in Å for this configuration.

Fig. 40 shows the outcome of geometry optimizations for a series of aggregates consisting of two anions and four pentapyrrole chains. Starting from the aggregate 40a now 6 - 14 ACN molecules were added in steps of two. As demonstrated in Table 15, the number of ACN molecules has a minor influence on the Ta...Ta distance, which varies between 9.4 Angstron for the aggregate with 12 ACN molecules and 10 Å for those with 10 or 0 ACN molecules, respectively. In most of the structures two of the pentapyrrole chains keep in a parallel pi-stacked arrangement while the remaining chains are not in close contact. Structure **40e** (12 ACN molecules) represents an exception: here the pi-stacked arrangement is loosened up to some degree to enable a contact of the methyl end of an ACN molecule with the pi-system of a pyrrole unit. Since evidently the anions are better "shielded" by four Py5 chains than they can be by only two chains, the ACN molecules are less likely to find their place close to an anion, and the number of

interactions between the pyrrole chains and ACN molecules such as through NH..N bridges or CH3..π contacts increases. On the other hand, this also means a reduced number of unfavourable dipole-dipole interactions between ACN molecules orienting towards the same anion. As a consequence, the average binding energy of an ACN molecule is fairly similar to that discussed before for the smaller aggregates: with 6 ACN molecules it amounts to 86 kJ/mol, and drops over 64, 53, and 43 to 37 kJ/mol with each added pair of ACN molecules, based upon the total binding energies shown in Table 20.

Chapter 7: Charged aggregates with solvent molecules

Taking into account that the polypyrrole chains in the material interact in a liquid medium while they function as charge carriers, in a final set of calculations the various aggregates considered so far were submitted at the same time to different oxidation states and the prescence of different groups of solvent molecules. Thus, we took the optimized structures from the previous chapter and calculated them with various total charges, limiting the number of positive charges per oligopyrrole chain to one for the sake of computational stability. Following this idea, the systems with two TaF_7^{2-} ions and two chains begin with a total charge of -4 (no chain oxidised, cf. Chapter 5), while adding one positive charge (at most one chain oxidised) leads to a total charge of -3 and adding two positive charges (both chains oxidised) to -2, of course. Along the same lines the total charges of the aggregates consisting of four oligopyrrole chains and two TaF_7^{2-} range between -4 (cf. Chapter 5) and 0. Again, all calculations were carried out with dispersion-corrected unrestricted Kohn-Sham density functional theory (DFT+D) employing the BP86 functional for high-spin electronic ground states.

7.1 Structures and binding energies for $[(TaF_7)_2(Py_5)_2(H_2O)_x]^{y-}$ with x= 4,6,8,10,12 y= 3,2

Here we will consider the same aggregates as in section 6.2, however with total charges of -3 (doublet spin state) and -2 (triplet spin state).

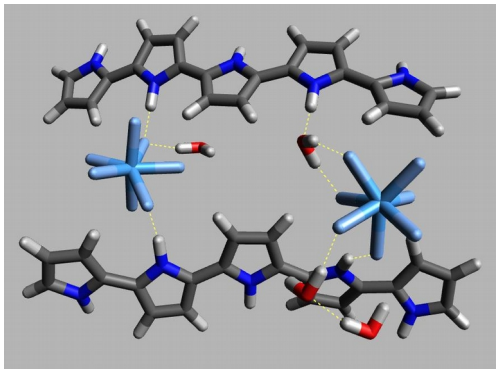

41a)

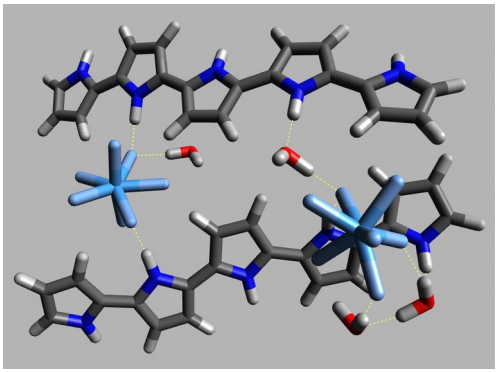

41b)

Figure **41.1**. Optimized structures for the first configuration with 2 Py_5-chains und 2 TaF_7^{2-} using 4 (a,b) WM, in the optimized OS: -3 (a) and -2 (b).

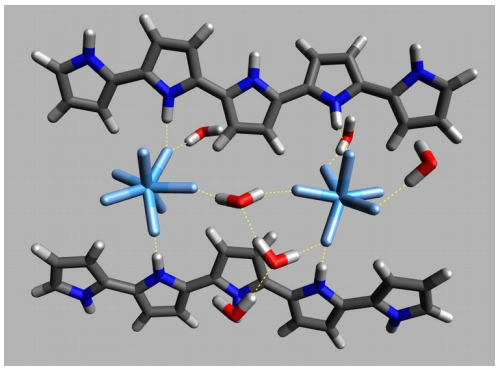

41c)

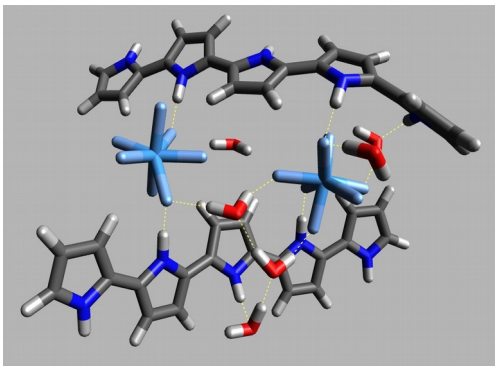

41d)

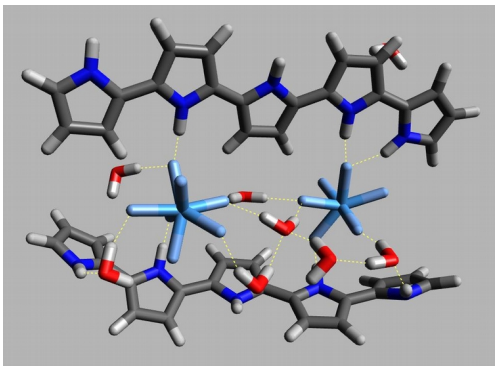

41e)

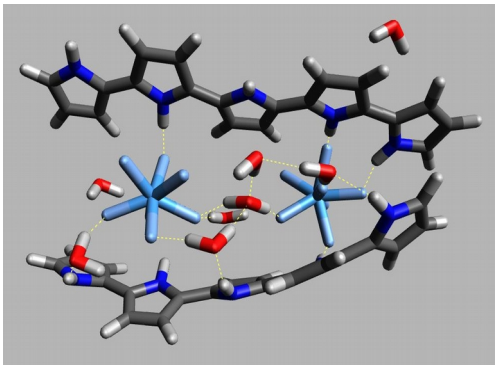

41f)

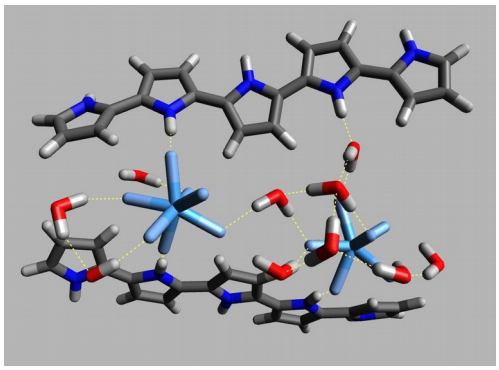

41g)

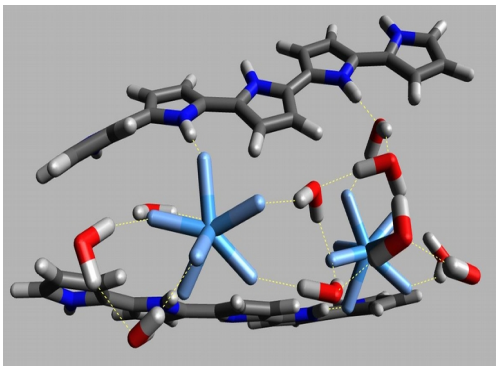

41h)

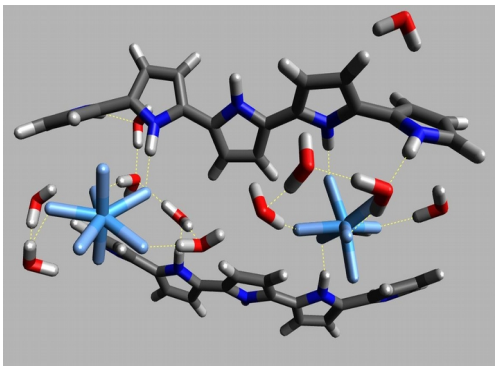

41i)

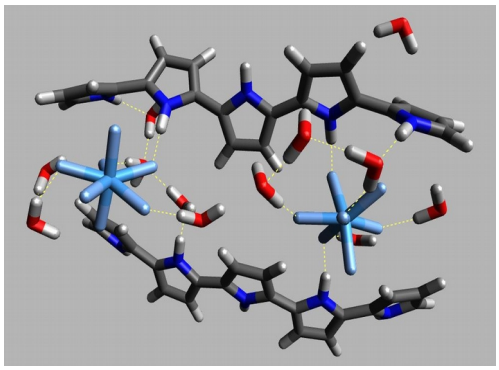

41j)

Figure **41.2**. Optimized structures for the first configuration with 2 Py_5-chains und 2 TaF_7^{2-} using 6 (c,d), 8 (e,f), 10 (g,h) and 12 (i,j) in the optimized OS: -3 (c,e,g,i) and -2 (d,f,h,j).

While the structure of the first aggregate with four WM (cf. Figure **30b** of Chapter 6.1) upon single oxidation is only slightly modified (cf. agregate **41a**) through a minor turning of one of the chains, changes are more pronounced in the doubly oxidised structure **41b**, where due to a diplacement of that TaF_7^{2-} ion which is surronded by 3 WM the corresponding ends of the oligopyrrole chains get into closer contact, as favoured by stronger cation-π interactions between the chains.

Similarly, the corresponding aggregate with six WM is hardly modified by a single oxidation (cf. Figures **30c** and **41c**), while double oxidation leads to a sigificant twist of one of the pentapyrrole chains which is accompanied by a major displacement of one of the WM: this WM no longer serves as a bridge between a pyrrole NH-group and a TaF_7^{2-} ion, but rather attaches to a NH group of a neighbouring pyrrole unit to make place for a direct NH..anion contact.

The singly oxidised aggregate **41e** containing eight WM differs appreciably from its non-oxidised parent **30d** through clear deviations of one of the pentapyrrole chains from planarity: besides an overall rotation of the lower chain in particular the ending pyrrole unit on the right-hand-side of this chain moves out of the approximate plane of the other pyrrol units to enable a NH..O bridge with a WM of the solvation shell of one of the anions, accompanied by significant out-of-plane bending of the corresponding NH-group. While this feature is conserved upon further oxidation (cf. **41f**) it should be noted that now the WM seem to concentrate even further in positions which may be regarded as in between the two anions.

Single oxidation of aggregate **30e** with ten WM does not lead to significant changes of the overall structure (cf. Gig. **41g**) while the doubly oxidised aggregate displays stronger structural modifications in particular regarding the ending pyrrole unit of the upper pentapyrrole chain of **41h** which seems to arrange itself in such a was as to optimize cation-anion interactions.When it comes to oxidation of aggregate **30f** containing twelve WM one should note that here already the parent structure shows strong distortions of the oligopyrrole chains from overall planarity, distortions, which help to establish an extended hydrogen bond network. The rigidity of this network probably contributes to the

observation, that neither the singly oxidised aggregate **41i** nor the doubly oxidised aggregate **41j** show stronger structural deviations from their parent.

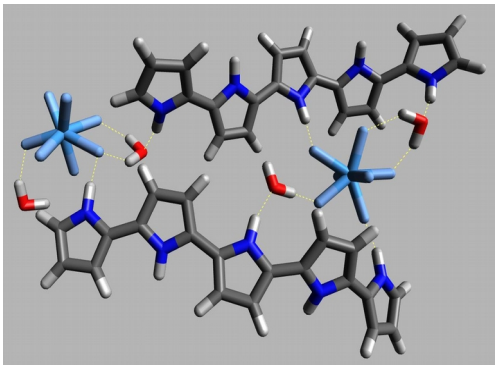
42a)

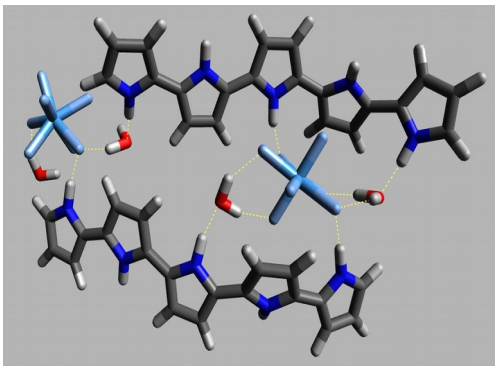
42b)

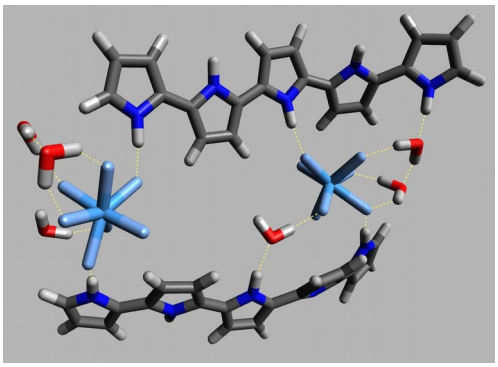
42c)

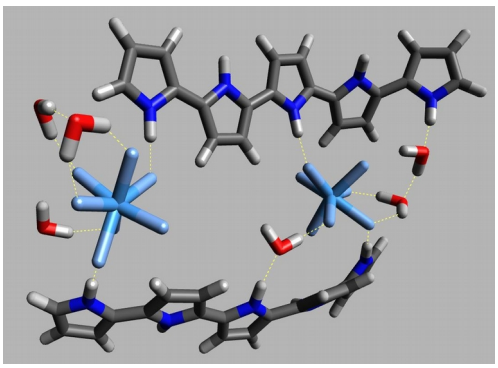
42d)

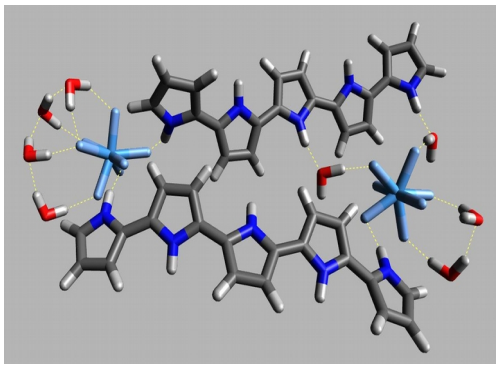
42e)

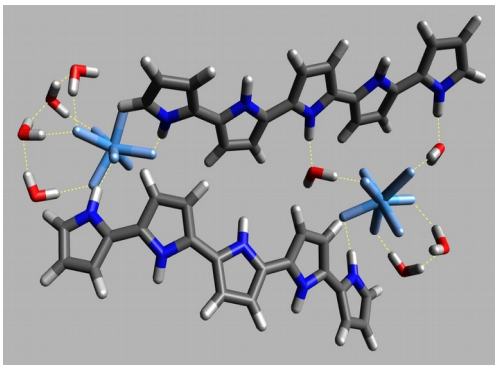
42f)

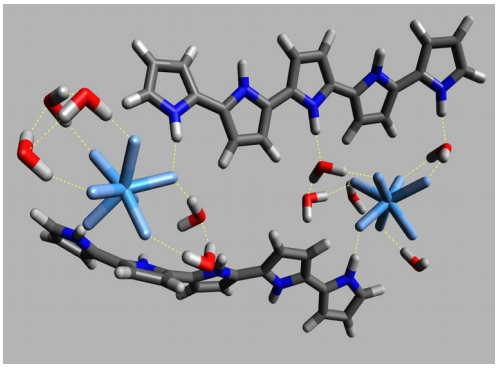
42g)

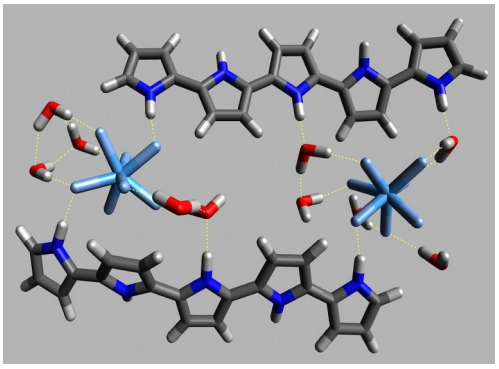
42h)

Fig.**42.1**. Optimized structures for the second configuration with 2 Py_5-chains und 2 TaF_7^{2-} using 4 (a,b), 6 (c,d), 8 (e,f), 10 (g,h) and 12 (i,j) in the optimized OS: -3 (a,c,e,g) and -2 (b,d,f,h).

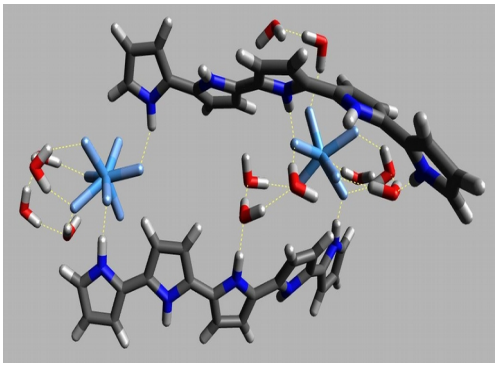

42i)

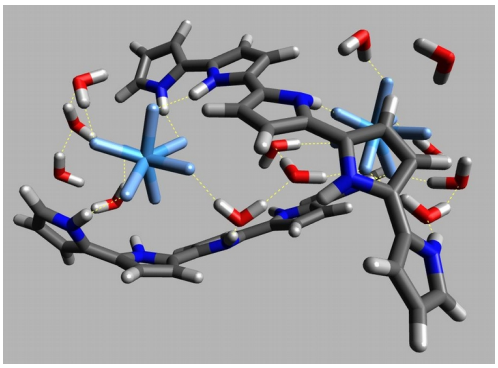

42j)

Fig.**42.2**. Optimized structures for the first configuration with 2 Py_5-chains und 2 TaF_7^{2-} using 12 (i,j) in the optimized OS: -3 (i) and -2 (j).

Comparing the aggregates **42a** and **42b** containing 4 WM with their parent **31b** one observes that oxidation introduces only minor structural modifications such as slight reorientations of the WM and pentayrrole chains leading to minor modifications of the hydrogen bonding pattern. In the case of the aggregates **42c** and **42d** with 6 WM no significant structural modifications as compared to the non-oxidised aggregate **31c** can be observed, and thus the hydrogen bonding pattern also remains intact upon oxidation of the chains. This is essentially also true for the aggregates containing 8 WM (**42e** and **42f**) and with 10 WM (**42g** and **42h**), characterized by microsolvation of each TaF_7^{2-} anions with four and five WM, respectively: in these aggregates the hydrogen bonding patterns remain unchanged from those in their respective parent aggregates **31d** and **31e**, respectively.

In anticipation of a discussion of Fig. 44, it should be noted, however, that in both cases oxidation has a significant effect on the interionic distances, which shrink significantly with each oxidation step as a result of a partial compensation of their Coulomb repulsion through Coulomb attraction with oxidised chains. Single oxidation of aggregate **31f** containing 12 WM leads to the possibility of relatively strong deviations of the oligopyrrole chains from planarity, as particularly noticeable for the upper chain shown in Fig. **42i**. On the other hand, the solvation shells of both anions are not strongly affected by single oxidation, whereas the second oxidation step introduces appreciable qualitative and quantitative differences: in aggregate **42j** one of the WM reorients to form a bridge between the solvation shell of the anion on the r.h.s. (right hand side) and a fluorine atome of the anion on the l.h.s. (left hand side), and also the curvature of the lower pentapyrrole chain is visibly increased.

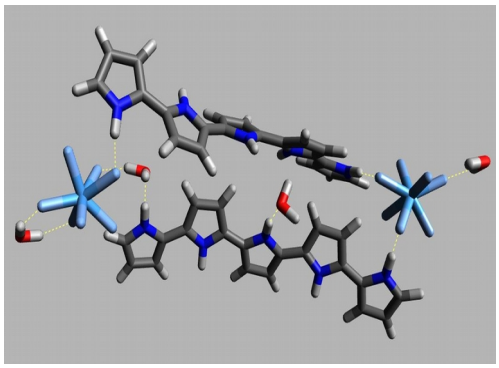
43a)

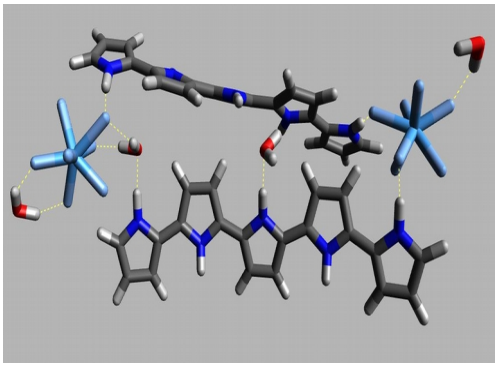
43b)

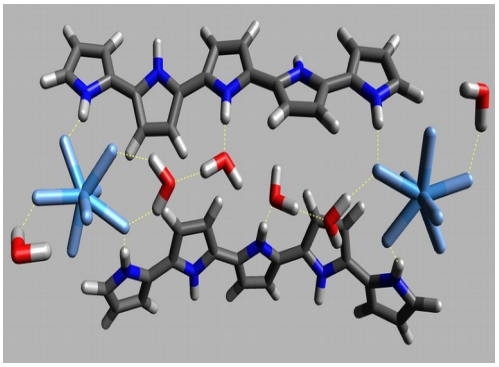
43c)

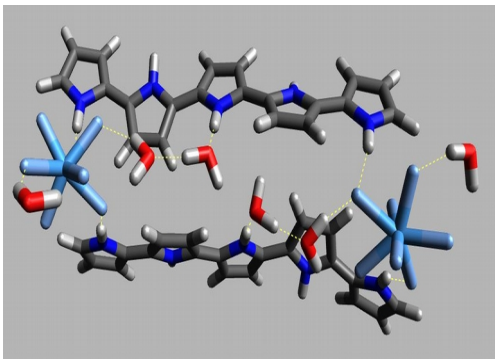
43d)

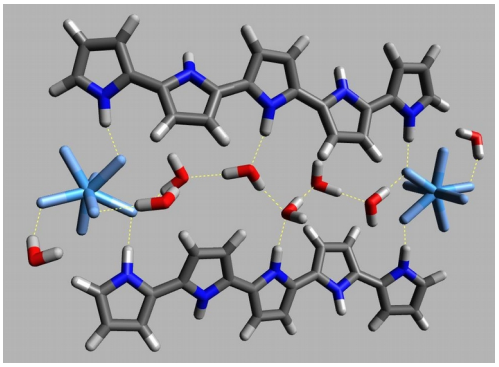
43e)

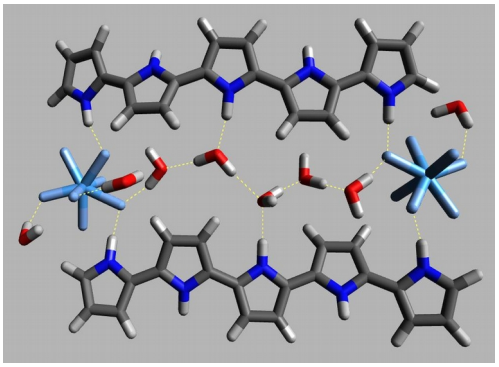
43f)

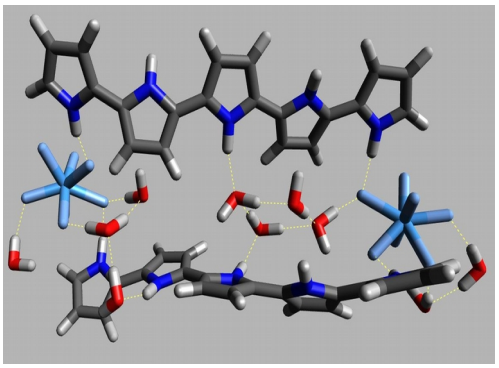
43g)

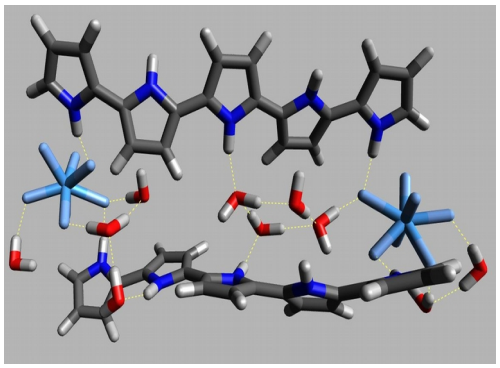
43h)

Figure **43.1**. Optimized structures for the third configuration with 2 Py_5-chains und 2 T-ions using 4 (a,b), 6 (c,d), 8 (e,f) and 10 (g,h) in the optimized OS: -3 (a,c,e,g) and -2 (b,d,f,h).

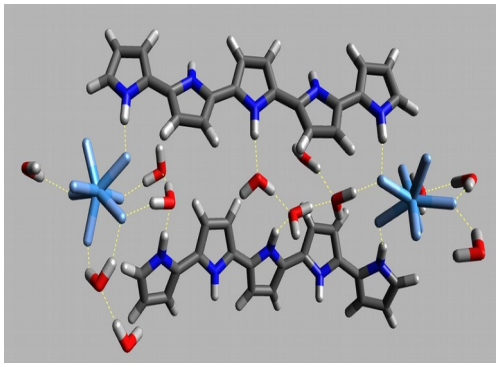

43i)

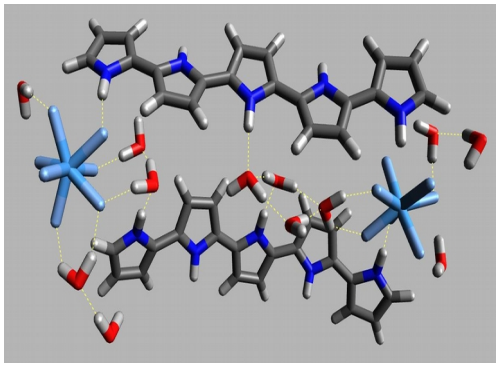

43j)

Figure **43.2**. Optimized structures for the third configuration with 2 Py_5-chains und 2 TaF_7^{2-} using 12 (i,j) WM, in the optimized OS: -3 (i) and -2 (j).

The last class of aggregates between two anions and two pentapyrrole chains considered here is characterized by large distances between the anions and possibility of the formation of chains of WM between them (cf. Fig. 32 and the corresponding discussion in Chapter 6.1). A glance at Fig. 43 shows that the essential structural parameters in nearly all of these aggregates are well conserved upon single and double oxidation, including the hydrogen bonding patterns and the relative orientation of the two pentapyrrole chains.

Figure 44 shows the binding energies (as before, defined with respect to dissociation into all components) along with the distances between the Ta atoms of the anions as a function of the number of positive charges (i.e., oxidation steps) on the oligopyrrole chains and the number of WM for the aggregates discussed hitherto. As expected, the binding energies systematically grow with both, the number of WM and the number of positive charges and the chains - apart from the aggregates with 10 WM for which the binding energies occasionally come close to those of corresponding aggregates with two less or two more WM, respectively.

The first finding is rationalized by the increasing possibilities for hydrogen bridges and other favourable interactions involving WM, and the second finding demonstrates that the Coulomb repulsion introduced between two positively charged chains is easily overcome by the increasing Coulomb attraction between the chains and the anions and that this effect is fairly independent on the formation of (partially filled) solvation shells around the ions. Also in line with expectation is the observation that the distances between the anions for each type of aggregate systematically shorten upon oxidation of the oligopyrrole

chains, rationalizable through more efficient screening by creation of delocalised positive charge distributions on the chains.

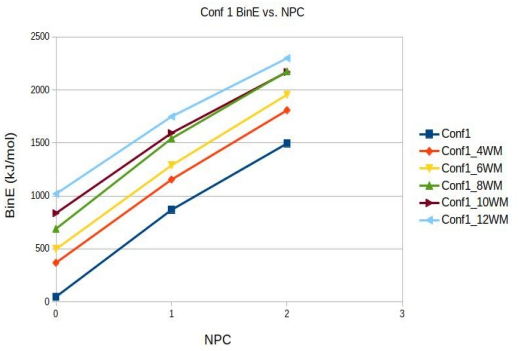

44a)

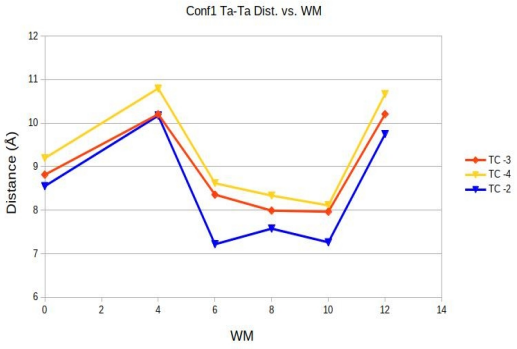

44b)

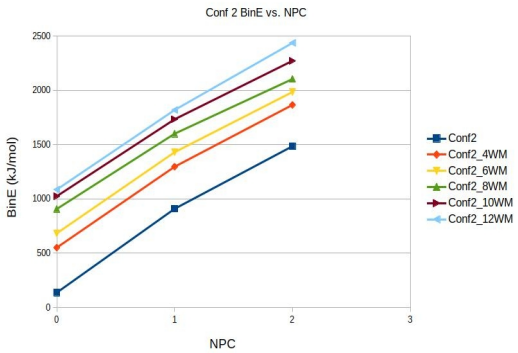

44c)

44d)

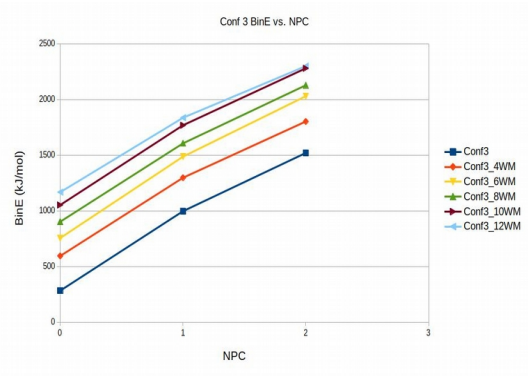

44e)

44f)

Figure **44**. Binding energy vs. number of positive charges and Ta-Ta distance vs. number of WM for the first configuration (a,b), second (c,d) and third (e,f).

While the magnitude of the binding energies sysytematically increases with each oxidation step, that is not neccessarily the case for the total energies, as seen from Figure **45**. The first type of aggregate (configuration 1) possesses the smallest distances between the anions, and here each loss of an electron in the oligopyrrole chains indeed always leads to a more negative energy, independent of the number of WM. Thus all of these

aggregates are most stable when their total charge is -2 (remember that total charges of -1 and 0 were not considered as they would require multiple oxidation of one or both chains). This is no longer the case for the second type of aggregates (configuration 2) with intermediate Ta..Ta distances: here the aggregate with 8 WM is most stable when only one of the oligopyrrole chains becomes oxidised.

For the third type of aggregates (configuration 3) possessing the largest distances between the anions it starts to become the rule that the most stable aggregates are singly oxidised only, with exception of the aggregate without any WM where the doubly oxidised form is clearly more stable and the aggregates with 6 and 8 WM, respectively, where the singly and doubly oxidised forms are nearly isoenergetic. Obviously increasing distances between the anions and increasing solvation diminish the need for second autoionisation of an aggregate.

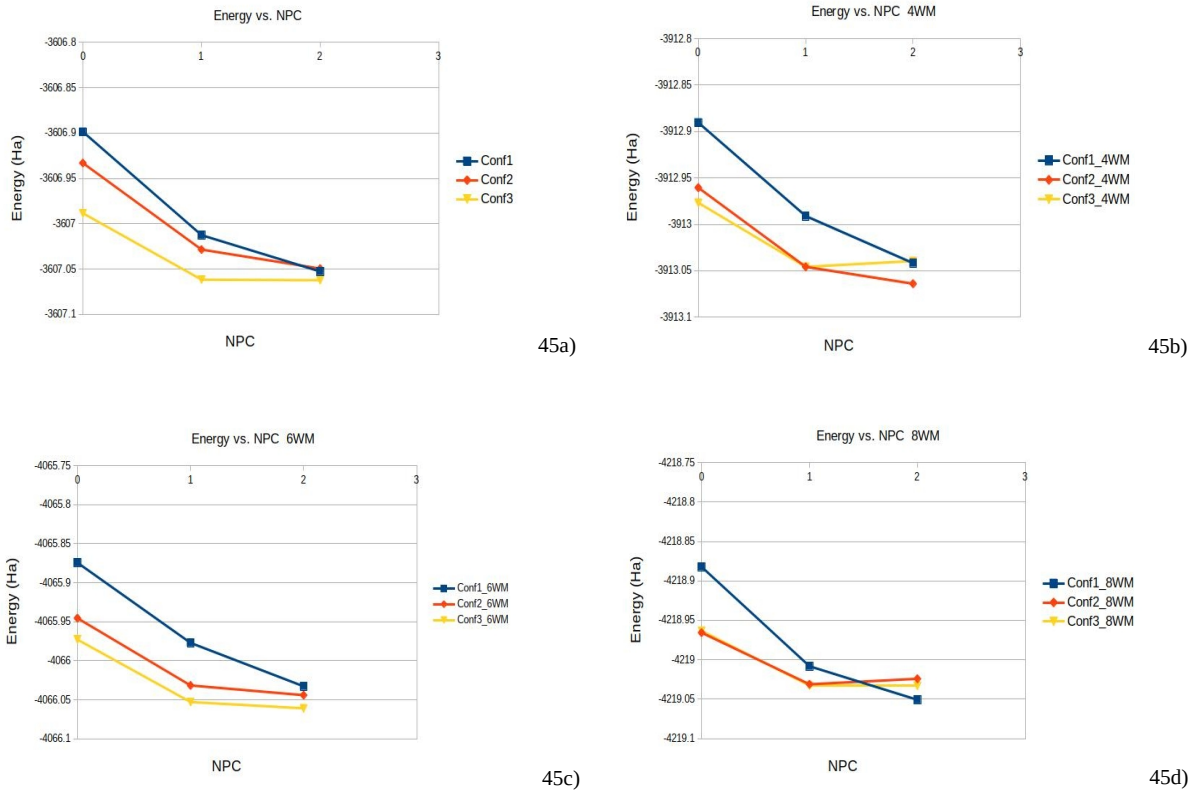

Figure **45.1**. Graphics of total energy vs. number of positive charges for all three studied configurations, separated by number of WM used in each calculation: no solvent present a), 4 b), 6 c) 8 d).

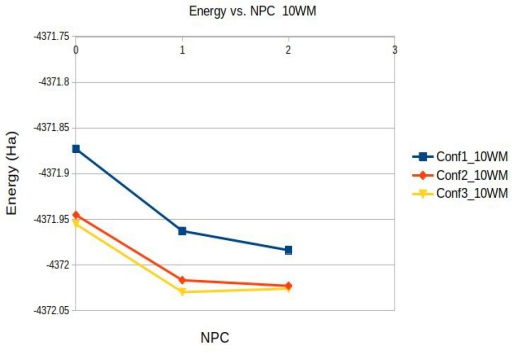

45e)

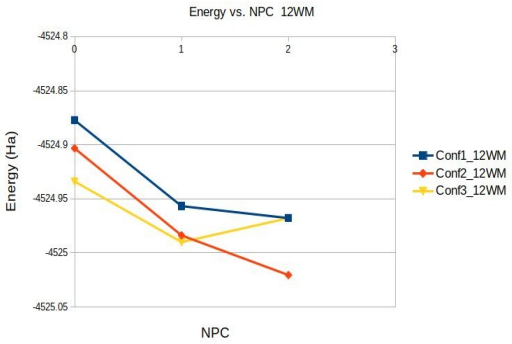

45f)

Figure **45.2**. Total energy vs. number of positive charges for all three studied configurations, separated by number of WM used in each calculation: 10 e) 12 f).

7.2. Structures and binding energies for $[(TaF_7)_2(Py_5)_4(H_2O)_x]^{y-}$ with x= 8,12,16,20,24 y= 3,2,1,0

In this section aggregates composed of four pentapyrrole chains and two heptafluorotantalate ions and 8 to 24 WM will be considered, where the number of WM was varied in steps of four. In line with the strategy to allow for up to single oxidation of each chain geometries, binding energies and total energies for total aggregate charges of -4, -3, -2, -1, and 0 were investigated, starting from the structures with total charge -4 as described in Chapter 6 and successiveley adding "positive" charges employing the high-spin unrestricted Kohn-Sham approach. While most of the optimized structures will be shown in appendix only (cf. Figures **57**-**61**), Figure **46** displays representative structures with a total charge of 0 and 24 added WM.

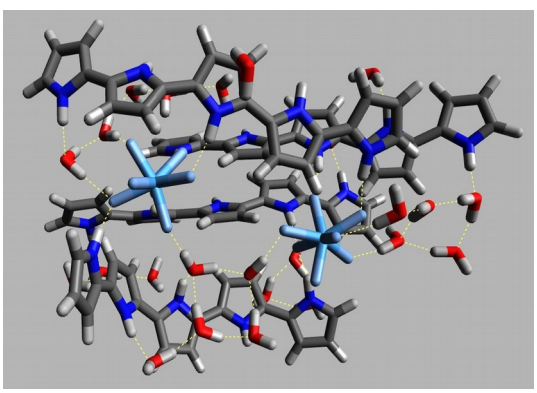

46a)

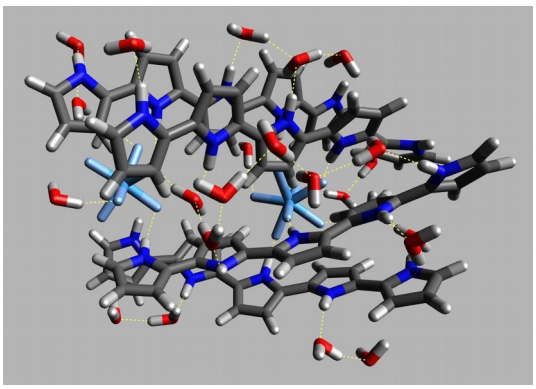

46b)

Figure **46**. Images of all 4 calculated configurations with 24 WM with total charge = 0 being first a), second b).

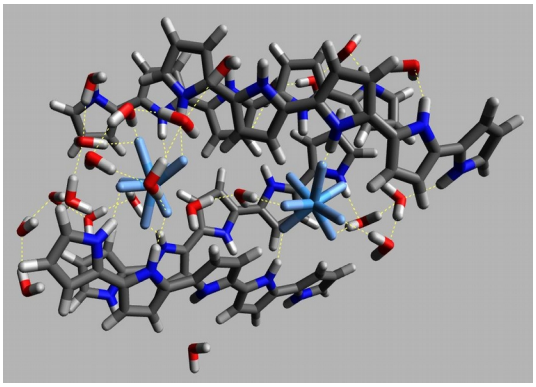

46c)

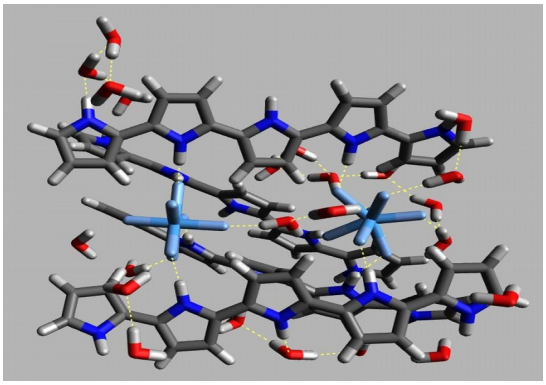

46d)

Figure **46**. Images of all 4 calculated configurations with 24 WM with total charge = 0 being third c) and fourth d).

Because of the fairly large size of the aggregates and the overall five charge states taken into account for each of them in the following geometrical changes observed as a function of the oxidation state and number of WM will not be discussed in great detail. The focus will rather be on larger geometrical changes, detected with the help of a script which first aligns two aggregates such as to minimize the root mean square distance between their atoms and then determines the atoms with the largest relative position shifts. Furthermore, as before binding energies, Ta..Ta distances and total energies will be considered.

The first type of aggregate (conformation 1) is characterized by one stack of π-π interacting oligopyrrole chains and two chains which essentially do not show close contacts when the total charge is -4 and no WM are present (cf. section **6.2**). Here changes in the oxidation state of the pentapyrrole chains may have significant geoemtrical consequences, as evidenced by the decrease of the Ta..Ta distance by nearly 2 Å upon addition of a positive charge on each of the four chains (cf. Fig. **47b**). Similarly, for the aggregate of conformation 1 with 12 WM one observes a major reduction of of the distance between the anions by about 2 Å for the cases of two and three oxidised oligopyrrole chains, along with other slight modifications. Adding more WM helps to stiffen the structure through hydrogen bond networks, thus also diminsihing the shortening of the Ta...Ta distances upon oxidation. Note, however, that this can only serve as a rule of thumb, with an obvious exception for the aggregate including the larges number of WM, i.e., 24 WM.

The second type of aggregate (conformation 2) contains two stacks of chains with π-π contacts and in the case of completely unoxidised oligopyrroles was observed to be relatively stiff as concerning the effects of added WM (cf. section **6.2**). As shown in Figure **47d** that means that the shortening of the Ta..Ta distance upon oxidation of an increasing number of chains tends to be quite systematic independent on the number of WM, with the occasional exceptions of the triply oxidised aggregate containing 8 WM and the fully oxidised aggregate containg 24 WM. With the help of the aforementiond script also changes of the dihedral angles of two "external" pyrroles by almost 10° were detected upon addition of 16 WM which, however, have no significant influence on the anion-anion distances.

Two π-π-stacked chains also consitute the main feature of the structure of the third type of aggregates (conformation 3). In this case, however, the stacks seem to be less decisive for a stiffening of the structure than the number of WM and their accompanying hydrogen bond network: from Figure **47f** it becomes evident that step-by-step oxidation of the "unsolvated" aggregate (0 WM) leads to much less systematic effects on the Ta..Ta distance than oxidation of the aggregates containing 12 WM and more. In particular in the aggregates with 20 and 24 WM the distance between the anions becomes nearly independent on the oxidation stage of the surrounding chains.

A similar effect is found in the last type of aggregate (conformation 4) which, as conformaation 1, contains only one stack of chains with direct π-π contacts. This aggregate is the one with the smallest Ta..Ta distances considered here, and these distances vary in the order of 1 Å only upon changing the oxidation state and the number of WM (cf. Fig. **47h**). In particular, though the anion-anion distance becomes largest in the aggregate with 24 WM, here the variation with the oxidation state amounts to less than 0.3 Å.

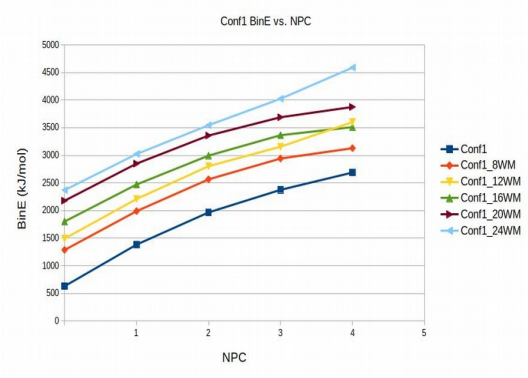

47a)

47b)

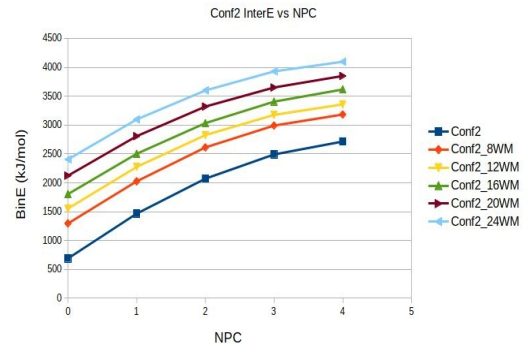

47c)

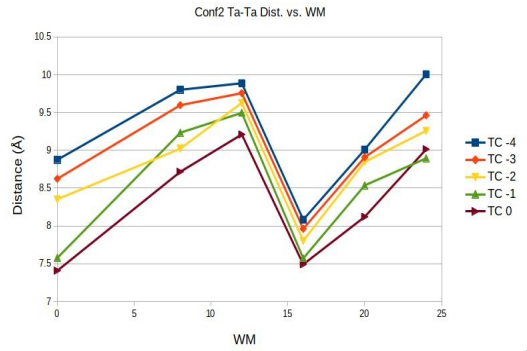

47d)

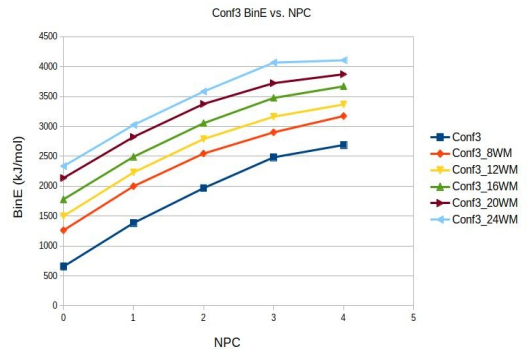

47e)

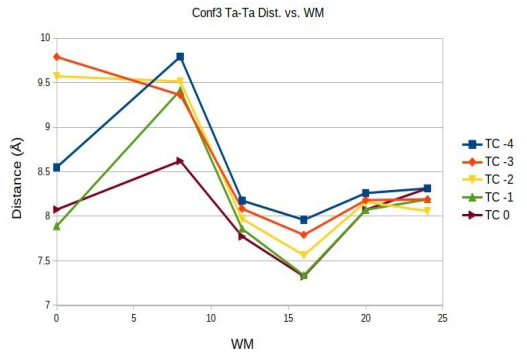

47f)

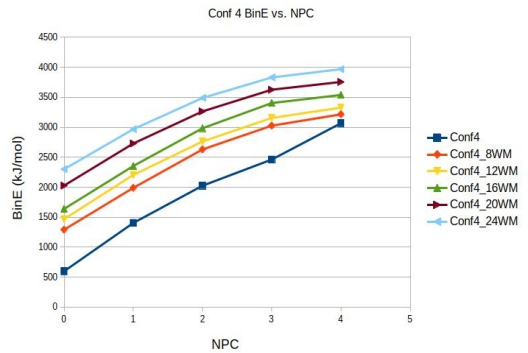

47g)

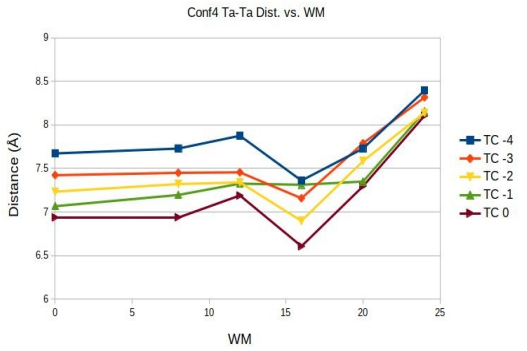

47h)

Figure **47**. Graphics of binding energy vs. number of positive charges (a,c,e,g) and Ta-Ta distance vs. number of WM. (b,d,f,h).

Figure **47** also contains the binding energies of the various aggregates, i.e., the energy gain upon formation of the aggregate from all of its molecular and ionic constituents. Their magnitude inevitably grows with the number of WM, and in all cases it also grows upon the number of positive charges on the pentapyrrole chains. The discussion of the reasons for these findings parallels the corresponding discussion in section 7.1 for the smaller aggregates and shall not be repeated. Here it may suffice to note that the only exception to the rule that more WM mean a higher magnitude of the binding energy is observed for the fully oxidised version of conformation 1 with 12 and 16 WM (cf. Fig. **47a**), which show strongly differing Ta..Ta distances.

The perhaps more interesting observation can be made from Figure **48**, which shows the total energies of the aggregates as a function of the number of positive charges on the chains. As seen in Fig. **48a**, for three out of the four considered conformations the minimum in the total energy is reached when two of the chains are oxidised, and in the remaining conformation (number 3) the doubly oxidised form is nearly isoenergetic with the triply oxidised form. Thus one has to conclude that usually only half of the chains will autooxidise as long as no solvent molecules are present. With increasing numbers of WM, however, the position of the energetic minimum shifts to smaller numbers of positive charges on the chains, and when 24 WM are reached (cf. Fig. **48f**) the singly oxidised form in two cases (conformations 1 and 4)is nearly isoenergetic with the doubly oxidised form, in one case (conformation 2) it is the clear minimum and only in the last case (conformation 3) the doubly oxidised form remains the most stable one. Evidently, stabilisation of the anions through at least partially filled solvation shells diminishes the energy to be gained from forming cationic oligopyrrole units since their attractive Coulomb interactions with the anions can be considered as partially screened through the solvent, thus making the apparently less efficiently screened repulsive Coulomb interactions between the extended cationic chains more unfavourable.

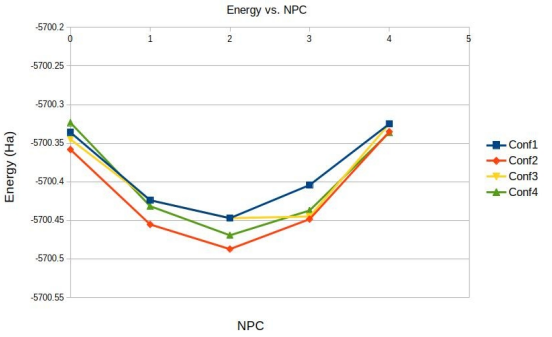

48a)

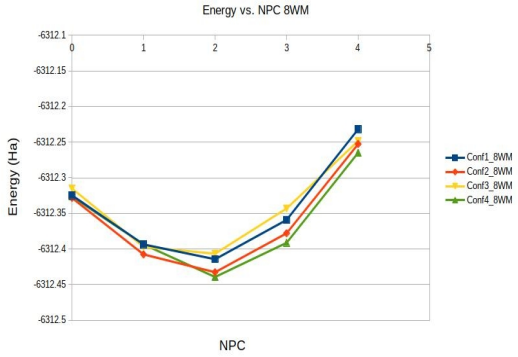

48b)

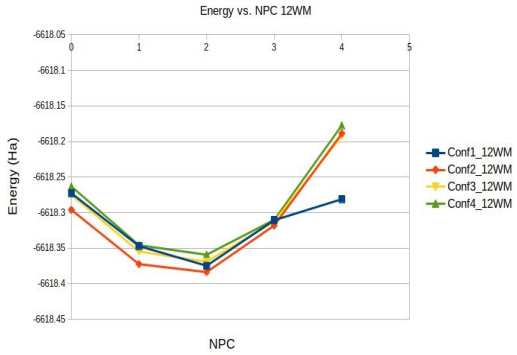

48c)

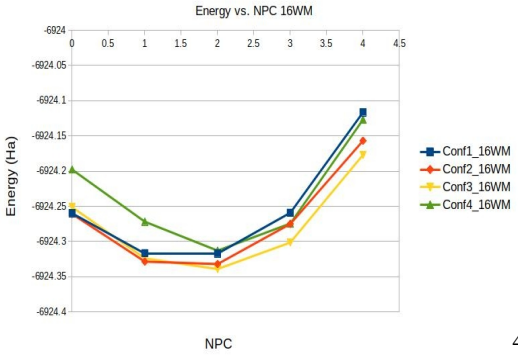

48d)

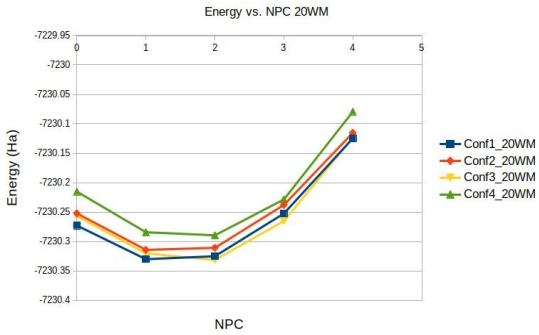

48e)

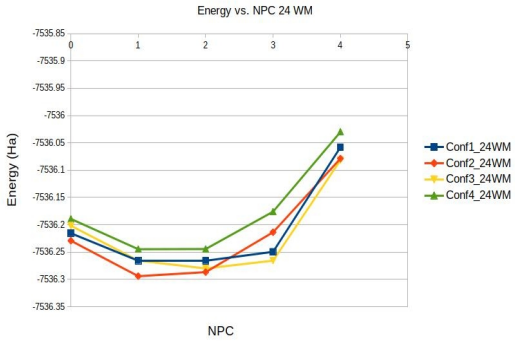

48f)

Figure **48**. Graphics of total energy vs. number of positive charges for pure structures a), 8 b), 12 c) and 16 d), 20 e) and 24 f) WM.

7.3 Structures and binding energies for $[(TaF_7)_2(Py_5)_2(ACN)_x]^{y-}$ with x= 4,6,8,10,12 y= 3,2

Following the same strategy as used in previous sections of this chapter in the following the effects of oxidising the geometry-optimized structures with randomly distributed acetonitrile (ACN) molecules presented in section 6.3 will be considered, using the same quantum chemical methods as before.

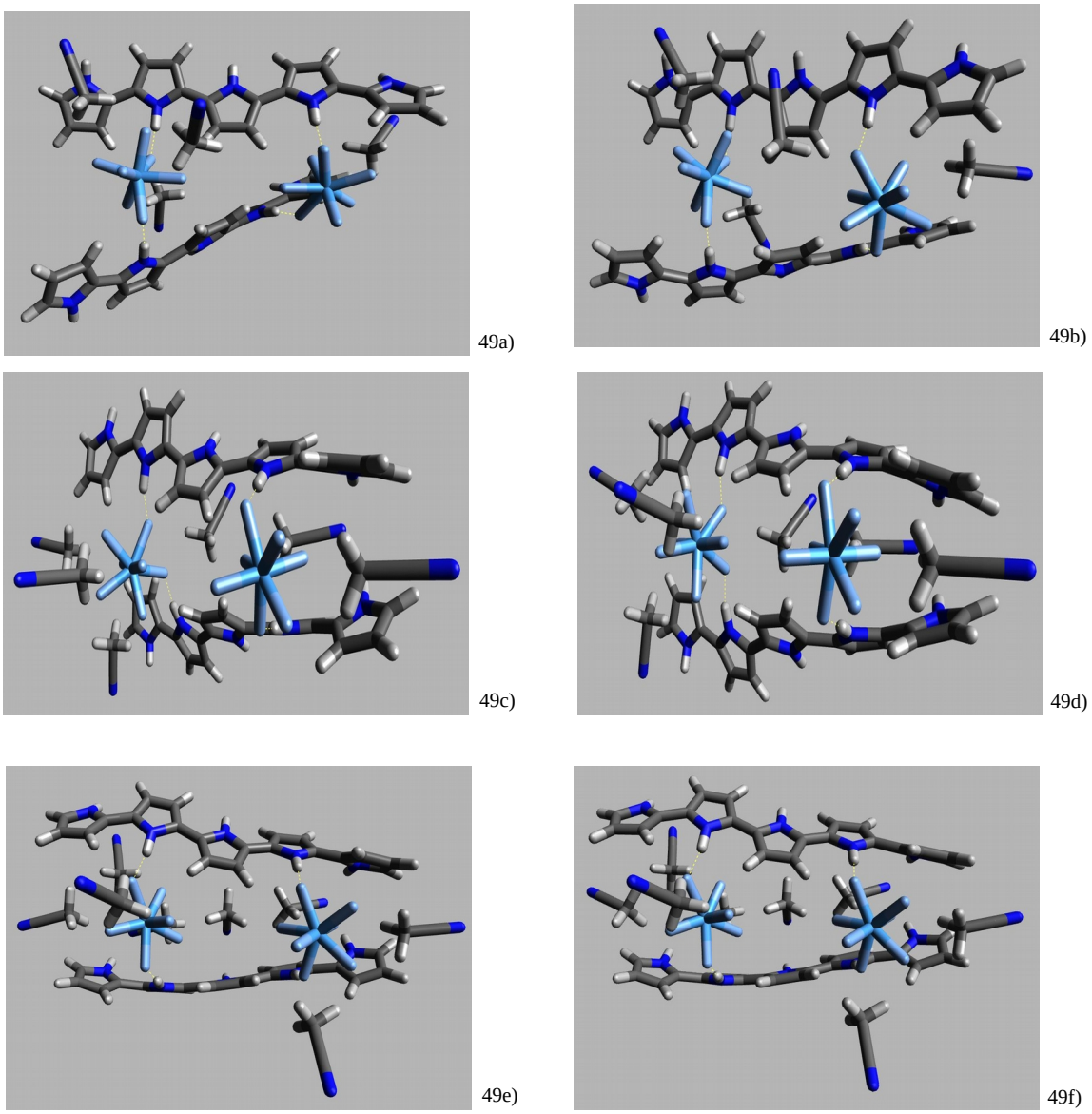

Figure **49.1**. Optimized structures for the first configuration with 2 Py_5-chains und 2 TaF_7^{2-} using 4 (a,b), 6 (c,d) and 8 (e,f) ACN in the optimized OS: -3 (a,c,e) and -2 (b,d,f).

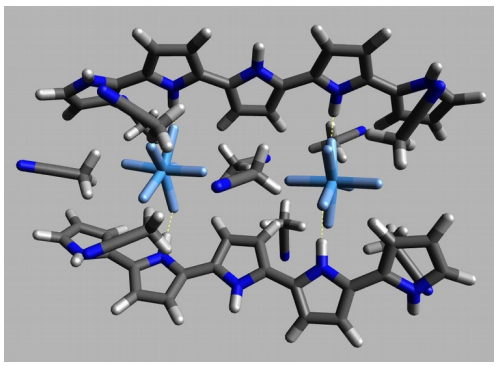
49g)

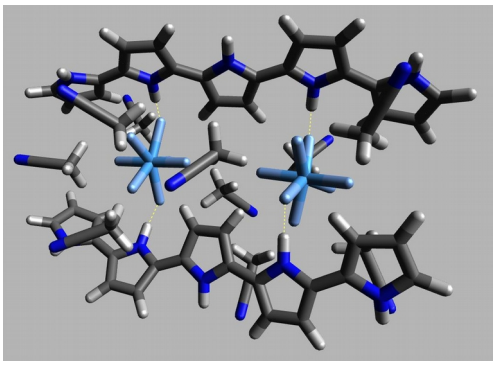
49h)

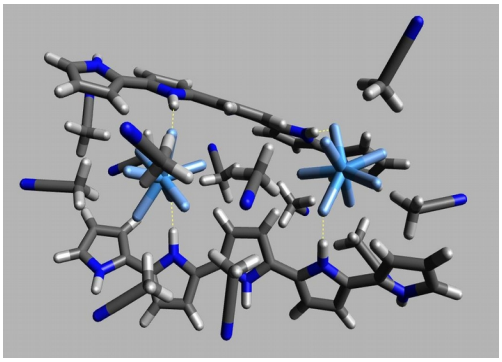
49i)

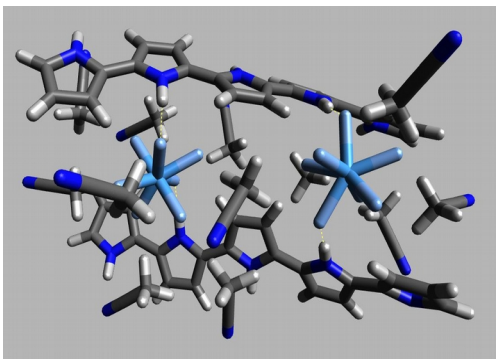
49j)

Figure **49.2**. Optimized structures for the first configuration with 2 Py_5-chains und 2 TaF_7^{2-} using 10 (g,h) and 12 (i,j) ACN in the optimized OS: -3 (g,i) and -2 (h,j).

For the aggregates composed of two pentapyrrole chains and two heptafluorotantalate ions total charges of -3 and -2 were investigated, corresponding to one and two oxidised chains, respectively. The first of the considered aggregates (configuration 1) is characterized by fairly short distances between the anions as they are sitting in neighbouring pockets of both pentapyrrole chains. This is true for all added numbers of ACN molecules (which range between 4 and 12 in steps of 2) as long as no chain is oxidised (cf. Chapter 6), but it also stays true after oxidising a single and two chains, respectively. This becomes clear from Figure 49 which also reveals that changes in the oxidation state do not lead to dramatic differences in this type of aggregate, apart from slight orientational changes of the ACN molecules and very minor chain twisting. In particular for larger numbers of ACN molecules differences between the various oxidation states are hardly perceptible anymore.

In the second of the considered aggregates (configuration 2) in most cases the two anions sit in immediately neighbouring pockets of one chain, while they show NH..F hydrogen bridges with two ending pyrrole units of the other chain, meaning that they leave the

pocket in between empty. The aggregates with 8 ACN solvent molecules, however, are an exception: as already mentioned in section 6.3 here one of the anions completely detaches from one of the two chains, yielding a fairly flexible structure with a strongly increased distance between the anions. This, in turn, results in much more significant changes of the aggregates structure upon oxidation than in the other cases containing 6, 10, and 12 ACN molecules, respectively. This can be perceived in Figure 50, as it was not possible to align the structures with total charges of -3 and -2 such as to not have strongly visible differences in one part of the aggregate or the other (cf. **50e** and **50f**), while for most of the other aggregates this was not a problem. The other case with larger structural changes is provided by the aggregate with only 4 ACN molecules (cf. **50a** and **50b**) where the relative orientation of the two pentapyrrole chains changes from roughly coplanar for one oxidised chain to roughly orthogonal upon oxidation of the second chain.

In the last of the considered aggregates the two anions attach to the ending pyrrole units of both pentapyrrole chains (configuration 3). This qualitative description does not change with the oxidation state of the aggregate, as can be seen from Fig. 51. While even the finer details of the structures of with 4, 6, and 8 ACN molecules agree very well for both considered oxidation states, one notes somewhat larger differences for the remaining aggregates, in particular as concerning the orientation of some of their 10 or 12 ACN molecules.

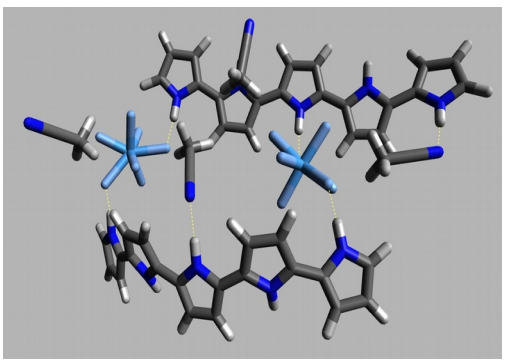

50a)

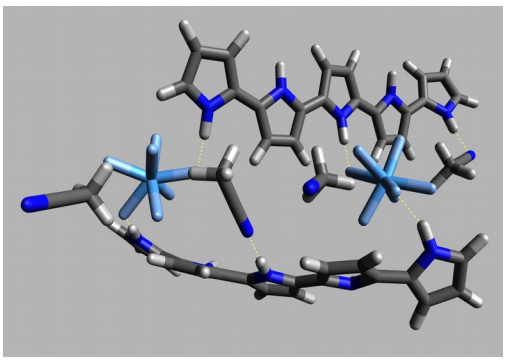

50b)

Figure **50.1**. Optimized structures for the second configuration with 2 Py_5-chains und 2 TaF_7^{2-} using 4 (a,b) ACN molecules in the optimized OS: -3 (a) and -2 (b).

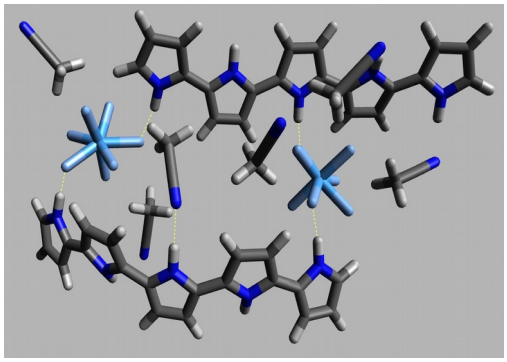

50c)

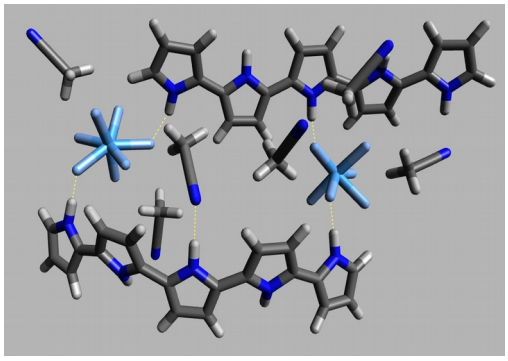

50d)

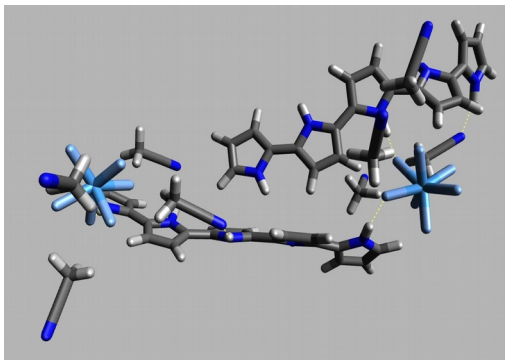

50e)

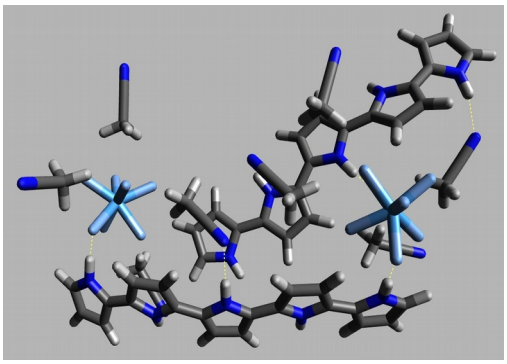

50f)

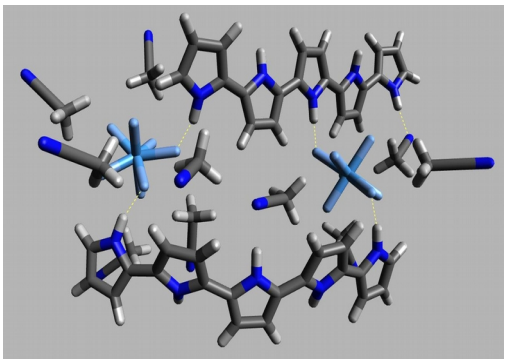

50g)

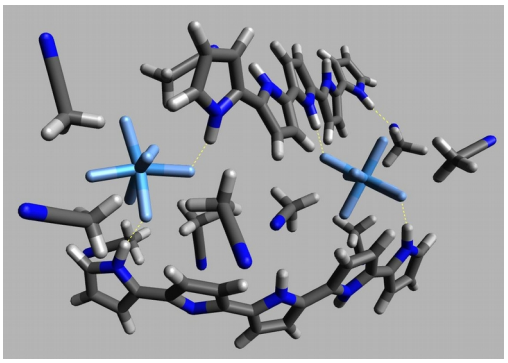

50h)

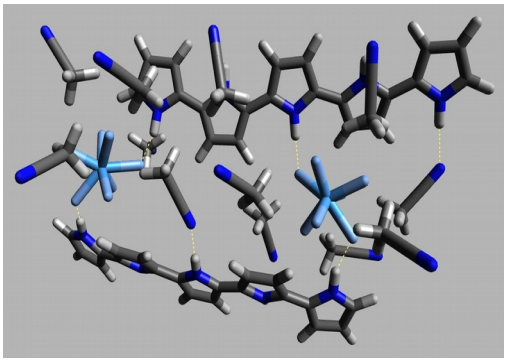

50i)

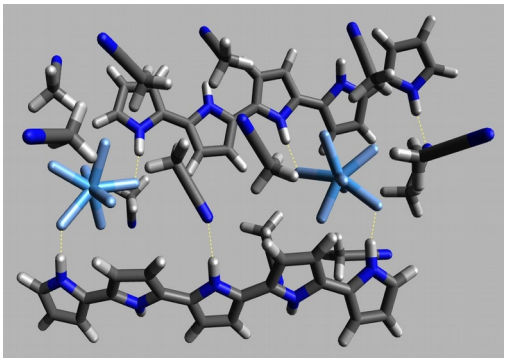

50j)

Figure **50.2**. Optimized structures for the second configuration with 2 Py_5-chains und 2 TaF_7^{2-} using 6 (c,d), 8 (e,f), 10 (g,h) and 12 (i,j) ACN in the optimized OS: -3 (c,e,g,i) and -2 (d,f,h,j).

While the binding energies of the aggregates closely follow the trends already observed previously, i.e., the systematically increases with both, the nubmer of solvent molecules and the number of positive charges on the chains, Figure 50 besides this, shows that in most cases the anion-anion distances also follow the same trends as found for the water-containing aggregates: they tend to shrink upon the first oxidation step and to shrink even further upon the second. Notable exceptions to this rule are configuration 2 with 4 and 6 solvent molecules and configuration 3 with 8 solvent molecules, highlighting that our previous general considerations of electrostatic screening as being responsible for the distance reduction occasionally must be supplemented by more specific considerations of chain and solvent molecule reorientation when this level of detail should become relevant.

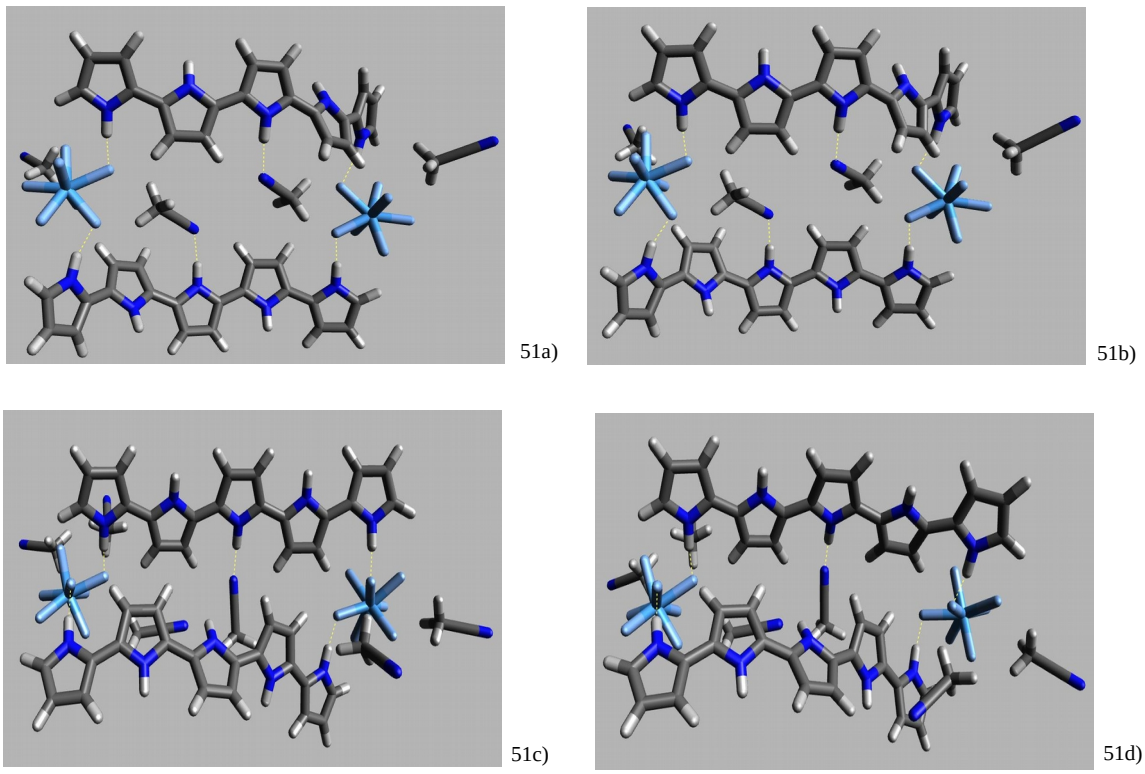

51a) 51b) 51c) 51d)

Figure **51.1**. Optimized structures for the third configuration with 2 Py_5-chains und 2 TaF_7^{2-} using 4 (a,b) and 6 (c,d) ACN molecules in the optimized OS: -3 (a,c) and -2 (b,d).

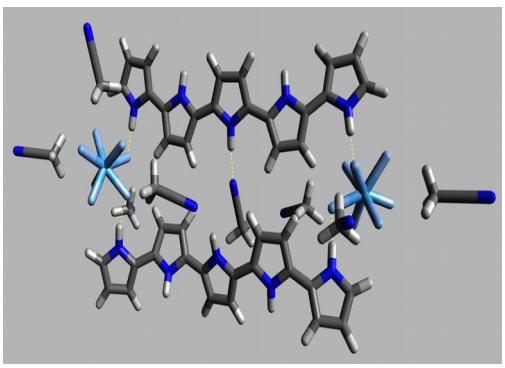
51e)

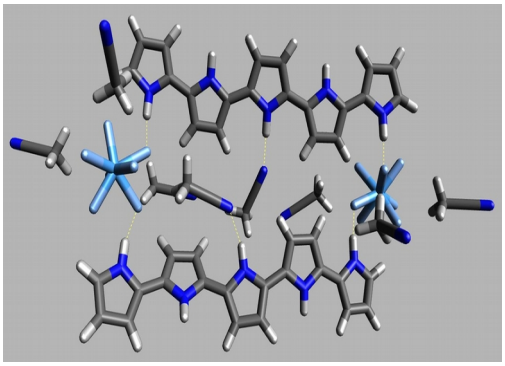
51f)

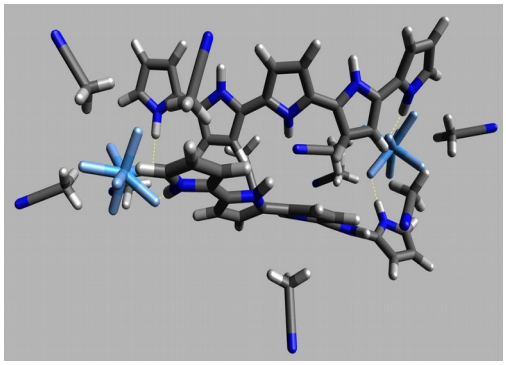
51g)

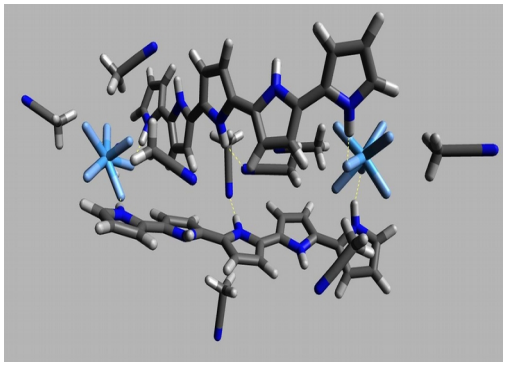
51h)

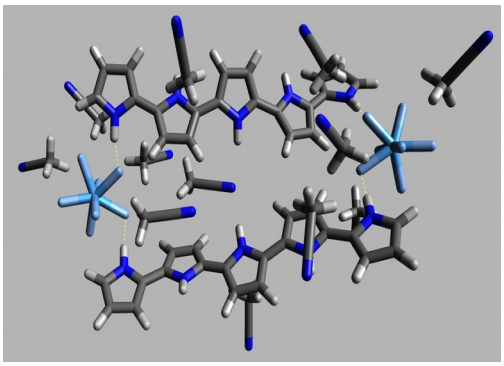
51i)

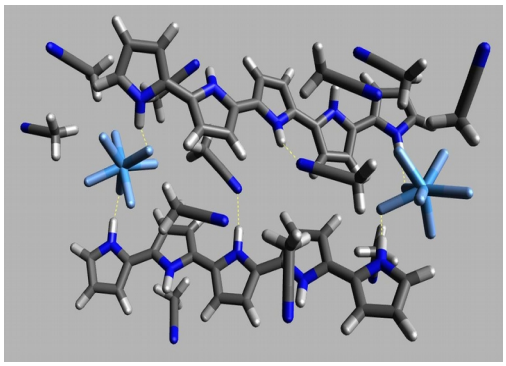
51j)

Figure **51.2**. Optimized structures for the third configuration with 2 Py_5-chains und 2 TaF_7^{2-} using 8 (e,f), 10 (g,h) and 12 (i,j) ACN molecules in the optimized OS: -3 (e,g,i) and -2 (f,h,j).

Here it may suffice to note that the strong reduction of the Ta..Ta distance observed for the second oxidation step of configuraiton 2 with 8 ACN molecules is certainly to be attributed to the flexibility of the partially detached anion (vide supra): a further positive charge on the chains pulls the anion back to both of them through Coulomb attraction. On the other hand, understanding the strong reduction of the Ta..Ta distance observed for the second oxidation step of configuration 3 with 12 ACN molecules would require careful consideration of the reorientation of the ACN molecules when they must adapt to the modified combined electric field of the chains.

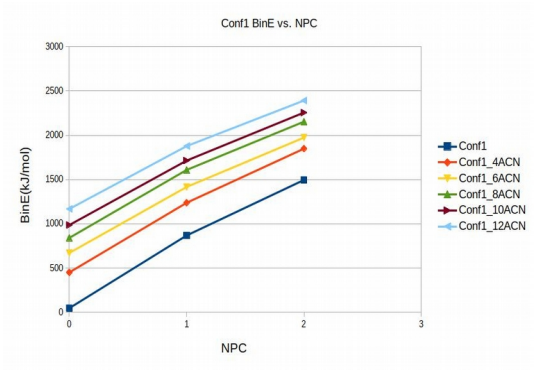

52a)

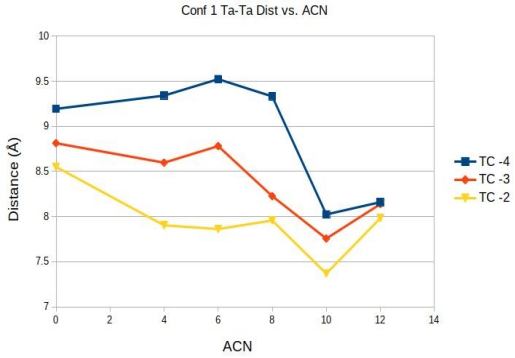

52b)

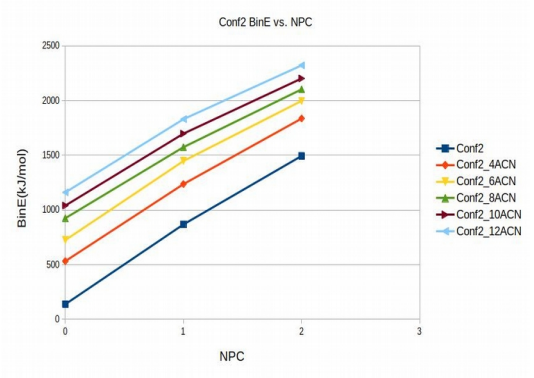

52c)

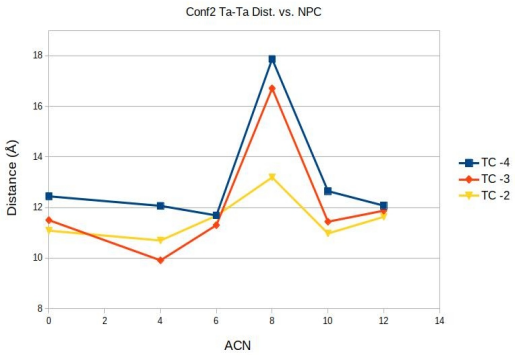

52d)

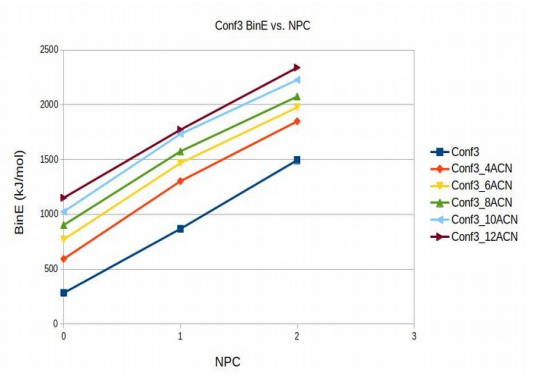

52e)

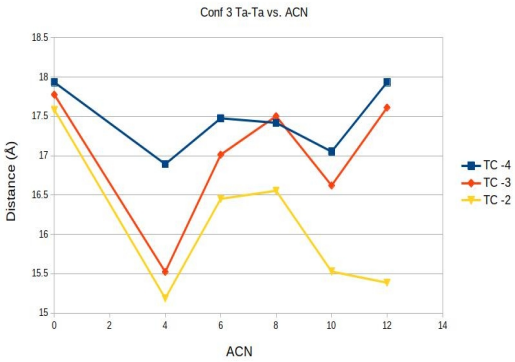

52f)

Figure **52**. Binding energy vs. number of positive charges and Ta-Ta distance vs. number of WM for the first (a,b), second (c,d) and the third configuration (e,f).

Figure 53 compares the total energies of the aggregtes containing various numbers of ACN molecules as a function of the positive charges on the oligopyrrole chains. Concentrating first on the aggregates containing four ACN molecules, it is seen that configuration 1 is the least stable, followed by configuration 2 and then configuration 3. This corresponds with the the distances between the anions, where configuration 1 has the smallest distance of about 9.2 Å, configuration 2 a distance of 12.4 Å, and

configuration 3 a distance of 16.9 Å (cf. Figs. **52b**, **52d**, and **52f**), meaning that the Coulomb repulsion between the anions reduces along the sequence. Interestingly, the total energies become more similar upon single oxidation of the aggregate and even very similar upon double oxidation. This can not be simply explained by corresponding changes in the Ta..Ta distances, as these even for two oxidised chains still differ significantly, ranging from 7.4 Å over 10.7 Å to 15.2 Å for the configurations 1 - 3, respectively. This rather has to be attributed to reorientation of the ACN molecules upon oxidising the chains: the negatively polarized nitrogen atoms in the cyano groups may get closer to positively charged pyrrole units without too strongly impairing the attraction of the positive dipole end (the methyl groups) to the heptafluorotantalate ions. Note that in configuration 3 with 4 ACN molecules hardly any reorientation is happening upon oxidation (cf. **51a** and **51b**) whereas significant ACN reorientation is observed for configurations 1 (cf. **49a** and **49b**) and 2 (cf. **50a** and **50b**), respectively.

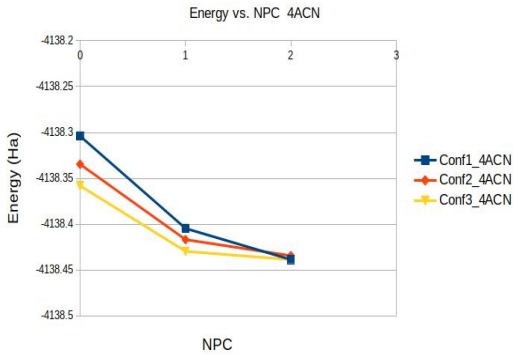

53a)

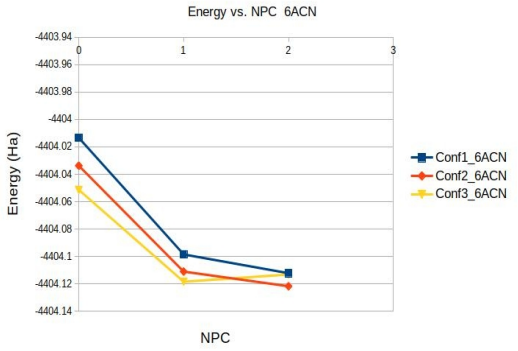

53b)

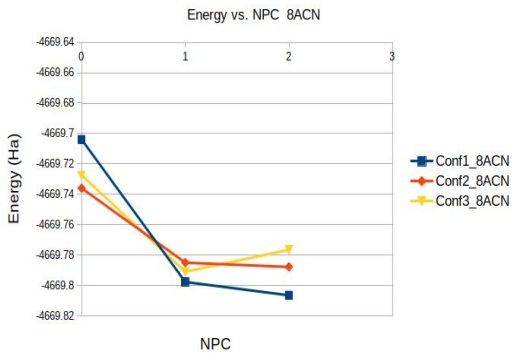

53c)

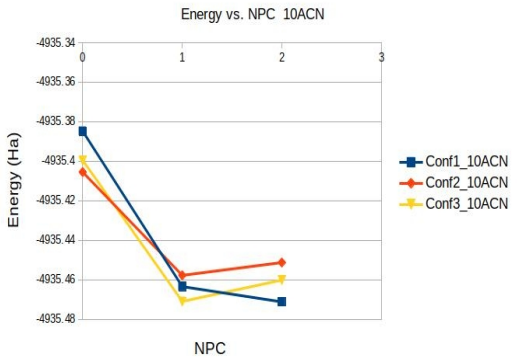

53d)

Figure **53.1**. Total energy vs. number of positive charges for 4 a), 6 b), 8 c), 10 d) ACN molecules.

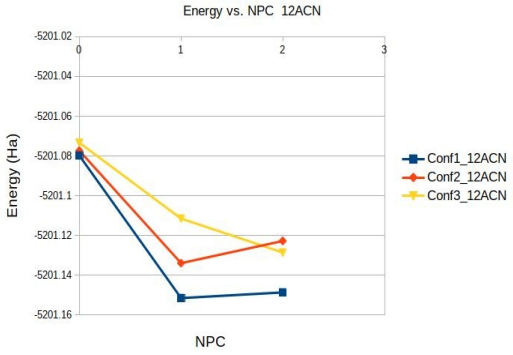

53e)

Figure **53.2**. Total energy vs. number of positive charges for 12 e) ACN molecules.

While the total energy consistently drops for the aggregates contaning 4 ACN molecules with increasing the number of positive charges on the chains, this is no longer the case for configuration 3 with 6 attached ACN molecules (cf. Fig. 53b). Here the singly oxidised form is the most stable one, as is also the case for configuration 3 with 8 ACN molecules (cf. Fig. 53c). When 10 ACN molecules are present, there are two configurations (2 and 3) out of three where the singly oxidised form is most stable, and this is also the case for the aggregates containing 12 ACN molecules (now for configurations 1 and 2). This resembles the situation for the aggregates containing water as solvent molecules, where also in a number of cases the singly oxidised form was more stable than the doubly oxidised one. Thus, dipolar solvents apparently help to stabilise aggregates between two heptafluorotantalate anions and two pentapyrrole chanis with a total charge of -3 rather than -2.

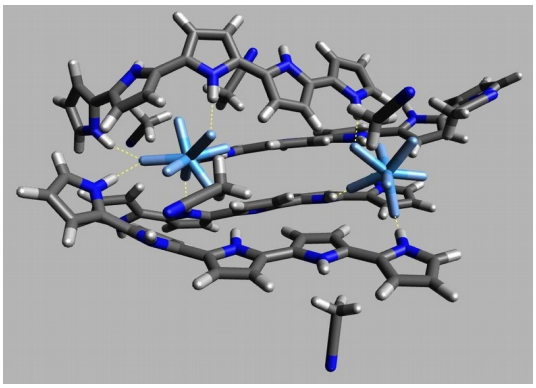

54a)

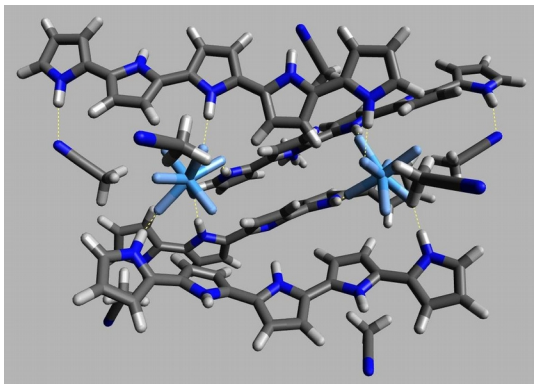

54b)

Figure **54.1**. Optimized structures for the first configuration with 4 Py_5-chains und 2 TaF_7^{2-} using 6 (a), 8 (b) and ACN molecules for the OS.

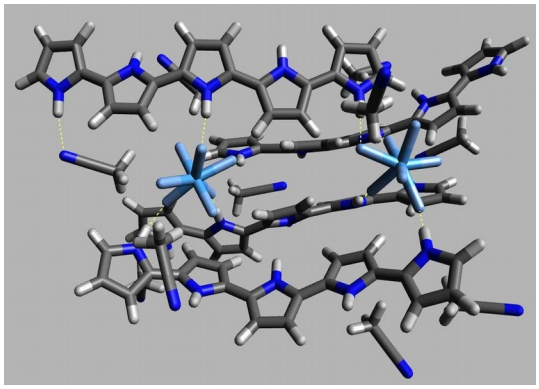

54c)

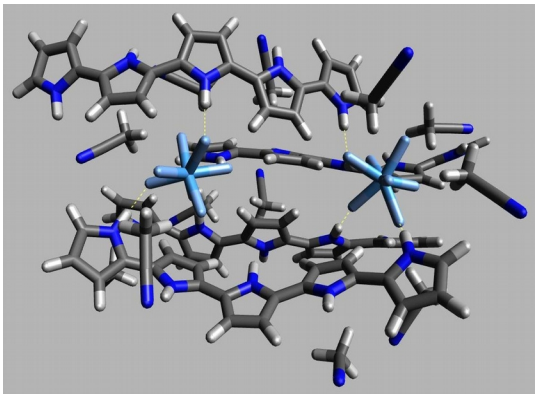

54d)

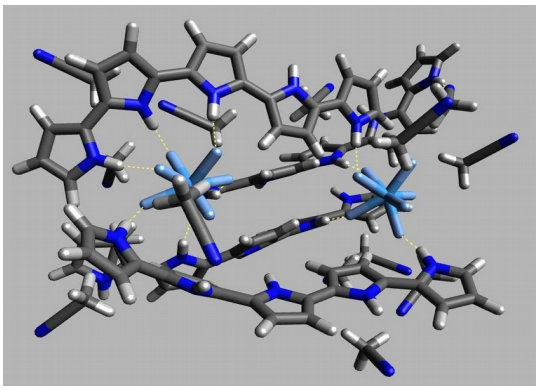

54e)

Figure **54.2**. Optimized structures for the first configuration with 4 Py_5-chains und 2 TaF_7^{2-} using 10 (c), 12 (d), and 14 (e) ACN molecules for the OS.

The largest of the investigated aggregate with ACN solvent molecules in different oxidation states is composed of two heptafluorotantalate ions and four pentapyrrole chains, to which 6 to 14 ACN molecules were added in random positions. While in section 6.3 this type of aggregate was considered with none of the chains oxidised, here now 1 to 4 positive charges were added. Figure 54 shows representative aggregates for two added positive charges, i.e., with total charges of -2. Let us recall that one of the main characteristics of most of these aggregates is a π-stack of two pentapyrrole chains, while the remaining chains do not show direct contacts between them. This is fairly independent on the oxidation state (cf. Figure 61 in appendix), at least as long as the total charge of the aggregate stays negative, while the aggergates with four oxidised chains show somewhat larger structural variation, though without breaking the π-stack. An exception is the aggregate containing 12 ACN molecules: here the π-stack is significantly perturbed for each of the oxidation states (cf. Fig. **61i**,**j**,**k**,**l** in the appendix).

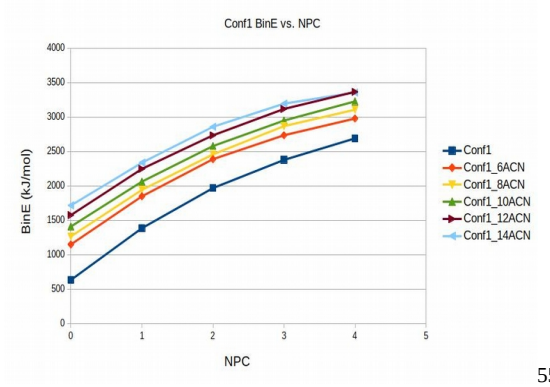

55a)

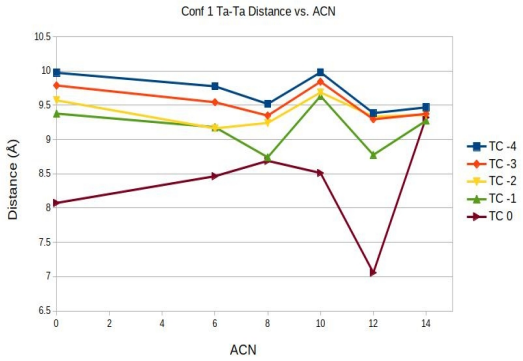

55b)

Figure **55**. Graphics of binding energy (a) vs. number of positive charges and Ta-Ta distance (b) vs. number of ACN.

While the trends in the binding energy as a function of the number of added positive charges and ACN molecules are very much as was to be expected (cf. Fig. **55a**), the plot of the Ta..Ta distance are in line with the above qualitative structural considerations: the aggregates with a total charge of 0 in most cases show significantly smaller distances between the anions as their analogs with negative total charges (cf. Fig. **55b**), and the aggregates containing 12 ACN molecules stand out in that here the distance reduction for four oxidised chains is even greater than for the aggregate without any solvent molecule, due to the structural flexibility of this aggregate accomanying the breakup of the π-stack.

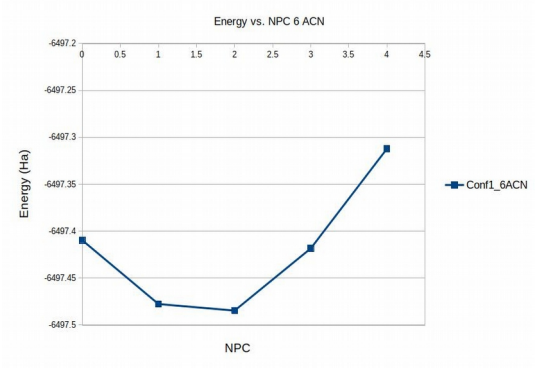

56a)

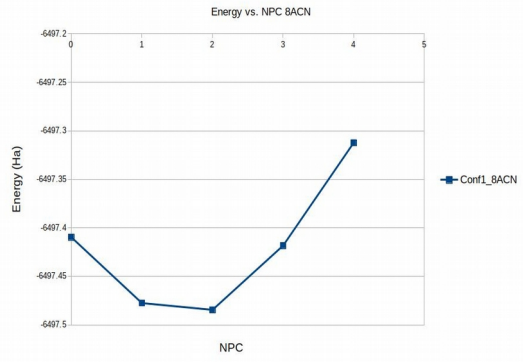

56b)

Figure **56.1**. Graphics of total energy vs. number of positive charges for 6 a) and 8 b) ACN molecules.

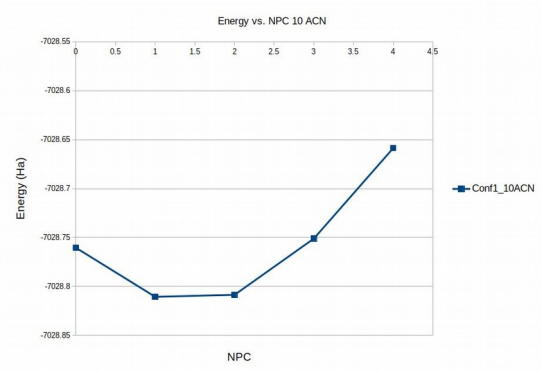

56c)

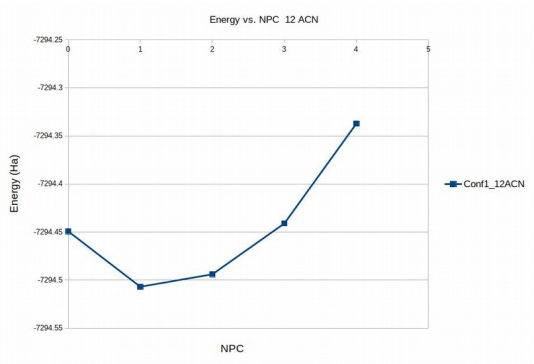

56d)

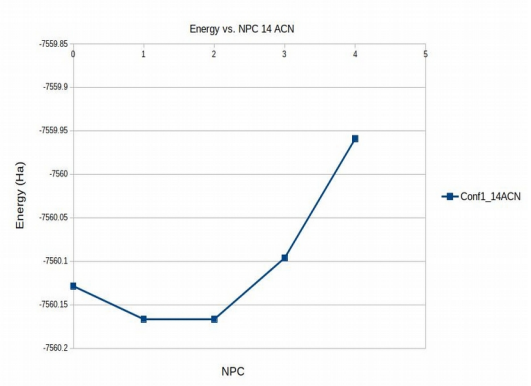

56e)

Figure **56.2**. Graphics of total energy vs. number of positive charges for 10 c), 12 d) and 14 e) ACN.

Fig. 56 demonstrates that also for this type of aggregate total charges of -3 and -2 lead to the lowest total energies: in the aggregates with 6 and 8 ACN molecules the preferred oxidation state corresponds to two oxidised pentapyrrole chains, with 10 and 12 ACN molecules a singly oxidised chains is preferred, and with 14 ACN molecules both oxidation states become nearly isoenergetic.

Chapter 8: Summary and Conclusions

Motivated by experimental investigations of amorphous polypyrrole doped with heptafluorotantalate ions[15] in this work aggregates formed by oligopyrroles and heptafluorotantalate ions have been investigated through quantum chemical calculations.

In a first step the structures and energies of the fundamental components, i.e., heptafluorotantalate and mono-, di-, and and tripyrrole, and of their aggregates were determined with dispersion-corrected density functional theory (DFT+D) and with second-order Møller-Plesset perturbation theory (MP2). The results for the anion yield an irregular structure with slightly differing Ta..F bond distances (2.00 - 2.02 Å with DFT+D, and 1.95 - 1.99 Å with MP2), essentially in agreement with crystallographical data[56] (1.92 - 1.98 Å). While the computational results for monopyrrole showed a maximum deviation of 0.02 Å from the experimental gas phase structure[57], demonstrating the validity of the theoretical approach, from the outcome of the calculations for the oligopyrroles a few relevant conclusions could be drawn:

(i) the pyrrole monomers twist around the C-C bonds linking them, with deviations from coplanarity in the order of 20-30 degree according to DFT+D and 10 degree more according to MP2.
(ii) as to be expected on the basis of dipole-dipole interactions between neighbouring pyrrole monomers in the oligopyrroles alternating monomer orientations are preferred over parallel orientations.
(iii) parallel arrangements of monomer units lead to curved oligopyrrole sections.

The combination of a heptafluorotantalate ion with monopyrrole showed the expected hydrogen bridge between the NH group of pyrrole and a fluorine atom of the anion, but also an auxiliary contact between an α-CH group and another fluorine atom, yielding a binding energy of 143 and 129 kJ/mol at the DFT+D and MP2 levels of theory, respectively, where no counterpoise correction was used at the DFT+D level while it was used for MP2. These binding energies increase to 175 and 147 kJ/mol, respectively, upon replacing monopyrrole with an alternating conformation of tripyrrole.

The corresponding structure is characterized by an NH..F bridge between the central pyrrole unit and the anion and two auxiliary contacts between β-CH groups of both neighbouring pyrrole units and two further fluorine atoms, forming an "ideal pocket". While even more stable conformations of an aggregate between tripyrrole and heptafluorotantalate can be obtained by switching pyrrole monomers around, replacing CH..F contacts with NH..F bridges, this structure was the most relevant for the further investigations since it allows for linear polypyrrole structures in the amorphous material. DFT+D calculations with two and four tripyrrole molecules showed that the anion is able to embed in several pockets, leading to an increase of the average NH..F and CH..F distances by 0.1 and 0.2 Å, respectively, with respect to the distances of 1.5 and 2.1 Å found for the aggregate of a single tripyrrole with the anion.

The second step of this study was devoted to DFT+D investigations of the questions of how many anions can be bound by a single oligopyrrole chain and, the other way round, how many chains can be bound by several anions? A pentapyrrole chain possesses two neighbouring pockets and, in fact, is able to bind two anions. However, the huge Coulomb repulsion between the anions leads to a twist of the chain which allows to increase the distance between the anions. Twisting of the chain can be avoided if the two anions bind to pockets at opposing sides of the chain. Chain twisting is also strongly reduced when two pentapyrrole chains accomodate two anions in immediately neighbouring pockets. In contrast to the aggregate containing only one chain, which was metastable, this aggregate was found to be weakly stable: it has a binding energy of 47 kJ/mol with respect to dissociation into two anions and two alternating pentapyrrole chains.

Other aggregates between two pentapyrrole chains and two anions, where one or both of the anions bind to "half-pockets" at the end of the chains were found to be more stable, of course, due to an increase of the ion-ion distances. It is remarkable that two chains are even able to bind three anions when two of them bind to half-pockets and one to the central pocket of both chains, though complete dissociation of this metastable aggregate would relase 546 kJ/mol. Two anions were found to be able to bind in pockets and half-pockets of four and five pentapyrrole chains, while a sixth chain was observed to unhitch. The smallest interionic distances in these stable aggregates amounted to 7.7 Å, only slightly more than the 7.1 Å between the NH groups in neighbouring pockets of free

oligopyrrole. Taking Coulomb repulsion between the anions explicitely into account but summing all other interaction and deformation energy contributions into anion "embedding energies" the latter were determined to be around 160 kJ/mol. The largest aggregate considered consisted in five heptapyrrole chains holding three anions. The distances between the anions here were around 7.4 Å and the embedding energy about 170 kJ/mol. The average NH..F and CH..F distances of 1.6 and 2.5 Å, respectively, were fairly similar to the corresponding numbers of 1.7 and 2.4 Å found for the aggregates containing three anions and four pentapyrrole chains.

These findings suggest that heptafluorotantalate anions indeed may be embedded in neighbouring pockets of polypyrrole material sections containing bundles of up to five chains in a more or less parallel arrangement. Assuming an embedding energy of 160 kJ/mol in each pocket the total embedding energy of an anion into a bundle of five chains would amount to 800 kJ/mol. This slightly overcomes the Coulomb repulsion of 780 kJ/mol with another anion in a neighbouring pocket, when the distance of 7.1 Å between two parallelly oriented NH groups is taken as the ion-ion distance. On the other hand it has to be taken into account that each anion has long-range Coulomb interactions with all other anions already present in the material, so that absorption has to come to an end long before each possible pocket has been filled. However, these considerations ignore three further factors: (i) the possibility of oxidation of polypyrrole chains, (ii) perturbation by solvent molecules,and (iii) embedding of counterions such as potassium cations.

Thus in further steps of the project at least the first two factors were investigated.

While the vertical and adiabatic ionisation potentials (IPs) of the heptafluortantalate ions were determined as about 120 and 54 kJ/mol, respectively, the corresponding numbers for monopyrrole amount to 801 and 786 kJ/mol on the DFT+D level of theory. While due to better charge delocalisation the vertical and adiabatic IP for pentapyrrole drop to 533 and 522 kJ/mol, at first sight one would still expect oxidation of the anion rather than of oligopyrrole in an aggregate combining both components. Yet, this is not the case: as shown by DFT+D calculations the vertical IPs dramatically drop down to about 41 - 90 kJ/mol for aggregates between a single anion and two tripyrrole in various structural arrangements, and one of these aggregates even had a slightly negative adiabatic IP of -3 kJ/mol after structure relaxation (with the adiabatic IP of the the remaining aggregates

being in the range 35 - 78 kJ/mol). A Mulliken population analysis confirmed that in the oxidised aggregates (possessing a doublet spin state) the tripyrrole components rather than the heptflurotantalate ion lost the electon, and that the positive charge on the tripyrrole components is fairly evenly delocalised over the backbone atoms of both oligopyrroles.

The oxidation of the oligopyrroles rather than of the anion evidently can be rationalized through the creation of a Coulomb attraction between the components of the aggregates upon oxidation. Furthermore, it was demonstrated that double oxidation (leading to triplet spin states) in these aggregates takes also place at the oligopyrrole components, and that the second oxidation step vertically requires 310 - 350 kJ/mol and adiabatically 280 - 310 kJ/mol. For larger aggregates composed of one anion and four tripyrroles and of two anions and two and four pentapyrrole chains single and double oxidation through population analysis was also shown to happen at the oligopyrrole components.

The aggregates between two anions and several pentapyrrole chains were of particular interest, as they all possess negative first adiabatic IPs in the range of -190 to -300 kJ/mol, and the second oxidation step still releases up to about 100 kJ/mol energy, producing an overall charge of -2. For the aggregates with four pentapyrrole chains third and fourth oxidation steps were also considered: here it was observed that the aggregates with an overall charge of -1 have roughly the same total energies as the singly oxidised aggregates with a charge of -3, while the total energies of the overall neutral aggregates are close to those of the non-oxidised aggregates with charge -4. As to be expected on the Coulomb attraction between anions and cations and partial screening of the Coulomb repulsion between the anions through the polarisable cations the anion-anion distances were found to decrease with each oxidation step, from 7.7 - 10.0 Å in the non-oxidised over 7.2 - 9.6 Å in the doubly oxidised to 6.9 - 8.1 Å in the fourfold oxidised aggregates.

In the next step of the project solvent molecules were added to the aggregates composed of two anions and two and four pentapyrrole chains, respectively. The effects of two different kinds of solvent molecules were thus investigated:

(i) water, as the most important example with hydrogen bridge- donor and acceptor capabilities
(ii) acetonitrile as an example with a large dipole moment and hydrogen bond acceptor capabilities only.

Another important difference between these classes of solvent molecules is their size. Accordingly, it was observed in the DFT+D level structure optimized aggregates that the small water molecules ocassionally may insert into NH..F hydrogen bridges to yield bridged NH..HOH..F structures, that they may serve as F..HOH..F bridges between two heptafluorotantalate anions, and that, not unexpectedly, they can form general hydrogen bond networks while essentially keeping the basic anion-oligopyrrole aggregate structure intact. For example, in the four considered aggregates composed of two anions and four pentapyrrole chains the anion-anion distances without water molecules were in the range of 8.5 - 10.6 Å, and these distances in each case changed by less than 1.2 Å when 8 to 24 water molecules were successively added in steps of four. An average binding energy per water molecule of 73 kJ/mol was obtained, which is about 10 kJ/mol less than the corresponding number for smaller aggregates consisting of two anions and only two pentapyrrole chains and up to 12 water molecules.

The comparatively large acetonitrile molecules in most cases were found to orient their methyl group ends towards the heptafluorotantalate ions, in agreement with expectation based on the orientation of their dipole moment. While the addition of acetonitrile molecules in most cases did not seem to have a large effect on the anion-anion distances, usually varying it by less than 1.2 Å, in one case a detachement of one of the anions from one of the chains was observed, resulting in a strong increase of the anion-anion distance by more than 5 Å. It has to be noted, however, that this concerned an aggregate with only two pentapyrrole chains, which leaves the anions fairly exposed to the attack of solvent molecules. In the considered aggregate of two anions and four pentapyrrole chains the anion-anion distance varied within a few tenths of an Å only, when 6 to 14 acetonitrile molecules were added in steps of two. In contrast to the case of water addition, the average contribution of each acetonitrile molecule to the total binding energy was found to systematically decrease with the number of added solvent molecules, from 86 kJ/mol for six to 37 kJ/mol for fourteen.

The final step of this study consisted in an investigation of the oxidation of the microsolvated aggregates, again by dispersion-corrected density functional theory. For the aggregates containing two pentapyrrole chains up to double oxidation was considered, and up to fourfold oxidation for the aggregates containing four chains. With water as solvent the anion-anion distances usually were found to decrease with each oxidation step. The total energy, on the other hand, displayed a similar behaviour as already found for the non-solvated oxidised aggregates: many of the aggregates with four pentapyrrole chains are energetically most stable when they are twofold oxidised.

There were aggregates, however, which were most stable in singly oxidised form - and that was also true for some of the aggregates containing two pentapyrrole chains only. Overall this was also observed whan water was replaced with acetonitrile. From this and the findings described above one is led to speculate that each heptafluorotantalate ion adsorbed into polypyrrole triggers a single autooxidation step when no solvent is present, while additional uptake of solvent molecules tends to reduce the amount of automatically generated positive charges in the material.

Bibliography

1. H. Shirakawa, E. J. Louis, E. J. MacDiarmid, C. K. Chiang, A. J. Hegger, *J. Chem. Soc., Chem. Commun.,* **1977**, *16*, 578-580.
2. C. K. Chiang, C. R. Fincher, Jr., Y. W. Park, A. J. Heeger, H. Shirakawa, E. J. Louis, S. C. Gau, A. G. MacDiarmid, *Phys. Rev. Lett.,* **1977,** *39,* 1098-1101.
3. P. Chandrasekhar, *Conducting Polymers, Fundamentals and Applications. Vol 1*. Dordrecht: Kluwer Academic Publisher., **1999**.
4. G. Inzelt, *J. Electrochem. Sci. Eng.,* **2018,** *8(1),* 3-37.
5. H. P. de Oliveira, S. A. Sydlik, T. M. Swager, *J. Phys. Chem. C,* **2013**,*117*, 10270-10276.
6. M. B. Runge, M. Dadsetam, J. Baltrusaitis, T. Ruesink, L. Lu, A. J. Windebank, M. J. Yaszemski, *Biomacromolecules,* **2010**, *11(11),* 2845-2853.
7. N. M. Dimitrijevic, S. Tepavcevic, Y. Liu, T. Rajh, S. C. Silver, D. M. Tiede, *J. Phys. Chem. C,* **2013**, *117,* 15540-15544.
8. B. Parakhonskiy, D. Shchukin, *Langmuir,* **2015**, *31*, 9214-9218.
9. R. Das, S. Giri, A. L. King Abia, B. Dhonge, A. Maity *ACS Sustainable Chemistry & Engineering,* **2017,** *5*(3), 2711-2724.
10. K. S. Jang, H. Lee, B. Moon, *Synthetic Metals,* **2004**, *143*, 289-294.
11. J. Heinze, B. Frontana-Uribe, S. Ludwigs, *Chem. Rev.,* **2010**, *110*, 4724-4771.
12. C. O. Yoon, H.K. Sung, J. H. Kim, Barsoukov, E. ; Lee, H. *Synthetic Metals* **1999**, *9*, (3), 201-212.
13. T. Eicher, S. Hauptmann, A. Speicher, *The Chemistry of Heterocycles: Structure, Reactions, Synthesis, and Applications*, Wiley-VCH, **2012**, pgs 108-124.
14. G. Zhang, J. Ma, J. J. Wen, *Phys. Chem. B*, **2007**, *111,(40)*, 11670-11679.
15. M. Sc. Thesis Document Gamarra, Jorge, “ Síntesis electroquímica y caracterización de películas de polipirrol dopadas con el anión heptafluorotantalato con potencial de alta capacitancia” Universidad de Los Andes Aug. **2012**, Bogotá, Colombia.
16. TURBOMOLE V7.0 2015, a development of University of Karlsruhe and Forschungszentrum Karlsruhe GmbH, 1989-2007, TURBOMOLE GmbH, since 2007; available from http://www.turbomole.com.

17. Electronic Structure Calculations on Workstation Computers: The Program System TURBOMOLE. R. Ahlrichs, M. Bär, M. Häser, H. Horn and C. Kölmel; *Chem. Phys. Letters,* **1989** *162*, 165-169.
18. H.-J. Werner, P. J. Knowles, G. Knizia, F. R. Manby, M. Schütz, WIREs *Comput Mol Sci* **2012** *2*, 242-253.
19. J. C. Lacroix, R.J. Valente, F. Maurel, P. C. Lacaze, *Chem. Eur. J.* **1998**, *4*,(9),1667-1677.
20. R. Colle, A. Curioni, *J. Am. Chem. Soc.* **1998,** *120,*(19), 4832-4839.
21. C. K. Lee, C. C. Hua, S. A. Chen, *J. Phys. Chem. B* **2009**, *113,(49)*, 15937–15948. A. A. Kocherzhenko, S. Patwardhan, F. C. Grozema, H. L. Anderson, L.D.A. Siebbeles, *J. Am. Chem. Soc.* **2009**, *131,(15)*, 5522–5529.
22. Ramachandran, K. I., *Computational chemistry and molecular modeling : principles and applications* Berlin : Springer, **2008**.
23. Z. L. Cai, M. J. Crossley, J. R. Reimers, R. Kobayashi, R. D. Amos, *J. Phys. Chem. B* **2006,** *110,*(31), 15624-15632.
24. S. Fantacci, F. De Angelis, J. Wang, S. Bernhard, A. Selloni, *J. Am. Chem. Soc.* **2004,** *126, (31)*, 9715-9723.
25. V. G. Ruiz, W. Liu, E. Zojer, M. Scheffler, A. Tkatchenko, *Phys. Rev. Lett.* **2012,** *108*, 146103.
26. R. Colle, P. Parruccini, A. Benassi, C. Cavazzoni, *J. Phys. Chem. B* **2007**, *111*, (11), 2800-2805.
27. J.U. Castillo, P. Guadarrama, S. Fomine, *Org. Electron.* **2013,** *14,(10)*, 2617-2627.
28. D.R. Armstrong, E. Brammer, T. Cadenbach, E. Hevia, A.R. Kennedy, *Organometallics* **2013**, *32*, 480−489.
29. B. Guo, Q. Kong, Y. Zhu, Y. Mao, Z. Wang, M. Wan, L. Chen, *Chem. Eur. J.* **2011,** *17*, 14878 – 14884.
30. A. Tkatchenko, M. Scheffer, *Phys. Rev. Lett.* **2009** ,*102*,(7) 073005(1-4).
31. S. Grimme, J. Antony, S. Ehrlich, H. Krieg, *J. Chem. Phys*. **2010** *132*, 154104.
32. Jensen, F. *Introduction to computational Chemistry,* Chichester, England ; Hoboken, NJ : John Wiley & Sons, **2007**.
33. P. Echenique, J. L. Alonso, *Mol. Phys.* **2007,** *105, (23-24),*3057-3098.
34. D.Cremer, *WIREs Comput. Mol. Sci.* **2011**, *1,* 509–530.
35. L. Claes, J.P. François, M. S. Deleuze, *J. Am. Chem. Soc.* **2002**, *124*, 7563-7572.

36. D. A. Scherlis, N. J. Marzari, *Phys. Chem. B* **2004** ,*108,(46)*, 17791-17795.
37. S.S. Zade, N. Zamoshchik, M. Bendikov, *Chem. Eur. J.* **2009**, *15*, 8613 – 8624.
38. J.D. Ripoll, A. Serna, D. Guerra, A. Restrepo, *J. Phys. Chem. A* 2010, *114, (41)*, 10917-10921.
39. R. Notario, M. Temprado, M. V. Roux, J. F. Liebman, *J. Phys. Chem. A* **2012**, *116*, 4363−4370.
40. G.R. De Maré, C.W. Bock, *Chem. Data Coll.***2018**, *15,* 97-106.
41. A. A. Skeltona, J. R. Fried Phys. Chem. Chem. Phys., **2013**,*15*, 4341-4354.
42. M.D. Hanwell, D.E. Curtis, D.C. Lonie, T. Vandermeersch, E. Zurek, G.R. Hutchison; “Avogadro: An advanced semantic chemical editor, visualization, and analysis platform” *Journal of Cheminformatics* **2012**, *4*, 17.
43. M. Häser, R. Ahlrichs, *J. Comp. Chem.,* **1989**, *10*, 104-111.
44. O. Treutler, R. Ahlrichs, J. Chem. Phys. **1995**, *102*, 346-354.
45. M. von Arnim, R. Ahlrichs, *J. Chem. Phys.* **1999**, *111*, 9183-9190.
46. C. Hättig, A. Hellweg, A. Köhn, *Phys. Chem. Chem Phys.,* **2006**, *8*, 1159-1169.
47. A. D. Becke, *Phys. Rev. A*, **1988**, *38*, 3098-3100.
48. P. Perdew, *Phys. Rev. B*, **1986**, *33*, 8822-8824.
49. S. Grime, J. Antony, E. Ehrlich, H. Krieg, *J. Chem. Phys.,* **2010**, *132*, 154104, (1-18).
50. F. Weigend, R. Ahlrichs, *Phys. Chem. Chem. Phys.*, **2005**, *7* , 3297-3305.
51. F. Weigend, *Phys. Chem. Chem. Phys.,* **2006,** *8,* 1057-1065.
52. F. Weigend, M. Häser, H. Patzelt, R. Ahlrichs, *Chem. Phys. Lett.* **1998**, *294*, 143-152.
53. A. Hellweg, C. Hättig, S. Höfener, W. Klopper, *Theor. Chem. Acc.,* **2007**, *117*, 587-597.
54. S. F. Boys and F. Bernardi, *Mol. Phys.,* **1970**, *19,* 553-566.
55. M. Gutowski, J.G.C.M van Duijneveldt-van de Rijdt, J.H. van Lenthe, F.B. van Duijneveldt, *J. Chem. Phys.*, **1993**, *98*, 4728-4737.
56. C.C. Torardi, L.H. Brixner, G. Blasse, *J. Solid State Chem.*, **1987**, *67*, 21-25.
57. L. Nygaard, J.T. Nielsen, ; J. Kirchheiner, G. Maltesen, J. Rastrup-Andersen, G. O. Sørensen, *J. Mol. Struct.,* **1969**, *3*, 491-506.

58. M. Kofranek, T. Kovář, A. Karpfen, H. Lischka, *J. Chem. Phys.,* **1992**, *96*, 4464-4473.
59. P. A. Steiner, W. Gordy, *J. Mol. Spectrosc.*, **1966**, *21*, 291-301.
60. J. D. Bernal, R. H. Fowler, *J. Chem. Phys.*, **1933**, *1*, 515-548.

Appendix

Structures and binding energies for $[(TaF_7)_2(Py_5)_4(H_2O)_x]^{y-}$ with x=8,12,16,20,24 y=3,2,1,0 .

Conf 1 (8WM and 12 WM)

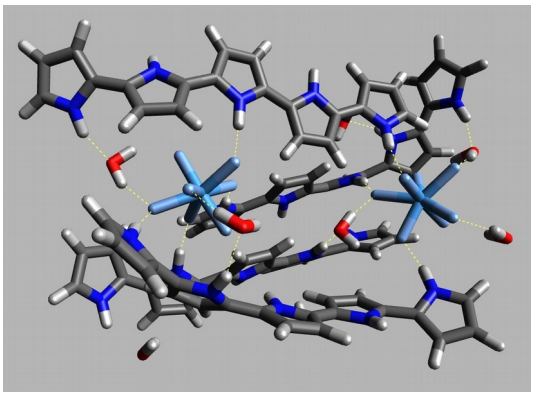

57a)

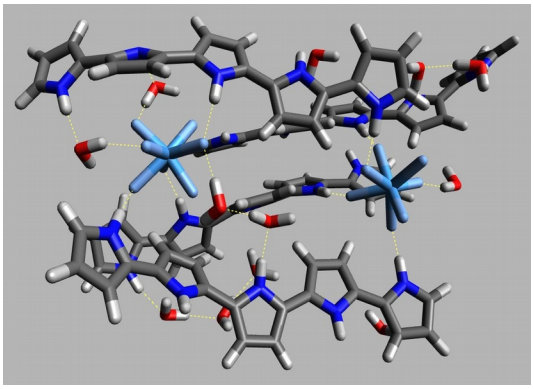

57e)

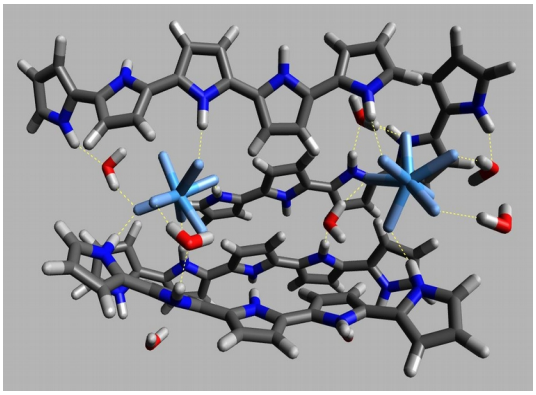

57b)

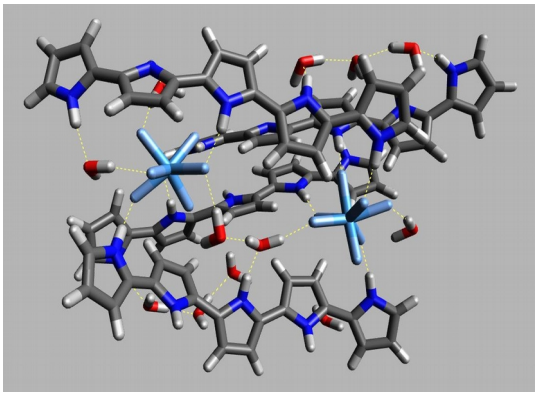

57f)

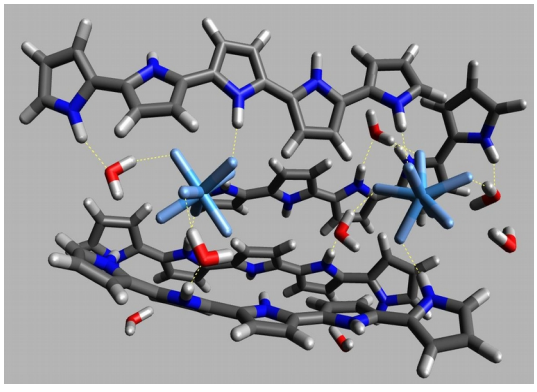

57c)

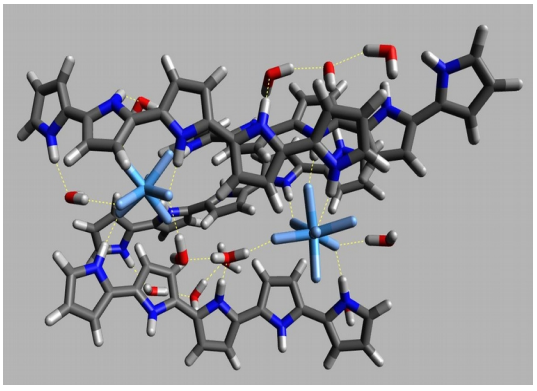

57g)

Figure **57.1**. The first configuration with 4 Py_5-chains und 2 TaF_7^{2-} with 8WM (left) and 12 WM (right) with oxidation state (OS), shown progressively: -3 (a,e), -2 (b,f) , -1 (c,g).

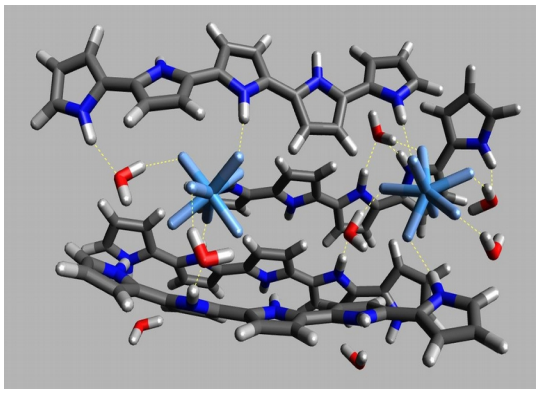

57d)

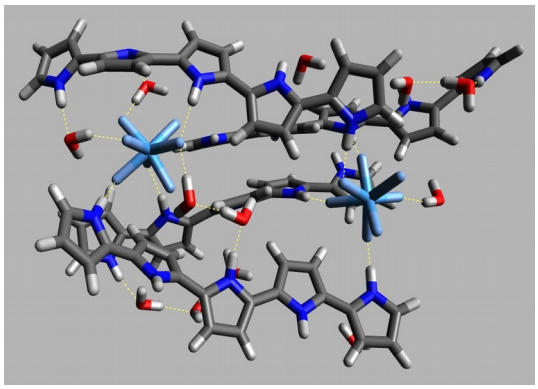

57h)

Figure **57.2**. The first configuration with 4 Py_5-chains und 2 TaF_7^{2-} with 8WM (left) and 12 WM (right) with oxidation state (OS), shown progressively: 0 (d,h).

Conf 1 (16 WM and 20 WM)

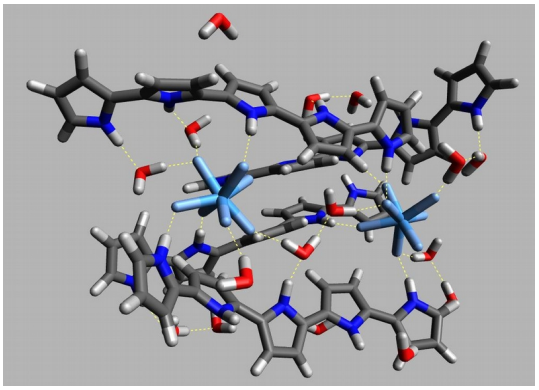

57i)

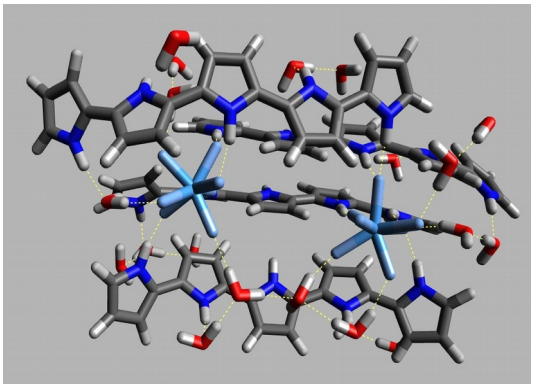

57m)

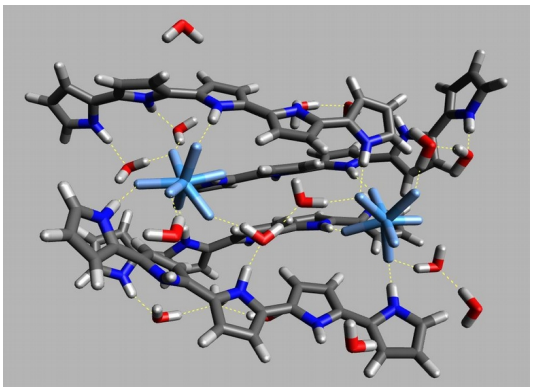

57j)

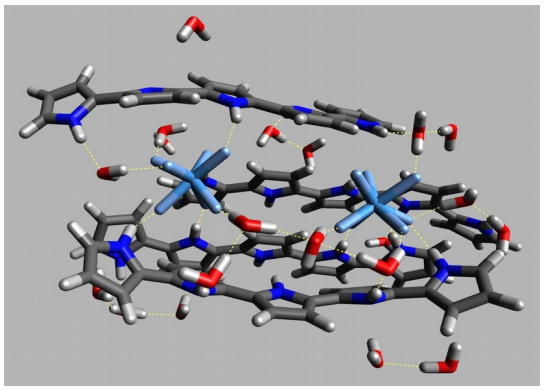

57n)

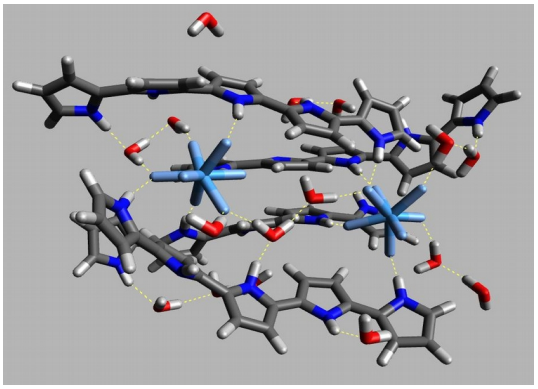

57k)

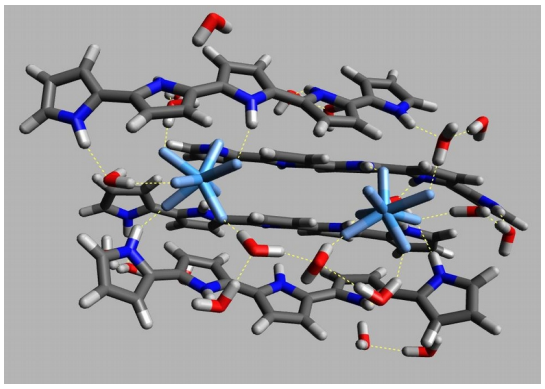

57o)

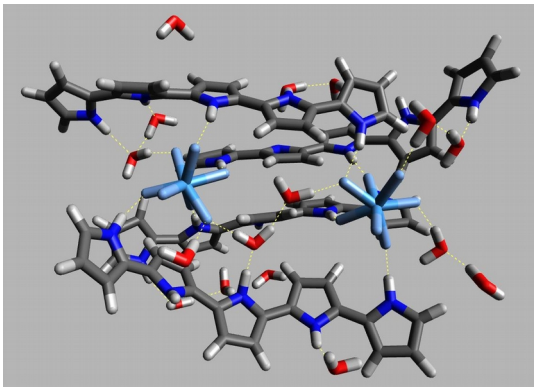

57l)

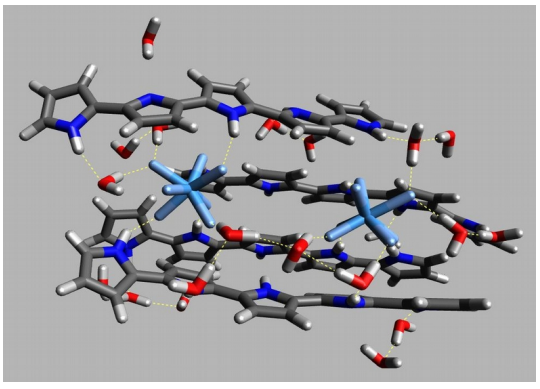

57p)

Figure **57.3**. The first configuration with 4 Py_5-chains und 2 TaF_7^{2-} with 16WM (left) and 20 WM (right) with oxidation state (OS), shown progressively: -3 (i,m), -2 (j,n) , -1 (k,o), 0 (l,p).

Conf 1 (24 WM)

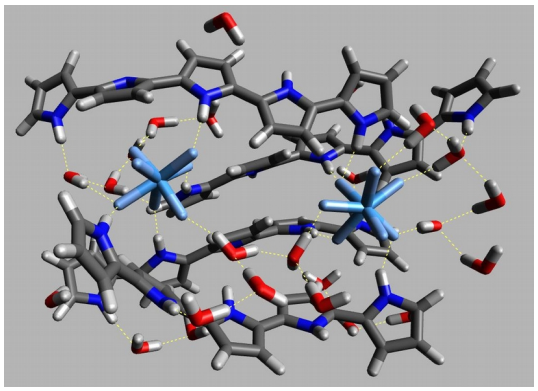

57q)

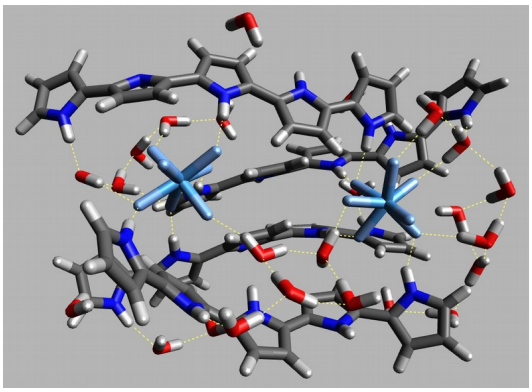

57r)

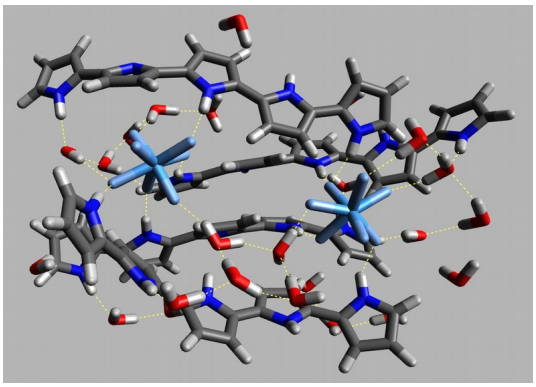

57s)

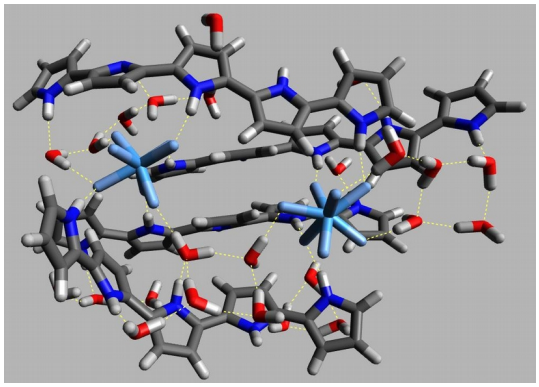

57t)

Figure **57.4**. The first configuration with 4 Py_5-chains und 2 TaF_7^{2-} with 24 WM with oxidation state (OS), shown progressively: -3 (q), -2 (r) , -1 (s), 0 (t).

Total energy (Ha)

System	Energy OS -4	Energy OS -3	Energy OS -2	Energy OS -1	Energy OS 0
No solvent	-5700.336053	-5700.424034	-5700.447283	-5700.404379	-5700.325008
8WM	-6312.324758	-6312.393697	-6312.414479	-6312.359260	-6312.231862
12WM	-6618.272800	-6618.347127	-6618.374744	-6618.310642	-6618.281174
16WM	-6924.260068	-6924.316725	-6924.317283	-6924.259279	-6924.116432
20WM	-7230.273031	-7230.330231	-7230.325229	-7230.252643	-7230.124657
24WM	-7536.215535	-7536.265776	-7536.265874	-7536.249488	-7536.265776

Binding energy (kJ/mol)

System	Energy OS -4	Energy OS -3	Energy OS -2	Energy OS -1	Energy OS 0
No solvent	630.62	1383.26	1965.94	2374.94	2688.19
8WM	1285.97	1988.61	2564.82	2941.48	3128.64
12WM	1492.06	2208.84	2803.00	3156.34	3600.61
16WM	1801.13	2471.53	2994.64	3363.99	3510.59
20WM	2177.67	2849.49	3358.00	3689.07	3874.68
24WM	2369.21	3022.76	3544.66	4023.29	4587.69

Ta-Ta distance (Å)

System	Energy OS -4	Energy OS -3	Energy OS -2	Energy OS -1	Energy OS 0
No solvent	9.974	9.788	9.571	9.378	8.075
8WM	10.585	10.318	10.297	9.936	10.038
12WM	10.637	10.607	9.072	8.923	10.895
16WM	9.834	9.766	9.622	9.287	9.179
20WM	8.477	8.328	7.955	7.995	7.98
24WM	9.865	9.05	9.055	8.934	8.413

Ionization energy (kJ/mol)

System	En. Diff (OS^{-3}-OS^{-4})	En. Diff.(OS^{-2}-OS^{-3})	En. Diff.(OS^{-1}-OS^{-2})	En. Diff.(OS^{0}-OS^{-1})	En. Diff.(OS^{0}-OS^{-4})
No solvent	-230.99	-61.04	112.64	208.39	29.00
8WM	-181.00	-54.56	144.98	334.48	243.90
12WM	-195.14	-72.51	168.30	77.37	-21.99
16WM	-148.75	-1.47	152.29	375.04	377.12
20WM	-150.18	13.13	190.57	336.03	389.56
24WM	-131.91	-0.26	43.02	-42.76	-131.91

Table **21**. Energetic and geometric data shown in this order: Total energy of the structures in each one of the OS, binding energy, inter- Ta ion distance and ionisation energy.

Conf 2 (8 WM and 12 WM)

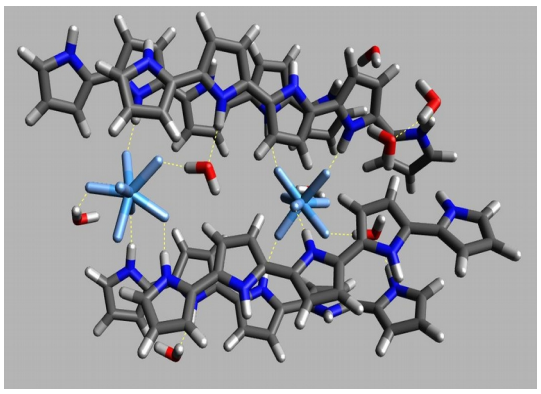

58a)

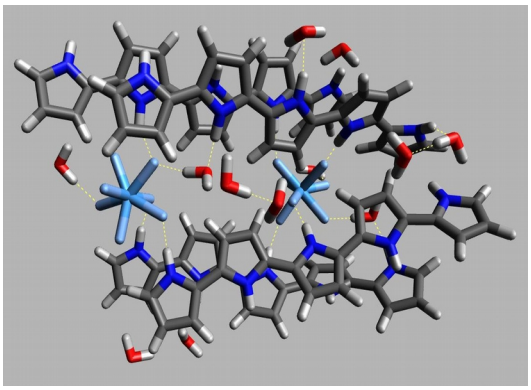

58e)

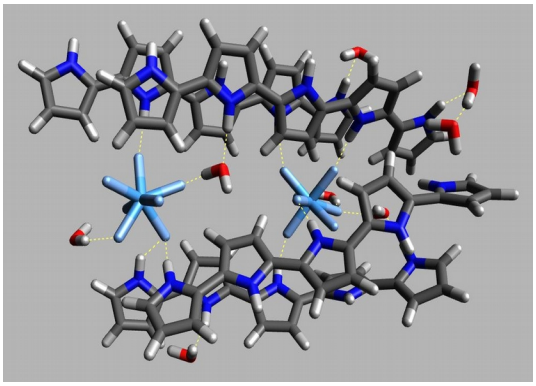

58b)

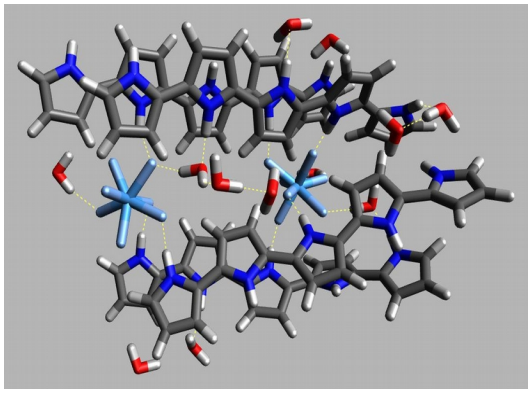

58f)

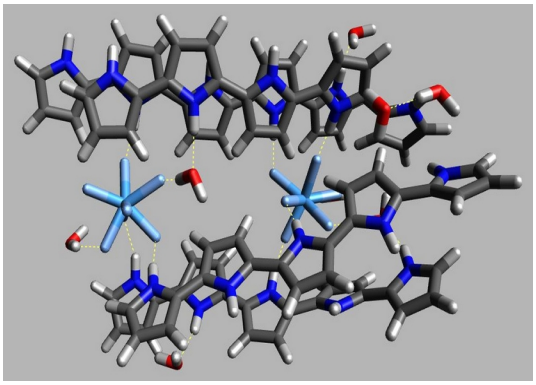

58c)

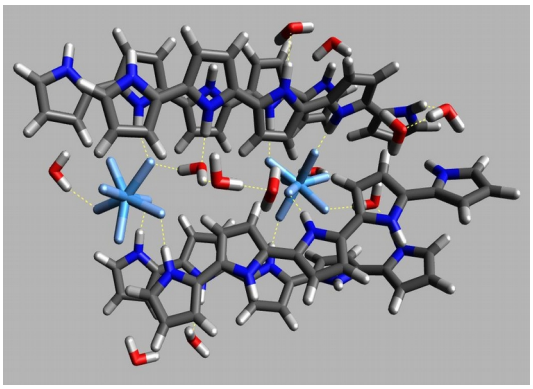

58g)

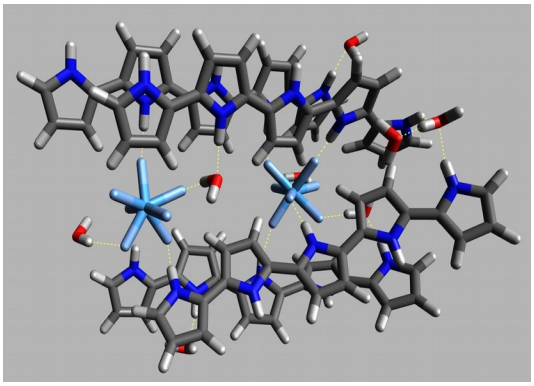

58d)

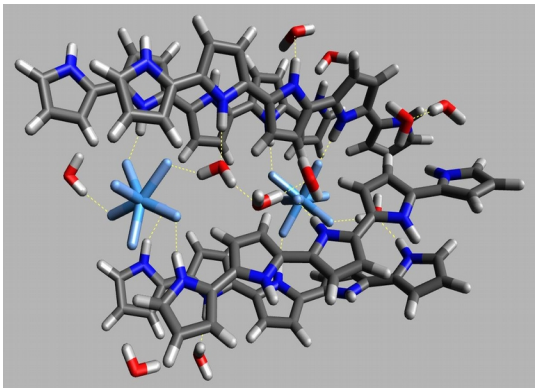

58h)

Figure **58.1**. The second configuration with 4 Py_5-chains und 2 TaF_7^{2-} with 8WM (left) and 12 WM (right) with oxidation state (OS), shown progressively: -3 (a,e), -2 (b,f) , -1 (c,g), 0 (d,h).

Conf 2 (16 WM and 20 WM)

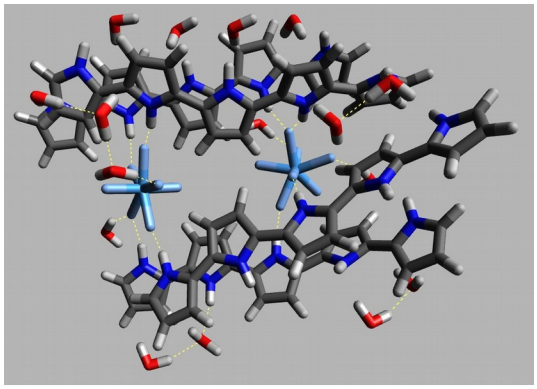

58i)

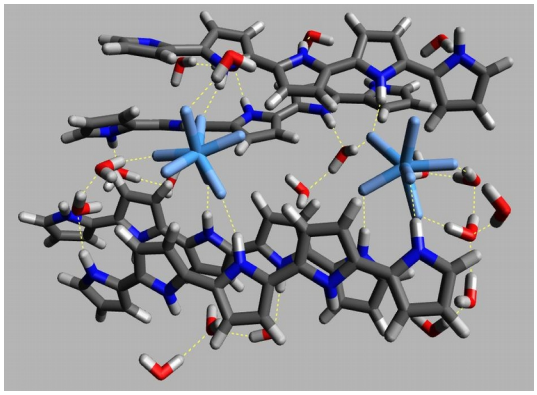

58m)

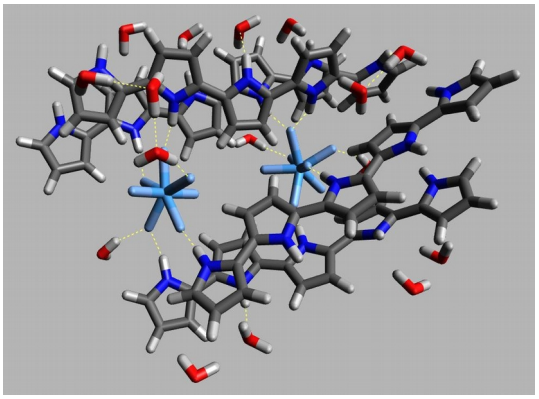

58j)

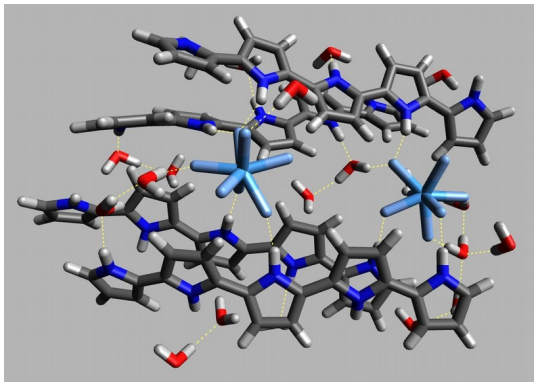

58n)

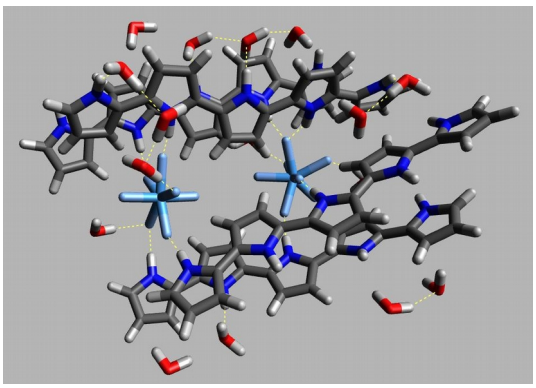

58k)

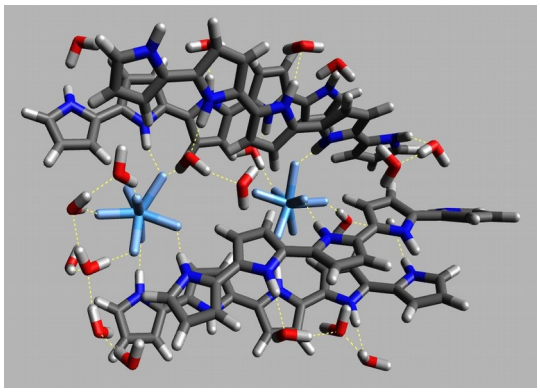

58o)

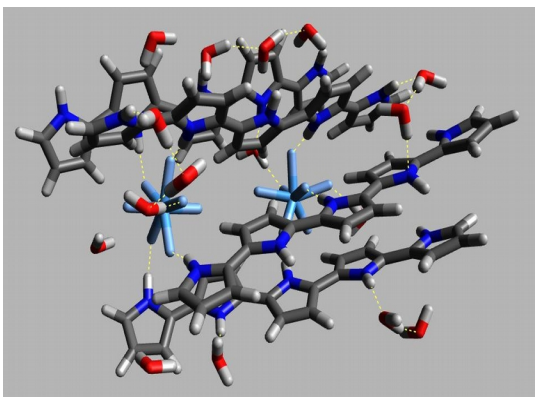

58l)

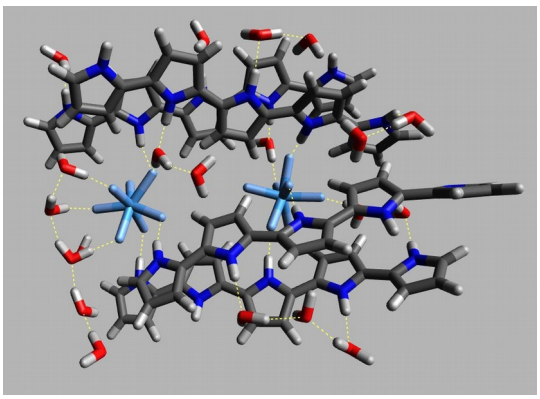

58p)

Figure **58.2**. The second configuration with 4 Py_5-chains und 2 TaF_7^{2-} with 8WM (left) and 12 WM (right) with oxidation state (OS), shown progressively: -3 (i,m), -2 (j,n) , -1 (k,o), 0 (l,p).

Conf 2 (24 WM)

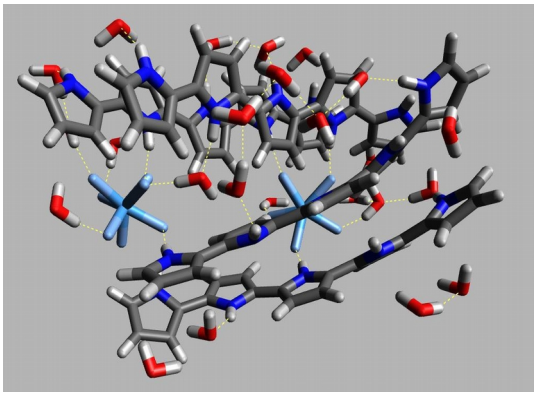

58q)

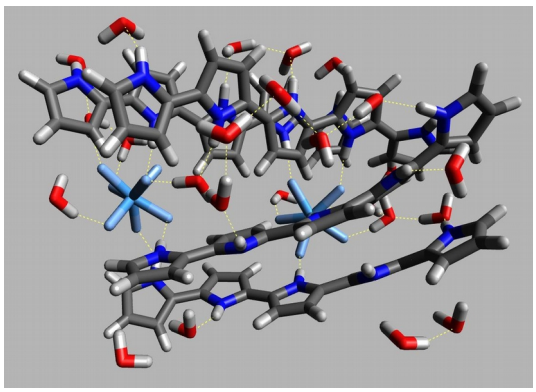

58r)

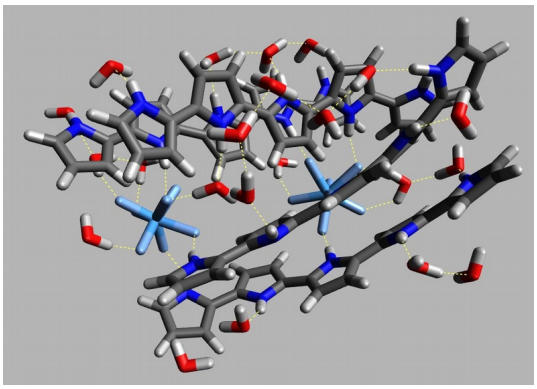

58s)

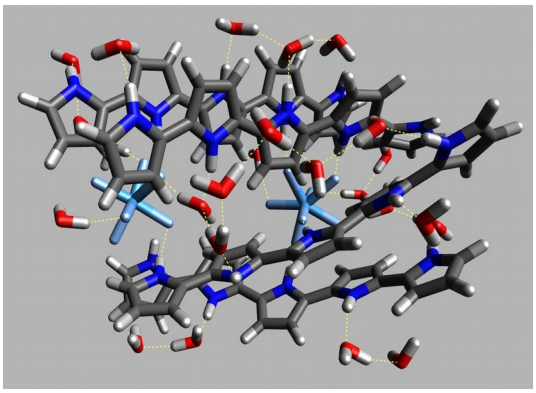

58t)

Figure **58.3**. The second configuration with 4 Py_5-chains und 2 TaF_7^{2-} with 24 WM with oxidation state (OS), shown progressively: -3 (q), -2 (r) , -1 (s), 0 (t).

Total energy (Ha)

System	Energy OS^{-4}	Energy OS^{-3}	Energy OS^{-2}	Energy OS^{-1}	Energy OS^{0}
No solvent	-5700.335233	-5700.448579	-5700.487386	-5700.455448	-5700.358389
8WM	-6312.252653	-6312.378025	-6312.432710	-6312.407720	-6312.328374
12WM	-6618.188847	-6618.318207	-6618.383652	-6618.372513	-6618.296222
16WM	-6924.156865	-6924.275119	-6924.332057	-6924.328601	-6924.260997
20WM	-7230.115344	-7230.238067	-7230.310952	-7230.314335	-7230.252339
24WM	-7536.078727	-7536.213707	-7536.286688	-7536.294156	-7536.229227

Binding energy (kJ/mol)

System	Energy OS^{-4}	Energy OS^{-3}	Energy OS^{-2}	Energy OS^{-1}	Energy OS^{0}
No solvent	689.26	1465.73	2071.23	2490.99	2715.04
8WM	1295.46	2025.43	2612.68	2990.75	3183.23
12WM	1553.55	2275.50	2826.38	3176.20	3358.21
16WM	1803.57	2502.71	3033.42	3405.57	3616.74
20WM	2123.34	2807.75	3320.51	3650.80	3850.23
24WM	2405.16	3097.28	3599.31	3929.34	4096.60

Ta-Ta distance (Å)

System	Energy OS^{-4}	Energy OS^{-3}	Energy OS^{-2}	Energy OS^{-1}	Energy OS^{0}
No solvent	8.876	8.624	8.353	7.578	7.409
8WM	9.802	9.598	9.022	9.234	8.717
12WM	9.888	9.757	9.628	9.497	9.211
16WM	8.083	7.962	7.803	7.571	7.492
20WM	9.011	8.909	8.847	8.537	8.121
24WM	10.007	9.463	9.259	8.895	9.015

Ionization energy (kJ/mol)

System	En. Diff (OS^{-3}-OS^{-4})	En. Diff.(OS^{-2}-OS^{-3})	En. Diff.(OS^{-1}-OS^{-2})	En. Diff.(OS^{0}-OS^{-1})	En. Diff.(OS^{0}-OS^{-4})
No solvent	-254.83	-83.85	101.89	297.59	60.80
8WM	-208.32	-65.61	143.58	329.16	198.81
12WM	-200.30	-29.24	171.83	339.63	281.91
16WM	-177.49	-9.07	149.49	310.47	273.40
20WM	-162.77	8.88	191.36	322.21	359.68
24WM	-170.47	19.61	191.61	354.39	395.14

Table **22**. Energetic and geometric data shown in this order: Total energy of the structures in each one of the OS, binding energy, inter- Ta ion distance and ionisation energy.

Conf 3 (8WM and 12 WM)

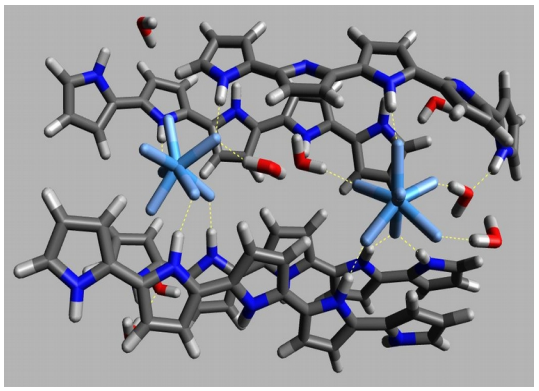

59a)

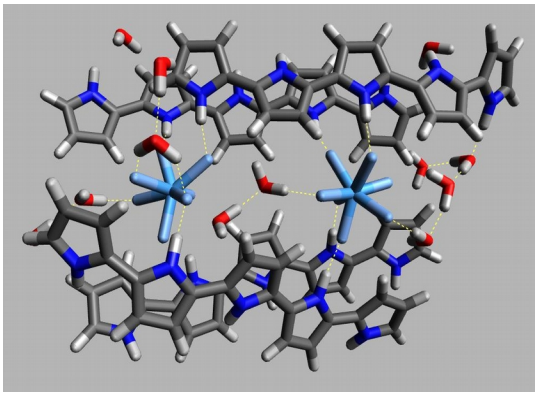

59e)

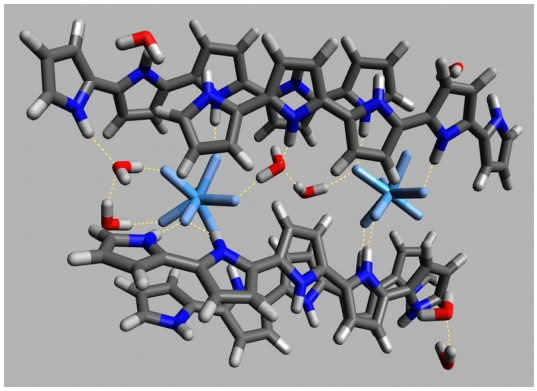

59b)

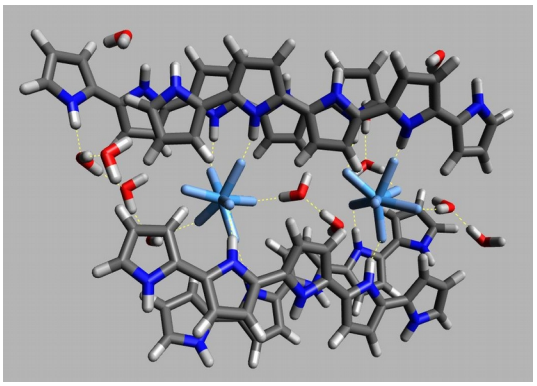

59f)

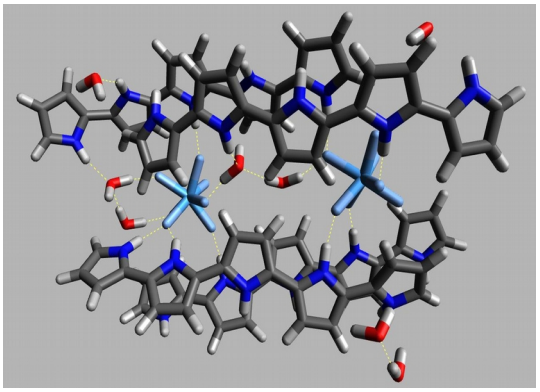

59c)

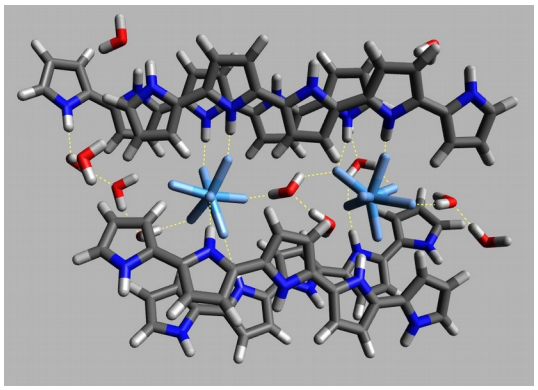

59g)

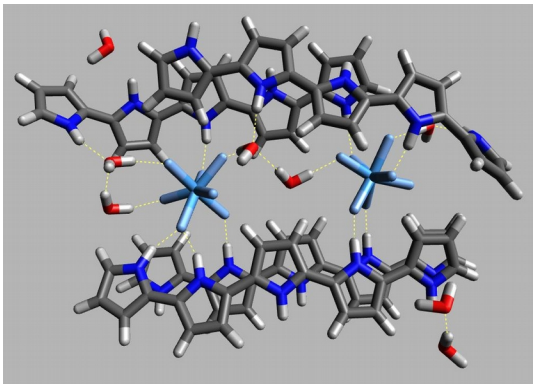

59d)

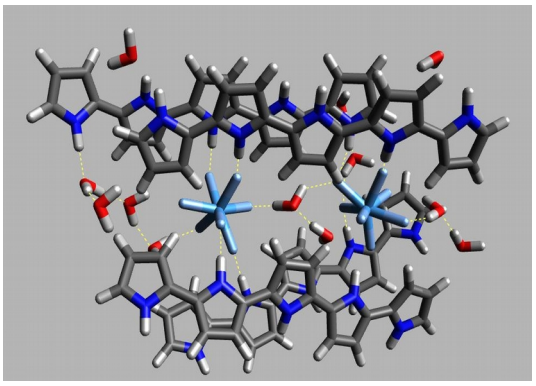

59h)

Figure **59.1**. The third configuration with 4 Py_5-chains und 2 TaF_7^{2-} with 8WM (left) and 12 WM (right) with oxidation state (OS), shown progressively: -3 (a,e), -2 (b,f) , -1 (c,g), 0 (d,h).

Conf 3 (16 WM and 20 WM)

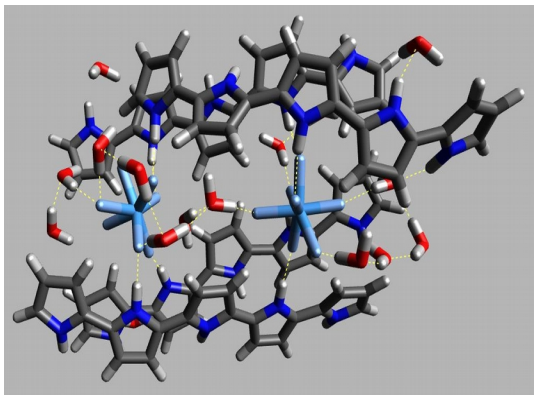

59i)

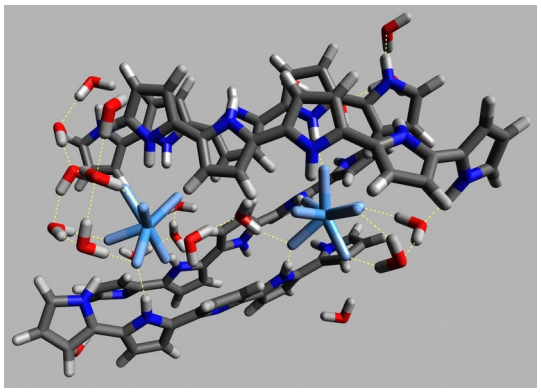

59m)

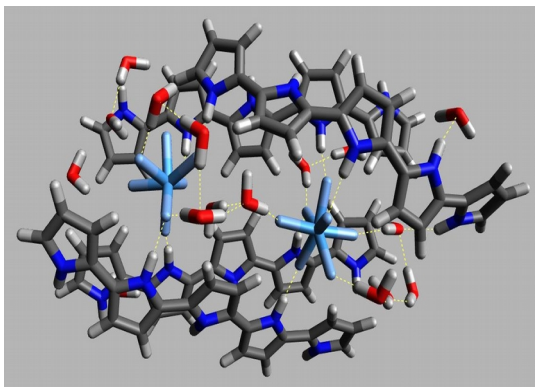

59j)

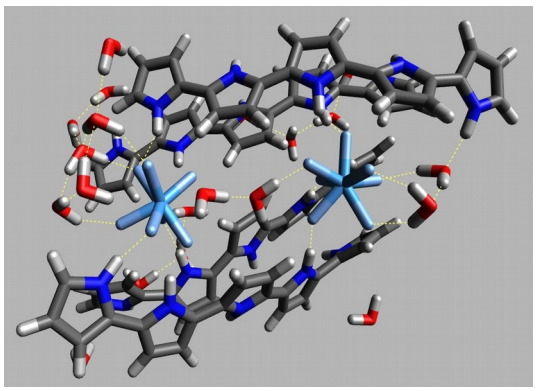

59n)

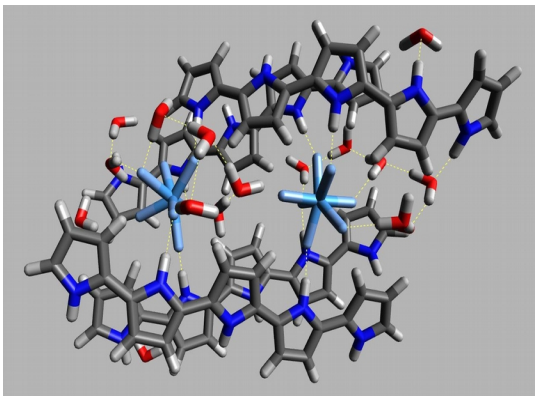

59k)

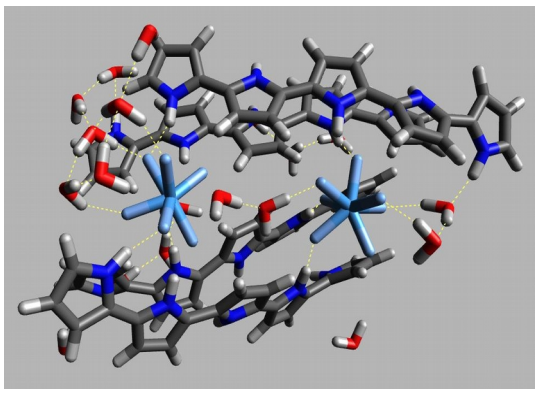

59o)

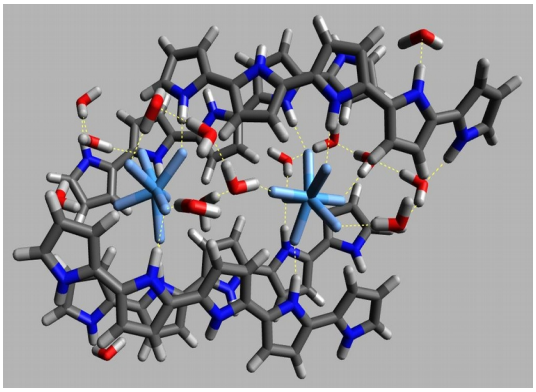

59l)

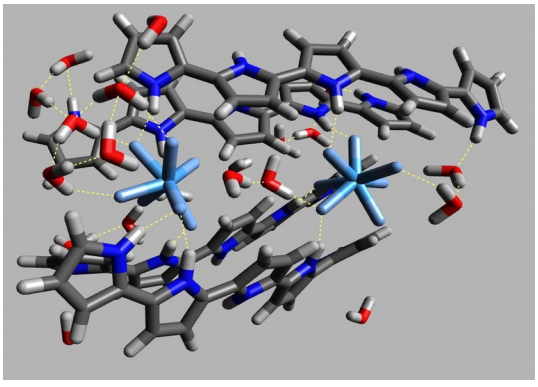

59p)

Figure **59.2**. The third configuration with 4 Py_5-chains und 2 TaF_7^{2-} with 16WM (left) and 20WM (right) with oxidation state (OS), shown progressively: -3 (i,m), -2 (j,n) , -1 (k,o), 0 (l,p).

Conf 3 (24 WM)

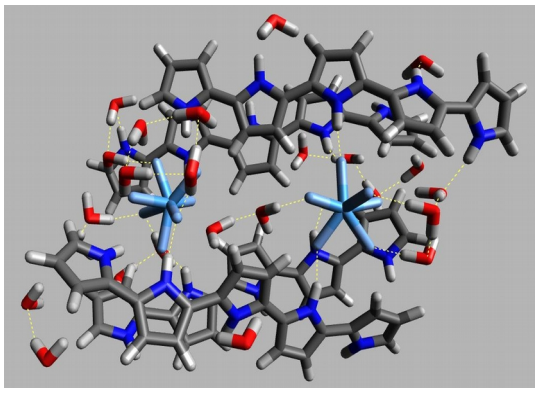

59q)

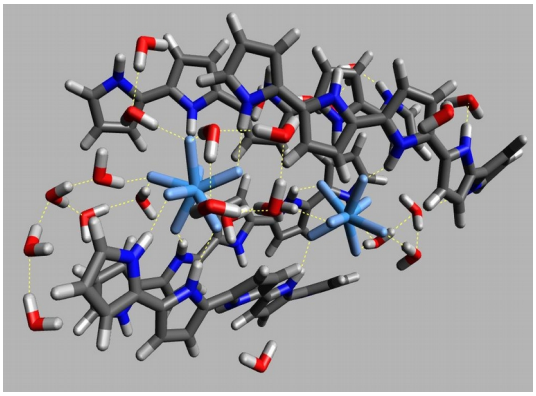

59r)

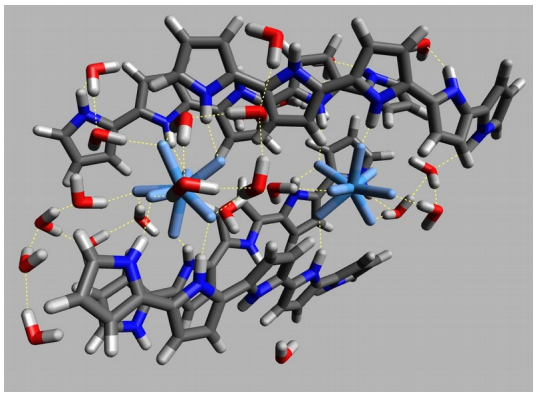

59s)

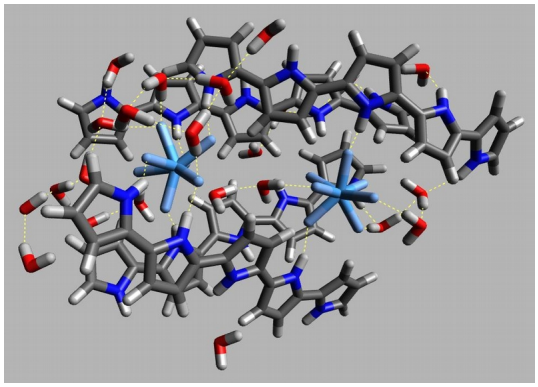

59t)

Figure **59.3**. The third configuration with 4 Py_5-chains und 2 TaF_7^{2-} with 24 WM with oxidation state (OS), shown progressively: -3 (q), -2 (r) , -1 (s), 0 (t).

Total energy (Ha)

System	Energy OS^{-4}	Energy OS^{-3}	Energy OS^{-2}	Energy OS^{-1}	Energy OS^{0}
No solvent	-5700.345086	-5700.424034	-5700.447283	-5700.445097	-5700.325008
8WM	-6312.315063	-6312.397150	-6312.406711	-6312.343207	-6312.248305
12WM	-6618.274931	-6618.354785	-6618.369048	-6618.312677	-6618.192066
16WM	-6924.251227	-6924.324073	-6924.339202	-6924.301455	-6924.176855
20WM	-7230.256695	-7230.320314	-7230.331552	-7230.265336	-7230.123355
24WM	-7536.201803	-7536.265646	-7536.280022	-7536.265646	-7536.081681

Binding energy (kJ/mol)

System	Energy OS^{-4}	Energy OS^{-3}	Energy OS^{-2}	Energy OS^{-1}	Energy OS^{0}
No solvent	654.34	1383.26	1965.94	2481.84	2688.19
8WM	1260.51	1997.68	2544.42	2899.34	3171.81
12WM	1497.65	2228.95	2788.04	3161.68	3366.66
16WM	1777.92	2490.82	3052.18	3474.72	3669.23
20WM	2134.78	2823.45	3374.60	3722.39	3871.27
24WM	2333.16	3022.42	3581.81	4065.71	4104.35

Ta-Ta distance (Å)

System	Energy OS^{-4}	Energy OS^{-3}	Energy OS^{-2}	Energy OS^{-1}	Energy OS^{0}
No solvent	8.550	9.788	9.571	7.891	8.075
8WM	9.791	9.361	9.514	9.415	8.621
12WM	8.176	8.085	7.971	7.859	7.774
16WM	7.960	7.791	7.563	7.337	7.326
20WM	8.260	8.181	8.161	8.073	8.073
24WM	8.313	8.190	8.057	8.190	8.313

Ionization energy (kJ/mol)

System	En. Diff (OS^{-3}-OS^{-4})	En. Diff.(OS^{-2}-OS^{-3})	En. Diff.(OS^{-1}-OS^{-2})	En. Diff.(OS^{0}-OS^{-1})	En. Diff.(OS^{0}-OS^{-4})
No solvent	-207.28	-61.04	5.74	315.29	52.72
8WM	-215.52	-25.10	166.73	249.16	175.27
12WM	-209.66	-37.45	148.00	316.66	217.56
16WM	-191.26	-39.72	99.11	327.14	195.27
20WM	-167.03	-29.50	173.85	372.77	350.08
24WM	-167.62	-37.74	37.74	483.00	315.38

Table **23**. Energetic and geometric data shown in this order: Total energy of the structures in each one of the OS, binding energy, inter- Ta ion distance and ionisation energy.

Conf 4 (8 WM and 12 WM)

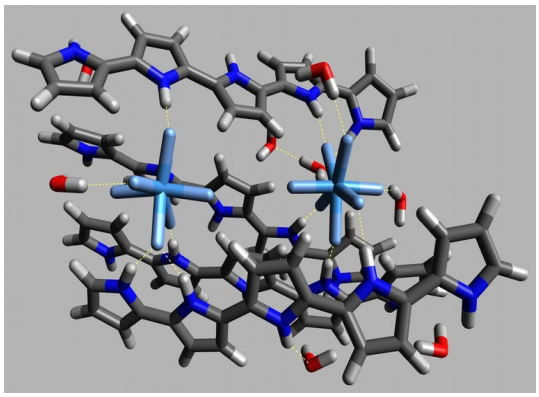
60a)

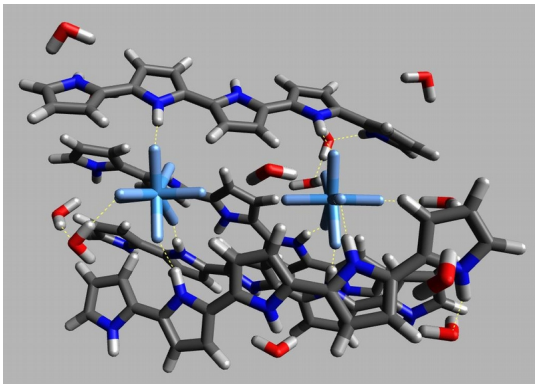
60e)

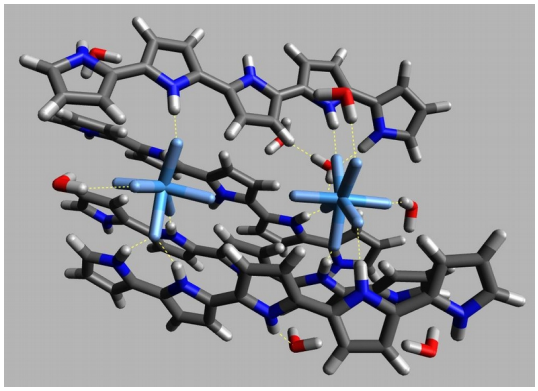
60b)

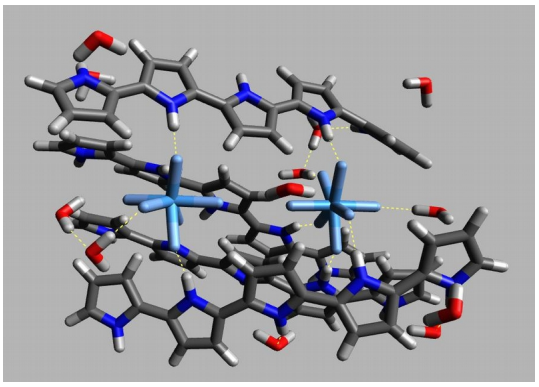
60f)

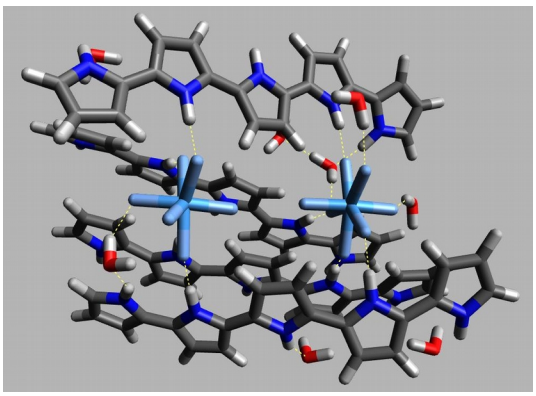
60c)

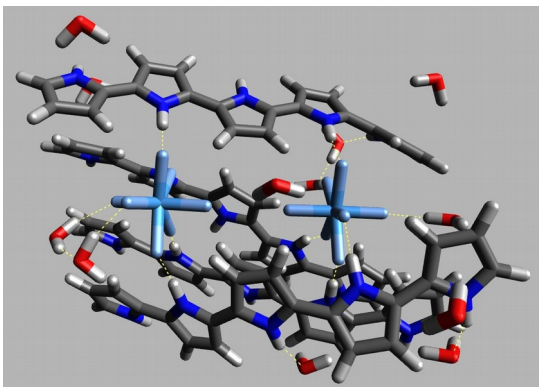
60g)

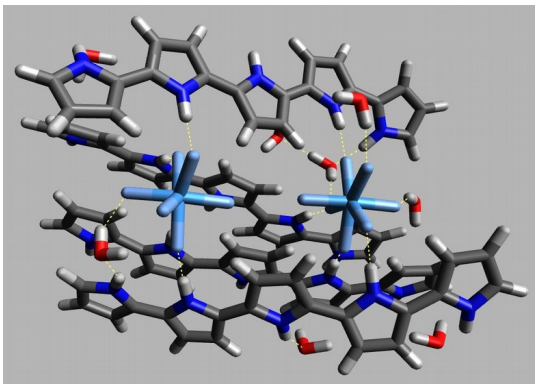
60d)

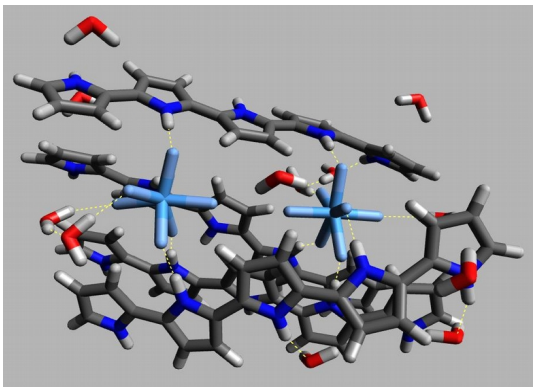
60h)

Figure **60.1**. The fourth configuration with 4 Py_5-chains und 2 TaF_7^{2-} with 8WM (left) and 12WM (right) with oxidation state (OS), shown progressively: -3 (a,e), -2 (b,f) , -1 (c,g), 0 (d,h).

Conf 4 (16 WM and 20 WM)

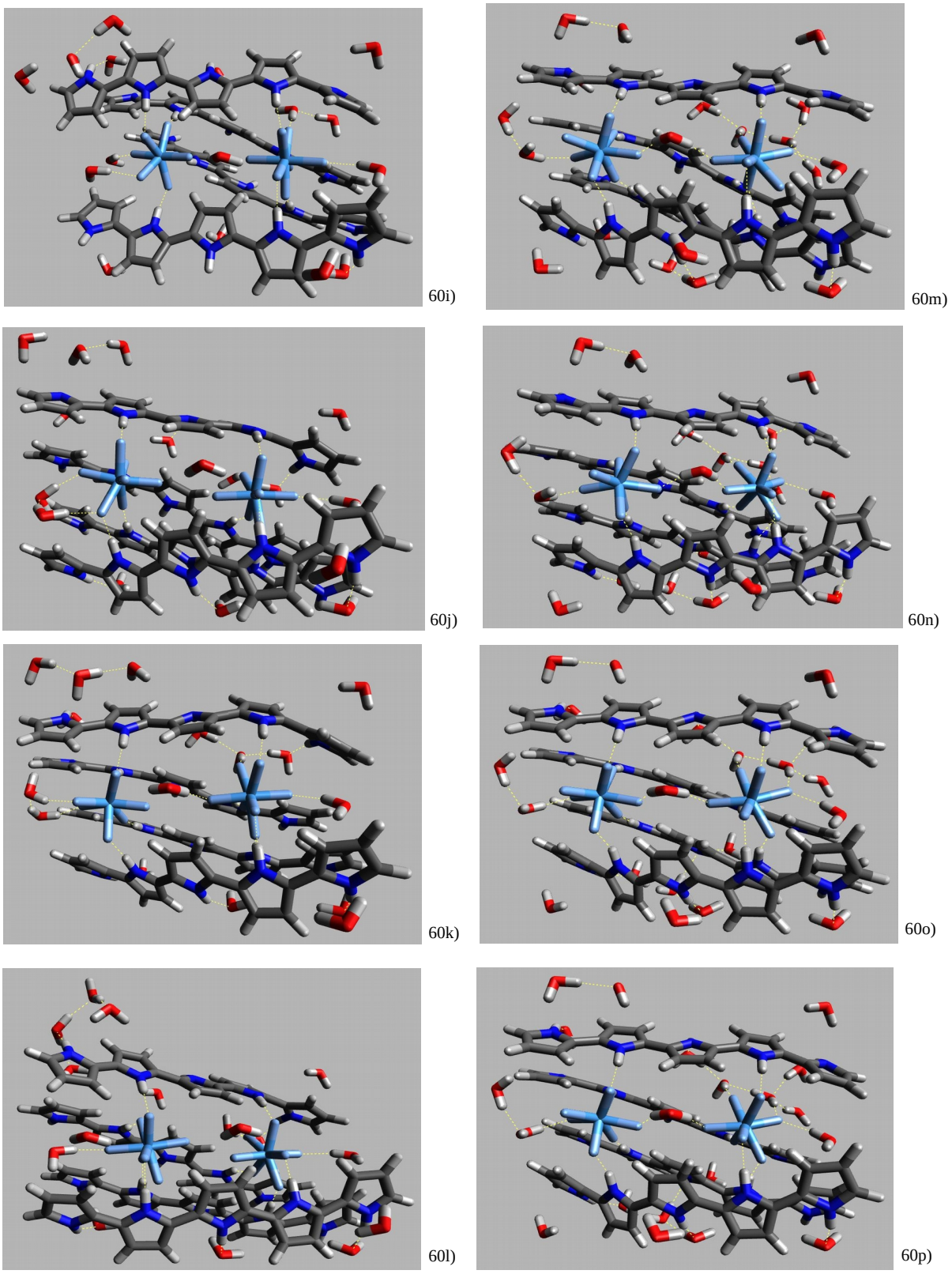

Figure **60.2**. The fourth configuration with 4 Py_5-chains und 2 TaF_7^{2-} with 16WM (left) and 20WM (right) with oxidation state (OS), shown progressively: -3 (i,m), -2 (j,n) , -1 (k,o), 0 (l,p).

Conf 4 (24 WM)

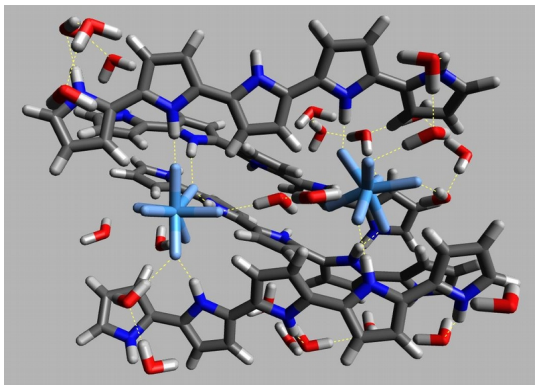

60q)

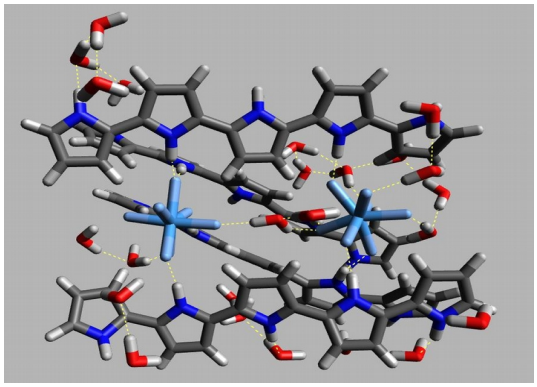

60r)

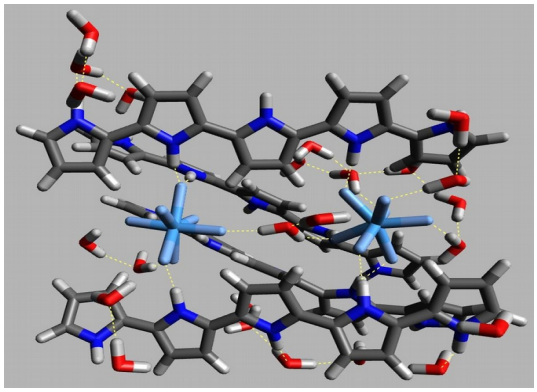

60s)

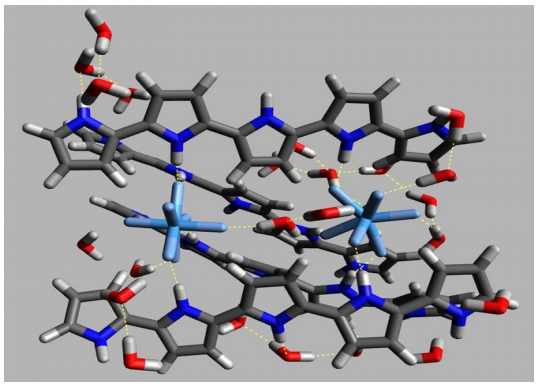

60t)

Figure **60.3**. The fourth configuration with 4 Py_5-chains und 2 TaF_7^{2-} with 24 WM with oxidation state (OS), shown progressively: -3 (q), -2 (r) , -1 (s), 0 (t).

Total energy (Ha)

System	Energy OS^{-4}	Energy OS^{-3}	Energy OS^{-2}	Energy OS^{-1}	Energy OS^{0}
No solvent	-5700.323519	-5700.431736	-5700.469489	-5700.437299	-5700.336136
8WM	-6312.326470	-6312.393697	-6312.439416	-6312.391421	-6312.264841
12WM	-6618.263286	-6618.345861	-6618.359287	-6618.310124	-6618.177251
16WM	-6924.197900	-6924.271976	-6924.313050	-6924.274521	-6924.126803
20WM	-7230.215450	-7230.284430	-7230.289654	-7230.228678	-7230.079379
24WM	-7536.189272	-7536.244757	-7536.244395	-7536.176017	-7536.030025

Binding energy (kJ/mol)

System	Energy OS^{-4}	Energy OS^{-3}	Energy OS^{-2}	Energy OS^{-1}	Energy OS^{0}
No solvent	597.71	1403.48	2024.24	2461.37	3067.53
8WM	1290.46	1988.61	2630.29	3025.92	3215.23
12WM	1467.08	2205.52	2762.41	3154.98	3327.77
16WM	1637.91	2354.04	2983.52	3404.01	3537.82
20WM	2026.49	2729.24	3264.60	3626.15	3755.81
24WM	2300.26	2967.58	3488.27	3830.39	3968.73

Ta-Ta distance (Å)

System	Energy OS^{-4}	Energy OS^{-3}	Energy OS^{-2}	Energy OS^{-1}	Energy OS^{0}
No solvent	7.672	7.422	7.233	7.066	6.937
8WM	7.728	7.449	7.320	7.195	6.939
12WM	7.875	7.455	7.339	7.325	7.189
16WM	7.360	7.157	6.897	7.312	6.606
20WM	7.728	7.788	7.584	7.349	7.295
24WM	8.395	8.316	8.140	8.155	8.106

Ionization energy (kJ/mol)

System	En. Diff (OS^{-3}-OS^{-4})	En. Diff.(OS^{-2}-OS^{-3})	En. Diff.(OS^{-1}-OS^{-2})	En. Diff.(OS^{0}-OS^{-1})	En. Diff.(OS^{0}-OS^{-4})
No solvent	-284.12	-99.12	84.51	265.60	-33.12
8WM	-176.50	-120.04	126.01	332.33	161.81
12WM	-216.80	-35.25	129.08	348.86	225.88
16WM	-194.49	-107.84	101.16	387.83	186.67
20WM	-181.11	-13.72	160.09	391.99	357.25
24WM	-145.68	0.95	179.53	383.30	418.10

Table **24**. Energetic and geometric data shown in this order: Total energy of the structures in each one of the OS, binding energy, inter- Ta ion distance and ionisation energy.

Conf 1 (6 ACN and 8 ACN)

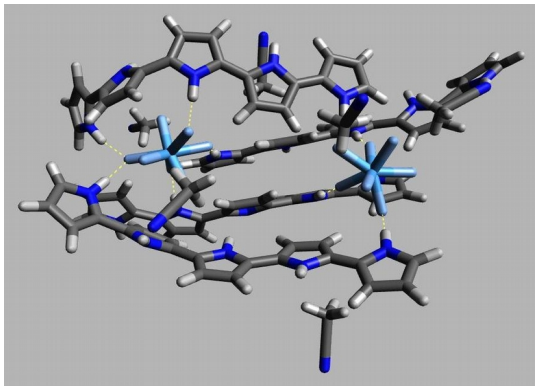
61a)

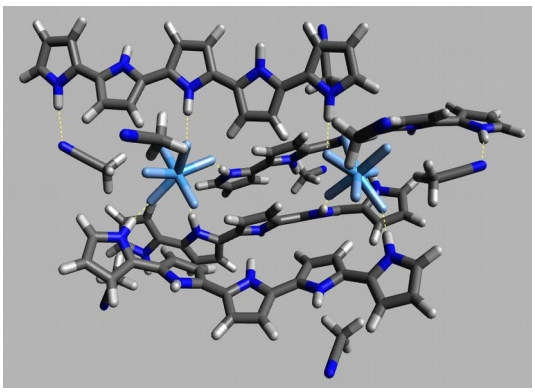
61e)

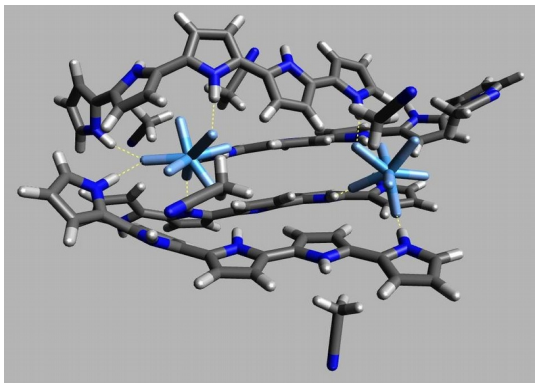
61b)

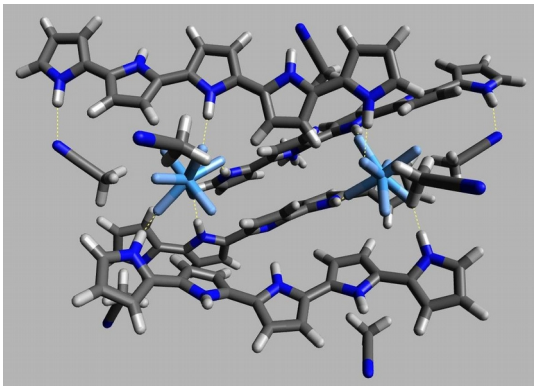
61f)

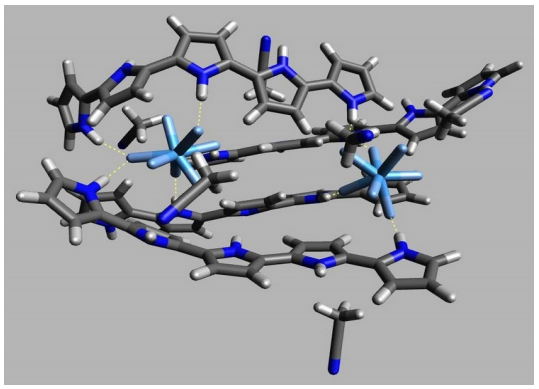
61c)

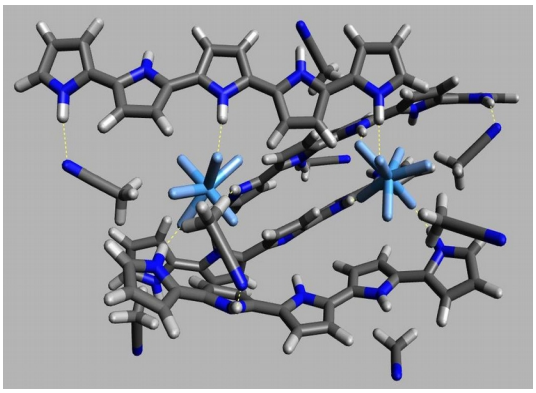
61g)

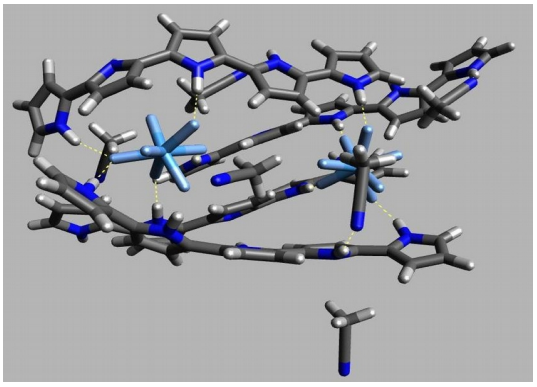
61d)

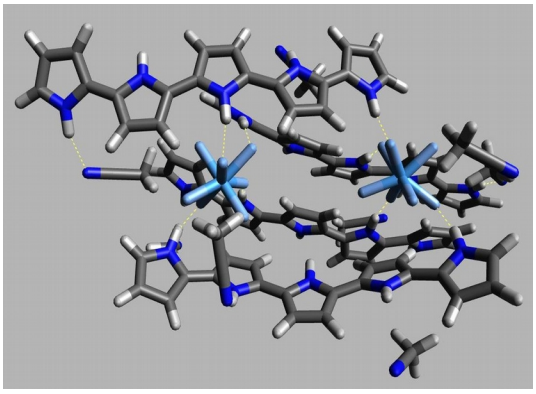
61h)

Figure **61.1**. The first configuration with 2 Ta ions and four pyrrole pentamers with 6 ACN (left) and 8 ACN (right) with oxidation state (OS), shown progressively: -3 (a,e), -2 (b,f) , -1 (c,g), 0 (d,h).

Conf 1 (10 ACN and 12 ACN)

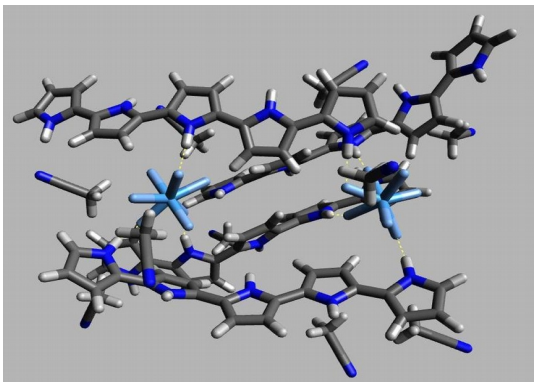

61i)

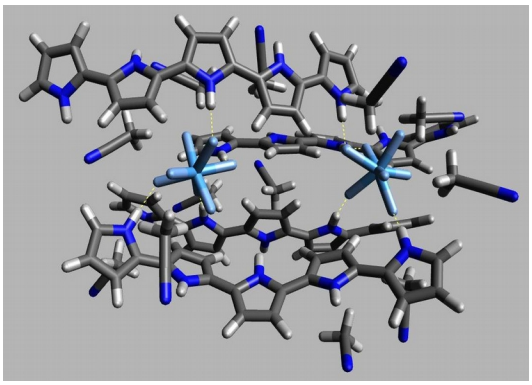

61m)

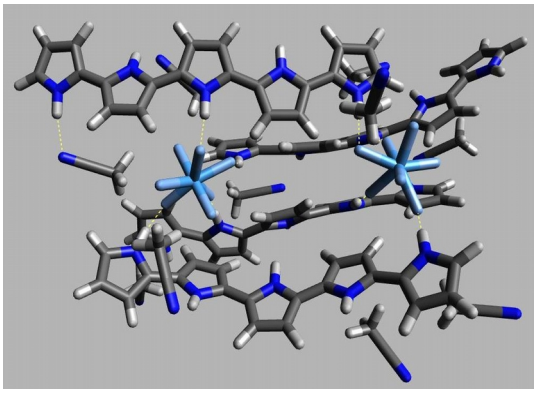

61j)

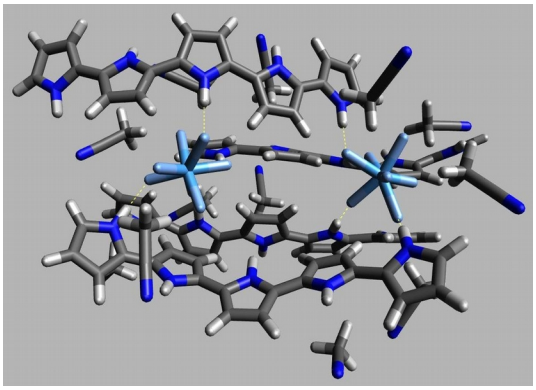

61n)

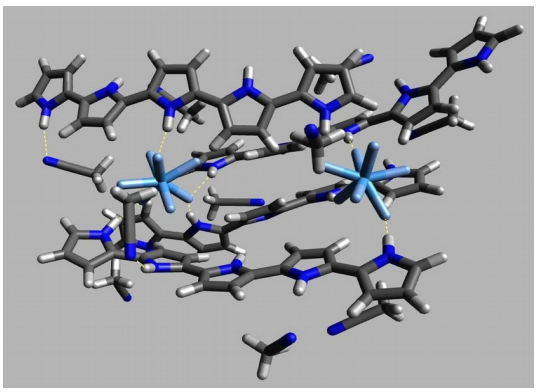

61k)

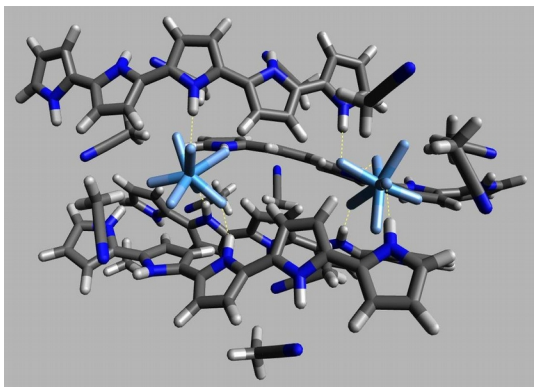

61o)

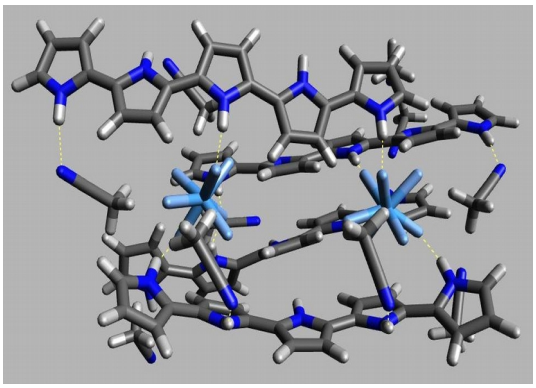

61l)

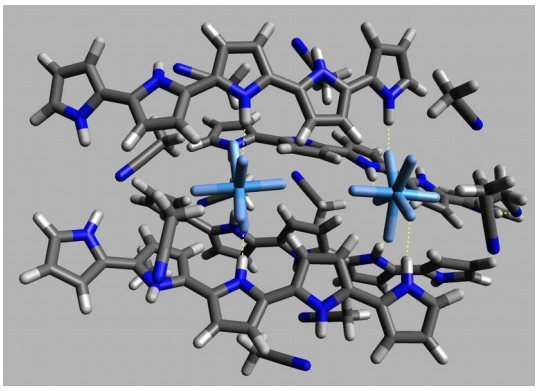

61p)

Figure **61.2**. The first configuration with 4 Py_5-chains und 2 TaF_7^{2-} with 10 ACN (left) and 12 ACN (right) with oxidation state (OS), shown progressively: -3 (i,m), -2 (j,n) , -1 (k,o), 0 (l,p).

Conf 1 (14 ACN)

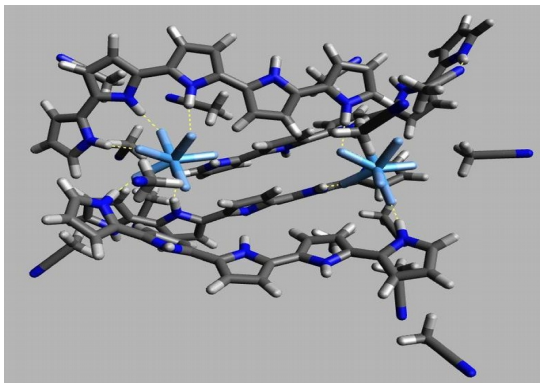

61q)

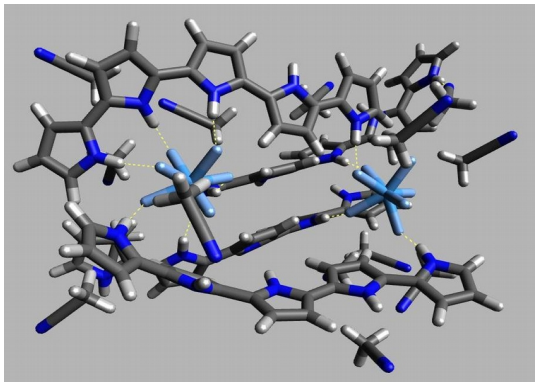

61r)

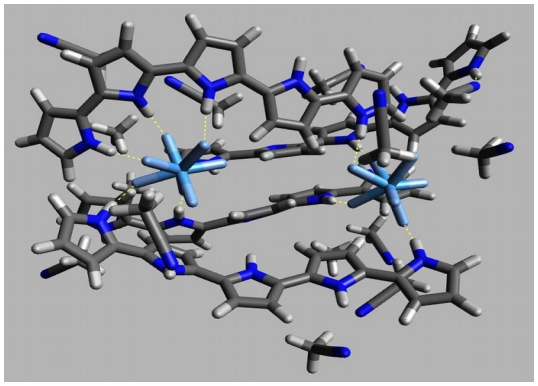

61s)

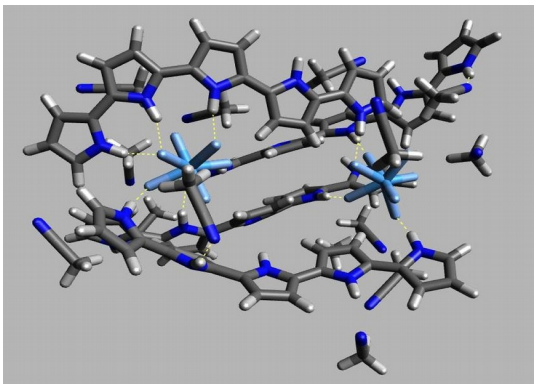

61t)

Figure **61.3**. The first configuration with 4 Py_5-chains und 2 TaF_7^{2-} with 14 ACN with oxidation state (OS), shown progressively: -3 (q), -2 (r), -1 (s), 0 (t).

Total energy (Ha)

System	Energy OS^{-4}	Energy OS^{-3}	Energy OS^{-2}	Energy OS^{-1}	Energy OS^{0}
No solvent	-5700.336053	-5700.424034	-5700.447283	-5700.404379	-5700.325008
6ACN	-6497.409675	-6497.477576	-6497.484527	-6497.418299	-6497.312168
8ACN	-6763.080210	-6763.139114	-6763.136644	-6763.094588	-6762.986875
10ACN	-7028.760459	-7028.810635	-7028.808626	-7028.751102	-7028.658623
12ACN	-7294.449266	-7294.506870	-7294.493897	-7294.441000	-7294.337091
14ACN	-7560.128613	-7560.166687	-7560.166756	-7560.096174	-7559.959072

Binding energy (kJ/mol)

System	Energy OS^{-4}	Energy OS^{-3}	Energy OS^{-2}	Energy OS^{-1}	Energy OS^{0}
No solvent	630.62	1383.26	1965.94	2374.94	2688.19
6ACN	1146.23	1846.15	2386.05	2733.81	2976.80
8ACN	1263.83	1940.13	2455.29	2866.51	3105.35
10ACN	1406.93	2060.31	2581.96	2947.29	3226.13
12ACN	1572.50	2245.38	2732.97	3115.73	3364.56
14ACN	1713.23	2334.84	2856.67	3193.00	3354.68

Ta-Ta distance (Å)

System	Energy OS^{-4}	Energy OS^{-3}	Energy OS^{-2}	Energy OS^{-1}	Energy OS^{0}
No solvent	9.974	9.788	9.571	9.378	8.075
6ACN	9.776	9.544	9.163	9.18	8.465
8ACN	9.519	9.349	9.242	8.741	8.689
10ACN	9.98	9.843	9.687	9.634	8.512
12ACN	9.385	9.295	9.336	8.776	7.058
14ACN	9.469	9.374	9.36	9.275	9.322

Ionization energy (kJ/mol)

System	En. Diff (OS^{-3}-OS^{-4})	En. Diff.(OS^{-2}-OS^{-3})	En. Diff.(OS^{-1}-OS^{-2})	En. Diff.(OS^{0}-OS^{-1})	En. Diff.(OS^{0}-OS^{-4})
No solvent	-230.99	-61.04	112.64	208.39	29.00
6ACN	-178.27	-18.25	173.88	278.65	256.00
8ACN	-154.65	6.48	110.42	282.80	245.05
10ACN	-131.74	5.27	151.03	242.80	267.37
12ACN	-151.24	34.06	138.88	272.81	294.52
14ACN	-99.96	-0.18	185.31	359.96	445.13

Table **25**. Energetic and geometric data shown in this order: Total energy of the structures in each one of the OS, binding energy, inter-Ta ion distance and ionisation energy.